



POLITECNICO DI TORINO
Repository ISTITUZIONALE

Design of a Multilayer Honey-Mimetic Antibacterial Wound Healing Device

Original

Design of a Multilayer Honey-Mimetic Antibacterial Wound Healing Device / Vasquez, JEDDAH MARIE. - (2019 Jul 18), pp. 1-298.

Availability:

This version is available at: 11583/2745713 since: 2019-08-02T08:35:00Z

Publisher:

Politecnico di Torino

Published

DOI:

Terms of use:

Altro tipo di accesso

This article is made available under terms and conditions as specified in the corresponding bibliographic description in the repository

Publisher copyright

(Article begins on next page)



ScuDo

Scuola di Dottorato ~ Doctoral School
WHAT YOU ARE, TAKES YOU FAR



Doctoral Dissertation
Doctoral Program in Energy Engineering (31st Cycle)

Design of a Multilayer Honey-Mimetic Antibacterial Wound Healing Device

Jeddah Marie Vasquez

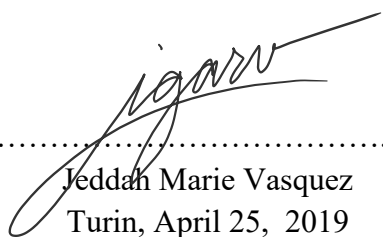
Supervisors

Prof. Valeria Chiono
Prof. Gianluca Ciardelli, Co-Supervisor
Prof. Wenxin Wang, Co-Supervisor
Dr. Udo Greiser, Co-Supervisor

Politecnico di Torino
April 25, 2019

This thesis is licensed under a Creative Commons License, Attribution - Noncommercial - NoDerivative Works 4.0 International: see www.creativecommons.org. The text may be reproduced for non-commercial purposes, provided that credit is given to the original author.

I hereby declare that, the contents and organisation of this dissertation constitute my own original work and does not compromise in any way the rights of third parties, including those relating to the security of personal data.


.....
Jeddah Marie Vasquez
Turin, April 25, 2019

Summary

My work was focussed on the development of a drug-free, antibacterial, multilayer honey-mimetic wound dressing, composed of: (1) a loaded antibacterial reactive oxygen species (ROS)-producing, injectable hydrogel, (2) an antibacterial glucose oxidase (GO) surface-functionalized electrospun polyurethane fibre patch protecting the hydrogel layer, and (3) a glucose-loaded hydrogel on top of the electrospun fibre wound dressing. Assembled all together, these materials would be applied on the wound site to facilitate healing and prevent bacterial infections.

In the development of the Layer (1) - wound dressing hydrogel -, an *in situ* quick forming, water absorbing hydrogel was developed, mimicking the antibacterial mechanism of honey. Within honey, antibacterial ROS such as hydrogen peroxide (H_2O_2) are continuously formed from the reaction of GO enzyme and glucose. The hydrogel was prepared by the Michael addition thiol-ene click chemistry between a synthesised hyperbranched polyethylene glycol diacrylate (HB PEGDA) and a commercially available thiolated hyaluronic acid (HA-SH). This reaction occurs rapidly in a physiological pH environment and causes a quick sol to gel transition of the mixed polymer solutions.

Four different HB PEGDA/HA-SH hydrogels were obtained by mixing HB PEGDA polymer solution (10-20 w/w %) with an equal volume of HA-SH solution (0.5-2 w/w %). Produced hydrogels differed for the relative content of the polymers (HB PEGDA dry weight: from 83.3 % w. to 90.9 % w.) and overall hydrogel concentration (from 6 to 12 % w./w.).

The hydrogel was screened based on its gelation time, water absorption profile, and degradation rate. Based on the results, HB PEGDA/HA-SH 10-1.0 was selected.

Mouldable and injectable HB PEGDA/HA-SH 10-1.0 hydrogels, prepared from HB PEGDA (10 w/w %) and HA-SH (1.0 w/w %) (dry weight composition: 90.9 wt.% HB PEGDA; 9.1 wt.% HA-SH; overall hydrogel concentration: 11 wt.%) were selected as their gelation time (63 s) may potentially allow *in vivo* injection. They displayed high water absorption (130%) after six weeks incubation in phosphate buffered saline solution. After 64 days, they showed no signs of degradation in terms of decreasing hydrogel mass.

A range of glucose oxidase concentrations (0-500 U/L) were tested with 2.5 w/w% glucose within the HB PEGDA/HA-SH 10-1.0 hydrogel. One final GO concentration was selected based on the amount of H₂O₂ produced (target range was 10-20 mM H₂O₂ per day) in 24 hours and cytocompatibility.

This HB PEGDA/HA-SH 10-1.0 hydrogel containing 250 U/L glucose oxidase and 2.5 w/w% glucose produced 9.11 ± 0.92 mM H₂O₂ in static conditions after 24 hours by pertitanic acid assay, and displayed cytocompatibility when tested in the presence of NIH/3T3 mouse fibroblast cells for 24 hours. Antibacterial ability was also measured against relevant Gram-positive bacteria and Gram-negative bacteria: *E. coli*, *S. aureus*, *P. aeruginosa*, MRSA, MRSE, etc.: the hydrogel had a higher antibacterial response to Gram-positive bacteria, which were more receptive to H₂O₂ due to their structural characteristics (they lack an outer membrane).

Layer (2) was made of Lubrizol Tecophilic SP60D60, a commercially available medical-grade thermoplastic polyurethane (TPU). This was coated with a polyDOPA (PDA) film to facilitate immobilization of GO enzyme as it grafts itself on PDA quinone functional groups. PDA coating by spontaneous oxidation of L-dihydroxyphenylalanine (L-DOPA) and self-polymerisation has been previously optimized at Politecnico di Torino to get a well-distributed coating layer using 7 hour time. To reduce oxidation/polymerisation time in PDA-coating, a novel protocol was developed by adding an oxidizing enzyme, lactoperoxidase (LPO) at various concentrations (0-1.4 U/mL). Furthermore, self-polymerisation approach was also tested at shorter times than 7 hours. PDA coating using 1.4 U/mL LPO was achieved in 3 hours. As a comparison, PDA coating was also prepared by self-polymerisation in 3 hours.

Glucose oxidase was successfully grafted into TPU-PDA fibre patches (with and without the use of LPO). One of the modified fibre patches of interest was TPU-PDA-GO-0-3, obtained by grafting GO to PDA deriving from DOPA self-polymerization in 3 hours. Such coating had an enzyme activity of 7.9 ± 1.9 U/g glucose oxidase. This was used as GO enzyme assay results showed that the addition of LPO did not play a significant role on increasing the amount of GO that can be grafted onto a PDA-coated substrate

For the top glucose-replenishing hydrogel (3), the material was prepared from UV-cured gelatin methacrylate (GelMA) loaded with 10 w/v glucose. GelMA was synthesized by following a literature protocol by Nichol, et al., 2010 (Cell-laden microengineered gelatin methacrylate hydrogels). GelMA was dissolved at a concentration of 15 w/v% into a PBS solution at pH 7.4 that contained 10 w/v% glucose and 1 w/v% Irgacure 2959. Hydrogels were formed by UV crosslinking under a UV lamp with an intensity of 4 mW/cm^2 at a wavelength of 365 nm. The bilayer device formed by glucose-loaded GelMA in combination with TPU-PDA-GO patches (obtained at different coating times and DOPA-oxidizing conditions) resulted cytocompatible in indirect contact tests with NIH/3T3 mouse fibroblast cells for 24 hours.

The image below (Figure 10.1) shows the schematic representation of the assembled multilayer wound healing device with the specific materials used for each layer.

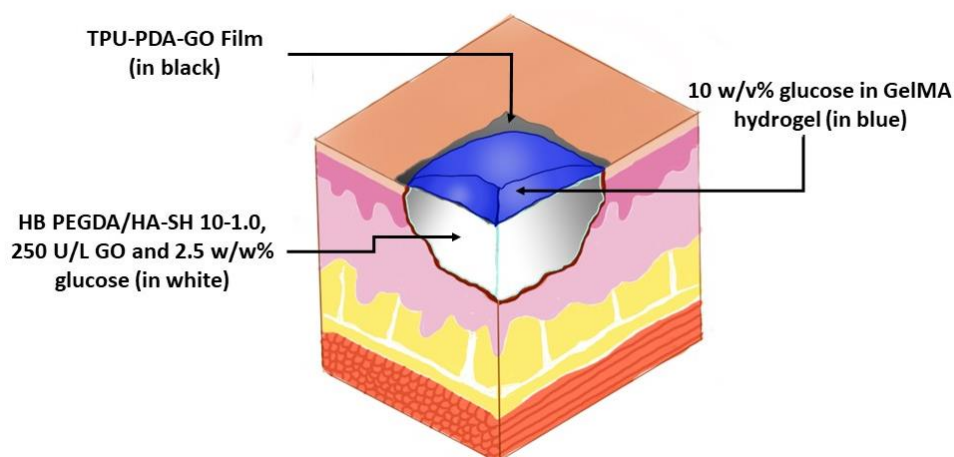


Figure 10.1 Multilayer wound healing device

The highest overall cytocompatibility of the multilayer device was $58.3 \pm 8.5\%$ with the use of TPU-PDA-GO-0-3 and glucose-loaded (10 w/v%) UV-crosslinked GelMA hydrogel. The obtained cytocompatibility for the multilayer was not considerably ideal: the GO/glucose concentrations in HB PEGDA/HA-SH 10-1.0 should be reduced when used with the TPU-PDA-GO fibre patch and glucose-loaded GelMA, as to reduce the amount of produced H_2O_2 . An alternative would be to apply the TPU-PDA-GO system to protect the *in situ* HB PEGDA/HA-SH 10-1.0 wound dressing from exposure and once the glucose from the HB PEGDA/HA-SH 10.1 hydrogel has almost depleted itself, the glucose-loaded GelMA hydrogel could be applied as an additional glucose source.

In future studies, the potential of drug-free GO enzyme/glucose ROS-producing systems to act on various bacterial strains, particularly Gram-positive antibiotic-resistant ones should be explored more in-depth, especially given concerns on the increasing antimicrobial resistance of bacteria. Further optimization of the overall H_2O_2 output will be required and be the subject of future studies.

Scope and Limitations of the Study

This Ph.D thesis focused on the use of a range of materials to produce drug-free antibacterial polymers as part of the objectives set by the EU Horizon 2020 Project HyMedPoly. To achieve this, the general concept of the study was to develop wound healing materials that are embedded with glucose oxidase and glucose that produce antibacterial hydrogen peroxide continuously until the glucose source is depleted. Several areas of research were involved:

- Polymer synthesis and characterization
- Material processing and modification by novel techniques
- Characterization of physicochemical properties of materials
- ROS-producing parameters and assay methods
- Assembly of multilayer wound healing device
- Cytocompatibility testing
- Antibacterial activity testing

The synthesis and characterization of two new types of hyperbranched polymers (hyperbranched polyethylene glycol diacrylate, HB PEGDA and hyperbranched polyethylene glycol diacrylate-co-glycidyl methacrylate, HB PEGDA-co-GMA) using free radical polymerization techniques was investigated. On the other hand, a known literature protocol was applied for the synthesis of gelatin methacrylate (GelMA). Additionally commercially available polymers, such as Vornia Ltd.'s

thiolated hyaluronic acid (HA-SH) and Lubrizol Tecophilic SP60D60 thermoplastic polyurethane (TPU A or TPU) were used in this work.

Material processing and modification was addressed to the development of functional hydrogels and electrospun fiber patches. Techniques investigated for material processing included:

- Hydrogel formation by crosslinking methods: Michael-addition thiol-ene crosslinking and UV-mediated crosslinking
- Electrospinning of thermoplastic polymers in solution (TPU) to form electrospun patches
- Use of enzymes for different applications: Glucose oxidase (GO) for hydrogen peroxide production in combination with glucose, and use of Lactoperoxidase (LPO) for increased oxidation rate of DOPA
- Enzyme immobilization methods: enzyme physical encapsulation in hydrogels, and its covalent-grafting to hydrogel polymers or solid substrates [via reacting with an epoxide group (HB PEGDA-co-GMA) or quinone group (polyDOPA)]
- Surface functionalization of a TPU fibre patch by polyDOPA coating methods

Table 0.1 lists the general characterization experiments of the materials and whether or not they were performed for a specific material. For example, HB PEGDA/HA-SH has a “Yes” under gelation time meaning that this was measured while it has “No” for static contact angle meaning that it was not analysed for this materials.

Table 0.1. List of characterization experiments performed on the materials (excluding GO-grafting and ROS-relevant experiments).

Characterization experiments	HB PEGDA/HA-SH	HBPEGDA-co-GMA/HA-SH	TPU	GelMA hydrogel
Gelation time	Yes	Yes	No	Yes
Rheological properties	Yes	Yes	No	No
Water absorption profile	Yes	Yes	Yes	No
Degradation profile	Yes	Yes	Yes	No
Tensile properties	No	No	Yes	No
Static contact angle	No	No	Yes	No
SEM analysis	No	No	Yes	No
FTIR analysis	No	No	Yes	Yes

Another important aim was to tailor GO and glucose contents within materials, to produce antibacterial H₂O₂ avoiding cytotoxic effects on cells. In this study, the final concentration of GO ranged from 0-1,000 U/L for hydrogel applications. A solution of 10,000 U/L of GO was used for GO-grafting the polyDOPA-coated TPU.

These concentrations define the amount of H₂O₂ that can be produced per unit of time from a glucose source. In this study, glucose amount was limited to a concentration range of 2.5-10 w/w% in hydrogels and 10 w/v% in phosphate buffer solution (PBS) pH 7.4 used to immerse TPU-PDA-GO fibre patches.

The method used for measuring H₂O₂ concentrations was a colorimetric pertitanic acid assay with a measurement range of 0-20 mM H₂O₂ based on the prepared hydrogen peroxide standards as the protocol stated that measurements beyond 20 mM H₂O₂ become more inaccurate.

Another aim was to fabricate a multilayer device composed of different layers, each with a specific function related to the production of antibacterial ROS:

- Layer 1: The bottom most layer was intended to be an injectable hydrogel that would be introduced as a liquid polymer solution and gel in *in situ* on the wound surface. This material would be capable of producing antibacterial ROS on its own.
- Layer 2: The intermediate layer was intended to be a functionalized protective layer with GO-grafted enzymes on its surface for additional antibacterial activity. This material would require a glucose source to produce antibacterial ROS.
- Layer 3: A glucose-loaded hydrogel that can be placed on top of Layer 2 and be removed and replaced to provide a glucose source for Layers 2 (and possibly Layer 1). This material would not have any antibacterial properties in and of itself but can be used for producing antibacterial ROS when combined with Layer 2.

A combination of [Layers 1 with 2], [Layer 2 with 3], and [Layer 1, 2, and 3] were intended to be used for wound healing applications. The multilayer wound healing device was intended only for preventing infections in common bacterial strains and some antibiotic resistant Gram-positive bacteria like (Methicillin-resistant *S. aureus*) MRSA and (Methicillin-resistant *S. epidermidis*) MRSE. Figure 10.2 below (taken from Chapter 10) illustrate the different proposed combinations that could be done with the materials developed.

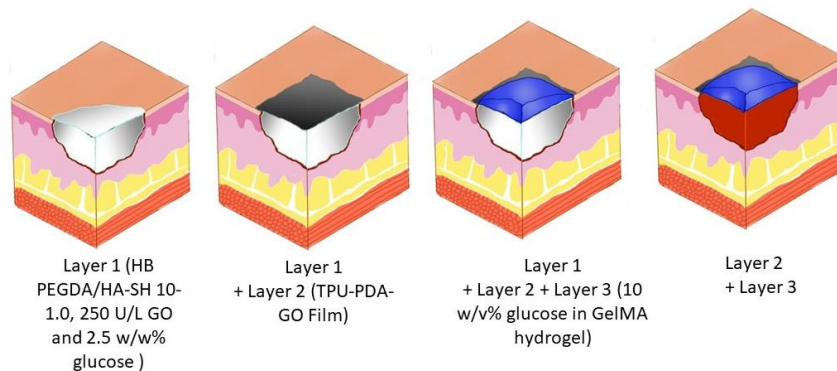


Figure 10.2: Possible configurations for assembling the materials developed in this thesis for an antibacterial wound healing patch using Layers 1 to 3.

In the assembly of the final multilayer wound healing device, Layer 1 (HB PEGDA/HA-SH 10-1.0 hydrogel) was limited to one GO/glucose concentration, which was 250 U/L glucose oxidase and 2.5 w/w% glucose. Layer 2 (TPU-PDA-GO-0-3 fibre patch) was selected from the material that would give an ideal H_2O_2 release and have cytocompatible properties. Layer 3 (glucose-loaded GelMA hydrogel) utilized one glucose composition of 10 w/v% glucose.

Preliminary cytocompatibility tests (CT 1) were performed using NIH/3T3 mouse fibroblast cells and an indirect, non-contact method. A different cytocompatibility test protocol (CT 2) however was for the testing of the multilayer device developed from ISO 10993 standards using eluates collected from the multilayer wound healing device.

Single and combined components of the wound healing device were tested, as summarized in Table 0.2 based on the cytocompatibility protocol used (CT1 or CT2), if ROS-production tests were performed on the material (Yes or No), or if antibacterial tests have been performed (Yes or No).

Table 0.2. List of experiments performed on the materials relevant to wound-healing applications.

Layer and combination	Cytocompatibility tested	ROS measurements	Antibacterial tests
Layer 1	CT 1	Yes	Yes
Layer 2	CT 1	Yes	No
Layer 3	CT 1	No	No
Layer 2+3	CT 1	Yes	No
Layer 1+2+3	CT 2	No	No

Antibacterial activity in nine bacterial strains (4 Gram-positive and 5 Gram-negative) was preliminarily tested on HB PEGDA/HA-SH hydrogels. The method used for assessing antibacterial activity was based on an agar diffusion test and the data gathered was reported in terms of zone of inhibition. Indeed such hydrogel can be used alone to treat infected wounds, while the other components can prolong the antibacterial activity. The complete device will be subject of future investigations.

Acknowledgements

This thesis would not have come into fruition without the help of so many. Though words may not be enough to convey what I feel, I would like to express my deepest gratitude to everyone who helped me realize this thesis.

Firstly, I would like to thank my supervisors, Prof. Valeria Chiono, Dr. Udo Greiser, Prof. Wenxin Wang, and Prof. Gianluca Ciardelli for their constant support and their faith in me. It has meant a lot to me to be mentored by them and learning how to be a better researcher.

Next, I would like to thank everyone in the EU Horizon 2020 HyMedPoly (Drug-Free Antibacterial Hybrid Biopolymers for Medical Applications) Project, especially Politecnico di Torino, Vornia Biomaterials, and Universitätsklinikum Knappschafts Krankenhaus Bochum. I am grateful to have been given the chance to participate in this project and I want to wish you all the best in your future careers too. The past three years have been an incredible learning experience for me, not just to things in the academia but with culture, language, and the history of many European countries.

I would like to thank the people from the different departments I have been involved in that have been a great help to me. From Politecnico di Torino's Department of

Mechanical and Aerospace Engineering: Susanna Sartori, Irene Carmagnola, Andrea Gallina, Chiara Tonda-Turo, Subha Purkayashtha. From Wenxin Wang's Wound Healing and Skin Research Laboratory in Charles Institute of Dermatology, especially to Sofia Kivotidi, Luca Pierucci, Sean McMahon, Sigen A, Xiaolin Li, Qian Xu, and Patrick Duffy. From Universtätsklinikum Knappschafts Krankenhaus Bochum: Dr. Jochen Salber, Ayesha Idrees, Patricia Varela.

There are so many people I owe my PhD journey to that have helped me in one way or another, and it would probably take forever to name everyone. For the sake of brevity, I will name only three: to Sugar and Garcy, my oldest and best friends back in Philippines for always being there for me even if we are miles away, and to my boyfriend Tiger.

Contents

Part I

Chapter 1	Wounds.....	2
1.1.	Abstract.....	2
1.2.	Introduction.....	2
1.2.1.	Structure of skin.....	3
1.2.2.	Types of wounds.....	4
1.3.	Wound healing and treatment.....	5
1.3.1.	Wound healing mechanism.....	5
1.3.2.	Complications in wound healing.....	7
1.3.3.	Role of Reactive Oxygen Species (ROS) in wound healing	8
1.4.	Antibiotic resistance.....	9
1.4.1.	Bacterial resistance in wounds.....	10
1.4.2.	Current antibacterial methods.....	10
1.4.3.	Research on natural sources for wound healing.....	11
1.5.	Role of enzymes in wound healing.....	12
1.5.1.	Glucose oxidase and ROS.....	13
1.6.	Hydrogels in regenerative medicine.....	14
1.6.1.	Hydrogels for wound care.....	14
1.6.1.1.	Properties relevant to wound care.....	15
1.6.1.2.	Click-chemistry thiol-ene hydrogels.....	16
1.6.1.3.	Hyperbranched hydrogels.....	18
1.7.	State of the art in antibacterial wound care.....	20
1.8.	References.....	24
Chapter 2	Preparation and Characterization of Hyperbranched PEGDA/HA-SH Hydrogels.....	34
2.1.	Abstract.....	34

2.2. Introduction.....	35
2.2.1. Free Radical Polymerization.....	35
2.2.2. Reversible-deactivation Radical Polymerization.....	36
2.3. Materials and methods.....	40
2.3.1. Polyethylene diacrylate (PEGDA).....	41
2.3.2. Thiolated hyaluronic acid (HA-SH).....	41
2.3.3. Reversible addition fragmentation chain transfer (RAFT) polymerization of HB PEGDA.....	42
2.3.4. Chemical characterization of HB PEGDA.....	43
2.3.5. Preparation of HB PEGDA/HA-SH hydrogels.....	44
2.3.6. Gelation time.....	45
2.3.7. Rheological characterization of hydrogel.....	46
2.3.7.1.1. Frequency sweep and strain sweep tests....	46
2.3.8. Swelling and water uptake profile.....	47
2.3.9. Degradation profile of hydrogels.....	48
2.4. Results and discussion.....	49
2.4.1. Chemical characterization of HB PEGDA.....	49
2.4.1.1. Gel Phase Chromatography.....	49
2.4.1.2. Nuclear Magnetic Resonance.....	50
2.4.2. Gelation time and rheological characterization of hydrogel.....	51
2.4.2.1. Gelation time.....	51
2.4.2.2. Results from frequency sweep and strain sweep tests.....	52
2.4.3. Physical characterization of hydrogel.....	55
2.4.3.1. Swelling and water uptake profile.....	55
2.4.3.2. Degradation profile.....	57
2.5. Conclusions.....	58
2.6. References.....	58

Chapter 3	Antibacterial Reactive Oxygen Species Production in HB PEGDA/HA-SH Hydrogel.....	61
3.1.	Abstract.....	61
3.2.	Introduction.....	62
3.2.1.	Common bacterial species found in wound sites.....	63
3.2.2.	Bactericidal effects of ROS.....	64
3.3.	Materials and methods.....	64
3.3.1.	Glucose oxidase.....	65
3.3.2.	Preparation of HB PEGDA/HA-SH hydrogel with glucose oxidase/glucose for the formation of ROS.....	66
3.3.3.	Pertitanic acid assay for the analysis of hydrogen peroxide formation and release.....	69
3.3.4.	Alamar Blue cytocompatibility tests.....	71
3.3.5.	Agar diffusion test.....	73
3.4.	Results and discussion.....	74
3.4.1.	H ₂ O ₂ production in HB PEGDA/HA-SH.....	74
3.4.2.	Alamar Blue cytocompatibility tests.....	78
3.4.3.	Antibacterial testing results.....	81
3.5.	Conclusions.....	87
3.6.	References.....	88
Chapter 4	Functionalization of HB PEGDA for Glucose Oxidase Immobilization.....	89
4.1.	Abstract.....	89
4.2.	Introduction.....	91
4.2.1.	Enzyme immobilization.....	91
4.2.2.	Methods for immobilizing glucose oxidase.....	91

4.2.3. Synthesis reaction for HB PEGDA-co-GMA and GO	
grafting strategy.....	93
4.3. Materials and Methods.....	96
4.3.1. Synthesis of HB PEGDA-co-GMA.....	97
4.3.2. Chemical characterization of HB PEGDA-co-GMA.....	99
4.3.3. Preparation of HB PEGDA-co-GMA/HA-SH hydrogels...	100
4.3.4. Characterization of HB PEGDA-co-GMA/HA-SH	
hydrogel.....	101
4.3.4.1. Gelation time.....	101
4.3.4.2. Rheological properties.....	102
4.3.4.3. Swelling and degradation profile.....	102
4.3.5. Immobilization of glucose oxidase.....	103
4.3.6. ROS production in HB PEGA-co-GMA/HA-SH.....	104
4.3.7. Alamar Blue cytocompatibility test.....	104
4.4. Results and Discussion.....	104
4.4.1. Chemical characterization of HB PEGDA-co-GMA.....	104
4.4.2. Gelation time.....	107
4.4.3. Rheological characterization of hydrogel.....	108
4.4.3.1. Frequency sweep.....	108
4.4.3.2. Strain sweep.....	109
4.4.4. Physical characterization of hydrogel.....	110
4.4.4.1. Water adsorption profile.....	110
4.4.5. Immobilization of glucose oxidase.....	112
4.4.6. ROS production in HB PEGA-co-GMA/HA-SH 10-1.0...	113
4.4.7. Alamar Blue cytocompatibility test.....	115
4.5. Conclusions.....	116
4.6. References.....	117

Part II

Chapter 5 Preparation and Characterization of Wound Healing

Thermoplastic Polyurethane Patches.....	121
5.1. Abstract.....	121
5.2. Introduction.....	123
5.2.1. Thermoplastic Polyurethanes.....	126
5.3. Materials and methods.....	128
5.3.1. Thermoplastic Polyurethanes for electrospinning.....	128
5.3.2. Physical and mechanical properties of TPU cast films.....	129
5.3.2.1. Static contact angle.....	129
5.3.2.2. Water absorption and dry weigh loss measurements.....	130
5.3.2.3. Tensile mechanical testing.....	130
5.3.3. Electrospinning of TPU patches, imaging of electrospun fibres, and optimization of process parameters.....	131
5.4. Results and discussion.....	132
5.4.1. Static contact angle of TPU cast films.....	132
5.4.2. Swelling and degradation results of TPUs.....	133
5.4.3. Mechanical test results.....	136
5.4.4. Electrospinning of whitelisted TPUs and morphological characterization.....	139
5.4.4.1. Morphological characterization of electrospun TPU patches.....	139
5.5. Conclusions.....	147
5.6. References.....	148

Chapter 6	Preparation and Characterization of "Bio-artificial"	
	Electrospun TPU Wound Healing Patch.....	152
6.1.	Abstract.....	152
6.2.	Introduction.....	153
6.2.1.	Improved design for wound healing and protection.....	153
6.2.2.	Requirements of wound healing patches.....	154
6.2.3.	State of the art of polymers for wound healing patches.....	154
6.2.4.	Coating techniques for wound healing patches.....	155
6.2.4.1.	Applications of polyDOPA coatings.....	156
6.2.4.2.	Immobilization of enzymes onPDA-coated surfaces.....	159
6.3.	Theoretical design of multilayer wound healing patch.....	162
6.4.	References.....	164
Chapter 7	PolyDOPA Surface Coatings of Selected Wound	
	Healing Thermoplastic Polyurethane Patch.....	168
7.1.	Abstract.....	168
7.2.	Introduction.....	169
7.2.1.	Oxidation mechanism of mussel inspired L-3,4- dihydroxyphenylalanine (DOPA).....	169
7.2.2.	Enhancing rate of oxidation of DOPA.....	172
7.2.3.	Oxidizing enzymes.....	173
7.3.	Materials and methods.....	174
7.3.1.	Preparation of LPO enzyme solutions.....	174
7.3.2.	Study of DOPA oxidation rate with lactoperoxidase.....	175
7.3.3.	Surface coating of electrospun TPU with polyDOPA (PDA) with/without LPO enhancement (Part I).....	176

7.3.4. Surface coating of electrospun TPU with polyDOPA (PDA) with/without LPO enhancement (Part II) – Scaled-up surface modification.....	176
7.3.5. SEM analysis of PDA-coated TPU.....	177
7.3.6. FTIR-ATR analysis of PDA-coated TPU.....	178
7.4. Results and discussion.....	178
7.4.1. PDA deposition as a function of LPO concentration.....	178
7.4.2. Determining time for “reference” oxidation level.....	183
7.4.3. SEM analysis of PDA-coated TPU.....	188
7.4.4. FTIR analysis of PDA-coated TPU.....	190
7.5. Conclusions.....	192
7.6. References.....	193

Chapter 8 Surface modification of PDA-TPU patches with

glucose oxidase.....	196
8.1. Abstract.....	196
8.2. Introduction.....	197
8.3. Materials and methods.....	199
8.3.1. Gelatin methacrylate.....	200
8.3.1.1. Preparation of glucose-loaded GelMA hydrogel...	202
8.3.2. Surface grafting of glucose oxidase on PDA-TPU patch...	204
8.3.3. Tests for analyzing the presence of immobilized glucose oxidase.....	204
8.3.3.1. SEM imaging.....	204
8.3.3.2. FTIR-ATR analysis.....	205
8.3.3.3. ROS production of GO-immobilized TPU patch...	205
8.3.3.3.1. Enzyme activity in the material.....	205
8.3.3.3.2. ROS production with a glucose-loaded hydrogel source.....	206

8.4. Results and discussion.....	207
8.4.1. Morphological analysis for GO-immobilized TPU patch...	207
8.4.2. FTIR-ATR analysis.....	209
8.4.3. ROS production of GO-immobilized TPU patch.....	215
8.4.3.1. GO enzyme in TPU-PDA-GO materials.....	215
8.4.3.2. ROS production of TPU-PDA-GO with a glucose- loaded hydrogel.....	217
8.5. Conclusions.....	219
8.6. References.....	220

Part III

Chapter 9 Assembly of Multilayer Wound Healing Patch.....	223
9.1. Abstract.....	223
9.2. Introduction.....	224
9.3. Materials and methods.....	226
9.3.1. HB PEGDA/HA-SH hydrogel.....	226
9.3.2. GO-immobilized TPU patch and glucose hydrogel source	226
9.3.3. Cytocompatibility of electrospun TPU fibre materials.....	227
9.3.4. Assembly of bilayer wound healing patch.....	228
9.3.5. Cytocompatibility evaluation of bilayer wound healing patch.....	229
9.3.6. Assembly of trilayer wound healing device.....	231
9.3.7. Cytocompatibility of trilayer wound healing device.....	232
9.4. Results and discussion.....	233
9.4.1. Cytocompatibility of TPUs.....	233
9.4.2. Cytocompatibility of bilayer wound healing device.....	234
9.4.3. Cytocompatibility of trilayer wound healing device.....	236

9.5. Conclusions.....	237
9.6. References.....	238
Chapter 10 General discussion and conclusion.....	240
10.1. General discussion.....	240
10.2. Conclusions and future development.....	249
10.3. References.....	251
 Appendices	
Appendix A: Synthesis and characterization of thermosensitive	
PLGA-PEG-PLGA hydrogel.....	A1
A1. Abstract.....	A1
A2. Introduction.....	A2
A3. Materials and methods.....	A3
A3.1. Polymer Synthesis.....	A4
A3.2. Chemical characterization by ¹ H NMR and Gel Phase Chromatography.....	A4
A3.3. Determination of gelation temperature.....	A4
A3.4. ROS measurement assays.....	A5
A4. Results and Discussion.....	A6
A4.1. Chemical characterization.....	A6
A4.2. Gelation temperature.....	A7
A4.3. ROS production in thermoresponsive hydrogels.....	A8
A.5. Conclusions.....	A9
A.6. References.....	A9
 Appendix B: Brochure copy of Vornia Biomaterials' PLGA-	
PEG-PLGA.....	A10

List of Tables

Table 0.1. List of characterization experiments performed on the materials (excluding GO-grafting and ROS-relevant experiments).

Table 0.2. List of experiments performed on the materials relevant to wound-healing applications.

Table 1.1. Examples of enzymes used for antimicrobial and antibiofilm strategies.

Table 2.1. Composition of prepared HB PEGDA/HA-SH hydrogels.

Table 3.1. Enzyme concentrations prepared for ROS formation in hydrogel.

Table 3.2. Glucose concentrations prepared for ROS formation in hydrogel.

Table 4.1. Composition of prepared HB PcG/HA-SH hydrogels.

Table 5.1. Summary of reported physical and mechanical properties of Lubrizol TPUs.

Table 5. 2. Shorthand for electrospinning parameter set-ups.

Table 5.3. Tabulation of fibre diameters of electrospun TPUs

Table 7.1. LPO enzyme concentrations used and their respective set-up codes.

Table 8.1. The glucose oxidase grafted sample codes

Table 10.1. Summary of materials with their highest H₂O₂ yielding parameters.

Table A.1. Concentration of GO and glucose used for preparing thermoresponsive PPP hydrogels.

List of Figures

Figure 1.1: Structure of skin.

Figure 1.2: Phases of wound healing.

Figure 1.3: Reactive oxygen species (ROS) and their role in wound healing. (Reproduced with permission from Dunill, et al. 2015. Full access).

Figure 1.4: ROS formation of H_2O_2 from glucose catalyzed by glucose oxidase (GO).

Figure 1.5: Swelling of hydrogel by absorbing water.

Figure 1.6: Thiol-Ene click chemistry reaction.

Figure 1.7: Hyperbranched polymer structure.

Figure 1.8: Description of the polymer units a hyperbranched polymer is composed of.

Figure 1.9: Market size of traditional and advanced wound dressings in North America.

Figure 1.10: Formation of antibacterial H_2O_2 .

Figure 1.11: Illustration of the hydrogel filling irregular shaped wound crevices.

Figure 2.1: Representation of chain growth polymerization.

Figure 2.2: Examples of molecular structures obtained by RDRP or CRP.

Figure 2.3: Structure and examples of RAFT agents.

Figure 2.4: RAFT reaction mechanism with thiolcarbonylthiol agent.

Figure 2.5: Chemical structure of PEGDA.

Figure 2.6: Chemical structure of HA-SH.

Figure 2.7: RAFT polymerization of PEGDA to HB PEGDA.

Figure 2.8: Hydrogel on rheometer plate: 20 mm parallel plate Rheometry was performed on a TA Discovery Hybrid Rheometer-2 (DHR-2) with 8 mm diameter parallel plates and TRIOS software for analysis of data.

Figure 2.9: GPC profile of HB PEGDA at different reaction times.

Figure 2.10: ^1H NMR spectrum of HB PEGDA Mw 16,656 Da.

Figure 2.11: Gelation time of hydrogels at different time points.

Figure 2.12: Frequency sweep profile of HB PEGDA/HA-SH hydrogels (at 10% oscillation strain).

Figure 2.13: Strain sweep profiles of HB PEGDA/HA-SH hydrogels (at 10 Hz frequency).

Figure 2.14: Hydrogel samples fabricated for characterization, a) 30 μL beads with 4 mm diameter, b) 200 μL beads with 7.5 mm diameter and 5 mm height.

Figure 2.15: Water adsorption profile of hydrogels.

Figure 2.16: Top illustration: Representation of the HB PEGDA/HA-SH hydrogel degradation. Bottom photographs: Progression of HB PEGDA/HA-SH 5.0-1.0 adsorbing water and degrading (left to right: day 4, 14, 20, 22).

Figure 2.17: Representative images of HB PEGDA/HA-SH 10-1.0 hydrogel at day 64 during water adsorption test.

Figure 3.1: Preparation of HB PEGDA/HA-SH hydrogel containing GO and glucose.

Figure 3.2: Standard solutions of H_2O_2 with ROS assay solution.

Figure 3.3: Calibration curve of H_2O_2 by the pertitanic acid assay.

Figure 3.4: Illustration of HB PEGDA/HA-SH hydrogel in a 24-well plate in DMEM medium with NIH/3T3 cells on well surface. Diameter of hydrogel, transwell insert, and individual well are in scale relative to each other.

Figure 3.5: H₂O₂ concentration after 24 hours from HB PEGDA/HASH 10.0/1.0 hydrogels containing varying amounts of enzyme and 2.5 w/w% glucose. Release was obtained in static conditions. Hydrogel composition: 10 w/w% HB PEGDA/1 w/w% HA-SH.

Figure 3.6: H₂O₂ production from HB PEGDA/HASH 10.0/1.0 hydrogel with 250 U/L and 500 U/L GO and 2.5 w/w% and 5.0 w/w% glucose concentrations. Measurements were obtained at t = 24 hours and t = 48 hours. Release was obtained in an incubator shaker operating at 15 rpm. Hydrogel composition: 10 w/w% HB PEGDA/1 w/w% HA-SH.

Figure 3.7: H₂O₂ concentration produced by HB PEGDA/HASH 10.0/1.0 and 5.0/1.0 hydrogels containing 250 U/L GO, 2.5 w/w% glucose at different time points. Release was obtained in an incubator shaker operating at 15 rpm.

Figure 3.8 : Cell viability of NIH/3T3 cells with HB PEGDA/HA-SH 10.0/1.0 hydrogels loaded with different concentrations of H₂O₂ after 24 hours after 24 hours in a static release (non-shaken method) set-up.

Figure 3.9: Cell viability of NIH/3T3 cells with HB PEGDA/HA-SH 10.0/1.0 hydrogels loaded with varying GO/glucose concentrations after 24 hours in a static release (non-shaken method) set-up.

Figure 3.10: Results of antibacterial agar diffusion tests on gram positive bacteria with HB PEGDA/HA-SH hydrogel 10-1.0 with fixed 2.5 w/w% glucose and varying GO concentrations labelled from 25-500 U/L (Data obtained from Ayesha Idrees).

Figure 3.11: Part 1 of results of antibacterial agar diffusion tests on gram negative bacteria with HB PEGDA/HA-SH hydrogel 10-1.0 with fixed 2.5 w/w% glucose and varying GO concentrations labelled from 25-500 U/L (Data obtained from Ayesha Idrees).

Figure 3.12: Part 2 of results of antibacterial agar diffusion tests on gram negative bacteria (*A. baumannii*) with HB PEGDA/HA-SH hydrogel 10-1.0 with fixed 2.5 w/w% glucose and varying GO concentrations labelled from 25-500 U/L (Data obtained from Ayesha Idrees).

Figure 3.13: Measured zones of inhibition of the HB PEGDA/HA-SH 10-1.0 (with 2.5 w/w% glucose) containing different GO concentrations for gram positive bacteria (Data obtained from Ayesha Idrees).

Figure 3.14: Measured zones of inhibition of the HB PEGDA/HA-SH 10-1.0 (with 2.5 w/w% glucose) containing different GO concentrations for gram negative bacteria (Data obtained from Ayesha Idrees).

Figure 4.1: Chemical structure of glycidyl methacrylate.

Figure 4.2: Possible reactions of lateral side groups in GO enzyme with a polymer containing an epoxide functional group.

Figure 4.3: Chemical structure of HB PEGDA-co-GMA or HB PcG.

Figure 4.4: Immobilization of glucose oxidase in HB PEGDA-co-GMA.

Figure 4.5: Steps in general ATRP synthesis with copper (II) chloride as the metal catalyst. L = ligand.

Figure 4.6: **a)** Separation column for removing copper from the polymer solution, **b)** an up-close look at the colour change as CuCl_2 forms a complex with Al_2O_3 .

Figure 4.7: GPC profile of HB PEGDA-co-GMA (5:1 PEGDA to GMA molar ratio) synthesized via DE-ATRP reaction.

Figure 4.8: ^1H NMR spectrum of HB PEGDA-co-GMA (5:1).

Figure 4.9: Gelation time of HB PEGDA-co-GMA/HA-SH hydrogels of varying compositions.

Figure 4.10: Frequency sweep of HB PEGDA-co-GMA/HA-SH 10-1.0 and 5.0-1.0 hydrogels at 10% strain.

Figure 4.11: Strain sweep of HB PEGDA-co-GMA/HA-SH 10-1.0 and 5.0-1.0 hydrogels at 10 Hz oscillation frequency.

Figure 4.12: Swelling profile of HB PEGDA-co-GMA/HA-SH 10-1.0 and HB PEGDA/HA-SH 10-1.0.

Figure 4.13: ^1H NMR spectra of [1] HB PEGDA-co-GMA with Glucose Oxidase Enzymes (in red), [2] HB PEGDA-co-GMA (in teal).

Figure 4.14: H₂O₂ production in HB PEGDA-co-GMA/HA-SH 10-1.0 at varying concentrations of GO enzyme (glucose concentration 2.5 w/w%) after 24 and 48 hours.

Figure 4.15: Cell viability of NIH/3T3 cells with HB PcG/HA-SH 10-1.0 and 5.0-1.0 hydrogels loaded with two different enzyme concentrations (250 U/L and 500 U/L) at a constant glucose concentration (2.5 w/w%) after 24 hours.

Figure 5.1: Schematic of formation of electrospun fibres.

Figure 5.2: Effect of applied voltage on electrospinning fibres.

Figure 5.3: Chemical structure of urethane bond by reaction of an isocyanate group and a hydroxyl group. When difunctional monomers react, a linear polyurethane forms.

Figure 5.4: Static Contact Angle Measurements of TPUs. Columns are the average values and bars are the standard deviation.

Figure 5.5: Short-term water adsorption results for TPUs.

Figure 5.6: Long-term water adsorption results for TPUs.

Figure 5.7: Stress-strain curves of the four TPUs (Trial 1 measurements).

Figure 5.8: Ultimate tensile strength properties of TPUs.

Figure 5.9: Stress-elongation curves of the four TPUs (Trial 1 measurements).

Figure 5.10: Ultimate Elongation Percentage of TPUs.

Figure 5.11: TPU A (SP-60D-60) electrospun fibres: a) 20 kV + 1.0 mL/h, b) 20 kV + 1.5 mL/h, c) 25 kV + 1.0 mL/h, d) 25 kV + 1.5 mL/h

Figure 5.12: Type C (SP-93A-100) TPU electrospun fibres: a) 20 kV + 1.0 mL/h, b) 20 kV + 1.5 mL/h, c) 25 kV + 1.5 mL/h, d) 25 kV + 1.0 mL/h

Figure 5.13: TPU A (left) and C (right) electrospun in 10 w/v% chloroform.

Figure 5.14: Electrospinning Setup I

Figure 5.15: Electrospinning Setup II

Figure 5.16: Electrospinning Setup III

Figure 5.17: Electrospinning Setup IV

Figure 5.18: Measurement of average fibre diameters.

Figure 6.1: Chemical structure of L-DOPA

Figure 6.2: Oxidation process of L-DOPA into polyDOPA

Figure 6.3: Structure of L-DOPA, dopamine, and their polymer derivatives

Figure 6.4: Possible reaction pathways in a PDA-coated surface (R' = polymeric backbone). Image drawn by the author, modified from Bazaka, K., et al. (2015).

Figure 6.5: PDA-coating of electrospun thermoplastic polyurethane fibre patch (end-product named as TPU-PDA).

Figure 6.6: Enzyme immobilization on TPU-PDA (end-product named as TPU-PDA-GO).

Figure 6.7: Reaction of several amino acids with a quinone group found in a PDA-coated substrate.

Figure 6.8: Overall multilayer antibacterial ROS-producing wound healing device

Figure 7.1: PDA-coating set-up for electrospun TPU fibres; the scheme of the set-up is shown on the left and the actual final product (TPU-PDA-LPO-1.4-7) is shown on the right.

Figure 7.2: Images of L-DOPA solutions (2 mg/mL) oxidizing into PDA with 0-1.4 U/mL LPO concentrations (1 column = 4 wells = 1 LPO concentration set-up) at different times (30 min, 3h and 5h)

Figure 7.3: Absorbance intensity at 450 nm of DOPA solutions containing different enzyme amounts as a function of time, as indicative of PDA formation (SO = Solution only).

Figure 7.4: Absorbance intensity at 450 nm as a function of time for DOPA solutions containing different enzyme amounts, during the incubation of a TPU patch. Absorbance values were indicative of PDA

deposition on the film, when compared to results in Figure 7.3 (SO = Solution only).

Figure 7.5: Comparison of absorbance values of DOPA solutions with the same concentration (LPO 0) with and without TPU film, as a function of time.

Figure 7.6: Comparison of absorbance times DOPA solutions of the same concentration (LPO 1.4) with and without TPU film.

Figure 7.7: Percentage oxidation of DOPA solutions in different conditions respect to the control set-up (SO)

Figure 7.8: Percentage oxidation of DOPA solutions in different conditions respect to the control set-up (WF)

Figure 7.9: Estimated time for reference oxidation in PDA-forming set-ups with LPO concentrations from 0 to 1.4 U/mL

Figure 7.10: SEM images (5000x magnification) of electrospun TPU fibrous membranes: a) uncoated, b) PDA-coated (7h), no LPO, c) PDA coated (7 h), 1.1 U/mL LPO, d) PDA coated (7h), 1.4 U/mL LPO.

Figure 7.11: Percentage of fibre size difference when coating electrospun TPU fibres with PDA in the presence of difference LPO concentrations. Data were derived from an average of 40 measurements per each SEM image by ImageJ software.

Figure 7.12: FTIR spectra of TPU membranes: purple = TPU; red = TPU-PDA (LPO 0); green = TPU-PDA (LPO 1.4). Coating time for reported spectra was 7 hours.

Figure 8.1: Chemical structure of gelatin functionalized to gelatin methacrylate (GelMA) with methacrylic anhydride.

Figure 8.2: **a)** 15 w/v% GelMA solution in “modified” PBS (with 10 w/v% glucose and 0.5 w/v% Irgacure 2959 in PBS pH 7.4). **b)** UV-crosslinked 100 μ L glucose-loaded GelMA hydrogel (diameter 7.5 mm). **c)** UV-crosslinking set-up of the GelMA hydrogels with intensity of 4 mW/cm² at 365 nm wavelength.

Figure 8.3: TPU-PDA-GO-1.4-7 (1 cm x 1 cm) with 100 μ L glucose-loaded GelMA hydrogel.

Figure 8.4: SEM images of TPU-PDA-LPO-0 coated at 3h and 7h (see the code), then immersed in GO enzyme solution for 24 hours.

Figure 8.5: SEM images of TPU-PDA-LPO-1.4 coated at 3h or 7h (see code), then immersed in GO enzyme solution for 24 hours.

Figure 8.6: FTIR spectra of TPU-PDA-0-3.

Figure 8.7: FTIR spectra of TPU-PDA-0-7.

Figure 8.8: FTIR spectra of TPU-PDA-1.4-3.

Figure 8.9: FTIR spectra of TPU-PDA-1.4-7.

Figure 8.10: FTIR spectra of gelatin methacrylate reported as a function of percent transmittance.

Figure 8.11: FTIR spectra of gelatin and GelMA from a study by Zhou, X., et al (2016). Reprinted Figure 3.A, reproduced with permission: Copyright (2019) American Chemical Society.

Figure 8.12: GO enzyme activity in TPU-PDA-GO fibre patches.

Figure 8.13: ROS production (after 24 hours) of TPU-PDA-GO patches with glucose-loaded GelMA hydrogel.

Figure 9.1: Assembly of multilayer wound healing device and their individual components.

Figure 9.2: Photos of glucose-loaded GelMA hydrogel bead alone, and on top of a TPU-PDA-GO to assemble the bilayer wound healing device.

Figure 9.3: Bilayer TPU-PDA-GO + glucose loaded GelMA hydrogel set-ups for cytocompatibility testing.

Figure 9.4: Trilayer ROS-producing wound healing device.

Figure 9.5: Viability of NIH/3T3 cells in indirect contact with electrospun TPU fibre mats (unmodified and GO enzyme grafted) after 24 hours.

Figure 9.6: Viability of NIH/3T3 cells in indirect contact with electrospun TPU-PDA-GO mats combined with glucose-loaded GelMA hydrogel beads after 24 hours.

Figure 9.7: Cell viability of NIH/3T3 cells tested with the eluates of the trilayer wound healing device after 24 hours.

Figure 10.1: Multilayer wound healing device.

Figure 10.2: Possible configurations for assembling the materials developed in this thesis for an antibacterial wound healing patch using Layers 1 to 3.

Figure A1: Polyethylene glycol (red) reacting with stannous octanoate (orange)

Figure A2: Ring opening reaction for PLGA-PEG-PLGA

Figure A3. Final PLGA-PEG-PLGA (PPP) product

Figure A4: ¹H NMR results of PLGA-PEG-PLGA with the GPC results for the Mn and Mw reported for 2, 4, and 6 hours

Figure A.5: Storage of 2PLGA-PEG-PLGA hydrogels as a function of temperature.

Figure A.6. H₂O₂ production in PLGA-PEG-PLGA at different time points.

Part I

Chapter 1 Wounds

1.1. Abstract

This chapter, introduces the foundation of the study by providing the background information relevant to the research project such as the structure of skin, the definition of wounds, the complications that might occur such as wound infections with antibacterial resistance and current methods of treating antibacterial infections. The design for a drug-free multilayer wound healing device is presented with the aim to protect injured tissue, stimulate healing, and prevent infections.

1.2. Introduction

Wounds are defined as injury to living tissue caused by a blow, sting, or cut, that breaks the skin. However, different sources have varying definitions, sometimes including lacerations, ulcers and burns as types of wounds^{1,2}.

Sales are driven by emerging technologies for wound treatment, particularly for chronic wounds, and traditional wound care will only account for 30% of the total

wound care market by 2024³. Market research forecasts that by 2024, traditional wound care devices (adhesives, gauzes, and nonadherents) will only comprise 30% of the market while more advanced wound care devices such as bioengineered skin, skin substitutes, foams, hydrogels will dominate the industry³.

1.2.1. Structure of skin

Skin consists of three layers: the epidermis, dermis, and deep subcutaneous tissue/hypodermis. The epidermis serves as the waterproof covering of the skin that also serves as a natural barrier against bacterial infections. Wounds often differ in depth and area, but generally they involve damaging the epidermal layer. The epidermis itself has no blood vessels but is nourished by the dermis. When wounds bleed, this usually indicates damage to the dermis at the very least⁴.

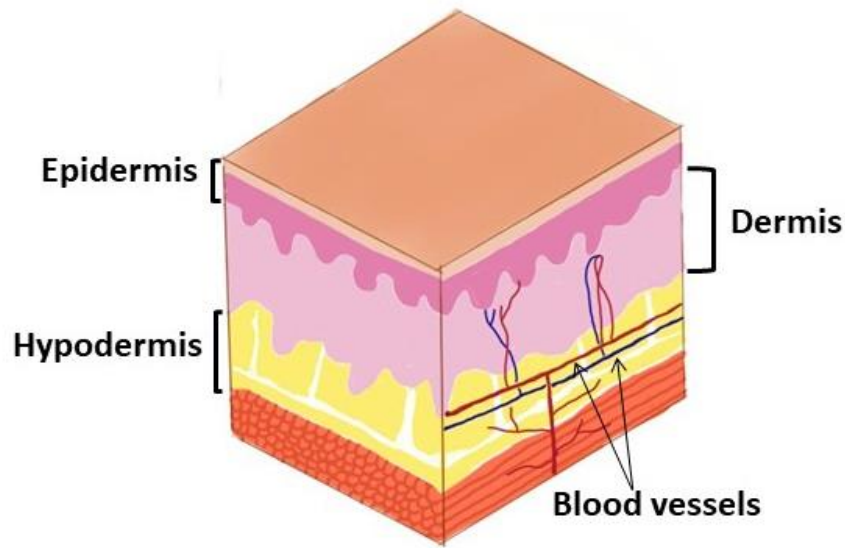


Figure 1.1: Structure of the skin.

1.2.2. Types of wounds

The most common types of wounds are punctures, ulcers, skin tears, and contusions⁵. A study on the global prevalence of wound types that occurred in 2015, indicates that surgical wounds, lacerations, and ulcers (diabetic, venous, and pressure) have the highest prevalence⁶.

In this Doctorate Thesis, the design of an antibacterial material for skin lesions of both wounds and ulcers will be focused upon. Normally, wounds are differentiated from ulcers in that wounds are physically inflicted by an external source, such as a jagged surface or surgical incision.

A skin ulcer is an open wound on the skin, which can be caused by a health problem such as infection, by a pressure sore, or by vein problems (venous skin ulcers)⁷.

These normally are much harder to heal and can occur chronically, particularly when a patient has a compromised immune system⁸.

1.3. Wound healing and treatment

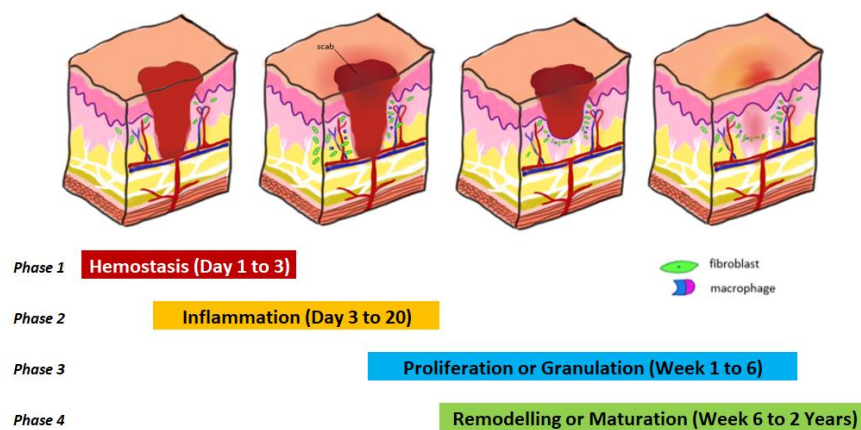


Figure 1.2. Phases of wound healing.

Wound healing is a natural process performed by the body. It is comprised of four phases as shown in Figure 1.2: hemostasis, inflammation, proliferation, and maturation⁹. The use of dressings and other wound care materials supports this healing process by protecting the wound from exposure, preventing infection and complications, and preserving skin function¹⁰.

1.3.1. Wound healing mechanism

The first event in wound healing is hemostasis consisting of the following factors that aim at decreasing blood loss: Platelets' aggregation and activation, blood clot

formation, vasoconstriction, and platelet release of chemokines as chemo-attractants to inflammatory cells at the wound site⁹.

During the inflammatory phase, the blood vessels dilate to allow cells, antibodies, growth factors, etc., to enter the wound area. This involves the actions of neutrophils, macrophages, and lymphocytes. Neutrophils are responsible for cleaning the wound from bacteria and necrotic tissues, while releasing inflammatory mediators and bactericidal oxygen free radicals⁹. Macrophages have many functions during wound healing such as providing host defense, controlling the inflammatory response as well as breaking down and removing dead cells¹¹. Lymphocytes are a type of white blood cells that are also responsible for the body's defense system against foreign particles¹². Also, by the time this stage takes place, the blood on the outermost surface will have formed into a scab to protect foreign objects from entering the body. This phase lasts four to six days.

During proliferation phase, the granulation tissue starts to form⁹. This tissue is comprised of collagen and extracellular matrices like hyaluronic acid¹³. Within this tissue new blood vessels are regenerated in a process called angiogenesis and the quality and health of the granulation tissue is dependent on the availability of oxygen and nutrients supplied to it by the blood vessels⁹. Wound contraction also occurs at this stage, with decrease in wound size⁹. Proliferation takes place anywhere between four to twenty-four days.

The last phase is maturation. Here, the newly deposited collagen forms crosslinks, increasing the tensile strength of the scar tissue⁹. Scars that have a raised appearance are called hypertrophic scars or keloid scars and occur when too much collagen has been produced¹⁴. Scars are made of the same type of collagen in normal skin but differ in fibre composition¹⁵. The collagen of normal skin's fibres is more randomly weaved while scar tissue's collagen is crosslinked and aligned in a single

direction¹⁵. Thus, scar tissue is more rigid and lacks the natural elasticity of skin¹⁵. This phase can take between 21 days to 2 years.

1.3.2. Complications in wound healing

Frequently not healing chronic wounds form because of the presence of bacterial biofilms and antibiotic-resistant bacteria in the wound bed, although there are other contributing factors such as foreign debris, diabetes, and inadequate nutrition⁸.

For example, *Pseudomonas aeruginosa* is a bacterial strain found in many chronic wounds that has a strong resistance to standard antibiotics, affecting people with compromised immune systems⁸. Wounds infected with *P. aeruginosa* may have a bluish tinge to them due to bacteria consuming fluids in the wound and then releasing waste back into the wound tissue⁸.

Some bacteria are also capable of quorum sensing. This ability lets them release chemical signals, often called autoinducers, to control their cell density before expressing a gene to release byproducts into the media they occupy such as extracellular matrices or virulent proteins¹⁶. These materials aggregate and lead to the formations of biofilms.

Biofilms are composites of bacterial or fungal cells, encased in extracellular matrix composed of hydrated polymers and debris, like polysaccharides, proteins, and DNA that are excreted by bacteria¹⁷. Bacteria in biofilms behave differently with respect to their planktonic status, in terms of structure, gene expression, antibiotic resistance, and interaction with the host¹⁷. Bacterial biofilm can be found on the surface of the skin, in the wound tissue, and in some cases deeper in the apparently normal tissue¹⁸.

Bacterial infections that involve biofilm formation are harder to recover from as the biofilm protects the bacteria from the host's immune response¹⁷. They also impede fibroblast development and inflammatory responses. Thus, it is unlikely that a wound can fully heal until the bacterial infection or biofilm is eliminated.

1.3.3. Role of Reactive Oxygen Species (ROS) in wound healing

The roles ROS play in wound healing differ at various stages in the wound healing process. This is briefly summarized and illustrated by Figure 1.3.

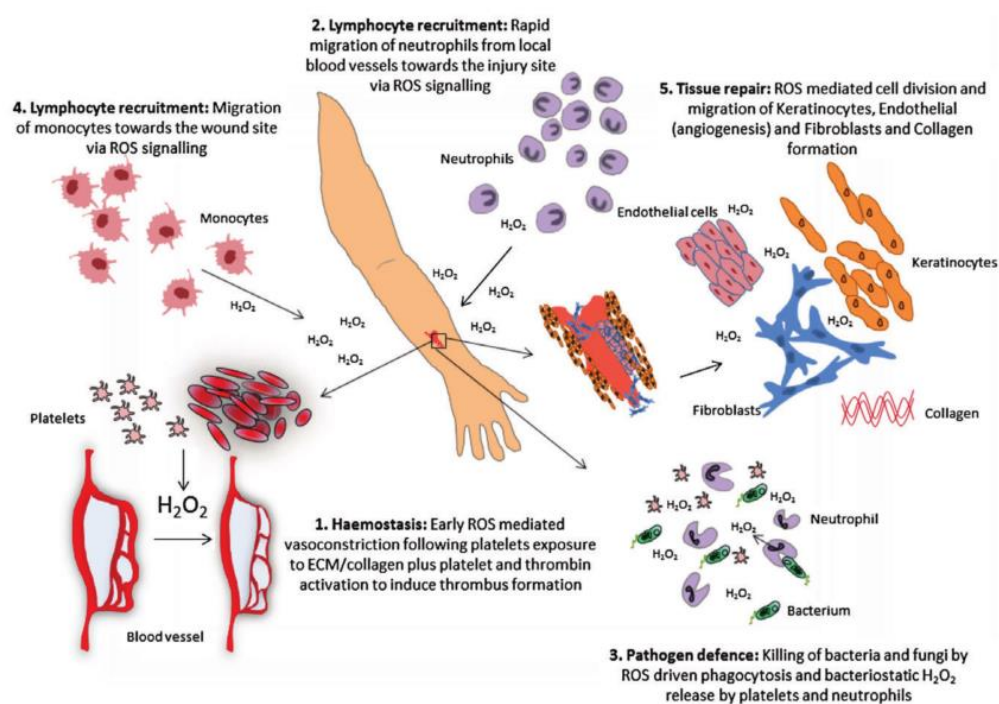


Figure 1.3: Reactive oxygen species (ROS) and their role in wound healing¹⁹.

(Reproduced with permission from Dunill, et al. 2015. Full access).

Reactive oxygen species (ROS), such as hydrogen peroxide, play a pivotal role in the orchestration of the normal wound-healing response. They are responsible for

killing bacteria during inflammation and are involved in the repair process by acting as secondary messengers to many immunocytes and non-lymphoid cells¹⁹. Harnessing the potential of ROS to be used within wound care devices provides the potential to accelerate the healing process and to prevent bacterial infections.

1.4. Antibiotic resistance

One of the pressing challenges in the biomedical sector is to fight antibiotic resistant bacteria. A study from the United Kingdom estimates that failure to address this issue could result in 10 million deaths per year by 2050 and cost 60 trillion GBP²⁰.

On 27th Feb 2017 the World Health Organization (WHO) published a list of bacteria that require new antibiotics to be developed²¹.

Priority 1: CRITICAL

- *Acinetobacter baumannii*, carbapenem-resistant
- *Pseudomonas aeruginosa*, carbapenem-resistant
- *Enterobacteriaceae*, carbapenem-resistant, Extended Spectrum β -Lactamase (ESBL)-producing

Priority 2: HIGH

- *Enterococcus faecium*, vancomycin-resistant
- *Staphylococcus aureus*, methicillin-resistant, vancomycin-intermediate and resistant
- *Helicobacter pylori*, clarithromycin-resistant
- *Campylobacter spp.*, fluoroquinolone-resistant
- *Salmonellae*, fluoroquinolone-resistant
- *Neisseria gonorrhoeae*, cephalosporin-resistant, fluoroquinolone-resistant

Priority 3: MEDIUM

- *Streptococcus pneumoniae*, penicillin-non-susceptible
- *Haemophilus influenzae*, ampicillin-resistant
- *Shigella spp.*, fluoroquinolone-resistant

1.4.1. Bacterial resistance in wounds

Antibiotic resistant species that can be found in wounds and ulcers include *Staphylococcus aureus*, *Pseudomonas aeruginosa*, *Escherichia coli*, *Enterococcus faecalis* and *Acinetobacter baumannii*, that occur in WHO's 2017 priority research list^{22,23}.

Given how the use of antibiotics lead to the risky development of antibacterial-resistant bacteria, especially in the case of patients overusing antibiotics, it is worth looking into alternative antibacterial methods that do not require the use of antibiotics and decrease the reliance on them²⁴. In developing an antibacterial wound healing device, the material efficiency against these species should be tested and proved to kill or prevent proliferation of some of these bacteria.

1.4.2. Current antibacterial methods

Antimicrobial intervention in wounds today are grouped as antibiotic and non-antibiotic based treatments. Antibiotics are drugs that are made (either naturally or synthetically) from fungi, molds, and other living organisms that can kill bacteria.

Non-antibiotic methods include the use of antiseptics such as silver, iodine, potassium permanganate (KMnO₄) topically applied on the wound tissue or

embedded in a wound dressing or gel as the most common method²⁵. Emerging non-antibiotic methods are being devised from more equipment intensive techniques such as cold plasma, ozone, phototherapy, and bacteriophage therapy²⁶⁻²⁸.

Polymers used for biomedical applications such as implants are often imbued with antibacterial properties in order to prevent possible infections from occurring. This can be accomplished by: i) adding an intrinsic antibacterial activity to the polymer, ii) conjugation of the polymer with an antibacterial agent, or iii) loading an antibacterial agent into the polymer matrix²⁹.

Meanwhile, many researchers are investigating ancient natural remedies to evaluate which antimicrobial strategies can be developed from them. Today's scientists have the advantage of being able to analyze the specific antibacterial mechanisms of these ancient remedies.

1.4.3. Research on natural sources for wound healing

As far back as 2000 BC, in ancient empires such as those of the Egyptians, Chinese, and Assyrians, healing of wounds sustained from war and combat was the concern of many healers^{30,31}. As they have been tasked to devise effective wound healing and antibacterial strategies, they looked to sources derived from plants and animals^{30,32}.

Today, several naturally occurring substances have been verified to display antibacterial properties such as honey, ginger, garlic, echinacea³³.

Research has been conducted on Manuka (*L. scoparium*) honey, which has been demonstrated to be effective against several human pathogens, including *Escherichia coli* (*E. coli*), *Enterobacter aerogenes*, *Salmonella typhimurium*, *Staphylococcus aureus* (*S. aureus*), β -haemolytic streptococci and vancomycin-resistant *Enterococci* (VRE) and *Pseudomonas aeruginosa* (*P. aeruginosa*)^{31,34}.

Honey has been noted in several studies to have a bactericidal effect^{34,35}. Its antibacterial effects are attributed to many factors, which include its phytochemical components, osmotic effect of sugar on bacterial cells, acidic pH that aids macrophages in destroying bacteria, and the enzymatic activity of Glucose Oxidase (GO) to produce hydrogen peroxide (H_2O_2) from glucose³⁵⁻³⁹. In this Doctorate thesis the effect of glucose oxidase in producing Reactive Oxygen Species (ROS) as an antibacterial agent will be analysed.

1.5. Role of enzymes in wound healing

Other enzymes have different functions in the wound healing process such as:

- Proteolytic enzymes produced endogenously (i.e. by the body cells) degrade necrotic tissue in the wound by hydrolysing peptide bonds⁴⁰.
- Anti-quorum sensing enzymes are used to prevent biofilm formation⁴¹.

The complete list of enzymes involved in wound healing can be found in Table 1.1.

Table 1.1. Examples of enzymes used for antimicrobial and antibiofilm strategies⁴¹

Proteolytic Enzymes	Polysaccharide-degrading Enzymes	Oxidative Enzymes
<ul style="list-style-type: none"> • Subtilins • Lysostaphin • Bacteriophages lysin 	<ul style="list-style-type: none"> • Lysozyme • Amylases • Dispersin B • Alginate lyase 	<ul style="list-style-type: none"> • Myeloperoxidase • Cellobiose dehydrogenase • Glucose oxidase • Horseradish peroxidase

1.5.1. Glucose oxidase and ROS

Glucose oxidase is an enzyme first identified in 1929 which was observed to form H₂O₂ from glucose and oxygen⁴². Its side product, D-gluconolactone is a common ingredient in most skin creams and anti-aging formulas, thus it is unlikely that it will demonstrate any adverse effects when it is produced in wound healing. Figure 1.4 illustrates the reaction of glucose oxidase on glucose in the presence of oxygen.

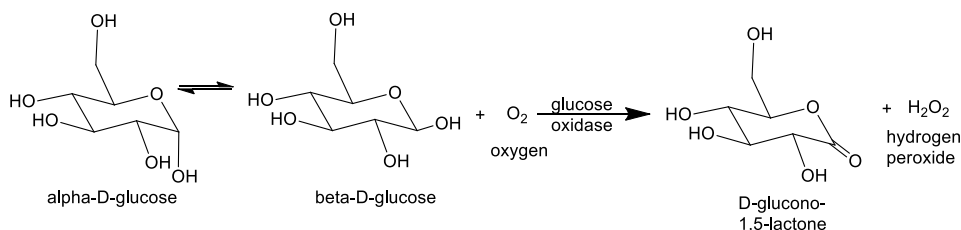


Figure 1.4: ROS formation of H₂O₂ from glucose catalyzed by glucose oxidase (GO). However, topical application of GO directly on the wound site in the form of a solution results in its rapid diffusion and becomes toxic to the wound by causing sudden glucose deprivation and burst release of ROS⁴³. Additionally, GO may be

quickly degraded due to the presence of endoproteases and peptidases in the healing tissue, even before exerting any antimicrobial effect⁴³.

To circumvent the problems associated with topical application of GO, in this work controlled release of hydrogen peroxide was obtained by incorporating GO and glucose in a two-component hydrogel.

1.6. Hydrogels in regenerative medicine

Hydrogels are water-swollen polymeric materials that maintain a distinct three-dimensional structure and were the first biomaterials designed for use in the human body as their resemblance to living tissue opens up many opportunities for applications in biomedical areas^{44,45}. They have been used for drug delivery, tissue scaffolds, wound healing, and bioprinting⁴⁶⁻⁵⁰.

1.6.1. Hydrogels for wound care

An ideal type of wound dressing is based on a material that can maintain a warm and moist environment around the wound as well as absorb exudates from the wound surface and reduce dehydration⁵¹. Other important characteristics that a wound dressing should have are: 1) composed of biocompatible materials, 2) permeability for oxygen and carbon dioxide, 3) prevent or inhibit bacterial growth 4) enhance growth factor activity⁵². To meet this challenge, a wound dressing system by using the versatile group of materials called hydrogels has been developed in this project.

1.6.1.1. Properties relevant to wound care

Hydrogels are formed when long chain polymers crosslink to form a three-dimensional network. This crosslinking can be made physically (polymer chain entanglements, ionic or hydrophobic interactions, hydrogen bonding, etc.) or chemically (functional groups of one polymer chain covalently bonded with other functional groups in other chains) by introducing a kind of stimuli, such as change in pH, temperature, or exposure to UV light^{53,54}. Hydrogel hydrophilic groups allow water absorption while hydrophobic groups prevent dissolution⁵⁴. Hence hydrogels are capable of absorbing high water contents when hydrated. This water absorption property, which ranges from 10-1000 wt%, satisfies one of the properties required for a wound dressing⁵⁵.

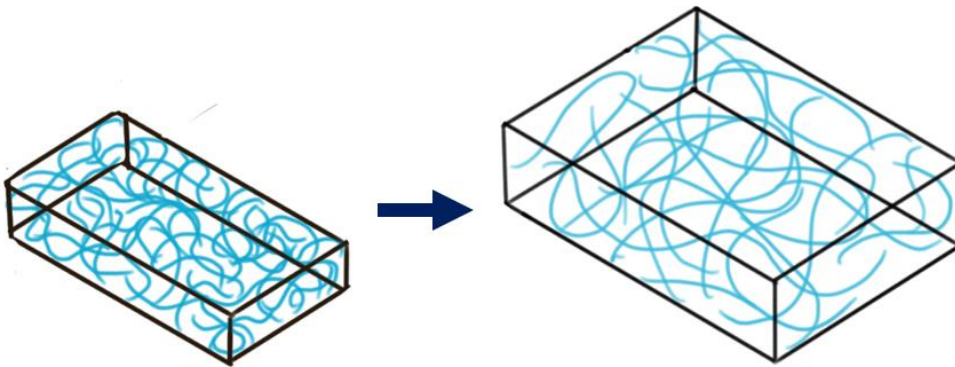


Figure 1.5: Swelling of hydrogel by absorbing water.

Hydrogels can be made of synthetic or natural polymers or their combination. While cells can easily attach to natural polymers that are part of the extracellular matrix (e.g. hyaluronic acid, collagen), due to the presence of ligands for cell receptors, the properties of natural polymers (such as molecular weight, molecular number, chemical groups that can be functionalized) can vary too widely and

despite the cytocompatible advantages of natural polymers, their physical and mechanical properties can be difficult to replicate and predict.

On the other hand, synthetic polymers have reproducible properties and can be easily tailored to have suitable mechanical properties and degradation rates for the application, as well as hydrophilic composition. Tailor-made synthesis allows the incorporation of a variety of functional groups into the polymer chain⁵⁶. Synthetic polymers generally suffer from poor cell attachment.

As hydrogels have porous crosslinked structure, this allows the material to be oxygen permeable, which aids in wound healing. In some applications, hydrogels have been used as contact lenses for this purpose^{57,58}.

Hydrogels can be embedded with antibacterial and wound healing agents that can diffuse into the wound tissue. Examples include silver nanoparticles, enzymes, and bioactive compounds (e.g. allicin and cinnamon aldehyde)^{43,49,59,60}. Hydrogels can also provide a scaffold for new cells to grow, as is the case with adipose-derived stem cells^{48,61}.

Additional properties that can be conferred to hydrogels for wound dressing are: quick forming ability, wound area coverage, adequate mechanical properties for handling and adhesive properties to the wound site.

1.6.1.2. Click-chemistry thiol-ene hydrogels

In order to design a hydrogel that is quick forming from a polymer solution (typically dissolved in water or phosphate buffer solution (PBS), a rapid

crosslinking is required. One possibility is to exploit the thiol-Michael addition reactions, specifically the thiol-ene click chemistry reaction.

First described in the 1960s, it is defined as an enolate-type carbonyl (e.g. a polymer with a thiol functional group) reacting in the presence of a catalyst to an α,β -unsaturated carbonyl (e.g. a polymer with an acrylate functional group)⁶². Figure 1.6 shows this reaction .

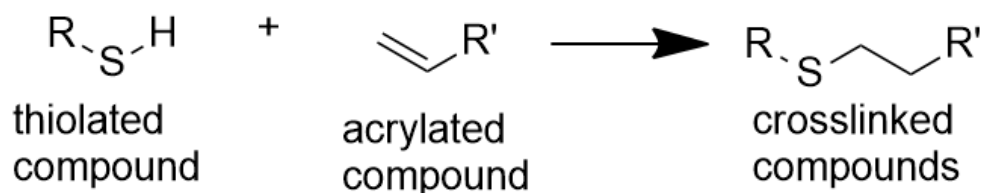


Figure 1.6: Thiol-Ene click chemistry reaction.

This thiol-ene click chemistry can either be base- or nucleophile-catalyzed⁶². For instance, a polymer, such as thiolated hyaluronic acid (HA-SH) dissolved in water at 1 w/v% concentration results in a solution with a pH of 3.5 . The introduction of a base such as sodium hydroxide (NaOH) to the acidic HA-SH solution to reach a pH of 7.4 allows the base-catalyzed reaction to occur in mild, physiological conditions.

Hyaluronic acid was chosen as the thiolated component for this research for a variety of reasons: it has previously shown cytocompatible properties, it is part of the extracellular matrix of skin tissue, and it has been proven to crosslink by click-chemistry with a wide range of acrylated polymers at physiological conditions^{49,59,63}.

1.6.1.3. Hyperbranched hydrogels

HB polymers are characterized to have abundant functional groups, an irregular 3D topology, low viscosity, and high solubility⁶⁴.

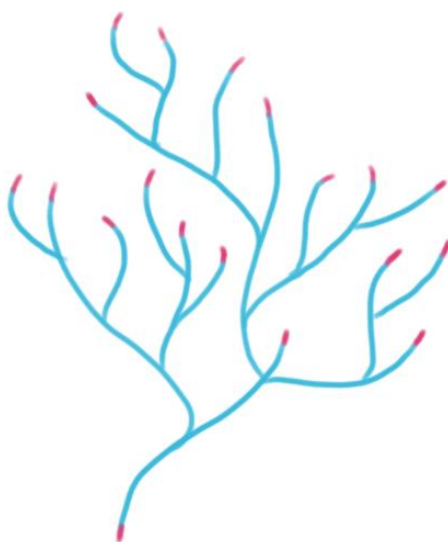


Figure 1.7: Hyperbranched polymer structure.

Such properties make them ideal to be used as components in an *in situ* formed hydrogel system. Their high solubility into low viscosity solutions allow them to be easily and rapidly dissolved in aqueous solution as a pre-hydrogel polymer solution. Their 3D topology and abundant functional groups allow rapid crosslinking with other polymer components, such as HA-SH thiol groups, forming a hydrogel with adequate stiffness.

Hyperbranched polymers can be characterized by their degree of branching (DB). DB is the ratio of the molar fraction of branched and terminal units relative to that of the total possible branching sites⁶⁴. For the polymerization of an AB₂ type

monomer, such as a diacrylate polymer illustrated in Figure 1.8, DB can be calculated from the equation⁶⁴:

$$DB = \frac{D + T}{D + T + L} \quad (eq. 1)$$

When a hyperbranched polymerization is assumed to have a high degree of polymerization (DP), the number of T approximates that of D, and the equation is reduced as follows:

$$DB = \frac{1}{1 + \frac{L}{2D}} \quad (eq. 2)$$

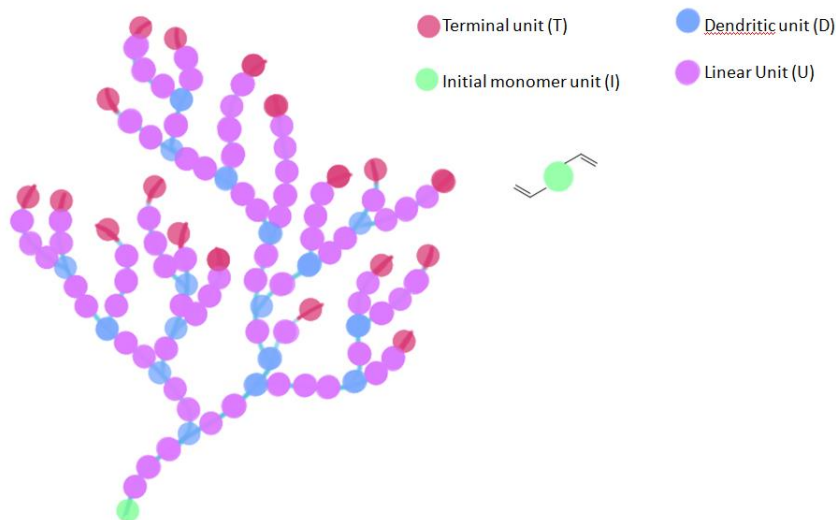


Figure 1.8: Description of the polymer units a hyperbranched polymer is composed of.

As a calculation example to obtain the DB, from Figure 1.9, there are 18 terminal units, 1 initial unit, 16 dendritic units, and 74 polymer units. Using equation 1, the DB is:

$$DB = \frac{D + T}{D + T + L} = \frac{16 + 18}{16 + 18 + 74} = 0.31$$

This means that for 1 mol of the hyperbranched polymer, there are 0.31 mol of dendritic and terminal functional groups.

Adding to this, the vinyl content (VC) for acrylate hyperbranched polymers can be calculated as:

$$VC = \frac{T}{D + T + L} \quad (eq. 3)$$

This equation will be useful when calculating the stoichiometry of the minimum amount of crosslinking material (such as HA-SH). This data can be obtained from analysis of a polymer's Nuclear Magnetic Resonance (NMR) spectra.

Hyperbranched polymers made from biocompatible materials such as polyethylene glycol (PEG)-based have been used as hydrogel components for biomedical applications^{48,49,59,65-67}. When crosslinked via Michael addition thiol-ene click chemistry, enzymes, cells, and bioactive compounds can be encapsulated in the hydrogel matrix⁴⁸.

For this study, the synthesis of a hyperbranched polyethylene glycol (PEG)-based hydrogel containing acrylate functional groups will be prepared to develop a quick forming, antibacterial wound dressing hydrogel.

1.7. State of the art in antibacterial wound care

Wound care devices can be sorted as traditional (gauze, adhesive, foams) and advanced (skin substitutes, stem cells, cold plasma treatment), with advanced wound care products growing each year, as observed from 2012 until the present day by market researchers^{27,68}. In Figure 1.9, the market size of the traditional

wound dressings remains approximately constant, while the market size for advanced wound dressings has been continuously increasing reaching approximately 60% of the entire market in 2018. Thus, with the rising threat of antimicrobial resistance (AMR) and the growth of elderly population percentage, there is a demand for effective drug-free antibacterial wound dressings.

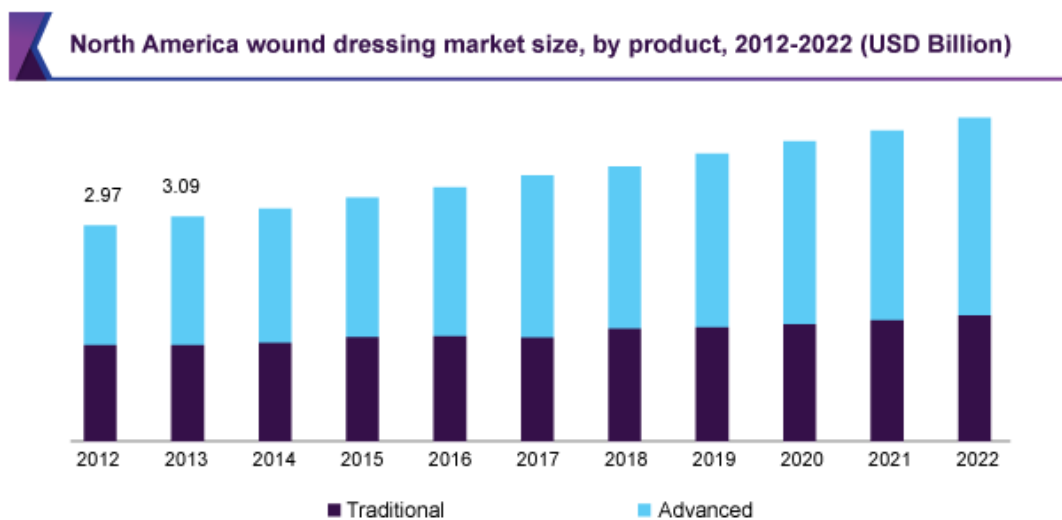


Figure 1.9: Market size of traditional and advanced wound dressings in North America⁶⁸.

A mechanism for killing bacteria in wounds that is often applied is through reactive oxygen species (ROS). The simplest of these methods is the application of a solution of hydrogen peroxide on the wound site for cleaning and disinfection. ROS can be formed in a variety of ways, ranging from chemical reactions to enzymatic reactions.

There are several ROS-based technologies that are currently in the market or applied in research. One of these commercial products is Surgihoney, an

antibacterial soft gel that can be applied on wounds³⁶. Surgihoney produces a maximum of 2.25 mM H₂O₂ after 24 hours of applications³⁶.

A second ROS-based commercially available wound dressing is Oxyzyme^{69,70}. It consists of one hydrogel patch embedded with glucose that is called the 'wound contact patch' while a smaller hydrogel patch, called the 'secondary wound patch', is embedded with glucose oxidase enzyme⁷¹. These hydrogels are stacked on top of each other, then a cover dressing is applied to protect the wound from exposure.

In the literature, a quick forming, *in situ* H₂O₂ releasing hydrogel (based on gelatin-hydroxyphenyl propionic acid) has been developed exploiting the mechanism of horseradish peroxidase enzyme (HRP) to produce an *in situ* gelling hydrogel with the help of the H₂O₂, ; the remaining H₂O₂ serves as the antibacterial component⁷². While H₂O₂ is being released into the wound, it is not continuously produced, like in the case of devices containing glucose oxidase enzyme + glucose antibacterial system.

From studies done by Loo, et al, 2012, topically applying 2.5 μmol of H₂O₂ in solutions with varying concentrations (10-166 mM) daily over a span of 10 days, it was found that a solution at a concentration of 10 mM enhances angiogenesis while 166 mM solution retards the wound closure⁷³. Thus, 10 mM per day is considered here as the target concentration to be achieved.

Based on the current state of the art, this research aims at producing a durable, mouldable, quick forming (transitioning from liquid state to a solid gel state) antibacterial hydrogel for wound dressing improving the current technologies mimicking the antibacterial properties of honey. The hydrogel will have higher mechanical stiffness than Surgihoney (a viscous solution) and higher GO/glucose content within the hydrogel compared to Oxyzyme.

This hydrogel will be formed when a hyperbranched polymer solution (containing GO enzyme) is mixed with a thiolated hyaluronic acid solution (containing glucose). As the two solutions are mixed and start to crosslink via thiol-ene click chemistry, the GO and glucose also interact and form antibacterial ROS (H_2O_2) as seen in Figure 1.10. Within the hydrogel matrix, glucose (molecular weight 180 g/mol) diffuses, while GO (molecular weight 160 kDa) is less mobile and is considered physically encapsulated⁷⁴. This potentially addresses the issue that topical application of GO may be quickly degraded due to the presence of endoproteases and peptidases in the healing tissue, even before exerting any antimicrobial effect⁴³.

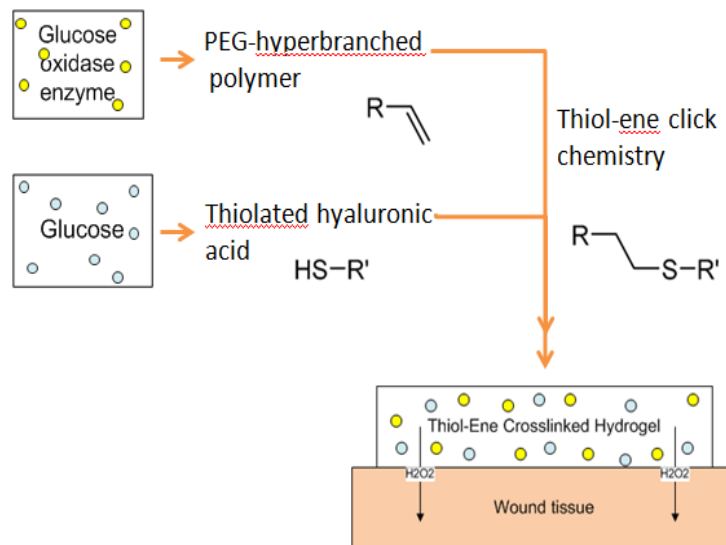


Figure 1.10: Formation of antibacterial H_2O_2 .

The mixed liquid that is subsequently becoming a gel can be extruded into a wound surface and give full coverage of the wound tissue even in irregular surfaces, as seen in Figure 1.11, compared to a layer of hydrogel or bandage. Gelation time is

targeted to be under two minutes, and when the material is completely crosslinked, a semi-rigid gel forms.

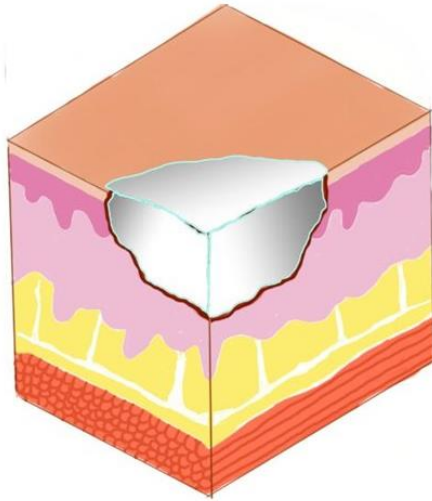


Figure 1.11: Illustration of the hydrogel filling irregular shaped wound crevices.

The rate of H_2O_2 formed can be tailored by manipulating the enzyme and glucose concentrations within the polymer solutions. This hydrogel should also have good swelling properties in order to absorb wound exudates as its secondary function. Due to its water absorbent properties, it can be possible to “recharge” the hydrogel with more glucose solution during the *in vivo application*, to allow continuous production of H_2O_2 once the original glucose has been depleted and to rehydrate the wound bed.

1.8. References

- (1) Wounds and Injuries <https://medlineplus.gov/woundsandinjuries.html> (accessed Feb 12, 2018).
- (2) Hermans, M. H. Wounds and Ulcers: Back to the Old Nomenclature. *Wounds* **2010**, 22 (11).
- (3) Driscoll, P. Growth in wound management from trends in prevalence,

technology – advanced medical technologies – blog

<http://blog.mediligence.com/2016/03/02/growth-in-wound-management-from-trends-in-prevalence-technology/> (accessed Jan 1, 2017).

- (4) Mir, M.; Murtaza, ; Ali, N.; Barakullah, A.; Gulzar, A.; Arshad, · Munam; Fatima, S.; Asad, M. Synthetic Polymeric Biomaterials for Wound Healing: A Review. **2018**, 7, 1–21. <https://doi.org/10.1007/s40204-018-0083-4>.
- (5) Advanced Tissue. Common Types of Wounds - Advanced Tissue <https://www.advancedtissue.com/common-types-of-wounds/> (accessed Feb 12, 2018).
- (6) MedMarket Diligence, L. Wound Management to 2024 | Medical Technology Market Analysis http://mediligence.com/s251/?_ga=2.161440446.288202397.1518427886-1394473983.1518427886 (accessed Feb 12, 2018).
- (7) Skin Ulcers Directory: Find News, Features, and Pictures Related to Skin Ulcers <https://www.webmd.com/skin-problems-and-treatments/skin-ulcers-directory> (accessed Feb 12, 2018).
- (8) 4 Likely Causes of a Chronic Wound That Will Not Heal <https://www.advancedtissue.com/4-likely-causes-of-a-chronic-wound-that-will-not-heal/> (accessed Jan 1, 2017).
- (9) Simon, Patrick E.; Moutran, Homere Al; Romo, T. I. Skin Wound Healing: Overview, Hemostasis, Inflammatory Phase <https://emedicine.medscape.com/article/884594-overview> (accessed May 15, 2018).
- (10) Wedro, B.; Davis, C. P. Wounds (Care) https://www.emedicinehealth.com/wound_care/article_em.htm#wound_care_facts (accessed May 16, 2018).
- (11) Koh, T. J.; Dipietro, L. A. Inflammation and Wound Healing: The Role of the Macrophage. <https://doi.org/10.1017/S1462399411001943>.
- (12) Martin, C. W.; Muir, I. F. K. The Role of Lymphocytes in Wound Healing. *Br. J. Plast. Surg.* **1990**, 43 (6), 655–662. <https://doi.org/10.1016/0007->

1226(90)90185-3.

- (13) Phases Of Wound Healing | Wound Care Education From CliniMed | CliniMed <https://www.clinimed.co.uk/wound-care/wound-essentials/phases-of-wound-healing> (accessed Nov 29, 2018).
- (14) Scars: Why They Form & Ways To Improve Appearance <https://www.webmd.com/skin-problems-and-treatments/scars> (accessed Nov 29, 2018).
- (15) Dallon, J. C.; Sherratt, J. A. *A Mathematical Model for Fibroblast and Collagen Orientation*; 1998; Vol. 60.
- (16) Miller, M. B.; Bassler, B. L. Quorum Sensing in Bacteria. *Annu. Rev. Microbiol.* **2001**, *55* (1), 165–199. <https://doi.org/10.1146/annurev.micro.55.1.165>.
- (17) Zhao, G.; Usui, M. L.; Lippman, S. I.; James, G. A.; Stewart, P. S.; Fleckman, P.; Olerud, J. E. Biofilms and Inflammation in Chronic Wounds. *Adv. wound care* **2013**, *2* (7), 389–399. <https://doi.org/10.1089/wound.2012.0381>.
- (18) Høgsberg, T.; Bjarnsholt, T.; Thomsen, J. S.; Kirketerp-Møller, K. Success Rate of Split-Thickness Skin Grafting of Chronic Venous Leg Ulcers Depends on the Presence of *Pseudomonas Aeruginosa*: A Retrospective Study. *PLoS One* **2011**, *6* (5), 4–9. <https://doi.org/10.1371/journal.pone.0020492>.
- (19) Dunnill, C.; Patton, T.; Brennan, J.; Barrett, J.; Dryden, M.; Cooke, J.; Leaper, D.; Georgopoulos, N. T. Reactive Oxygen Species (ROS) and Wound Healing: The Functional Role of ROS and Emerging ROS-Modulating Technologies for Augmentation of the Healing Process. *Int. Wound J.* **2015**, *14* (1), 89–96. <https://doi.org/10.1111/iwj.12557>.
- (20) de Kraker, M. E. A.; Stewardson, A. J.; Harbarth, S. Will 10 Million People Die a Year Due to Antimicrobial Resistance by 2050? *PLoS Med.* **2016**, *13* (11), 1–6. <https://doi.org/10.1371/journal.pmed.1002184>.
- (21) Davies, O. L.; Bennet, S. WHO publishes list of bacteria for which new

- antibiotics are urgently needed <http://www.who.int/news-room/detail/27-02-2017-who-publishes-list-of-bacteria-for-which-new-antibiotics-are-urgently-needed> (accessed May 21, 2018).
- (22) Janssen, H.; Janssen, I.; Cooper, P.; Kainyah, C.; Pellio, T.; Quintel, M.; Monnheim, M.; Groß, U.; Schulze, M. H. Antimicrobial-Resistant Bacteria in Infected Wounds, Ghana, 2014 1. *Emerg. Infect. Dis.* **2018**, *24* (5), 2016–2019.
 - (23) Pîrvănescu, H.; Bălăeoiu, M.; Ciurea, M. E.; Bălăeoiu, A. T.; Mănescu, R. Wound Infections with Multi-Drug Resistant Bacteria. **2014**, No. 1, 73–79.
 - (24) Llor, C.; Bjerrum, L. Antimicrobial Resistance: Risk Associated with Antibiotic Overuse and Initiatives to Reduce the Problem. *Ther. Adv. Drug Saf.* **2014**, *5* (6), 229–241. <https://doi.org/10.1177/2042098614554919>.
 - (25) Ngan, V. Antiseptic | DermNet New Zealand <https://www.dermnetnz.org/topics/antiseptic/> (accessed May 21, 2018).
 - (26) Carson, C. F.; Riley, T. V. *Non-Antibiotic Therapies for Infectious Diseases*; Commonwealth Department of Health and Ageing, 2003.
 - (27) Betancourt-ángeles, M.; Peña-eguiz, R.; López-callejas, R.; Alberto, N.; Valencia-alvarado, R.; Moreno-tapia, J. A. Case Report Treatment in the Healing of Burns with a Cold Plasma Source. *Int. J. Burn Trauma* **2017**, *7* (7), 142–146.
 - (28) Leite, S. N.; de Andrade, T. A. M.; Masson-Meyers, D. dos S.; Leite, M. N.; Enwemeka, C. S.; Frade, M. A. C. Phototherapy Promotes Healing of Cutaneous Wounds in Undernourished Rats. *An. Bras. Dermatol.* **2014**, *89* (6), 899–904. <https://doi.org/10.1590/abd1806-4841.20143356>.
 - (29) Idrees, A.; Varela, P.; Ruini, F.; Vasquez, J. M.; Salber, J.; Greiser, U.; Wang, W.; McMahon, S.; Sartori, S.; Ciardelli, G.; et al. Drug-Free Antibacterial Polymers for Biomedical Applications. *Biomed. Sci. Eng.* **2018**, *2* (1). <https://doi.org/10.4081/bse.2018>.
 - (30) Honey in history. Prehistory, Ancient Egypt, Ancient China. <https://healthywithhoney.com/honey-in-history-prehistory-ancient-egypt->

- ancient-china/ (accessed May 21, 2018).
- (31) Mandal, M. D.; Mandal, S. Honey: Its Medicinal Property and Antibacterial Activity. *Asian Pac. J. Trop. Biomed.* **2011**, *1* (2), 154–160. [https://doi.org/10.1016/S2221-1691\(11\)60016-6](https://doi.org/10.1016/S2221-1691(11)60016-6).
- (32) Bhattacharya, S. Wound Healing through the Ages. *Indian J. Plast. Surg.* **2012**, *45* (2), 177–179. <https://doi.org/10.4103/0970-0358.101255>.
- (33) Dresden, D.; Wilson, D. R. 7 best natural antibiotics: Uses, evidence, and effectiveness <https://www.medicalnewstoday.com/articles/321108.php> (accessed May 22, 2018).
- (34) Shenoy, Vishnu Prasad; Ballal, Mamatha; Shivanada, PG; Bairy, I. Honey as an Antimicrobial Agent. *J. Glob. Infect. Dis.* **2012**, 102–105. <https://doi.org/https://dx.doi.org/10.4103/0974-777X.96770>.
- (35) Molan, P. C. Honey as a topical antibacterial agent for treatment of infected wounds <http://www.worldwidewounds.com/2001/november/Molan/honey-as-topical-agent.html> (accessed Feb 2, 2018).
- (36) Cooke, J.; Dryden, M.; Patton, T.; Brennan, J.; Barrett, J.; O'Dowd, A.; Godlee, F.; Smith, R.; Coast, J.; Cooke, J.; et al. The Antimicrobial Activity of Prototype Modified Honeys That Generate Reactive Oxygen Species (ROS) Hydrogen Peroxide. *BMC Res. Notes* **2015**, *8* (1), 20. <https://doi.org/10.1186/s13104-014-0960-4>.
- (37) Cooper, R. A.; Molan, P. C.; Harding, K. G. Antibacterial Activity of Honey against Strains of Staphylococcus Aureus from Infected Wounds. *J. R. Soc. Med.* **1999**, *92* (6), 283–285. <https://doi.org/10.1177/014107689909200604>.
- (38) Abuharfeil, N.; Al-Oran, R.; Abo-Shehada, M. The Effect of Bee Honey on the Proliferative Activity of Human B-and T-Lymphocytes and the Activity of Phagocytes. *Food Agric. Immunol.* **1999**, *11* (2), 169–177. <https://doi.org/10.1080/09540109999843>.
- (39) Bogdanov, S. Nature and Origin of the Antibacterial Substances in Honey. *LWT - Food Sci. Technol.* **1997**, *30* (7), 748–753.

- <https://doi.org/10.1006/fstl.1997.0259>.
- (40) Sinclair, R. D.; Ryan, T. J. Proteolytic Enzymes in Wound Healing: The Role of Enzymatic Debridement. *Australas. J. Dermatol.* **1994**, *35* (1), 35–41. <https://doi.org/10.1111/j.1440-0960.1994.tb01799.x>.
- (41) Thallinger, B.; Prasetyo, E. N.; Nyanhongo, G. S.; Guebitz, G. M. Antimicrobial Enzymes: An Emerging Strategy to Fight Microbes and Microbial Biofilms. *Biotechnol. J.* **2013**, *8* (1), 97–109. <https://doi.org/10.1002/biot.201200313>.
- (42) Viswanathan, S.; Li, P.; Choi, W.; Filipek, S.; Balasubramaniam, T. A.; Renugopalakrishnan, V. Protein–Carbon Nanotube Sensors: Single Platform Integrated Micro Clinical Lab for Monitoring Blood Analytes. *Methods Enzymol.* **2012**, *509*, 165–194. <https://doi.org/10.1016/B978-0-12-391858-1.00010-1>.
- (43) Arul, V.; Masilamoni, J. G.; Jesudason, E. P.; Jaji, P. J.; Inayathullah, M.; Dicky John, D. G.; Vignesh, S.; Jayakumar, R. Glucose Oxidase Incorporated Collagen Matrices for Dermal Wound Repair in Diabetic Rat Models: A Biochemical Study. *J. Biomater. Appl.* **2012**, *26* (8), 917–938. <https://doi.org/10.1177/0885328210390402>.
- (44) Badalà, F.; Nouri-mahdavi, K.; Raoof, D. A. NIH Public Access. *Computer (Long. Beach. Calif.)* **2008**, *144* (5), 724–732. <https://doi.org/10.1038/jid.2014.371>.
- (45) Caló, E.; Khutoryanskiy, V. V. Biomedical Applications of Hydrogels: A Review of Patents and Commercial Products. *Eur. Polym. J.* **2015**, *65*, 252–267. <https://doi.org/10.1016/j.eurpolymj.2014.11.024>.
- (46) Qiao, M.; Chen, D.; Hao, T.; Zhao, X.; Hu, H.; Ma, X. Injectable Thermosensitive PLGA-PEG-PLGA Triblock Copolymers-Based Hydrogels as Carriers for Interleukin-2. *Pharmazie* **2008**, *63* (1), 27–30. <https://doi.org/10.1691/ph.2008.7115>.
- (47) Park, J.; Lee, S. J.; Chung, S.; Lee, J. H.; Kim, W. D.; Lee, J. Y.; Park, S. A. Cell-Laden 3D Bioprinting Hydrogel Matrix Depending on Different

- Compositions for Soft Tissue Engineering: Characterization and Evaluation. *Mater. Sci. Eng. C* **2017**, *71*, 678–684.
<https://doi.org/10.1016/j.msec.2016.10.069>.
- (48) Dong, Y.; Hassan, W. U.; Kennedy, R.; Greiser, U.; Pandit, A.; Garcia, Y.; Wang, W. Performance of an in Situ Formed Bioactive Hydrogel Dressing from a PEG-Based Hyperbranched Multifunctional Copolymer. *Acta Biomater.* **2014**, *10* (5), 2076–2085.
<https://doi.org/10.1016/j.actbio.2013.12.045>.
- (49) McMahon, S.; Kennedy, R.; Duffy, P.; Vasquez, J. M.; Wall, J. G.; Tai, H.; Wang, W. Poly(Ethylene Glycol)-Based Hyperbranched Polymer from RAFT and Its Application as a Silver-Sulfadiazine-Loaded Antibacterial Hydrogel in Wound Care. *ACS Appl. Mater. Interfaces* **2016**, *8* (40), 26648–26656. <https://doi.org/10.1021/acsami.6b11371>.
- (50) Wang, S.; Lee, J. M.; Yeong, W. Y. Smart Hydrogels for 3D Bioprinting. *Int. J. Bioprinting* **2015**, *1* (1), 3–14.
<https://doi.org/http://ijb.whioce.com/index.php/int-j-bioprinting/article/view/01005>.
- (51) Kamoun, E. a.; Kenawy, E. R. S.; Tamer, T. M.; El-Meligy, M. a.; Mohy Eldin, M. S. Poly (Vinyl Alcohol)-Alginate Physically Crosslinked Hydrogel Membranes for Wound Dressing Applications: Characterization and Bio-Evaluation. *Arab. J. Chem.* **2013**, *8* (1), 38–47.
<https://doi.org/10.1016/j.arabjc.2013.12.003>.
- (52) Zaman, H. U.; Islam, J. M. M.; Khan, M. A.; Khan, R. A. Physico-Mechanical Properties of Wound Dressing Material and Its Biomedical Application. *J. Mech. Behav. Biomed. Mater.* **2011**, *4* (7), 1369–1375.
<https://doi.org/10.1016/j.jmbbm.2011.05.007>.
- (53) Chai, Q.; Jiao, Y.; Yu, X. Hydrogels for Biomedical Applications: Their Characteristics and the Mechanisms behind Them. *Gels* **2017**, *3* (1), 6.
<https://doi.org/10.3390/gels3010006>.
- (54) Sannino, A.; Demitri, C.; Madaghiale, M. Biodegradable Cellulose-Based

- Hydrogels: Design and Applications. *Materials (Basel)*. **2009**, 2 (2), 353–373. <https://doi.org/10.3390/ma2020353>.
- (55) Yacob, N.; Hashim, K. Morphological Effect on Swelling Behaviour of Hydrogel. *AIP Conf. Proc.* **2014**, 1584 (2014), 153–159. <https://doi.org/10.1063/1.4866123>.
- (56) Ahmed, E. M. Hydrogel : Preparation , Characterization , and Applications : A Review. **2015**, 105–121.
- (57) Compañ, V.; Andrio, A.; López-Alemany, A.; Riande, E.; Refojo, M. F. Oxygen Permeability of Hydrogel Contact Lenses with Organosilicon Moieties. *Biomaterials* **2002**, 23 (13), 2767–2772. [https://doi.org/10.1016/S0142-9612\(02\)00012-1](https://doi.org/10.1016/S0142-9612(02)00012-1).
- (58) Heiting, G. Silicone Hydrogel Contact Lenses - A Complete Guide <https://www.allaboutvision.com/contacts/silicone-hydrogel.htm> (accessed May 22, 2018).
- (59) Dong, Y.; Qin, Y.; Dubaa, M.; Killion, J.; Gao, Y.; Zhao, T.; Zhou, D.; Duscher, D.; Geever, L.; Gurtner, G.; et al. A Rapid Crosslinking Injectable Hydrogel for Stem Cell Delivery, from Multifunctional Hyperbranched Polymers via RAFT Homopolymerization of PEGDA. *Polym. Chem.* **2015**, 6182–6192. <https://doi.org/10.1039/C5PY00678C>.
- (60) Lee, S. C.; Kwon, I. K.; Park, K. Hydrogels for Delivery of Bioactive Agents: A History Perspective. *Adv. Drug Deliv. Rev.* **2013**, 65 (1), 17–20. <https://doi.org/10.1080/10810730902873927>.Testing.
- (61) Kennedy, R.; Ul Hassan, W.; Tochwin, A.; Zhao, T.; Dong, Y.; Wang, Q.; Tai, H.; Wang, W. In Situ Formed Hybrid Hydrogels from PEG Based Multifunctional Hyperbranched Copolymers: A RAFT Approach. *Polym. Chem.* **2014**, 5 (6), 1838–1842. <https://doi.org/10.1039/C3PY01513K>.
- (62) Nair, D. P.; Podgórski, M.; Chatani, S.; Gong, T.; Xi, W.; Fenoli, C. R.; Bowman, C. N. The Thiol-Michael Addition Click Reaction: A Powerful and Widely Used Tool in Materials Chemistry. *Chem. Mater.* **2014**, 26 (1), 724–744. <https://doi.org/10.1021/cm402180t>.

- (63) Dong, Y.; Hassan, W.; Zheng, Y.; Saeed, A. O.; Cao, H.; Tai, H.; Pandit, A.; Wang, W. Thermoresponsive Hyperbranched Copolymer with Multi Acrylate Functionality for in Situ Cross-Linkable Hyaluronic Acid Composite Semi-IPN Hydrogel. *J. Mater. Sci. Mater. Med.* **2012**, *23* (1), 25–35. <https://doi.org/10.1007/s10856-011-4496-z>.
- (64) Zheng, Y.; Li, S.; Weng, Z.; Gao, C. Hyperbranched Polymers: Advances from Synthesis to Applications. *Chem. Soc. Rev.* **2015**, *44* (12), 4091–4130. <https://doi.org/10.1039/C4CS00528G>.
- (65) Bandyopadhyay, A.; Sengupta, S.; Das, T. *Hyperbranched Polymers for Biomedical Applications*; Springer US, 2018. <https://doi.org/https://doi.org/10.1007/978-981-10-6514-9>.
- (66) Tai, H.; Duvall, C. L.; Hoffman, A. S.; Stayton, P. S.; Wang, W. PH-Responsive Hyperbranched Copolymers from One-Pot RAFT Copolymerization. *Macromol. Mater. Eng.* **2012**, *297* (12), 1175–1183. <https://doi.org/10.1002/mame.201200227>.
- (67) A, S.; Xu, Q.; Zhou, D.; Gao, Y.; Vasquez, J. M.; Greiser, U.; Wang, W.; Liu, W.; Wang, W. Hyperbranched PEG-Based Multi-NHS Polymer and Bioconjugation with BSA. *Polym. Chem.* **2017**, *8*, 1283–1287. <https://doi.org/10.1039/C6PY01719C>.
- (68) *Global Wound Dressing Market Size, Share | Industry Report 2012-2022*; 2018.
- (69) Oxyzyme Dressings Datacard <http://www.dressings.org/Dressings/oxyzyme.html> (accessed May 23, 2018).
- (70) Moffatt, C. J.; Stanton, J.; Murray, S.; Doody, V.; Davis, P. J.; Franks, P. J. A Randomised Trial to Compare the Performance of Oxyzyme® and Iodozyme® with Standard Care in the Treatment of Patients with Venous and Mixed Venous/Arterial Ulceration. *Wound Med.* **2014**, *6*, 1–10. <https://doi.org/10.1016/j.wndm.2014.08.002>.
- (71) Eaton, A. Oxyzyme Application and Removal Video - YouTube

- <https://www.youtube.com/watch?v=N5BVAC8oTtU> (accessed May 23, 2018).
- (72) Lee, Y.; Choi, K.-H.; Park, K. M.; Lee, J.-M.; Park, B. J.; Park, K. D. In Situ Forming and H₂O₂-Releasing Hydrogels for Treatment of Drug-Resistant Bacterial Infections. *ACS Appl. Mater. Interfaces* **2017**, *9* (20), 16890–16899. <https://doi.org/10.1021/acsami.7b03870>.
- (73) Loo, A. E. K.; Wong, Y. T.; Ho, R.; Wasser, M.; Du, T.; Ng, W. T.; Halliwell, B. Effects of Hydrogen Peroxide on Wound Healing in Mice in Relation to Oxidative Damage. *PLoS One* **2012**, *7* (11). <https://doi.org/10.1371/journal.pone.0049215>.
- (74) Glucose Oxidase Product Sheet
<https://www.sigmaaldrich.com/content/dam/sigmaaldrich/docs/Sigma/Datasheet/7/g2133dat.pdf> (accessed May 24, 2018).

Chapter 2 Preparation and Characterization of Hyperbranched PEGDA/HA-SH Hydrogels

2.1. Abstract

This work was aimed at the preparation of a hyperbranched PEG-based acrylate polymer that could crosslink with thiolated hyaluronic acid. In order to synthesize this polymer, Reversible Atom Chain-Transfer Fragmentation (RAFT) polymerization was applied. Hyperbranched polyethylene glycol diacrylate (HB PEGDA) was successfully synthesized, with a molecular weight of 16,656 Da and vinyl content of 57% under a reaction time of 2 hours and 40 minutes. Hydrogels were obtained by mixing HB PEGDA polymer solutions (10-20 w/w%) with an equal volume of thiolated hyaluronic acid (HA-SH, 0.5-2 w/w%), based on the mechanism of thiol-ene click chemistry. Gelation time of 1000 μ L volume of hydrogels, obtained by the vial-tilt method, ranged from 42 to 585 seconds, depending on the HB PEGDA/HA-SH composition. The rheological properties,

swelling and water uptake, and degradation profile of hydrogels were obtained. Based on the physical criteria that a wound dressing hydrogel should be quick forming, mouldable, have high water absorption properties, have a minimum degradation time of one week, HB PEGDA/HA-SH hydrogel has potentiality for further studies in this application. This part of the activity was carried out at Wenxin Wang's Wound Healing and Skin Research Laboratory in Charles Institute of Dermatology, School of Medicine, University College Dublin, Ireland.

2.2. Introduction

2.2.1. Free Radical Polymerization

The Michael addition thiol-ene reaction has been exploited for a wide variety of material science applications. Given that reaction can occur in mild conditions and at fast reaction rates, it is the objective of this chapter to synthesize a PEG-based acrylate hyperbranched polymer that can react with a thiolated polymer, namely thiolated hyaluronic acid (HA-SH) to form a quick forming hydrogel with good mechanical properties, retaining large amounts of water¹.

There are two methods for synthesizing polymers: chain reaction (addition) polymerization and step reaction (condensation) polymerization². For monomers with vinyl groups, chain reaction polymerization is generally the method of choice.

For chain reaction polymerization, a catalyst such as a free radical from a peroxide molecule is required. In this reaction, the double bond of the vinyl group is attacked and opens up to bond with other monomers (initiation). The polymer chain continues to grow with the free electron from the radical passing into the outermost carbon. (propagation). The polymer chain then ends when one chain containing a

free radical reacts with another chain containing a free radical (termination by combination). Other alternative termination reactions that occur are termination by disproportionation and termination by transfer reaction^{3,4}. Figure 2.1 shows as an example the polymerization of polyethylene from ethylene occurring through three steps of initiation, propagation, and termination by combination.

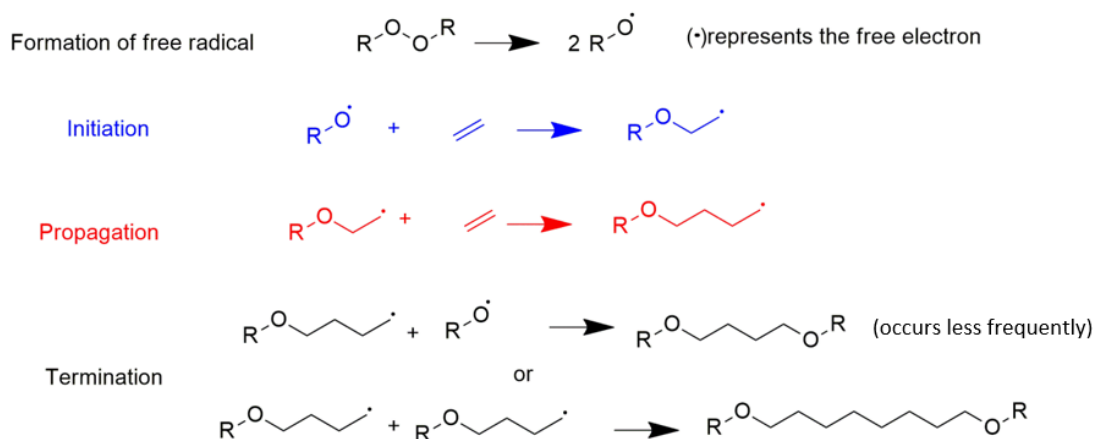


Figure 2.1: Representation of chain growth polymerization.

2.2.2. Reversible-deactivation Radical Polymerization

A drawback of conventional Free Radical Polymerization is the termination reaction between radicals is difficult to be controlled, thus it is challenging to obtain a specific polymer structure, molecular weight and polydispersity index⁵.

On the contrary, Reversible-deactivation radical polymerization, RDRP (also known as "Controlled/Living polymerization, CRP" and variations like Living Radical Polymerization, or Living Free Radical Polymerization), are defined as a form of chain growth polymerization where chain transfer and chain termination are absent⁵. This method allows a more controllable synthesis of polymers with different compositions, functionalities and architectures as shown in Figure 2.2.

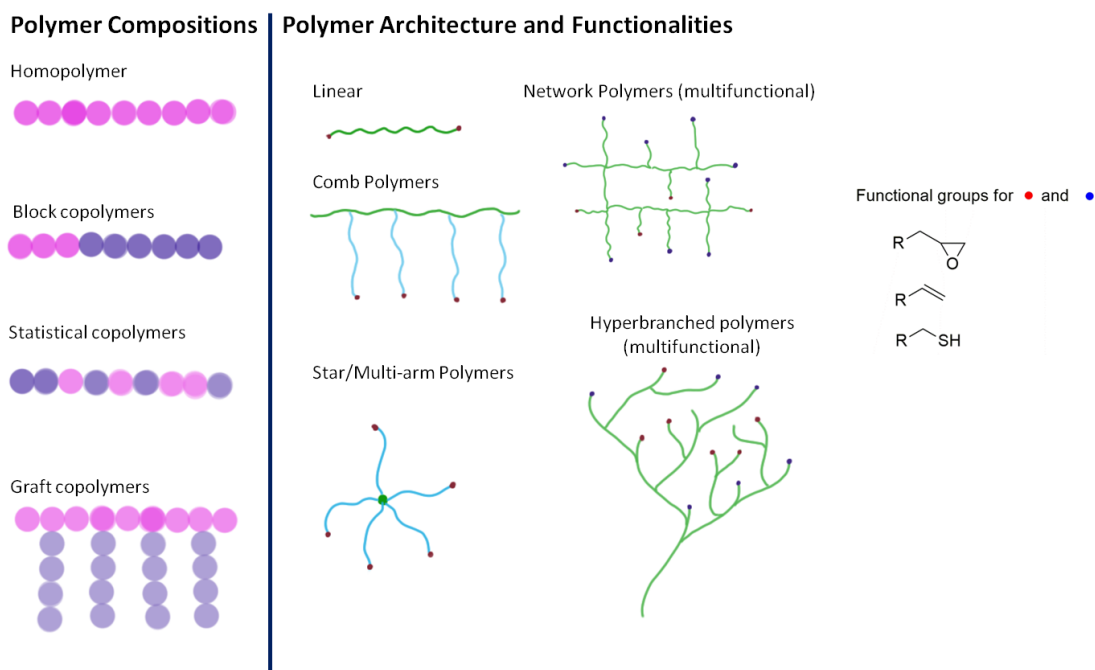


Figure 2.2: Examples of molecular structures obtained by RDRP or CRP.

The three most promising CRP methods of polymerizations are: 1) stable free radical polymerization (SFRP) or nitroxide mediated polymerization (NMP); 2) transition-metal-catalyzed atom transfer radical polymerization (ATRP), 3) reversible addition- fragmentation chain transfer (RAFT) polymerization⁵.

Within CRP, the most versatile method for synthesizing hyperbranched polymers for biomedical applications is RAFT polymerization. Compared to ATRP methods, it does not require a metal catalyst like copper chloride. This can often interfere with the biocompatibility of the material, when trace elements still exist in the end product of the reaction even after extensive purification methods. Synthesis in RAFT polymerization occurs much faster compared to SFRP, which requires 30-70 hours⁶.

RAFT agents are typically carbonylthio compounds as shown in Figure 2.3. In RAFT polymerization, the components for the reaction are: 1) monomer, 2) a radical source (eg. azobisisobutyronitrile or AIBN), 3) the RAFT agent (see Figure 2.3), 4) solvent⁷

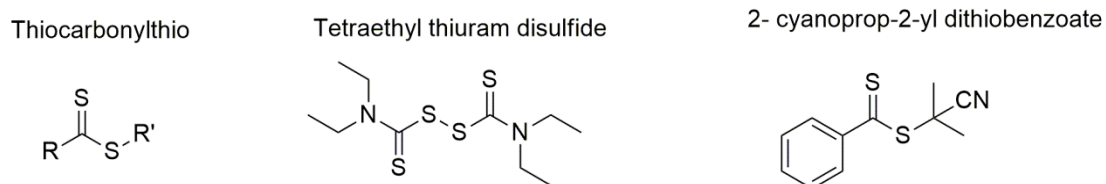
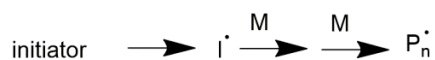


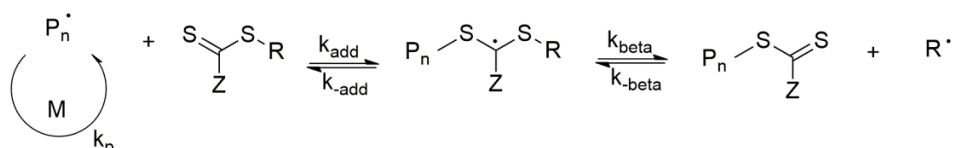
Figure 2.3: Structure and examples of RAFT agents^{7,8}.

In the RAFT polymerization mechanism, initiation and radical-radical termination occur similar to that of conventional polymerization, described in Figure 2.1. The detailed mechanism of RAFT polymerization and how it differs from conventional polymerization is illustrated below in Figure 2.4

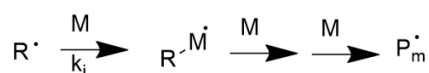
Initiator



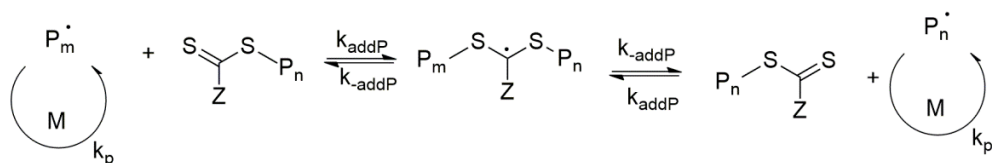
Reversible chain transfer



Reinitiation



Chain equilibration



Termination

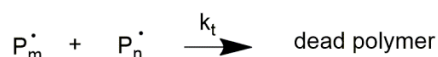


Figure 2.4: RAFT reaction mechanism with thiolcarbonylthio agent.

During the reversible chain transfer phase, which is in the early stage of polymerization, the propagating radical (P_n^\bullet) reacts to the thiocarbonylthio compound, which then fragments off the intermediate radical (R^\bullet), and a polymeric carbonylthio compound is formed.

In the re-initiation stage, R^\bullet reacts with other monomers and forms a new propagating radical polymer (P_m^\bullet).

Due to rapid equilibrium between the active propagating radicals, (P_n^\bullet and P_m^\bullet) and the dormant polymeric thiocarbonylthio compounds, there is equal probability for

all chains to grow and this results in polymers with narrow polydispersity index. When the polymerization is completed, most of the polymer chains retain the thiocarbonylthio end group and can be isolated as stable materials. The stability of the polymer formed via RAFT was proven, synthesizing two hyperbranched polymers with close molecular weights and polydispersity index, using both RAFT and DEATRP methods. For example, a hyperbranched PEG-based polymer was synthesized in Wenxin Wang's research group using the two methods: RAFT synthesis gave a weight-average molecular weight (Mw) of 16,656 Da and DEATRP gave a Mw of 19,881 Da. Upon collection of the polymers via lyophilization, the DEATRP-synthesized polymer self crosslinked while the RAFT-synthesized polymer maintained its initial chemical characteristics. A possible explanation is that some of the DE-ATRP polymers became activated as radicals and reacted with the other vinyl groups in the polymer chains.

In this chapter, the synthesis of a hyperbranched (HB) polymer to be used for the preparation of an antibacterial hydrogel is described. The methods and results of the chemical characterization of this material are also detailed in this chapter. Afterwards, this HB polymer was crosslinked with thiolated hyaluronic acid to form a hydrogel. The physical and chemical characteristics of the hydrogel were then determined and described in this chapter.

2.3. Materials and methods

2,2'-Azobis(isobutyronitrile) (AIBN), Tetraethylthiuram disulfide (DSDA), Polyethylene glycol Diacrylate, MW = 575 Da (PEGDA), Butanone, Hexane, Diethyl Ether, Acetone, Glucose, Glucose Oxidase enzyme (E.C. 1.1.3.4), Phosphate Buffer Solution pH 7.4 (PBS) were bought from Sigma Aldrich, UK.

Thiolated Hyaluronic acid (HA-SH, 80% degree of thiolation, 400 kDa) was provided by Vornia Ltd., Ireland.

Experiments were performed in Professor Wenxin Wang's Wound Healing and Skin Research Laboratory in Charles Institute of Dermatology, School of Medicine, University College Dublin, Ireland.

2.3.1. Polyethylene diacrylate (PEGDA)

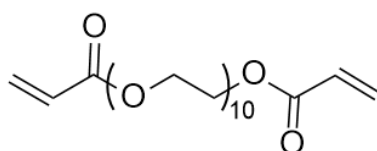


Figure 2.5: Chemical structure of PEGDA.

PEGDA has been used as a monomer to synthesize polymers for biomedical applications. Its acrylate functional groups allow it to polymerize with itself or other monomers to form a hyperbranched copolymer⁹⁻¹¹.

2.3.2. Thiolated hyaluronic acid (HA-SH)

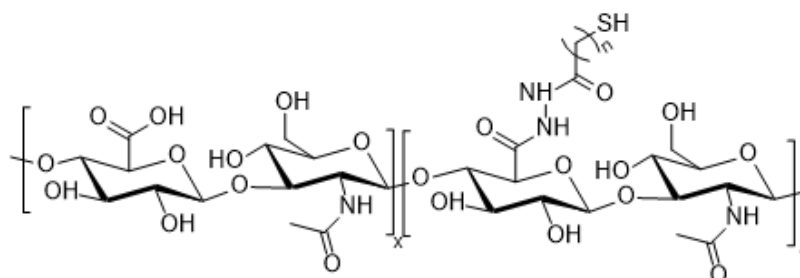


Figure 2.6: Chemical structure of HA-SH.

The synthesis protocol of HA-SH was described by Shu, et al., 2002¹². HA-SH is highly likely to form disulfide bonds with itself when exposed to oxygen, and forms a gel with itself if left in a solution in open air after several hours. This is due to the formation of disulfide bonds in oxidative environment.

In this research, the limitations of handling HA-SH were taken into consideration when developing industrial applications for this product.

2.3.3. Reversible addition fragmentation chain transfer (RAFT) polymerization of HB PEGDA

HB PEGDA was synthesized via Reversible Atom Chain-Transfer Fragmentation (RAFT) polymerization. Briefly, in a 250 mL double-neck flask, the following reagents were dissolved in 160 mL butanone: 46 g PEGDA, 948.92 mg DSDA (chain transfer agent) and 735.66 mg AIBN (reaction initiator). The solution was sealed and purged with Argon, and placed into an oil bath at 70°C for 2-3 hours. Samples were taken hourly to be analyzed by Gel Phase Chromatography (GPC) analysis to monitor the molecular weight increase of the polymer and the molar conversion (described in the section 2.3.4. Chemical characterization of HB PEGDA). When the molecular weight reached 10-20 kDa, the reaction was stopped by removing the mixture from the heating bath and opening the flask to let oxygen enter to prevent polymer gelling within the flask. The polymer was purified first by precipitating in a 2:1 volume ratio of diethyl ether: hexane and then by dialysis. The dialyzed solution was then lyophilized in a freeze dryer for 4 days.

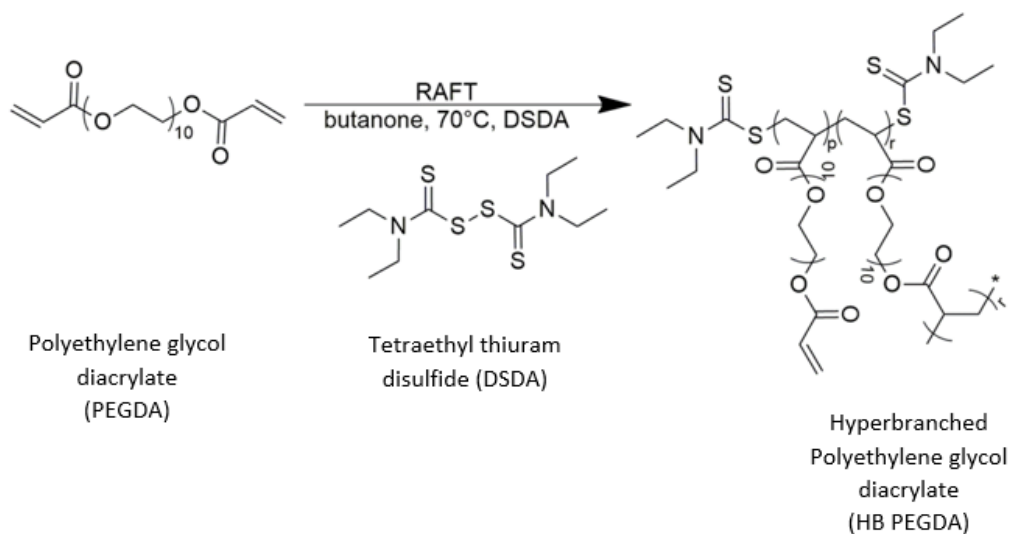


Figure 2.7: RAFT polymerization of PEGDA to HB PEGDA.

2.3.4. Chemical characterization of HB PEGDA

Samples for GPC analysis were prepared by dissolving 3 mg of polymer in 1 mL of dimethyl formamide (DMF). The samples were filtered (0.45 μm pore size) through a filter syringe into small amber GPC vials. The samples were analyzed in an Agilent 1260 Infinity GPC/SEC system (Agilent Technologies) to monitor molecular weight, molar conversion and polydispersity as the reaction proceeded. This system is equipped with a refractive index detector (RI), with two columns in series (30 cm PLgel mixed-C) and eluted using DMF (containing 0.1% LiBr) as mobile phase.

For characterizing molecular structure, ^1H Nuclear Magnetic Resonance (NMR) was used. The final polymer samples were dissolved in chloroform-D (CDCl_3) and ^1H NMR analysis was carried out on a 400 MHz Varian NMR spectroscopy system. Data were analyzed using MesReNova 6.1 processing software.

According to literature, HB polymers are characterized to have abundant functional groups, an irregular 3D topology, low viscosity, and high solubility¹³. These particular properties make them ideal to be used as one of the components in an *in situ* formed hydrogel system. Low viscosity and high solubility allow them to be dissolved easily in an aqueous solution as pre-hydrogel polymer solution. Their 3D topology and abundant functional groups allow ease of contact when crosslinking with HA-SH's thiol groups and the formation of a mechanically strong hydrogel structure.

2.3.5. Preparation of HB PEGDA/HA-SH hydrogels

To prepare hydrogel samples for further characterization, HB PEGDA polymer was dissolved in 1X 7.4 PBS buffer at concentrations from 10-20 w/w% (Table 2.1). HA-SH solution was prepared at concentrations of 1-4 w/w% (Table 1). To form a hydrogel, equal volumes of HB PEGDA and HA-SH solutions were mixed and pipetted into a 7.5 mm diameter cylinder mold or into a Teflon surface to form a bead. Total volume of this hydrogel cylinder was 200 μ L (hydrogel has a height of approximately 5 mm).

Table 2.1: Composition of prepared HB PEGDA/HA-SH hydrogels.

Hydrogel code	HB PEGDA solution concentration - Prehydrogel (% wt./wt.)	HA-SH solution concentration - Prehydrogel (% wt./wt.)	Hydrogel relative HB PEGDA/HA-SH amount (dry wt./dry wt.)	Overall hydrogel composition (wt./wt.)
5.0-1.0	10.0	2.0	5.0: 1.0	6.0%
10-0.5	20.0	1.0	20.0: 1.0	10.5%
10-1.0	20	2.0	10.0: 1.0	11.0%
10-2.0	20	4.0	5.0: 1.0	12.0%

Except for gelation time, all characterizations were performed on HB PEGDA/HA-SH 5.0-1.0 and 10.0-1.0

2.3.6. Gelation time

The gelation time for the hydrogels was obtained using the vial-tilt method¹⁴. Briefly, 500 μ L HB PEGDA solution was combined with 500 μ L HA-SH solution, using the concentrations shown in Table 2.1. These vials were tilted side to side and observed for 5 s. The gelation was considered complete when no flow was observed for 5 s.

2.3.7. Rheological characterization of hydrogel

Rheometry is used to study the flow of matter, particularly liquids and "soft solids". This allows the properties of hydrogels to be characterized and compared with each other. Gelation, in rheological terms, can be defined as the change of a substance from viscoelastic liquid to a viscoelastic solid¹⁵.

2.3.7.1. Frequency Sweep and Strain Sweep Tests

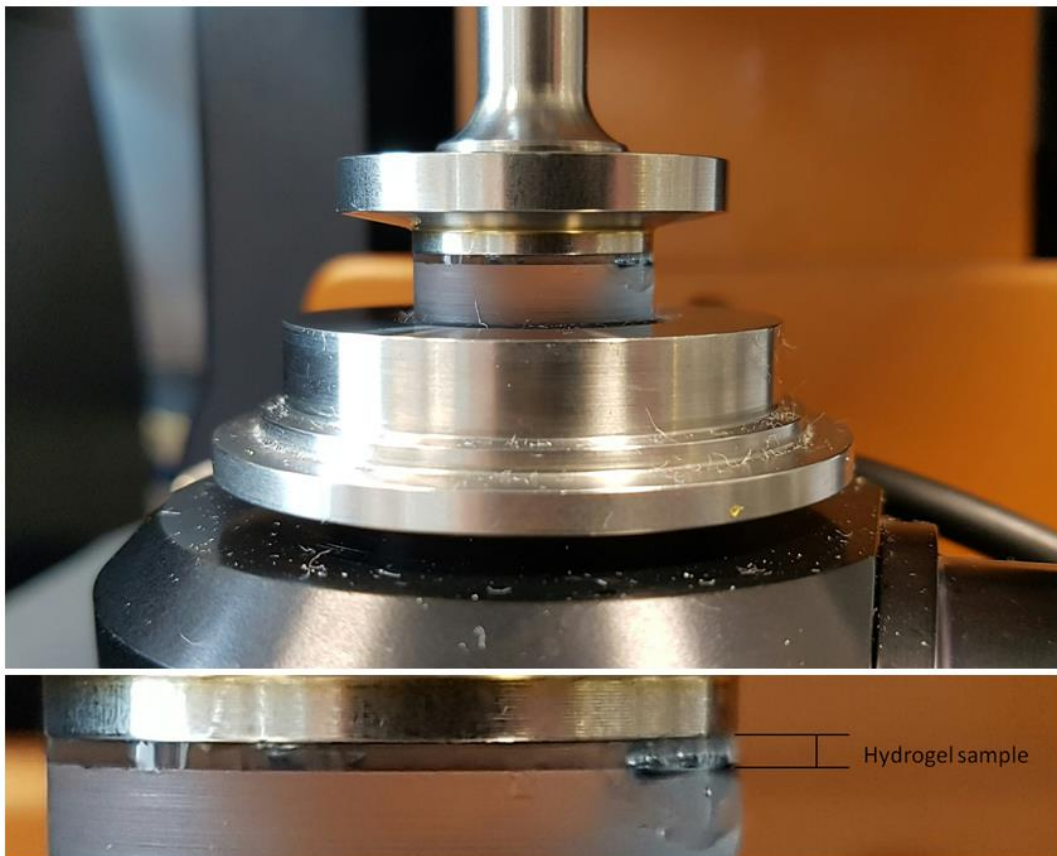


Figure 2.8: Hydrogel on rheometer plate: 20 mm parallel plate Rheometry was performed on a TA Discovery Hybrid Rheometer-2 (DHR-2) with 8 mm diameter parallel plates and TRIOS software for analysis of data.

With the aim of determining the rheological properties of the HB PEGDA/HA-SH hydrogels, detailed dynamic rheological assessments were conducted on hydrogels. Rheological profiles were obtained by pipetting an excess 90 μL of pre-forming HB PEGDA/HA-SH hydrogel (the individual components were mixed, but the solution was still liquid) into the rheometer plate at room temperature. The 8 mm disc plate was lowered until a height of 1.5 mm was achieved. Estimated volume of analyzed hydrogel was 75.4 μL .

Storage moduli (G') and loss moduli (G'') were measured from sweep tests. A frequency sweep profile (at 10% strain) was obtained at a range of 0.1 to 100 Hz. Strain sweep profile (at 10 Hz) was obtained at a range of 0.1% to 100% strain.

The shear elastic (or storage) modulus, G' , gives a measure of the energy that is stored elastically by the system per cycle when subjected to frequency oscillation¹⁵. It is what gives a viscoelastic material its characteristic "solidness". Meanwhile, the shear viscous (or loss) modulus, G'' , represents a measure of the energy that is dissipated during flow per cycle of oscillation¹⁵. It describes how "liquid" a viscoelastic material is. When G' is greater than G'' , then a material can be describe as behaving more like a solid.

2.3.8. Swelling and water uptake profile

In order to determine the water absorption profile of hydrogels, 200 μL samples of 10-1 and 5-1 HB PEGDA/HA-SH hydrogels were prepared. These were selected by considering the HA-SH composition constant and observing the physical properties of the hydrogel based on the HB PEGDA present. These samples were placed in pre-weighed 20 mL scintillation vials and weighed. Then 2 mL 1X 7.4 pH PBS was added to these vials. The samples were incubated at 37°C.

At different time points (initially every 2 hours for the first 8 hours, then every 24 hours for the first week and every 2 days onward) up to 6 weeks, PBS was removed and the bottle was weighed. After weighing, 2 mL of fresh PBS solution was added again and the bottle was returned to the incubator. Measurements were performed in quadruplicates.

Water absorption was calculated based on this formula:

$$\text{Percent absorption} = \frac{W_t - W_0}{W_0} * 100\% \quad (\text{eq. 4})$$

Where W_t = weight of hydrogel at time point t in, W_0 = initial weight of the hydrogel.

2.3.9. Degradation profile of hydrogels

The degradation profile was obtained from the swelling and water uptake profile performed in Par. 2.3.8. Degradation was considered to occur when the *Percent absorption* of the hydrogel began to decrease after reaching its highest attainable *Percent absorption*. Since the data did not give a decrease in percent absorption as far as Day 64 for HB PEGDA/HA-SH 10-1.0 (with the planned study intended to last only for 28 days), the degradation point for HB PEGDA/HA-SH 5.0-1.0 was taken as the time period where the samples dissolved into the system as there was no gradual decrease after the maximum swelling point was obtained.

2.4. Results and discussion

2.4.1. Chemical characterization of HB PEGDA

2.4.1.1. Gel Phase Chromatography

GPC analysis showed that polymer weight-average molecular weight (M_w) after 2 hours and 40 minutes reaction was 16,656 Da, while number-average molecular weight (M_n) was 11,060 Da, polydispersity index was 1.5, and molar conversion from monomer to polymer was 32.5%. These properties were obtained from the Agilent GPC software by integrating the GPC curve measured on samples polymerized at the corresponding time (Figure 2.9).

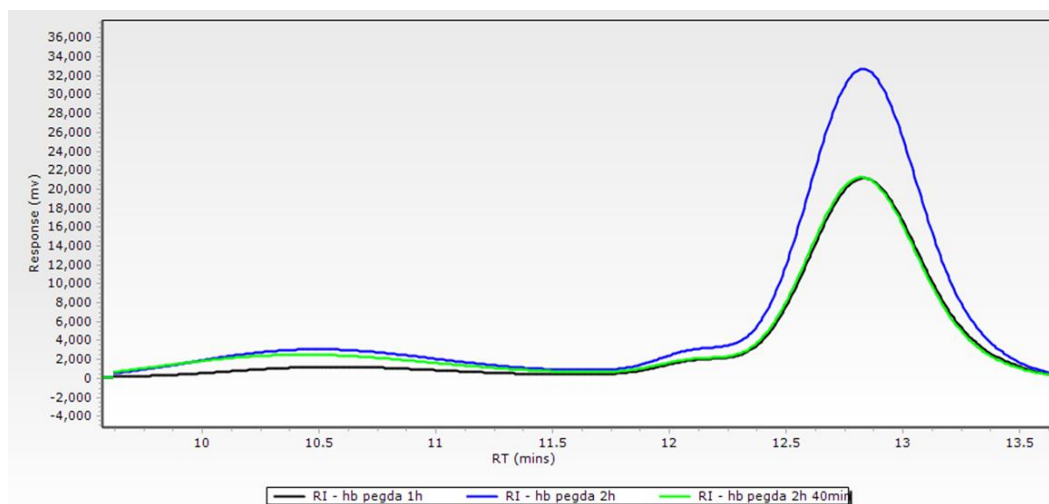


Figure 2.9: GPC profile of HB PEGDA at different reaction times.

In other syntheses, by not fully purging the reaction flask with Argon, the reaction could be slowed down to 7-10 hours, in order to obtain a hyperbranched polymer of the same molecular weight.

2.4.1.2. Nuclear Magnetic Resonance

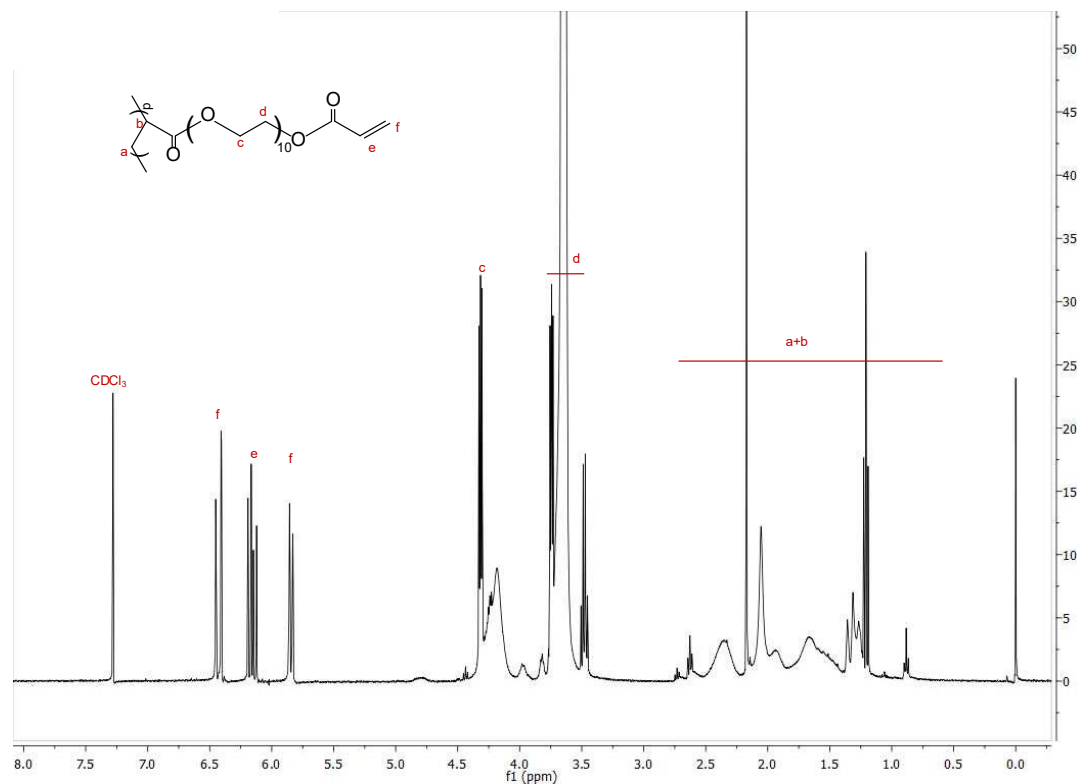


Figure 2.10: ¹H NMR spectrum of HB PEGDA Mw 16,656 Da.

¹H NMR spectra (Figure 2.10) allowed the analysis of the branched structure and amount of pendant acrylate groups. The pendant acrylate groups were identified as three characteristic chemical shifts at 6.4-5.8 ppm. The PEG groups were identified as the chemical shift at 4.34-3.95 ppm. From these shifts, the vinyl ratio was calculated to be 57 mol% and the vinyl content was 0.99 mmol vinyl/g polymer. The higher the vinyl content, the greater were the chances for the polymer to crosslink faster. The DB for hyperbranched polymers has been typically ranged at 40-60%, thus the calculated value (57%) suggested high degree of branching¹⁷.

2.4.2. Gelation time and rheological characterization of hydrogel

2.4.2.1. Gelation time

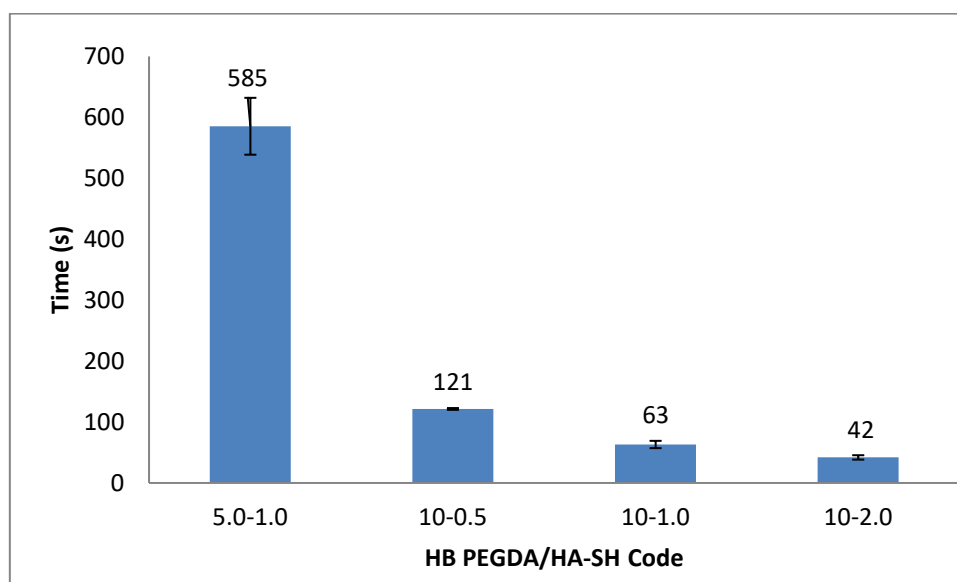


Figure 2.11: Gelation time of hydrogels at different time points.

Gelation time is reported in Figure 2.11 as a function of hydrogel composition. Results showed that an increased amount of HB PEGDA from 83% (5.0:1.0) to 95% (20.0: 1.0) caused a marked decrease in the gelation time. This result could be attributed to the higher availability of acrylate groups for crosslinking. However, gelation time further decreased in the case of the 10.0:1.0 hydrogel which showed a slightly lower HB PEGDA content (91%) respect to 20.0: 1.0 hydrogel (Figure 2.10). Both hydrogels showed very close overall hydrogel concentration (Table 2.1). Hence, this result suggests that gelation was minimized by a proper relative amount of HB PEGDA to HASH.

The gelation time was also affected by hydrogel overall concentration (overall concentration was 6%, 10.5%, 11%, 12% for HB PEGDA/HASH 5.0:1.0, 20.0: 1.0, 10.0:1.0, 10-2.0, respectively). A comparison between the first (5.0:1.0) and fourth

(10-2.0) compositions in Figure 2.10, having the same relative amount of polymers and a different hydrogel overall concentration (6% versus 12%), suggested that a more concentrated hydrogel favored gelation. This result was due to lower water content, accelerating gelation. Indeed, the lowest gelation time (42 s) was measured for 10-2.0 hydrogel (83% HB PEGDA, 12% overall concentration) while the highest gelation time (585 s) was measured for 5.0:1.0 hydrogel (83% HB PEGDA, 12% overall concentration). Hence the gelation time decreased by 93% while concentration was increased by 50%. Such gelation rate was extremely fast and incompatible with perspective clinical application.

The hydrogels synthesized in this study showed slightly lower gelation times than those reported in previous studies. Previous literature described the synthesis of hyperbranched PEG-based polymers to be crosslinked with HA-SH and, for a variety of concentrations, gelation times ranging from one to five minutes were reported ¹⁰.

As a conclusion, based on the gelation time values, HB PEGDA/HASH 10.0:1.0 was selected as an optimal hydrogel: its gelation rate was fast but compatible with a perspective clinical application. As a comparison HB PEGDA/HASH 5.0:1.0 hydrogel was also further characterized.

2.4.2.2. Results from frequency sweep and strain sweep tests

The frequency sweep profiles of the HB PEGDA/HA-SH hydrogels 5.0-1.0 and 10-1.0 at 10% oscillation strain are depicted in Figure 2.12. For a perfect solid, these storage and loss values are $G''=0$ and $G'=a \text{ finite value}$ ¹⁵. For a perfect liquid, $G''=a \text{ finite value}$ and $G'=0$ ¹⁵. As hydrogels are neither perfect solids or perfect liquids, their G' and G'' values are higher than zero. When $G''>G'$, the sample is considered

more viscous than elastic (solution), when in $G'' < G'$, the sample is more elastic than viscous (hydrogel). From Figure 2.11, in both 5.0-1.0 and 10-1.0 compositions, the storage moduli were consistently higher than the loss moduli at all time points, meaning that the material was in hydrogel form.

Storage modulus is also connected to how well-crosslinked a material is. A hydrogel that has more crosslinked junctions is able to store more deformation energy in an elastic manner. From the data, when the frequency was increased, this caused the hydrogel to increase its G' and G'' as it stored the energy exerted on it, to prevent the gel from deforming. As there is little observable difference in the G' and G'' values between 5.0-1.0 and 10-1.0, both hydrogels were similarly crosslinked.

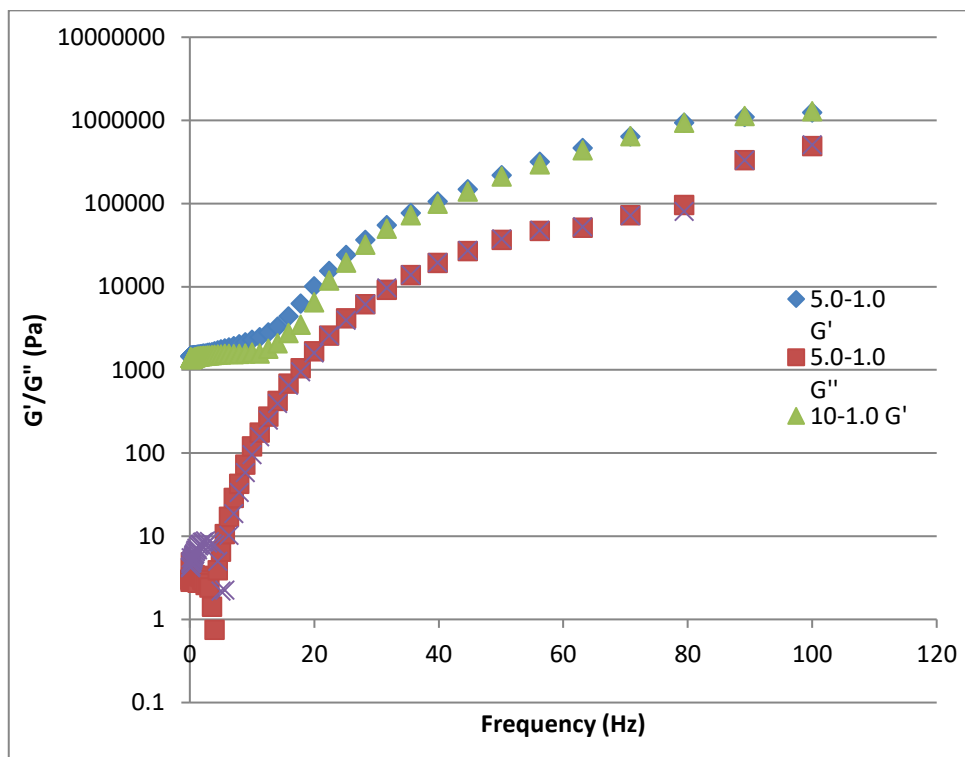


Figure 2.12: Frequency sweep profile of HB PEGDA/HA-SH hydrogels (at 10% oscillation strain).

In Figure 2.13, the strain sweep profiles of the HB PEGDA/HA-SH hydrogels are shown, under a constant frequency of 10 Hz. As with Figure 2.11, the storage moduli were consistently higher than the loss moduli for both polymer compositions. However, in this profile, when the rotational strain on the hydrogel was increased, the G'' decreased slightly, while the G' slightly increased, with the storage and loss moduli points gradually diverging from each other. This means that in higher strains, the hydrogels behaved more like a solid material.

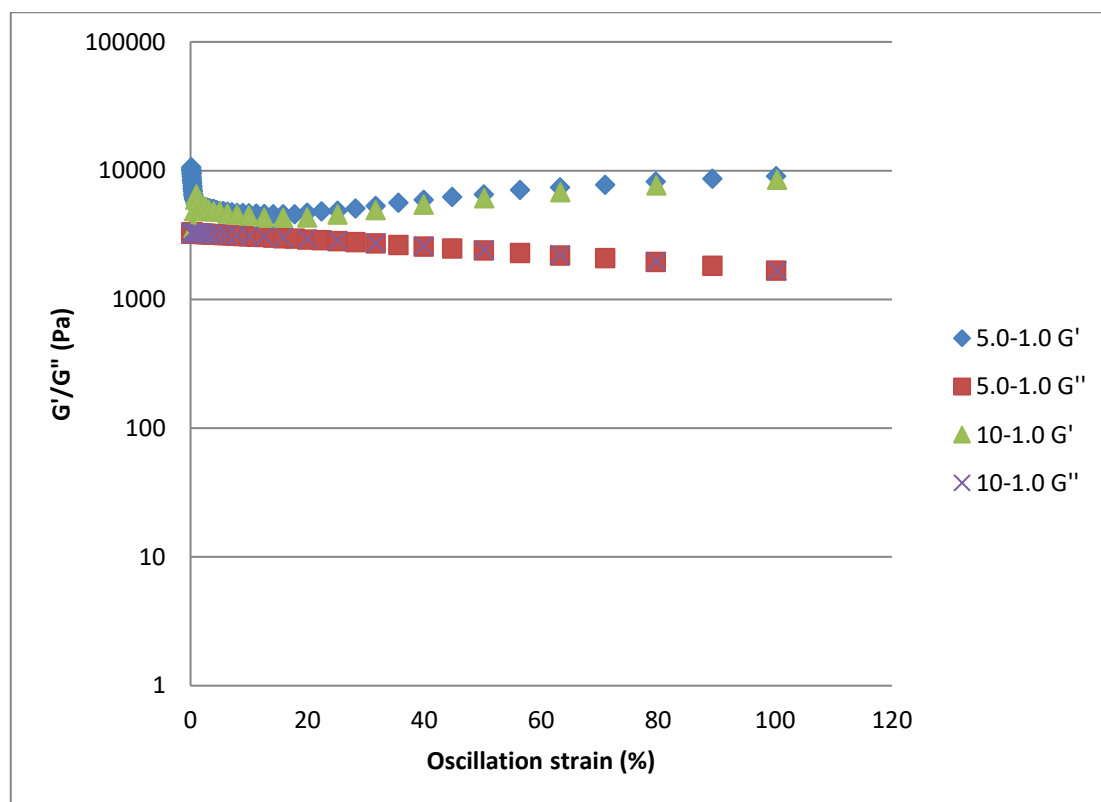


Figure 2.13: Strain sweep profiles of HB PEGDA/HA-SH hydrogels (at 10 Hz frequency).

2.4.3. Physical characterization of hydrogel

The selected hydrogel compositions were used to form hydrogel beads, by pipetting 30 μL of HB PEGDA/HA-SH pre-crosslinked solution onto a hydrophobic Teflon surface. The average diameter of these beads was 4 mm (see Figure 2.14 a). Such hydrogels could also be poured into moulds to produce cylindrical hydrogels (see Figure 2.14 b).

When producing these hydrogels, the operator should be fast as to avoid time hydrogel crosslinking within the pipette.



Figure 2.14: Hydrogel samples fabricated for characterization, a) 30 μL beads with 4 mm diameter, b) 200 μL beads with 7.5 mm diameter and 5 mm height.

2.4.3.1. Swelling and water uptake profile

Figure 2.15 shows water adsorption percentage as a function of time. The hydrogels displayed the trend to adsorb water as time progressed. In the first two weeks, adsorbed water was less than 10% of hydrogel initial mass, but as the entangled polymers in the hydrogel began to uncoil, more water was taken in progressively.

HB PEGDA/HA-SH 5.0-1.0, which contained a lower overall polymer amount (overall concentration 6%) and a different HB PEGDA/HASH dry weight ratio

(83/17) respect to HB PEGDA/HA-SH 10-1.0 (overall concentration: 11%; HB PEGDA/HASH dry weight ratio of 91/9) was completely dissolved after 28 days. HB PEGDA/HA-SH 5.0-1.0 hydrogel was able to take water up to a maximum of 57% of its weight in 27 days while HB PEGDA/HA-SH 10-1.0 hydrogel was able to absorb up to 131% of its weight in 64 days.

HB PEGDA/HA-SH 10-1.0 hydrogel was resistant in a water environment for at least 64 days: such hydrogel contained a higher overall polymer quantity than the HB PEGDA/HA-SH 5.0-1.0 hydrogel and it was probably better crosslinked thanks to an optimal HB PEGDA/HA-SH ratio.

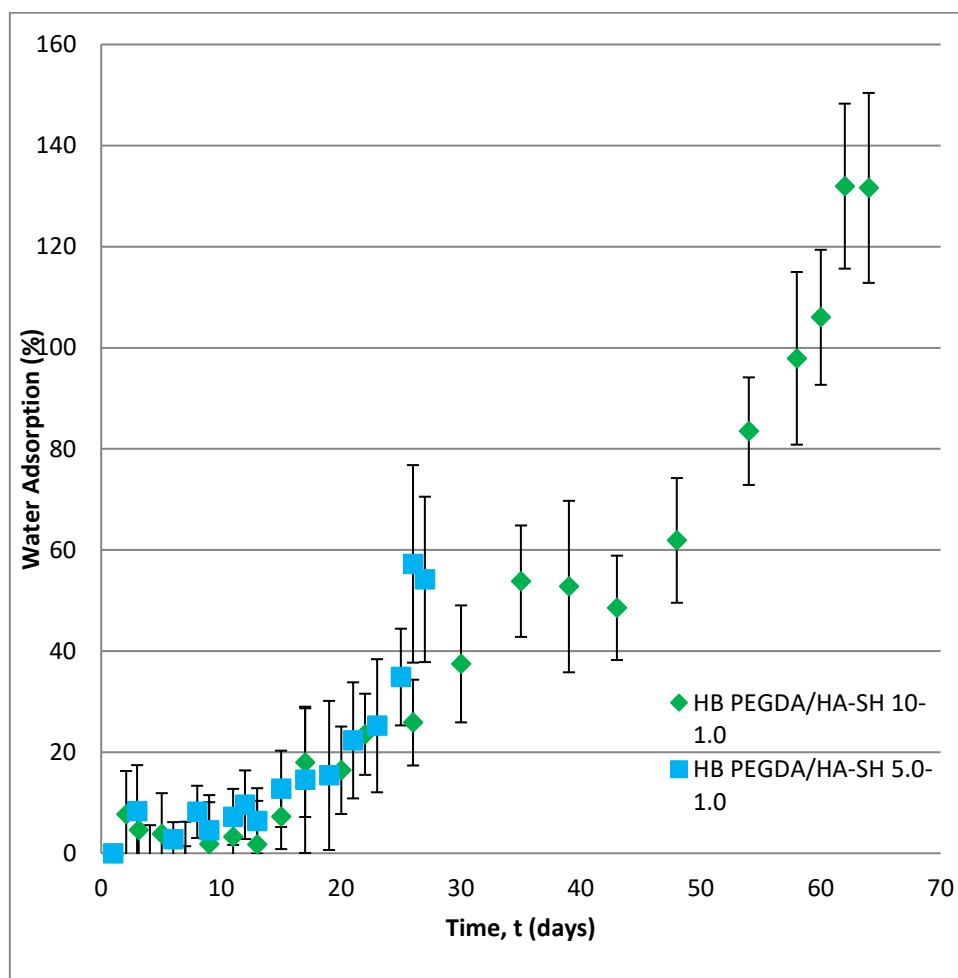


Figure 2.15: Water adsorption profile of hydrogels.

2.4.3.2. Degradation profile

The degradation studies in most hydrogels often do not take more than 3 weeks^{9,18}. As observed for HB PEGDA/HA-SH 5.0-1.0, degradation did not start until day 28, then "burst" after day 28. For this hydrogel, it continued to swell and take in water despite its more altered shape. In its final stages, it appeared as a semi-solid flat gel until it was finally indistinguishable from the PBS medium where it was soaked in. Figure 2.16 illustrates the progression.

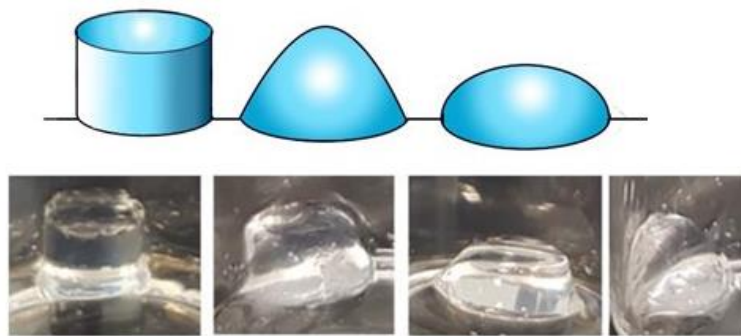


Figure 2.16: Top illustration: Representation of the HB PEGDA/HA-SH hydrogel degradation. Bottom photographs: Progression of HB PEGDA/HA-SH 5.0-1.0 adsorbing water and degrading (left to right: day 4, 14, 20, 22).

For HB PEGDA/HA-SH 10-1.0, there was some alteration in its shape but it continued to hold an overall cylindrical structure on day 64, as seen in Figure 2.17.



Figure 2.17: Representative images of HB PEGDA/HA-SH 10-1.0 hydrogel at day 64 during water adsorption test.

As a conclusion, the hydrogels demonstrated their slow degradation which is fundamental for *in vivo* applications. Particularly, HB PEGDA/HA-SH 10-1.0 hydrogel also showed shape retention, which is an important ability for its future perspective applications in wound healing.

2.5. Conclusions

In this chapter, HB PEGDA was synthesized and chemically characterized. This polymer had a vinyl content of 0.99 mmol/gram polymer, molecular weight of 16,656 Da, and a polydispersity of 1.5. Using this polymer, HB PEGDA/HA-SH hydrogels were formed via thiol-ene click chemistry. The gelation time of the material ranged from 42 to 585 seconds, depending on the HB PEGDA and HA-SH relative amount and hydrogel overall concentration. The HB PEGDA/HA-SH 10.0/1.0 hydrogel composition (91 wt.% HB PEGDA; 11 wt./v. % hydrogel overall concentration) was selected as it showed a relatively fast gelation time at 63 s, which was compatible with a possible future *in vivo* application. Additionally, water adsorption test showed that HB PEGDA/HA-SH 10.0/1.0 hydrogel retained its shape after 64 days incubation, with no signs of degradation and a progressive swelling up to 131% after 64 days. Rheological analyses indicated that PEGDA/HA-SH 10.0/1.0 was a weak hydrogel with G' in the 5-10 kPa range at 10 Hz frequency and within 0-100% strain (strain sweep tests). Hence it was suitable for applications in the regeneration of soft tissues such as skin.

2.6. References

- (1) Fenoli, C. R.; Bowman, C. N. The Thiol-Michael Addition Click Reaction: A Powerful and Widely Used Tool in Materials Chemistry. **2013**.

- (2) Carraher, C. E. *Polymer Chemistry*, 6th ed.; Marcel Dekker, Inc.: New York, 2003.
- (3) Wesley R. Mariott; Antonio Rodriguez-Delgado, A.; Chen*, E. Y.-X. Chain Termination and Transfer Reactions in the Acrylate Polymerization by a Monometallic Chiral Zirconocenium Catalyst System. *Macromolecules* **2006**, *39* (4), 1318–1327. <https://doi.org/10.1021/MA052305+>.
- (4) Ribelli, T. G.; Augustine, K. F.; Fantin, M.; Krys, P.; Poli, R.; Matyjaszewski, K. Disproportionation or Combination? The Termination of Acrylate Radicals in ATRP. *Macromolecules* **2017**, *50* (20), 7920–7929. <https://doi.org/10.1021/acs.macromol.7b01552>.
- (5) Spanswick, J.; Matyjaszewski, K. Controlled / Living Radical Polymerization. *Mater. Today* **2005**, *8* (3), 26–33. [https://doi.org/https://doi.org/10.1016/S1369-7021\(05\)00745-5](https://doi.org/https://doi.org/10.1016/S1369-7021(05)00745-5).
- (6) Dollin, M.; Szkurhan, A. R.; Georges, M. K. Rapid Additive-Free TEMPO-Mediated Stable Free Radical Polymerizations of Styrene. *J. Polym. Sci. Part A Polym. Chem.* **2007**, *45*, 5487–5493. <https://doi.org/10.1002/pola>.
- (7) Moad, G.; Rizzardo, E.; Thang, S. H. Radical Addition-Fragmentation Chemistry in Polymer Synthesis. *Polymer (Guildf)*. **2008**, *49* (5), 1079–1131. <https://doi.org/10.1016/j.polymer.2007.11.020>.
- (8) Kennedy, R.; Ul Hassan, W.; Tochwin, A.; Zhao, T.; Dong, Y.; Wang, Q.; Tai, H.; Wang, W. In Situ Formed Hybrid Hydrogels from PEG Based Multifunctional Hyperbranched Copolymers: A RAFT Approach. *Polym. Chem.* **2013**. <https://doi.org/10.1039/C3PY01513K>.
- (9) Dong, Y.; Hassan, W.; Zheng, Y.; Saeed, A. O.; Cao, H.; Tai, H.; Pandit, A.; Wang, W. Thermoresponsive Hyperbranched Copolymer with Multi Acrylate Functionality for in Situ Cross-Linkable Hyaluronic Acid Composite Semi-IPN Hydrogel. *J. Mater. Sci. Mater. Med.* **2012**, *23* (1), 25–35. <https://doi.org/10.1007/s10856-011-4496-z>.
- (10) Dong, Y.; Qin, Y.; Dubaa, M.; Killion, J.; Gao, Y.; Zhao, T.; Zhou, D.;

- Duscher, D.; Geever, L.; Gurtner, G.; et al. A Rapid Crosslinking Injectable Hydrogel for Stem Cell Delivery, from Multifunctional Hyperbranched Polymers via RAFT Homopolymerization of PEGDA. *Polym. Chem.* **2015**, 6182–6192. <https://doi.org/10.1039/C5PY00678C>.
- (11) McMahon, S.; Kennedy, R.; Duffy, P.; Vasquez, J. M.; Wall, J. G.; Tai, H.; Wang, W. Poly(Ethylene Glycol)-Based Hyperbranched Polymer from RAFT and Its Application as a Silver-Sulfadiazine-Loaded Antibacterial Hydrogel in Wound Care. *ACS Appl. Mater. Interfaces* **2016**, 8 (40), 26648–26656. <https://doi.org/10.1021/acsami.6b11371>.
- (12) Shu, X. Z.; Liu, Y.; Luo, Y.; Roberts, M. C.; Prestwich, G. D. Disulfide Cross-Linked Hyaluronan Hydrogels. **2002**, 1304–1311. <https://doi.org/10.1021/bm025603c>.
- (13) Zheng, Y.; Li, S.; Weng, Z.; Gao, C. Hyperbranched Polymers: Advances from Synthesis to Applications. *Chem. Soc. Rev.* **2015**, 44 (12), 4091–4130. <https://doi.org/10.1039/C4CS00528G>.
- (14) Deshmukh, M.; Singh, Y.; Gunaseelan, S.; Gao, D.; Stein, S.; Sinko, P. J. Biodegradable Poly(Ethylene Glycol) Hydrogels Based on a Self-Elimination Degradation Mechanism. *Biomaterials* **2011**, 31 (26), 6675–6684. <https://doi.org/10.1016/j.biomaterials.2010.05.021>. Biodegradable.
- (15) Moura, M. J.; Figueiredo, M. M.; Gil, M. H. Rheological Study of Genipin Cross-Linked Chitosan Hydrogels. *Biomacromolecules* **2007**, 8, 3823–3829.
- (16) Sandle, T. *Pharmaceutical Microbiology : Essentials for Quality Assurance and Quality Control*.
- (17) Wang, D.; Zhao, T.; Zhu, X.; Yan, D.; Wang, W. Bioapplications of Hyperbranched Polymers. *Chem. Soc. Rev.* **2015**, 44 (12), 4023–4071. <https://doi.org/10.1039/C4CS00229F>.
- (18) Omer, R. A.; Hughes, A.; Hama, J. R.; Wang, W.; Tai, H. Hydrogels from Dextran and Soybean Oil by UV Photo-Polymerization. *J. Appl. Polym. Sci.* **2015**, 132 (6), n/a-n/a. <https://doi.org/10.1002/app.41446>.

Chapter 3 Antibacterial

Reactive Oxygen Species

Production in HB PEGDA/HA-SH

Hydrogel

3.1. Abstract

HB PEGDA/HA-SH 10-1.0 and HB PEGDA/HA-SH 5.0-1.0 hydrogels were used to encapsulate glucose oxidase (GO) enzyme and glucose to produce an antibacterial injectable hydrogel for wound dressing. Varying amounts of GO (0-2000 U/L) were dissolved in HB PEGDA solutions (20 w/w% and 10 w/w%). Glucose (1-20 w/w%) was dissolved in 2 w/w% HA-SH solution. In 24 hours, 250 U/L GO and 2.5 w/w% glucose in the HB PEGDA/HA-SH 10-1.0 hydrogel produced 16.02 ± 4.16 mM H_2O_2 in shaken conditions and 9.11 ± 0.92 mM H_2O_2 in static conditions. This hydrogel also demonstrated cytocompatibility with NIH/3T3 mouse fibroblast cells after 24 hours. Hydrogen peroxide continuously produced by the HB PEGDA/HA-SH 10-1.0 (w/w%) hydrogel loaded with 250 U/L glucose oxidase and 2.5 w/w% glucose demonstrated antibacterial activity against several

strains of bacteria, primarily Gram-positive bacteria (*S. aureus*, *A. baumannii*, *S. epidermidis*, and *A. baumannii*) and antibiotic-resistant Gram-positive bacteria (MRSA, MRSE). On the other hand, hydrogel antibacterial activity on Gram-negative bacteria (*E. coli* and *P. aeruginosa*) and antibiotic-resistant *P. Aeruginosa* was less relevant with reduced inhibition zones in the agar diffusion test. When the glucose oxidase concentration in the hydrogel was increased from 250 U/L to 500 U/L, the material demonstrated antibacterial activity on antibiotic resistant *E. coli*. Thus, these hydrogels have the potential to be used as *in situ* forming antibacterial wound dressings.

The main experiments were performed in Professor Wenxin Wang's Wound Healing and Skin Research Laboratory in Charles Institute of Dermatology, School of Medicine, University College Dublin, Ireland. Antibacterial agar diffusion tests were performed by the PhD candidate Ayesha Idrees (Politecnico di Torino) during her secondment period at Universitätsklinikum Knappschaftskrankenhaus Bochum – Department of Experimental Surgery/ Clinic of Surgery under Dr. Jochen Salber's supervision, as a part of the EU Horizon 2020 “HyMedPoly” project.

3.2. Introduction

Enzymes are complex proteins obtained from living organisms that are capable of catalyzing a number of reactions¹. Their functions are often defined in their name. The six classes of enzymes are:

- Hydrolases
- Oxidoreductases
- Transferases
- Lyases

- Isomerases
- Ligases

Oxidoreductases, such as glucose oxidase work by catalyzing the transfer of electrons from the reducing agent or electron donor, to the oxidizing agent or electron acceptor¹. In the reaction previously described in Chapter 1, Figure 1.5, GO works to specifically oxidize glucose in order to produce the antibacterial reactive oxygen species, H₂O₂. The specific selectivity of this enzyme for glucose eliminates oxidation of other substrates.

The enzyme unit (U) is a unit for the amount of a particular enzyme and its value is typically given in the product specifications of a purchased enzyme instead of mass². One U is defined as the amount of the enzyme that produces a certain amount of enzymatic activity, and for this study, one unit is the amount that catalyzes the conversion of 1 micro mole of glucose substrate into 1 micro mole H₂O₂ per minute².

As previously mentioned, it was found that 10 mM H₂O₂ can enhance angiogenesis in wound healing, while 166 mM can retard wound closure³. In this chapter, the concentration of enzyme and glucose within the hydrogel required to produce 10-20 mM H₂O₂/day was determined.

3.2.1. Common bacterial species found in wound sites

The presence of bacteria in wounds may cause complications and slow the healing process. In a retrospective study performed on 213 patients by Bessa, et al., 2013, *Staphylococcus aureus* was found to be the most common bacterial species in different types of wounds (37%), followed by *Pseudomonas aeruginosa* (17%),

Proteus mirabilis (10%), *Escherichia coli* (6%) and *Corynebacterium spp.* (5%)⁴. Early chronic wounds contain mostly Gram-positive organisms while wounds that have not healed for several months that have a deep structure involvement which contain anaerobic and Gram-negative micro-organisms⁵.

3.2.2. Bactericidal effects of ROS

One of the objectives of this research was to synthesize a drug-free antibacterial material. As previously discussed in Chapter 1, honey contains enzymes which catalyze the formation of ROS from glucose and oxygen, that have the potential to prevent or inhibit bacterial infections. However, the antibacterial effect of ROS might come at the cost of cell cytotoxicity when ROS concentration exceeds a maximum value. Thus, by encapsulating glucose oxidase enzyme and glucose within a hydrogel, the rate of formation and release of hydrogen peroxide can be controlled at some extent. In this work, testing HB PEGDA/HA-SH hydrogel on several bacterial strains, some of which antibiotic-resistant, was aimed at observing its activity and measure zones of inhibition in relation to the GO enzyme concentration.

3.3. Materials and methods

Hyperbranched poly(ethylene glycol diacrylate) (HB PEGDA) was synthesized as discussed in Chapter 2.

Glucose, Titanium oxysulfate (TiOSO₄), Sulfuric acid (H₂SO₄), Glucose oxidase enzyme (E.C. 1.1.3.4), Phosphate buffer solution tablets (PBS 7.4), Hank's buffer

solution, High-Glucose Dubelcco's Modified Eagle Medium (DMEM), Fetal Bovine Serum (FBS), Resazurin sodium salt, Penicillin-Streptomycin (PS) were provided by Sigma Aldrich, UK. Thiolated Hyaluronic acid (HA-SH, 80% degree of thiolation, 400 kDa) was provided by Vornia Ltd., Ireland. NIH/3T3 mouse fibroblast cells (ATCC® CRL-1658™) were obtained from ATCC, UK.

Experiments on ROS characterization and cytocompatibility testing in NIH/3T3 mouse fibroblast cells were performed in Professor Wenxin Wang's Wound Healing and Skin Research Laboratory in Charles Institute of Dermatology, School of Medicine, University College Dublin, Ireland. Antibacterial agar diffusion tests (described in the next paragraph) were performed by the PhD candidate Ayesha Idrees (Politecnico di Torino) during her secondment period at Universtätsklinikum Knappschafts Krankenhaus Bochum – Department of Experimental Surgery/ Clinic of Surgery under Dr. Jochen Salber's supervision, as a part of the EU Horizon 2020 "HyMedPoly" project. A. Idrees also performed cell tests on hydrogels prepared by J.M. Vasquez, which are discussed in A. Idrees's accepted PhD thesis.

3.3.1. Glucose oxidase

Glucose oxidase is a protein dimer with the molecular weight of 160 kDa⁶. The active site where the glucose binds is located in a deep pocket. The ideal pH for glucose oxidation is 5.5 but it can be performed over a pH range of 4-7. The activity of this enzyme is quantified in terms of units. The commercially available enzyme that we utilized in these studies has an activity of 19,290 U/g. This value was used to stoichiometrically calculate the amount required to prepare a stock GO solution of 10,000 U/L in PBS at pH 7.4.

3.3.2. Preparation of HB PEGDA/HA-SH hydrogel with glucose oxidase/glucose for the formation of ROS

Enzyme solutions listed in Table 3.1 grouped as Solution A were prepared from the 10,000 U/L stock solution by dilution with PBS at pH 7.4 until the desired concentration was obtained. A volume of Solution A was mixed with an equal volume of 40 w/w% HB PEGDA solution to obtain Solution B. For comparison on the ROS produced between two different polymer compositions in the hydrogel with an identical enzyme concentration, 1000 U/L solution A was mixed with 20 w/w% HB PEGDA and 10 w/w% HB PEGDA; the end product was a hydrogel with 250 U/L in HB PEGDA/HA-SH 10-1.0 and HB PEGDA/HA-SH 5.0-1.0.

Table 3.1. Enzyme concentrations prepared for ROS formation in hydrogel.

Enzyme solution in PBS 7.4 (U/L) (Solution A)	Concentration in HB PEGDA (U/L) (Solution B)	Enzyme Concentration in hydrogel (U/L)	Enzyme Concentration Code in graphs
0	0	0	0
100	50	25	25 U/L
200	100	50	50 U/L
500	250	125	125 U/L
1000	500	250	250 U/L
2000	1000	500	500 U/L

Glucose solutions, grouped under Solution C and listed in Table 3.2, were prepared by dissolving glucose in PBS at pH 7.4. A volume of Solution C was mixed with an equal volume of 4 w/w% HA-SH in order to obtain Solution D.

Table 3.2 Glucose concentrations prepared for ROS formation in hydrogel.

Glucose solution prepared (w/w%) (Solution C)	Concentration in HA-SH (w/w%) (Solution D)	Concentration in hydrogel (w/w%)	Code in graphs
20	10	5	5.0%
10	5	2.5	2.5%
1	0.5	0.25	0.25%
0	0	0	0

Solution B was mixed with an equal volume of Solution D. After several seconds for proper dispersion, the mixture solution was pipetted into beads or cylindrical molds as described in Chapter 2. Using the HB PEGDA/HA-SH hydrogel 10.0/1.0 containing 250 U GO, and 2.5 w/w% glucose, Figure 3.1 illustrates the preparation of solutions B and D before they are combined together to form a hydrogel.

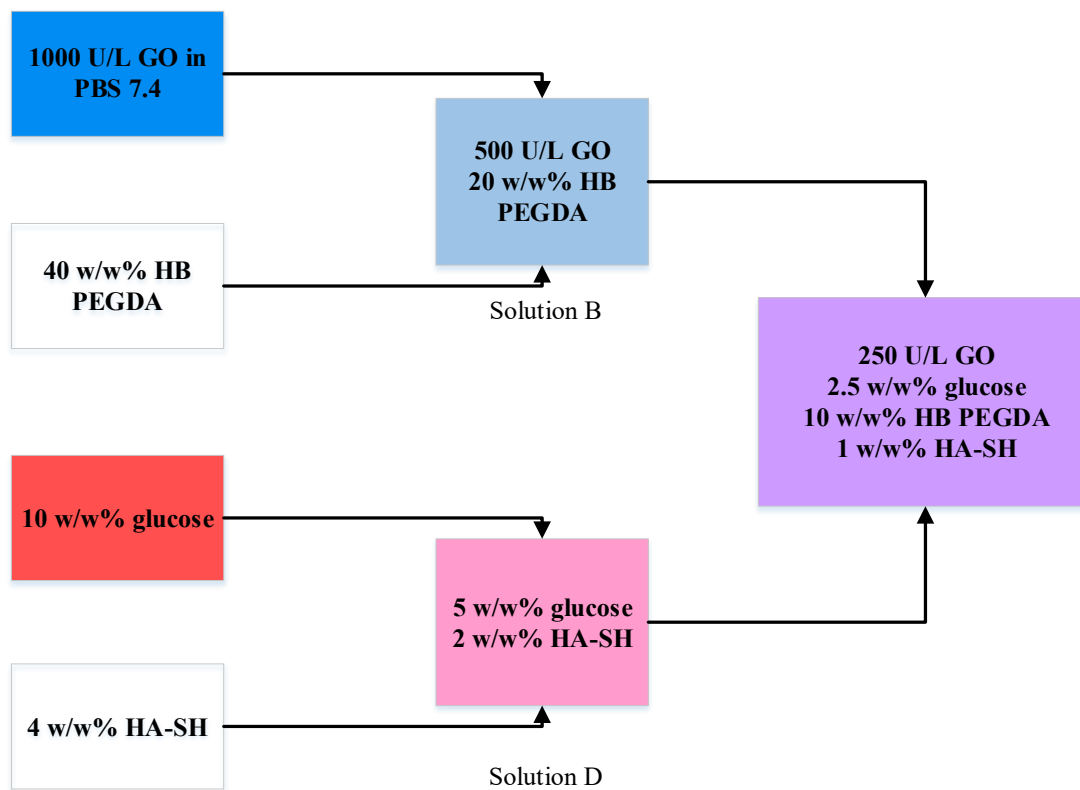
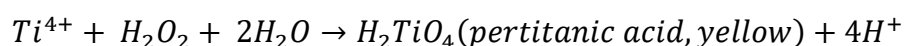


Figure 3.1: Preparation of HB PEGDA/HA-SH hydrogel containing GO and glucose.

The moment the hydrogel is formed as a crosslinked semi-rigid gel is considered as the initial time point ($t = 0$) in time-related characterizations such as the concentration of ROS produced at a particular time point.

3.3.3. Pertitanic acid assay for the analysis of hydrogen peroxide formation and release

Once the GO and glucose have been combined, it is assumed that they begin to produce H₂O₂. The production of hydrogen peroxide was quantified by colorimetric pertitanic assay⁷. The assay solution was prepared by dissolving 25 grams of TiSO₄ in 1 L of 2M sulfuric acid (H₂SO₄) solution. The reaction that occurs with H₂O₂ is:



The amount of pertitanic acid can be used to identify the amount of H₂O₂ formed by measuring solution absorbance intensity at the wavelength of 407 nm. For obtaining the standard curve, 100 μL of solutions with 0-20 mM H₂O₂ were pipetted into a 96-well plate as shown in Figure 3.2. Then, 50 μL of the prepared assay solution (ROS assay solution) was added into each well containing a sample. The plate was shaken in the the plate reader for 15 s before the absorbance was read in a SpectraMax M3 Multi-Mode Microplate Reader (Molecular Devices), with Soft-Max Pro Software used to obtain and analyze the data.

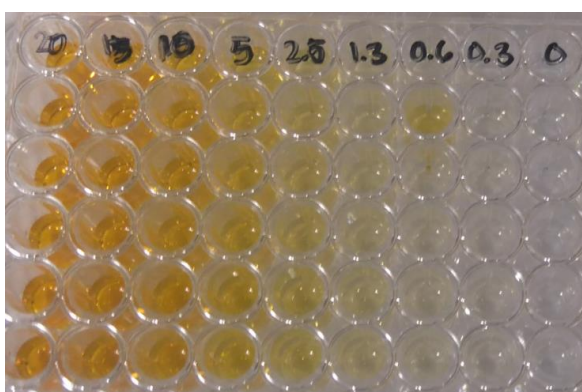


Figure 3.2: Standard solutions of H₂O₂ with ROS assay solution.

The equation to obtain the H₂O₂ concentration (mM) can be derived from the standard curve shown in Figure 3.3.

$$H_2O_2 = \frac{\text{Absorbance} - 0.0724}{0.1777} \quad (\text{eq.5})$$

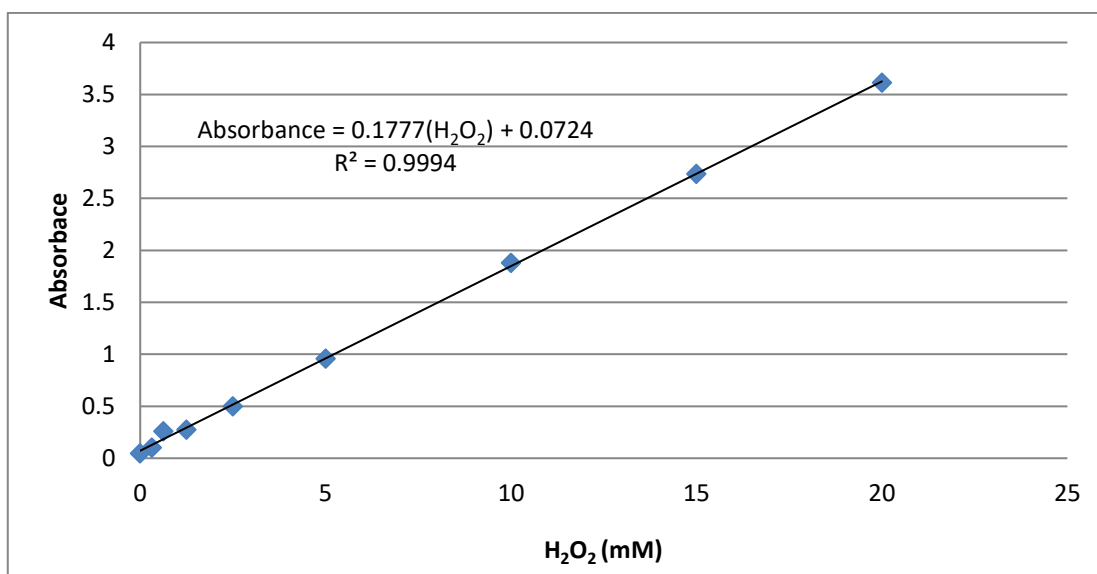


Figure 3.3: Calibration curve of H₂O₂ by the pertitanic acid assay.

To measure the H₂O₂ produced by a hydrogel at a given time point, 200 μL of hydrogel was placed in a scintillation vial. Afterwards, 9800 μL PBS pH 7.4 was added as the medium for H₂O₂ diffusion. These vials were placed in an incubator at 37°C to simulate body temperature. 100 μL of this solution was transferred to a 96-well plate. The absorbance was then measured at 407 nm after adding 50 μL ROS assay solution and shaking the plate to allow the reaction to occur. This diluted concentration was then used to calculate the actual concentration of H₂O₂ produced and released from the hydrogel. Each measurement was done in 4 replicates.

3.3.4. Alamar Blue cytocompatibility tests

Before the hydrogel samples were prepared for this test, the polymer solutions B and D were sterilized by passing the solutions through a 0.25 μm syringe filter. All preparation steps were performed inside a fume hood and UV-sterilized apparatus was used.

Hydrogel samples were prepared by pipetting 30 μL of the pre-crosslinked hydrogel solution on a hydrophobic Teflon surface. The hydrophobic material creates a surface tension with the solution, hence the hydrogel forms a semi-spherical bead as previously shown in Figure 2.13.

Hydrogels were tested for cytocompatibility using a non-contact method by placing them in a transwell insert in a 24-well plate as illustrated in Figure 3.4. In this cytocompatibility assay, the viability of the cells was tested while H_2O_2 was continuously produced and released into the cell medium.

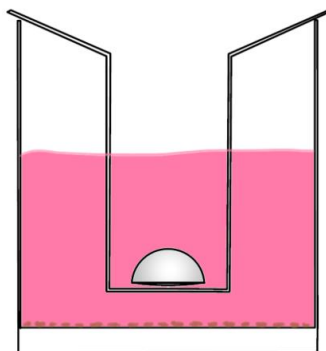


Figure 3.4: Illustration of HB PEGDA/HA-SH hydrogel in a 24-well plate in DMEM medium with NIH/3T3 cells on well surface. Diameter of hydrogel, transwell insert, and individual well are in scale relative to each other.

Cytotoxicity of the HB PEGDA/HA-SH hydrogel was evaluated using NIH/3T3 mouse fibroblast cells (ATCC® CRL-1658™). Briefly, cell suspension containing 30,000 cells/mL was cultured in full cell medium (High-Glucose Dulbecco's

Modified Eagle Mixture, containing 10 v/v% Fetal Bovine Serum, and 1 v/v% Penicillin-Streptomycin) in a 24-well plate. Then, 1 mL of the prepared full cell medium was added to each well and incubated at 37°C overnight.

The day after the cells were incubated, the wells were washed with sterile Hanks Buffer Solution. Afterwards, 1 mL of fresh full cell culture medium was added to each well and transwell inserts containing hydrogel samples were placed. Positive control (PC) for this experiment was a set of wells that did not contain any hydrogel or transwell insert. Each setup was done in 4 replicates.

The plate was incubated for 24 hours at 37°C, after which the Alamar Blue assay was performed. The transwell inserts were removed and the cells were washed once again. Then 1 mL of Alamar Blue solution was added to each well, and the plate was returned to incubate for 6 hours at 37°C. Alamar Blue solution was prepared by dissolving 3 mL of resazurin blue in 27 mL Hanks Buffer Solution to obtain a 10 v/v% Alamar Blue solution.

The absorbance and fluorescence were then measured using the SpectraMax M3 Multi-Mode Microplate Reader (Molecular Devices) with the preset method Alamar Blue (AB) protocol to quantify the value of each well. This value was obtained from taking the fluorescence measurements at 530-560 nm and the absorbance measurements at 570 nm and 600 nm which the protocol processed and simplified into a single final reading. The percent cell viability was calculated as:

$$\begin{aligned} & \textit{Cell viability (\%)} \\ &= \frac{\textit{Reading of Sample Well} - \textit{Reading of Alamar Blue}}{\textit{Reading of No treatment Well} - \textit{Reading of Alamar Blue}} \\ & * 100\% \quad (\textit{eq. 6}) \end{aligned}$$

3.3.5. Agar diffusion test

In testing for the antibacterial activity of the honey-mimetic hydrogels, the agar diffusion test method was used. According to the protocol, a suspension of the bacteria ($1-2 \times 10^8$ CFU/mL) was prepared to a McFarland 0.5, then spread evenly onto an appropriate agar (such as Müller-Hinton agar) in a Petri dish. The agar typically contains (w/v%): 30.0% beef infusion, 1.75% casein hydrolysate, 0.15% starch, 1.7% agar with the pH adjusted to neutral at 25 °C⁸. Thermo Scientific Oxoid wafer discs are loaded with antibiotic solution (Oxacillin for Gram-positive bacteria and Gentamicin for Gram-negative bacteria) and placed onto the surface of the agar. For this set of experiments, the HB PEGDA/HA-SH 10-1.0 (w/w%) hydrogel half-spherical beads loaded with 0-500 U/L GO enzyme and 2.5 w/w% glucose were placed on agar surface. After 24 hours of incubation at 37°C, zones of growth inhibition around each of the hydrogel beads were measured to the nearest millimeter. Data was presented as images of these petri dish samples and compiled into a graph of inhibition zone diameter versus glucose oxidase concentration in hydrogel. Samples were done in duplicates.

Bacterial strains used were: *Staphylococcus aureus* (ATCC 29213 of wound source), *Staphylococcus epidermidis* (ATCC 12228), *Escherichia coli* (ATCC 25922), *Pseudomonas aeruginosa* (ATCC 27853), *A. baumannii*. Antibiotic-resistant strains used were: Methicillin-resistant *Staphylococcus aureus* (MRSA), Methicillin-resistant *Staphylococcus epidermidis* (MRSE), VIM-2 producing drug resistant *Pseudomonas aeruginosa*, and KPC-2 producing drug resistant *Escherichia coli*.

3.4. Results and discussion

3.4.1. H₂O₂ production in HB PEGDA/HA-SH

Effect of enzyme concentration on ROS production

Figure 3.5 shows the H₂O₂ concentrations with a varying amount of glucose oxidase enzyme (at constant 2.5 w/w% glucose concentration) produced within a span of 24 hours in HB PEGDA/HASH 10.0-1.0 hydrogel. This set-up was performed in static conditions.

ROS production increased as a function of enzyme concentration from 25 to 250 U/L, while keeping constant the glucose concentration at 2.5 w/w%. However, statistical analysis showed that there was no significant increase in ROS production between 250 U/L and 500 U/L enzyme concentration with production of 9.11 ± 0.92 and 8.21 ± 0.47 mM H₂O₂, respectively. Since the objective was to have a hydrogel producing 10-20 mM H₂O₂/day, GO concentrations of 250 U/L and 500 U/L were selected. Statistical analysis ($p = 0.06$) showed that the hydrogen peroxide concentrations between 250 U/L and 500 U/L were not significantly different.

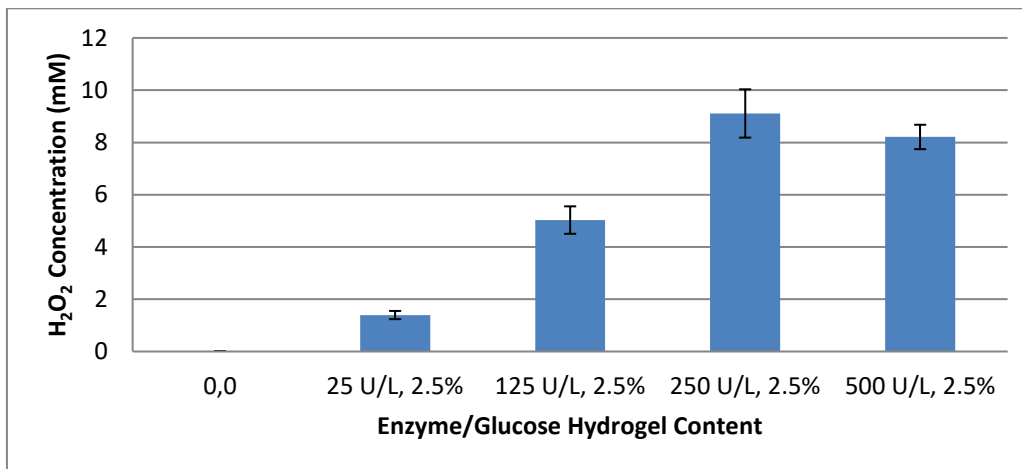


Figure 3.5: H₂O₂ concentration after 24 hours from HB PEGDA/HASH 10.0/1.0 hydrogels containing varying amounts of enzyme and 2.5 w/w% glucose. Release was obtained in static conditions.

Hydrogel composition: 10 w/w% HB PEGDA/1 w/w% HA-SH.

Effect of mixing and glucose concentration on H₂O₂ production

Figure 3.6 shows H₂O₂ production from hydrogels with two enzyme concentrations (250 and 500 U/L) and two glucose concentrations (2.5 and 5.0 w/w %). In this experiment, slightly higher concentrations of hydrogen peroxide were obtained by putting the samples in an incubator shaker operating at 15 rpm instead of using a stationary incubator. Agitation improved the efficiency of the GO and glucose to form hydrogen peroxide. An independent-sample t-test was conducted to compare ROS production with or without shaking (using the measurements with parameters held constant: 250 U/L GO, 2.5 w/w% glucose in HB PEGDA/HA-SH 10-1.0). There was a significant difference in the ROS concentrations using the non-shaking method (9.07 ± 0.67 mM H₂O₂) and with shaking method (16.02 ± 4.16 mM H₂O₂) conditions ($p < 0.01$). These results suggest that incubating the samples in an incubator shaker produces a higher H₂O₂ production than incubating the samples without any agitation, as expected. The subsequent experiments were conducted in an incubator shaker.

In determining the effect of glucose concentration on the ROS production, an independent-sample t-test was conducted to compare 2.5 w/w% glucose versus 5.0 w/w% glucose with 250 U/L GO at 24 hours in HB PEGDA/HA-SH 10-1.0. There was no significant difference in the 2.5 w/w% glucose (16.02 ± 4.16 mM H_2O_2) and 5.0 w/w% glucose (19.53 ± 3.36 mM H_2O_2) conditions ($p = 0.18$). This was due to glucose oxidase being the limiting agent, producing hydrogen peroxide at a rate depending on its enzyme activity. Thus, using 250 U/L GO, optimal glucose concentration was 2.5 w/w% after 24 h.

Similar results are obtained for the three other settings, when time and enzyme concentration were held constant: no significant difference in ROS concentration when the glucose concentration was increased from 2.5 w/w% to 5.0%. Hence for each time and enzyme concentration, optimal glucose concentration was 2.5 w/w%.

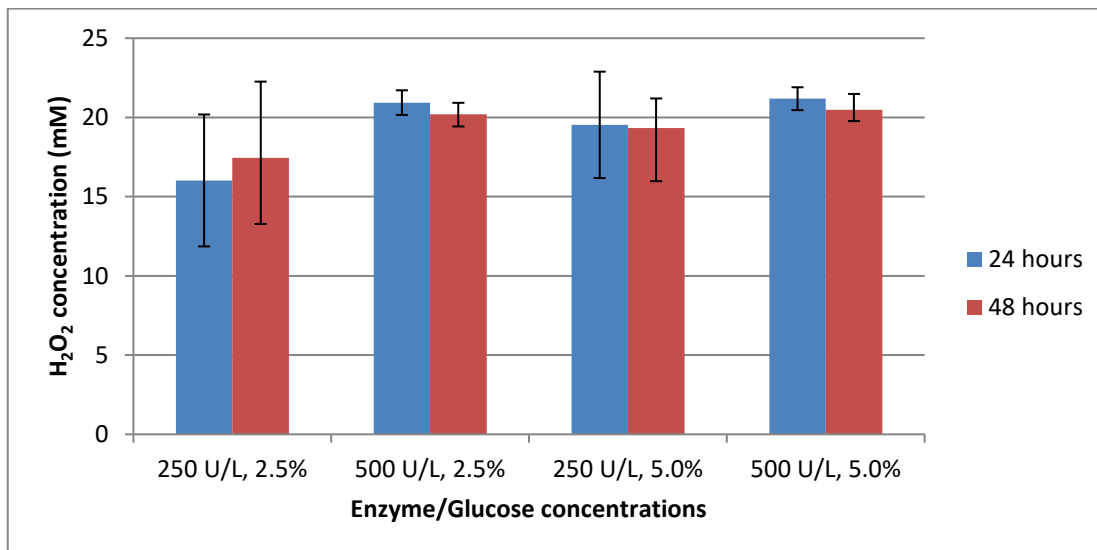


Figure 3.6: H_2O_2 production from HB PEGDA/HASH 10.0/1.0 hydrogel with 250 U/L and 500 U/L GO and 2.5 w/w% and 5.0 w/w% glucose concentrations. Measurements were obtained at $t = 24$ hours and $t = 48$ hours. Release was obtained in an incubator shaker operating at 15 rpm.

Hydrogel composition: 10 w/w% HB PEGDA/1 w/w% HA-SH.

H₂O₂ Formation Profile at Varying Hydrogel Compositions

Figure 3.7 shows H₂O₂ concentration produced from hydrogels with different polymer compositions (HB PEGDA/HASH 10.0/1.0 and 5.0/1.0) and as a function of time. The concentration of H₂O₂ was found to increase with time. In the case of HB PEGDA/HASH 5.0/1.0, this concentration reached a peak at 24 hours, as glucose progressively reduced during the reaction and/or diffused out of the hydrogel network.

The hydrogels based on 5 w/w% HB PEGDA produced more hydrogen peroxide consistently at different time points except at 48 hours. However, the independent-samples t-test that compared H₂O₂ production in HB PEGDA/HA-SH 10-1.0 and HB PEGDA/HA-SH 5.0-1.0 (at 24 hours, 250 U/L GO, and 2.5 w/w% glucose parameters held constant) showed that this difference was not statistically significant ($p = 0.18$). This suggested that hydrogel composition did not significantly affect ROS production, therefore it would be preferable to use HB PEGDA/HA-SH 10-1.0 as it has other interesting properties for wound healing applications, such as shape retention, water stability for longer and quick crosslinking, respect to HB PEGDA/HA-SH 5.0-1 hydrogel.

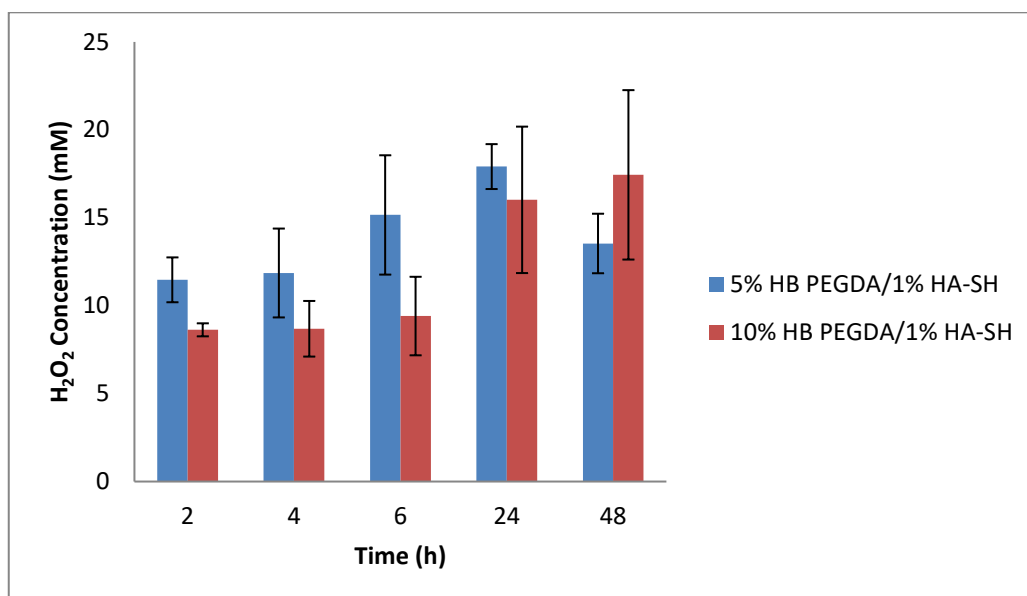


Figure 3.7: H₂O₂ concentration produced by HB PEGDA/HASH 10.0/1.0 and 5.0/1.0 hydrogels containing 250 U/L GO, 2.5 w/w% glucose at different time points. Release was obtained in an incubator shaker operating at 15 rpm.

A drop in H₂O₂ production 24 hours to 48 hours was observed from for HB PEGDA/HASH 5.0/1.0 hydrogel. Statistical results showed that this decrease was significant. This could be due to a release of glucose from the less concentrated hydrogel into the medium or to the saturation of the solution with H₂O₂ and its incubation at 37°C for an extended period of time causing H₂O₂ to decompose into water and oxygen (hydrogen peroxide decomposition requires two H₂O₂ molecules to decompose in the balanced equation: $2H_2O_2 \rightarrow 2H_2O + O_2$). HB PEGDA/HA-SH 10-1.0 showed a superior concentration, therefore both glucose and H₂O₂ were probably slowed down.

3.4.2. Alamar Blue cytocompatibility tests

Figure 3.8 and 3.9 show the results of the cytocompatibility of NIH/3T3 mouse fibroblasts when indirectly incubated for 24 hours with HB PEGDA/HA-SH 10-1.0

loaded with 0-20 mM H₂O₂ (Figure 3.8) and GO enzyme/glucose (Figure 3.9) for 24 hours. The hydrogels were placed in transwell inserts with the produced H₂O₂ diffusing into the cell culture media. PC represents the positive control, the set of wells with no treatment and used as a reference for calculating the cell viability. In Figure 3.8 and 3.9, NIH/3T3 mouse fibroblast cells grown in tissue culture plates served as the positive control. In Figure 3.8, the samples (except the positive control) were hydrogels loaded with different concentrations of hydrogen peroxide to initially test their cytocompatibility in concentrations similar to those produced by the GO/glucose loaded hydrogels from Figures 3.5 to 3.7. Non-contact cytocompatibility analysis showed that the cell viability for these hydrogels were higher than 100% which means that hydrogels with 0-20 mM H₂O₂ were cytocompatible with NIH/3T3 cells.

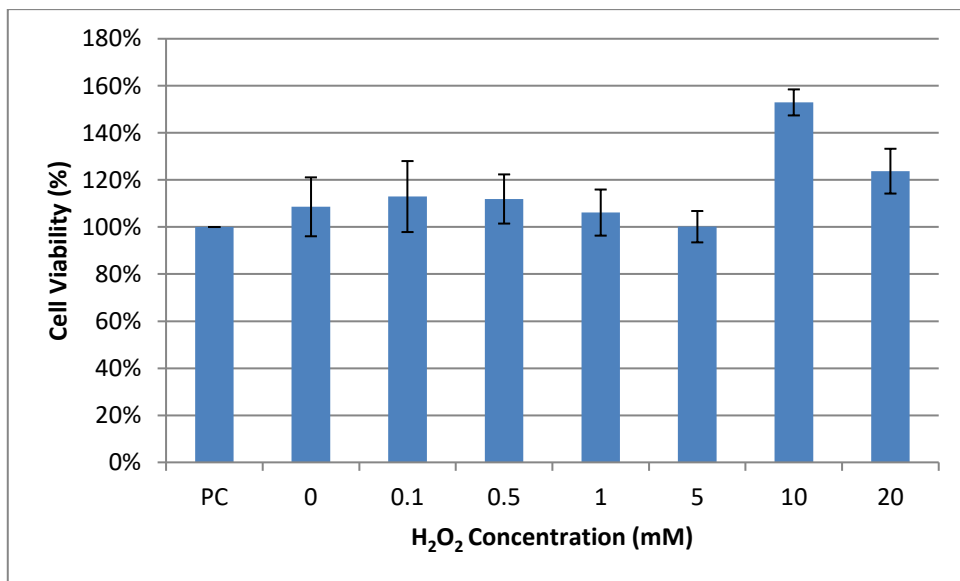


Figure 3.8 : Cell viability of NIH/3T3 cells with HB PEGDA/HA-SH 10.0/1.0 hydrogels loaded with different concentrations of H₂O₂ after 24 hours after 24 hours in a static release (non-shaken method) set-up.

Non-contact cytocompatibility data in Figure 3.9 included different conditions.

Some of these conditions (2.5 U/L GO-0.25% glucose; 2.5 U/L GO-2.5% glucose; 25 U/L GO-0.25% glucose; 25 U/L-2.5% glucose) did not reach the target H₂O₂ concentration range of 10-20 mM/day, however they were also included in the cytocompatibility analysis.

Figure 3.9 shows positive cell viability in all GO/glucose concentrations except for 500 U/L-2.5% and 1000 U/L-2.5% (cell viability less than 80%).

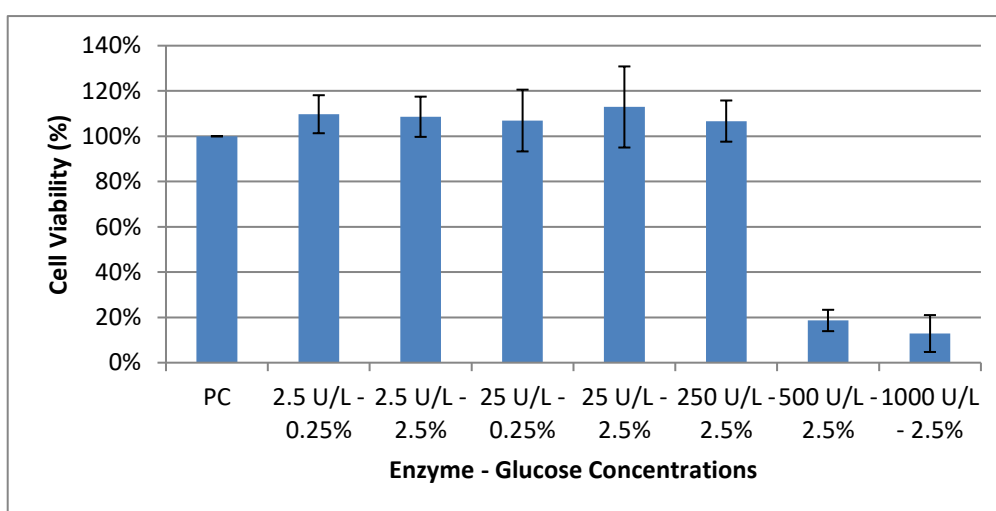


Figure 3.9: Cell viability of NIH/3T3 cells with HB PEGDA/HA-SH 10.0/1.0 hydrogels loaded with varying GO/glucose concentrations after 24 hours in a static release (non-shaken method) set-up.

Results showed that with 20 mM H₂O₂ production (Figure 3.8), a cytocompatibility of 123% with respect to the positive control was measured. However, in Figure 3.9, cell viability analysis for hydrogels with 500 U/L GO -2.5% glucose (expected to produce 8.21±0.47 mM H₂O₂ in 24 hours) showed their significantly lower cytocompatibility of 19%. This lower cytocompatibility could be attributed to the differences in the rate of released H₂O₂ between the systems, i.e. it is likely the majority of the H₂O₂ in the hydrogels of Fig. 3.8 was released in the first hours, decomposing into water and oxygen after 24 h.

GO-glucose amounts of 1000 U/L-2.5% (Fig. 3.9) were added to confirm the low cytocompatibility with high GO concentration. Thus, the highest tested cytocompatible concentration was 250 U/L glucose oxidase with 2.5 w/w% glucose for NIH/3T3 mouse fibroblast cells.

3.4.3. Antibacterial testing results

Disc diffusion results are shown in Figures 3.10 to 3.12 and sorted according to tested bacterial type: Gram-positive (Fig. 3.10) and Gram-negative bacteria (Fig.3.11. and Fig. 3.12). The overall trend was that increasing the GO enzyme concentration increased the measured zone of inhibition. Also, it can be observed that the hydrogels produced greater zones of inhibition in the Gram-positive group than in the negative group. This is likely due to the Gram-positive bacteria's lack of an outer cell membrane which made them more vulnerable to the oxidative damage ROS like H_2O_2 produced. Even antibiotic resistant Gram-positive bacteria displayed zones of inhibition as seen in Figure 3.10.

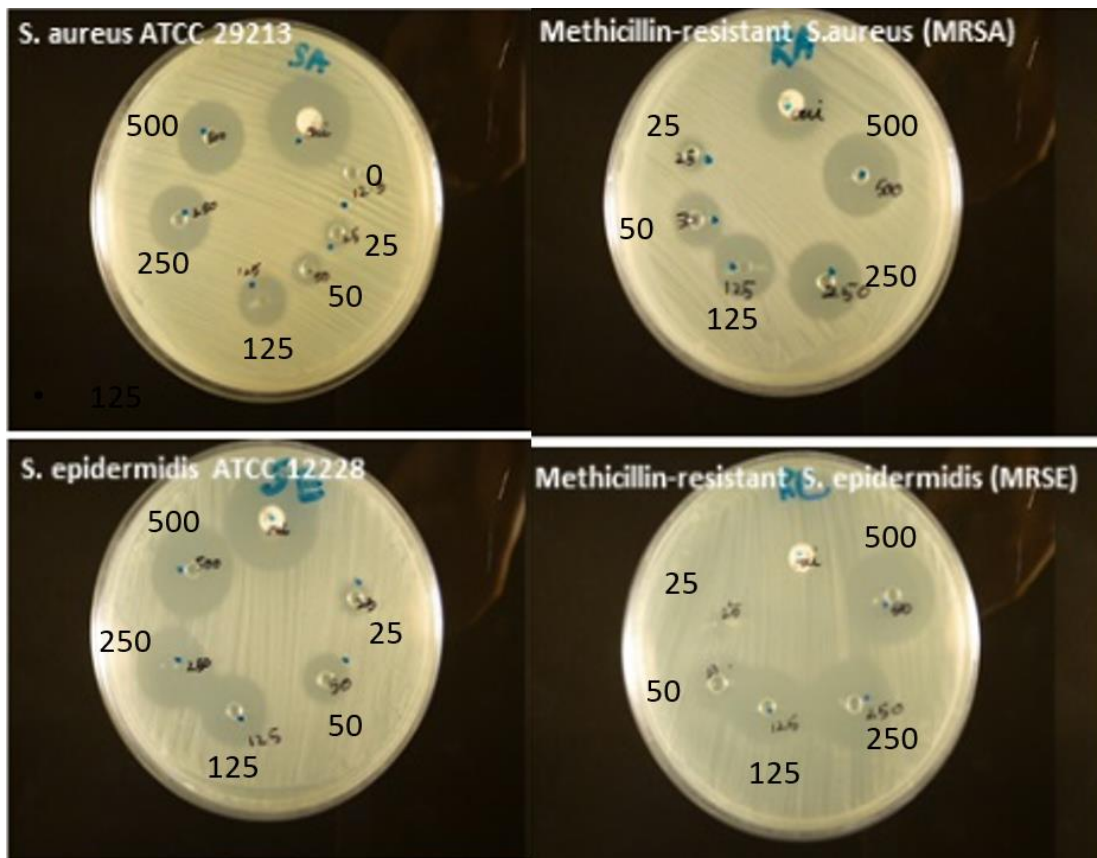


Figure 3.10: Results of antibacterial agar diffusion tests on Gram-positive bacteria with HB PEGDA/HA-SH hydrogel 10-1.0 with fixed 2.5 w/w% glucose and varying GO concentrations labelled from 25-500 U/L (Data obtained from Ayesha Idrees).

From Figures 3.11 and 3.12, the zones of inhibition of the Gram-negative bacteria appeared more reduced and were present only in concentrations 250 U/L and 500 U/L. To obtain a proper assessment of the zones of inhibition, they were measured using ImageJ software and are presented in Figures 3.13 and 3.14

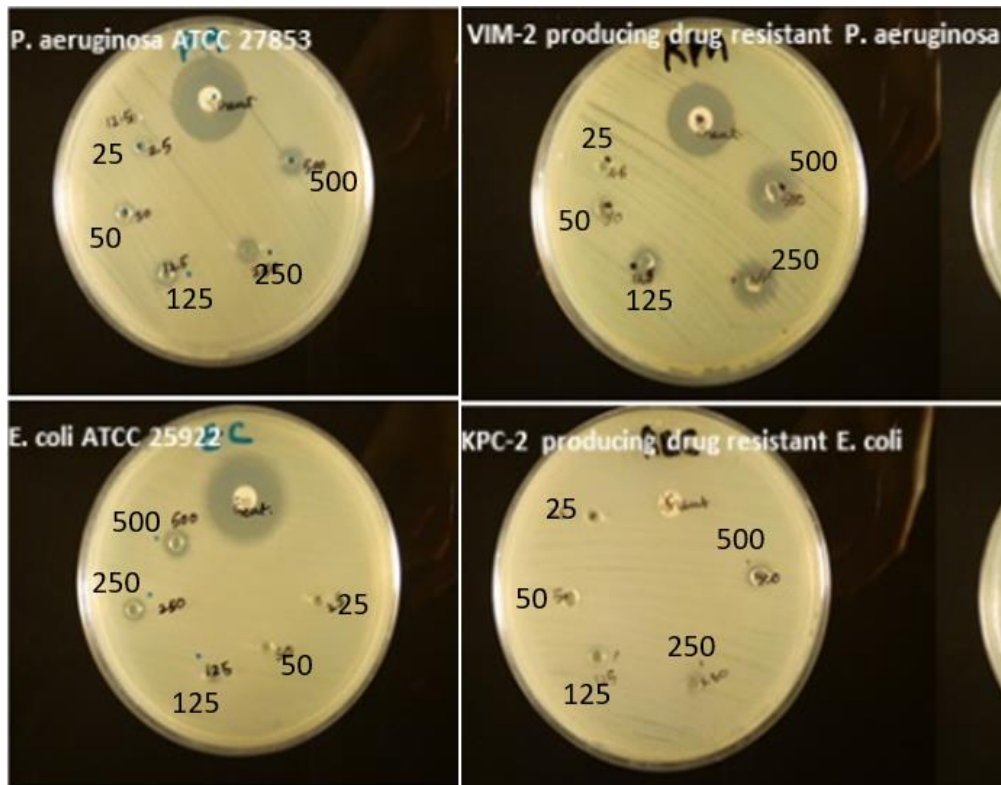


Figure 3.11: Part 1 of results of antibacterial agar diffusion tests on Gram-negative bacteria with HB PEGDA/HA-SH hydrogel 10-1.0 with fixed 2.5 w/w% glucose and varying GO concentrations labelled from 25-500 U/L (Data obtained from Ayesha Idrees).

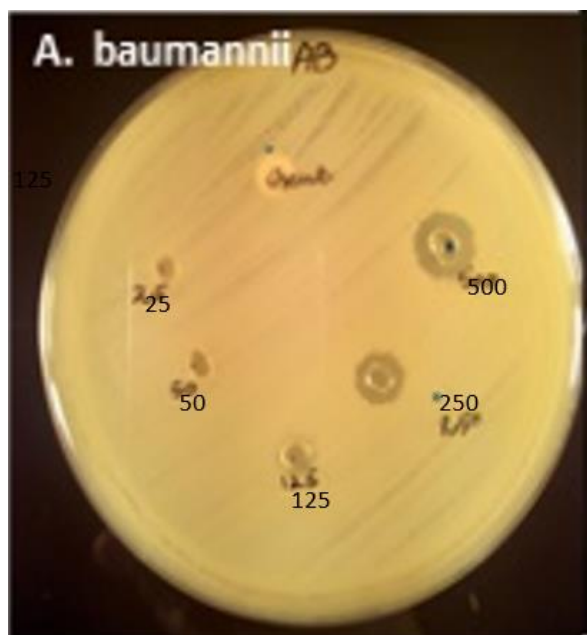


Figure 3.12: Part 2 of results of antibacterial agar diffusion tests on Gram-negative bacteria (*A. baumannii*) with HB PEGDA/HA-SH hydrogel 10-1.0 with fixed 2.5 w/w% glucose and varying GO concentrations labelled from 25-500 U/L (Data obtained from Ayesha Idrees).

From Figures 3.13 and 3.14, the zones of inhibition were measured and grouped according to the GO concentrations used and type of bacteria. Figure 3.13 shows the zone of inhibition values of Gram-positive bacteria and Figure 3.14 shows the zone of inhibition values of Gram-negative data.

Figure 3.13 shows that at a concentration as low as 25-50 U/L, zones of inhibition could be measured for MRSA and MRSE. It is possible that the altered structure of MRSA and MRSE made them more vulnerable to hydrogen peroxide than their *S. aureus* and *S. epidermidis* counterparts. As the concentration is increased to 125 U/L, zones of inhibition were observed in *S. aureus*, *S. epidermidis*.

In 125 U/L the zones of inhibition for MRSA and MRSE were increased, meaning that increasing the GO concentration increases the antibacterial activity within the same bacterial strain. While inhibition zones were observed much earlier for the

antibiotic-resistant bacteria, their normal strains displayed larger zones of inhibition in later concentrations

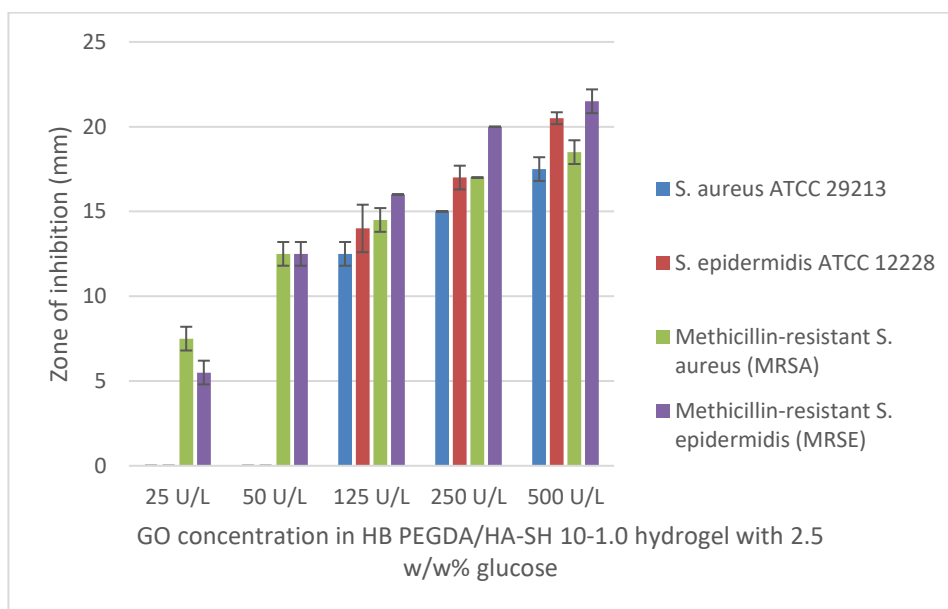


Figure 3.13: Measured zones of inhibition of the HB PEGDA/HA-SH 10-1.0 (with 2.5 w/w% glucose) containing different GO concentrations for Gram-positive bacteria (Data obtained from Ayesha Idrees).

In Figure 3.14, no zones of inhibition were observed for 25 U/L and 50 U/L glucose oxidase, which meant that they had no antibacterial activity for the Gram-negative bacteria at these particular GO concentrations. As the concentration is increased to 125 U/L, zones of inhibition were observed in *P. aeruginosa*, and VIM-2 producing drug-resistant *P. aeruginosa*. Further increasing the concentration to 250 U/L, *E. coli* and *A. baumannii* displayed zones of inhibition, thus this concentration showed antibacterial activity already in 8 out of the 9 bacterial species used.

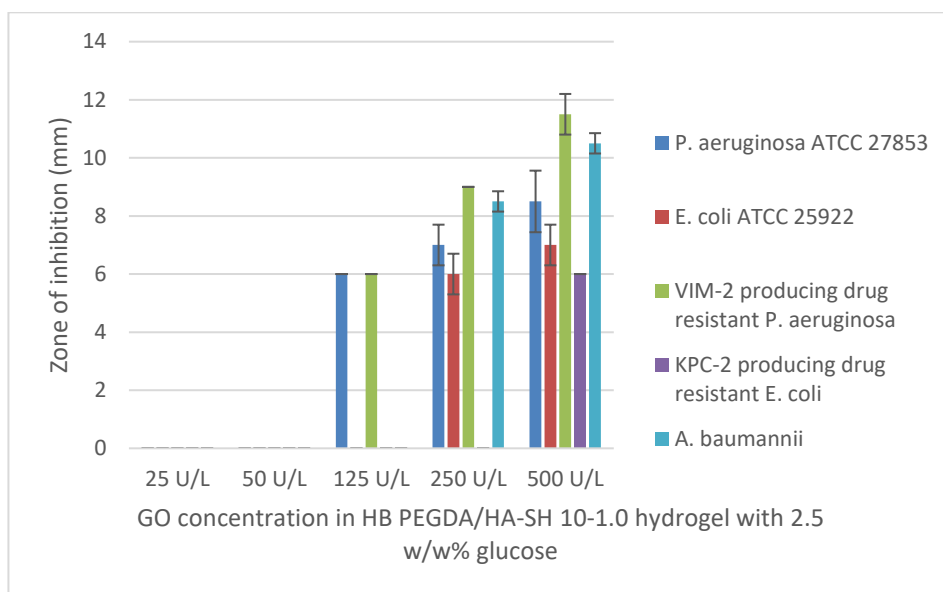


Figure 3.14: Measured zones of inhibition of the HB PEGDA/HA-SH 10-1.0 (with 2.5 w/w% glucose) containing different GO concentrations for Gram-negative bacteria (Data obtained from Ayesha Idrees).

The highest GO concentration at which NIH/3T3 mouse fibroblasts showed positive cell viability was 250 U/L. The 500 U/L GO enzyme concentration did not have a positive cell viability with NIH/3T3 mouse fibroblasts (see Par. 3.4.2) but was nonetheless tested for antibacterial activity. Results showed that at this concentration, inhibition zones were observed in KPC-2 drug resistant *E. coli*. However, the use of a concentration of 500 U/L GO to produce H₂O₂ could be applied only for applications where bacteria can be primarily attacked, e.g. as a first treatment of highly infected wounds. Alternatively, in the future efforts should be spent to the development of novel tailored delivery systems able to deliver ROS only to bacteria and not to cells.

3.5. Conclusions

Glucose oxidase and glucose produced ROS in the form of hydrogen peroxide within an *in situ* HB PEGDA/HA-SH (10-1.0 and 5.0-1.0) hydrogel with the former being the more preferred hydrogel composition to use in terms of its physical characteristics (lower gelling time and higher water absorption and shape stability). In 24 hours in an incubator shaker (37°C, 15 rpm), 250 U/L GO and 2.5 w/w% glucose in the HB PEGDA/HA-SH 10-1.0 hydrogel produced 16.02 ± 4.16 mM H₂O₂. This same material produced also 9.11 ± 0.92 mM H₂O₂ in static conditions. This concentration, and those lower than it, were cytocompatible in *in vitro* tests using NIH/3T3 mouse fibroblast cells.

Hydrogen peroxide continuously produced by the HB PEGDA/HA-SH 10-1.0 (w/w%) hydrogel loaded with 250 U/L GO and 2.5 w/w% glucose demonstrated antibacterial activity in several strains of bacteria, primarily Gram-positive bacteria (*S. aureus*, *A. baumannii*, *S. epidermidis*, and *A. baumannii*) and antibiotic-resistant Gram positive bacteria (MRSA, MRSE). It showed antibacterial activity, albeit with lower zones of inhibition on Gram-negative bacteria (*E. coli* and *P. aeruginosa*) and antibiotic-resistant *P. Aeruginosa*. When the concentration was increased from 250 U/L to 500 U/L GO in the hydrogel, the material demonstrated additionally antibacterial activity on antibiotic resistant *E. coli*. However, as cytocompatibility in NIH/3T3 mouse fibroblast cells within 24 hours was only positive up to the concentration of 250U/L, the best antibacterial activity accompanied by positive cell viability was achieved using HB PEGDA/HA-SH 10-1.0 (w/w%) with 250 U/L GO and 2.5 w/w% glucose.

The results obtained from this chapter allowed the researchers to select HB PEGDA/HA-SH 10-1.0 (w/w%) with 250 U/L GO and 2.5 w/w% glucose as a promising hydrogel, to be used as a drug-free antibacterial wound dressing for

combatting antimicrobial resistance, especially considering it displays antibacterial activity in three antibiotic-resistant bacteria.

3.6. References

- (1) Toone, E. J.; Nord, F. F. *Advances in Enzymology : And Related Areas of Molecular Biology*; Wiley, 2011.
- (2) NC-IUB. Units of Enzyme Activity. *Eur. J. Biochem.* **1979**, *97*, 319–320.
<https://doi.org/10.1111/j.1432-1033.1979.tb13116.x>.
- (3) Loo, A. E. K.; Wong, Y. T.; Ho, R.; Wasser, M.; Du, T.; Ng, W. T.; Halliwell, B. Effects of Hydrogen Peroxide on Wound Healing in Mice in Relation to Oxidative Damage. *PLoS One* **2012**, *7* (11).
<https://doi.org/10.1371/journal.pone.0049215>.
- (4) Bessa, L. J.; Fazii, P.; Di Giulio, M.; Cellini, L. Bacterial Isolates from Infected Wounds and Their Antibiotic Susceptibility Pattern: Some Remarks about Wound Infection. *Int. Wound J.* **2015**, *12* (1), 47–52.
<https://doi.org/10.1111/iwj.12049>.
- (5) Dow, G.; Browne, A.; Sibbald, R. G. Infection in Chronic Wounds: Controversies in Diagnosis and Treatment. *Ostomy. Wound. Manage.* **1999**, *45* (8), 23–27, 29-40; quiz 41-2.
- (6) Glucose Oxidase Product Sheet
<https://www.sigmaaldrich.com/content/dam/sigma-aldrich/docs/Sigma/Datasheet/7/g2133dat.pdf> (accessed May 24, 2018).
- (7) Eisenberg, G. Colorimetric Determination of Hydrogen Peroxide. *Ind. Eng. Chem. Anal. Ed.* **1943**, *15* (5), 327–328.
<https://doi.org/10.1021/i560117a011>.
- (8) Sandle, T. *Pharmaceutical Microbiology : Essentials for Quality Assurance and Quality Control*.

Chapter 4 Functionalization of HB PEGDA for Glucose Oxidase Immobilization

4.1. Abstract

An improvement to the HB PEGDA/HA-SH hydrogel system is to redesign the hyperbranched polymer to have functionalities for enzyme grafting. Covalent immobilization of the GO enzyme into a hyperbranched substrate, in contrast to simple encapsulation of the enzyme within the hydrogel as described in Chapter 3, may provide some benefits, such as a prolonged enzyme activity within the hydrogel, both avoiding its diffusion and protecting the enzyme from possible degradation or denaturation. Through Deactivation-Enhanced Atom Transfer Radical Polymerization (DE-ATRP) a hyperbranched polyethylene glycol diacrylate-co-glycidyl methacrylate (HB PEGDA-co-GMA or HB PcG) was synthesised with PEGDA to GMA molar ratio of 5:1. The epoxy group of the glycidyl methacrylate can be exploited for reaction with the amine and amide groups of the GO enzyme. ¹H NMR analysis suggested successful GO immobilization to the the HB PcG polymer. The HB PcG demonstrated similar

characteristics to HB PEGDA in its ability to crosslink and form a hydrogel when mixed with HA-SH solution. Gelation time ranged from 1.1 to 9.4 minutes depending on HB PcG and HA-SH concentration. This hydrogel was able to swell to a maximum of 139% of its weight at day 20 and underwent complete dissolution/degradation after 6 days. Using 250 U/L GO and 2.5 w/w% glucose (the ideal GO and glucose concentrations established for HB PEGDA/HA-SH 10-1.0 honey-mimetic hydrogen peroxide-producing system) 8.3 mM H₂O₂ was produced after 24 hours. However, HB PEGDA-co-GMA/HA-SH 10-1.0 hydrogel showed less cytocompatibility when compared to HB PEGDA/HA-SH 10-1.0 hydrogels with the same enzyme/glucose concentration . For example, while HB PEGDA/HA-SH 10-1.0 with 250 U/L GO, and 2.5 w/w% glucose had a cell viability of 107% when using NIH/3T3 cells after 24 hours, HB PEGDA-co-GMA/HA-SH 10-1.0 only had 65% cell viability. This means that while HB PEGDA-co-GMA has the potential to be used as an enzyme immobilizing material, able to form a hydrogel *in situ* with HA-SH, its biocompatibility is still suboptimal. Improvements to the system can be done by decreasing the molar ratio of GMA with respect to HB PEGDA to decrease the cytotoxic effect of its epoxide groups. An alternative is to ensure the epoxide groups are successfully deactivated, either by reacting and immobilizing the enzyme or by the addition of some other reagent (such as converting it into an alcohol functional group). This activity was performed in Professor Wenxin Wang's Wound Healing and Skin Research Laboratory in Charles Institute of Dermatology, School of Medicine, University College Dublin, Ireland.

4.2. Introduction

4.2.1. Enzyme immobilization

Enzyme immobilization onto a substrate provides many benefits. These include being able to reuse the enzyme without diffusing into its surrounding environment (e.g. enzymes entering and coming into contact with wound tissue) or being washed away by solvents in *in vivo* or *in vitro* experiments, stabilizing the enzyme, and increasing the thermal stability of the enzyme¹. Enzymes may be immobilized physically binding them to a substrate or by chemical conjugation. Covalent binding of enzymes to substrates may exploit the reaction between the lateral reactive groups of the enzymes (e.g. -NH₂ groups in arginine and lysine, -CONH₂ in glutamine, and -SH in cysteine) with functional groups in the substrate such as imidazole, indolyl, phenolic hydroxyl, etc¹.

Glucose oxidase is often used as the model enzyme in immobilization tests. It has been immobilized in various substrates such as surface-grafted acrylic acid electroactive polyaniline films, pyrolytic graphite (based on simple absorption methods), and pyrrole-functionalized polystyrene²⁻⁴. In creating a more stable, covalently immobilized substrate it is necessary to modify the material into a copolymer or surface modify it in order to have the immobilizing functional groups.

4.2.2. Methods for immobilizing glucose oxidase

In one study performed by Valentova et al., 1981 glucose oxidase was immobilized on two substrates: bead cellulose and a copolymer containing glycidyl methacrylate (GMA)⁵. Through a shake flask method, glucose oxidase was dissolved in a PBS buffer solution with pH 7.5, then the carrier material was incubated for 16 hours at

4°C. As glycidyl methacrylate, shown in Figure 4.1 contains a vinyl group and an epoxy group (also known as an oxirane group), the vinyl group can be used for free radical polymerization to create a hyperbranched copolymer by reacting with polyethylene glycol diacrylate (PEGDA).

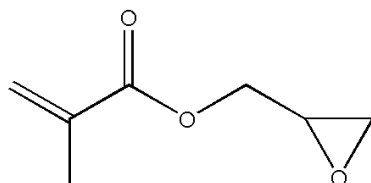


Figure 4.1: Chemical structure of glycidyl methacrylate.

Possible reactions of certain amino acids in the protein with the oxirane group are shown in Figure 4.2. These amino acids may also react with other groups as aldehydes, as shown in a study performing lipase immobilization in poly(vinyl acetate [PVA]-acrylamide) microspheres⁶. Glucose oxidase has also been immobilized in PVA nanofibres for sensor applications⁷. A hyperbranched copolymer can also be made from these other monomers, but for this study the focus will be on an epoxide-functionalized copolymer.

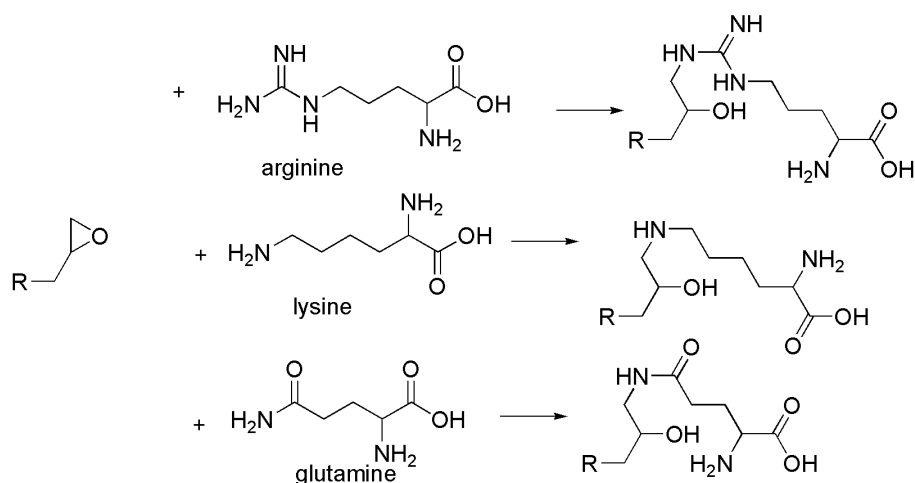


Figure 4.2: Possible reactions of lateral side groups in GO enzyme with a polymer containing an epoxide functional group.

This reaction has been already described for HB PEGDA synthesis in Chapters 2 and 3. In the final bifunctional HB polymer, the epoxy group may react with the amine and amide groups found in the GO enzyme. Another variation in Valentova's study is that the polymer substrate synthesized in this study is liquid and can form a hydrogel when mixed with a thiolated polymer via Michael addition crosslinking. In most immobilization studies, the enzymes are immobilized onto a solid substrate (eg. electrodes, films, beads) and can be separated from the enzyme medium by simple decanting and washing. In this proposed polymer synthesis, recovering the copolymer with immobilized enzymes from the rest of the not immobilized enzymes requires liquid-liquid separation methods, such as centrifugation.

As a side note, another study has immobilized glucose oxidase in a polydopamine-coated substrate⁸. This method of immobilizing glucose oxidase will be investigated in later chapters 5 to 8 as an alternative form of GO immobilization. This system makes use of the quinone groups found in polydopamine which react with available amine, amide, or thiol groups in the enzyme via Michael addition reaction.

4.2.3. Synthesis reaction for HB PEGDA-co-GMA and GO grafting strategy

HB PEGDA was synthesized in Wenxin Wang's Wound Healing and Skin Research Laboratory both through RAFT (discussed in Chapter 2) and DE-ATRP. The reason why DE-ATRP synthesized HB PEGDA was not discussed in detail was that it self-crosslinked while undergoing lyophilization for removal of water and trace organic solvents after dialysis.

On the other hand, DE-ATRP was used for synthesizing HB PEGDA-co-GMA copolymer as it tends to give higher molar conversion yields than RAFT synthesis during the comparison of DE-ATRP-synthesized HB PEGDA (62.0%) with RAFT-synthesized HB PEGDA (32.5%, reported in Chapter 2). The theoretical structure of HB PEGDA-co-GMA is presented below in Figure 4.3.

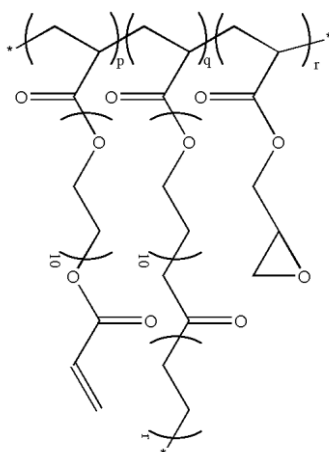


Figure 4.3. Chemical structure of HB PEGDA-co-GMA or HB PcG.

When GO enzyme is mixed with the HB PcG polymer solution and reacted with the polymer substrate at 4 °C for at least 16 hours in a flask with continuous shaking, a reaction, as shown in Figure 4.4, is expected to occur⁵. This immobilization step should leave the vinyl groups intact and allow them to react via Michael-addition thiol-ene crosslinking with a polymer such as thiolated hyaluronic acid.

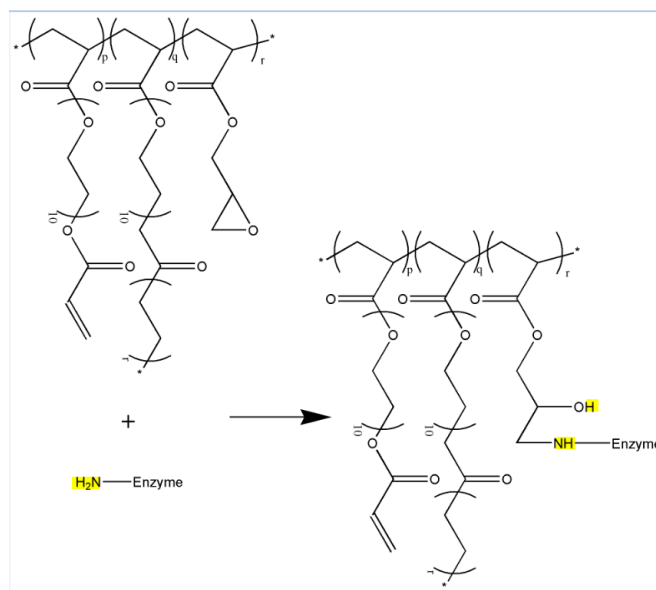


Figure 4.4: Immobilization of glucose oxidase in HB PEGDA-co-GMA.

DE-ATRP is a free radical polymerization reaction which differs from RAFT in that it makes use of a metal catalyst in the initiation and propagation steps to have a higher rate of reaction than the termination stage. When a radical is generated in the ATRP system, there are three possible situations: 1) propagation with the monomer, 2) termination, 3) deactivation into dormant species⁹. These reactions can happen simultaneously with the dominant event depending on its rate relative to the other two. Figure 4.5 depicts the general steps that occur in an ATRP synthesis, with copper (II) chloride as the metal catalyst.

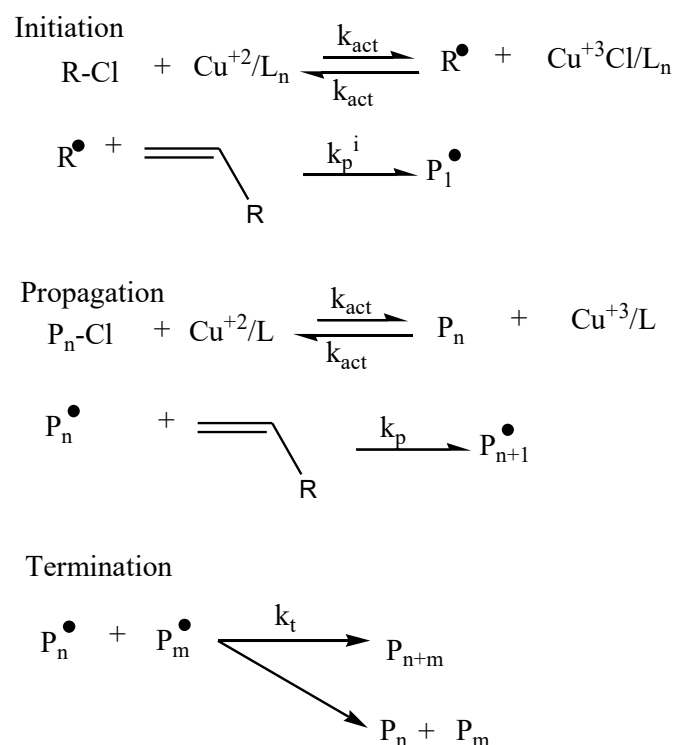


Figure 4.5: Steps in general ATRP synthesis with copper (II) chloride as the metal catalyst. L = ligand

Following a similar DE-ATRP synthesis performed by A, et al., 2017, HB PEGDA-co-GMA was synthesized using the similar reagents for the metal catalyst, initiator, ligand, and reducing agent¹⁰.

4.3. Materials and Methods

Polyethylene glycol diacrylate (PEGDA, MW 575), glycidyl methacrylate (GMA), ethyl α -bromoisobutyrate (EBriB), N,N,N',N'',N''-Pentamethyldiethylenetriamine (PMDETA), copper (II) chloride, ascorbic acid, hexane, butanone, acetone, aluminium oxide (Al₂O₃), diethyl ether, glucose, glucose oxidase enzyme (GO, E.C. 1.1.3.4), phosphate buffer solution pH 7.4 (PBS), Hank's buffer solution, high-

glucose Dubelcco's modified eagle medium (DMEM), fetal bovine serum (FBS), resazurin sodium salt and penicillin-streptomycin (PS) were bought from Sigma Aldrich, UK. Thiolated Hyaluronic acid (HA-SH, 80% degree of thiolation, 400 kDa) was provided by Vornia Ltd., Ireland. NIH/3T3 mouse fibroblast cells (ATCC® CRL-1658™) were obtained from ATCC, UK.

Experiments were performed in Professor Wenxin Wang's Wound Healing and Skin Research Laboratory in Charles Institute of Dermatology, University College Dublin, Ireland.

4.3.1. Synthesis of HB PEGDA-co-GMA

HB PEGDA-co-GMA (PEGDA to GMA molar ratio of 5:1) was synthesized via DE-ATRP synthesis. Briefly, in a 250 mL double-neck flask, the following reagents were dissolved in 120 mL butanone: 34.5 g PEGDA, 2.13 g GMA, 3.90 g EBriB (initiator), 86.65 mg PMDETA (ligand), and 67.23 mg copper (II) chloride (metal catalyst). The solution was sealed and purged with Argon for 30 minutes. After that, 22 mg of ascorbic acid dissolved in 100 μ L H₂O (reducing agent) was added. The solution was purged with Argon again for another 15-20 minutes. It was then sealed and placed into an oil bath at 50°C for 6-8 hours. Samples were taken out hourly to be analyzed by GPC analysis to monitor the molecular weight increase of the polymer and the molar conversion. When the molecular weight reached 10-20 kDa, the reaction was stopped by removing the mixture from the heating bath and opening the flask to let oxygen enter to prevent polymer gelling within the flask.

The polymer was purified first by precipitating in a 2:1 volume ratio of diethyl ether: hexane solution. After the precipitating the polymer (which settled into the bottom layer), the solution of diethyl ether and hexane (containing the unreacted

monomers and other reagents) was decanted, 30 mL of acetone was added to decrease the viscosity for the next stage, the removal of the copper catalyst.

A chromatography column was prepared in order to remove the copper from the solution afterwards. As shown in Figure 4.6, the column was prepared by assembling layers, from bottom to top of: 1-2 cm cotton, 2-4 cm sand, 20-30 cm aluminum oxide, and approximately 0.5 cm sand again (to cover aluminum oxide and prevent it from being removed).



Figure 4.6: a) Separation column for removing copper from the polymer solution, b) an up-close look at the color change as CuCl_2 forms a complex with Al_2O_3

At the bottom of the separation column a double neck flask was placed, with one neck connected to the column and the other to a vacuum pump. This column was washed with acetone first to wet the column before the polymer solution was poured down. Excess solvents were removed from the recovered polymer solution in an evaporating flask before being dialyzed and freeze-dried for the final step of the purification process. It was noted that DE-ATRP synthesized HB PcG was more stable than DE-ATRP synthesized HB PEGDA as it did not self-crosslink in the lyophilization process. It is probable that the addition of the epoxide group inhibited the contact between the acrylate groups from interacting with each other, as later results would show that HB PcG contained a lower vinyl content than HB PEGDA.

4.3.2. Chemical characterization of HB PEGDA-co-GMA

The procedure for chemical characterization was then same applied for HB PEGDA and described in Chapter 2, section 2.3.4, except that for every hourly sample taken from the reacting flask for GPC analysis, the copper was removed by passing the sample through a Pasteur pipette containing aluminum oxide and cotton (to prevent the Al_2O_3 passing through the pipette). Afterwards 100 μL of this polymer solution (containing varying amounts of butanone, formed polymer, and monomers) was diluted in 900 μL dimethyl formamide (DMF). Additionally, the final sample for GPC analysis was prepared by dissolving 3 mg of polymer in 1 mL of Dimethyl Formamide (DMF).

The DMF-dissolved samples were filtered (0.45 μm pore size) through a filter syringe into small amber GPC vials. The samples were analyzed in an Agilent 1260 Infinity GPC/SEC system (Agilent Technologies) to monitor molecular weight, molar conversion and polydispersity as the reaction proceeded. The used system is

equipped with a refractive index detector (RI), with two columns in series (30 cm PLgel mixed-C), eluted using DMF (containing 0.1% LiBr) as mobile phase.

For characterizing molecular structure, ^1H Nuclear Magnetic Resonance (NMR) was used. The final polymer samples were dissolved in chloroform-D (CDCl_3) and ^1H NMR analysis was carried out on a 400 MHz Varian NMR spectroscopy system. Data were analyzed using MesReNova 6.1 processing software.

Chemical characterization from the ^1H NMR spectra calculated the degree of hyperbranching based on vinyl groups and the amount of available epoxide groups. According to literature, HB polymers are characterized to have abundant functional groups, an irregular 3D topology, low viscosity, and high solubility¹¹. These particular properties make them ideal to be used as one of the components in an *in situ* formed hydrogel system. Their low viscosity and high solubility allow these polymers to be dissolved easily in an aqueous solution as pre-hydrogel polymer solution. Their 3D topology and abundant functional groups allow ease of contact when reacting with HA-SH thiol groups and the formation of a mechanically strong hydrogel structure.

4.3.3. Preparation of HB PEGDA-co-GMA/HA-SH hydrogels

To prepare hydrogel samples for further characterization, HB PEGDA-co-GMA (or HB PcG) polymer was dissolved in 1X 7.4 PBS buffer at concentrations from 10-20 w/w% (Table 1). HA-SH solution was prepared at a concentrations of 1-4 w/w% (Table 1). To form a hydrogel, equal volumes of HB PcG and HA-SH solutions were mixed and pipetted into a 7.5 mm diameter cylinder mold or into a teflon surface to form a bead. Total volume of this hydrogel cylinder was 200 μL (hydrogel has a height of approximately 5 mm).

Table 4.1: Composition of prepared HB PcG/HA-SH hydrogels

Hydrogel code	HB PcG solution concentration - Prehydrogel (% wt./wt.)	HA-SH solution concentration - Prehydrogel (% wt./wt.)	Hydrogel relative HB PcG/HA-SH amount (dry wt./dry wt.)	Overall hydrogel composition (wt./wt.)
5.0-1.0	10.0	2.0	5.0 : 1.0	6.0%
10-1.0	20	2.0	10.0 : 1.0	11.0%
10-2.0	20	4.0	5.0 : 1.0	12.0%

Except for gelation time and cytocompatibility assays, characterizations were performed only on HB PEGDA-co-GMA/HA-SH 10.0-1.0 to compare its properties with those of HB PEGDA/HA-SH 10-1.0 hydrogel.

4.3.4. Characterization of HB PEGDA-co-GMA/HA-SH hydrogel

4.3.4.1. Gelation time

The gelation time for the hydrogels was obtained using the vial-tilt method¹². Briefly, 500 μ L HB PEGDA-co-GMA solution was combined with 500 μ L HA-SH solution, using the concentrations collected in Table 2.1. These vials were tilted side to side and observed for 5 s. The gelation was considered complete when no flow was observed for 5 s.

4.3.4.2. Rheological properties

Rheometry was performed on a TA Discovery Hybrid Rheometer-2 (DHR-2) with 8 mm and 20 mm diameter parallel plates and TRIOS software for analysis of data.

With the aim of determining the rheological properties of the HB PEGDA-co-GMA/HA-SH hydrogels, detailed dynamic rheological assessments were conducted on hydrogels. Rheological profiles were obtained by pipetting excess 90 μL pre-forming HB PEGDA/HA-SH hydrogel (the individual components were mixed, but the solution was still liquid) into the rheometer plate, at room temperature. The 8 mm disc plate was lowered until a height of 1.5 mm was achieved. Estimated volume of analyzed hydrogel was 75.4 μL .

Storage moduli (G') and loss moduli (G'') were measured from sweep tests. A frequency sweep profile (at 10% strain) was obtained at a range of 0.1 to 100 Hz. Strain sweep profile (at 10 Hz) was obtained at a range of 0.1% to 100% strain.

4.3.4.3. Swelling and degradation profile

In order to determine the water absorption profile of hydrogels, 200 μL samples of 10-1.0 and 5.0-1.0 HB PcG/HA-SH hydrogels were prepared. These samples were placed in pre-weighed 20 mL scintillation vials and weighed. Then 2 mL 1X 7.4 pH PBS was added to these vials. The samples were incubated at 37°C.

At different time points (initially every 2 hours for the first 8 hours, then every 24 hours for the first week, then every 2 days onward up to 4 weeks), PBS was removed and the vial containing hydrogel was weighed. After weighing, 2 mL of fresh PBS solution was added again and the vial was returned to the incubator. Measurements were performed in quadruplicates.

Water absorption was calculated based on this formula, taken from Chapter 2:

$$\text{Percent absorption} = \frac{W_t - W_0}{W_0} * 100\% \quad (\text{eq. 4})$$

Where W_t = weight of hydrogel at time point t in, W_0 = initial weight of the hydrogel.

Degradation was observed when the water absorption percentage was negative. The time for complete degradation was the time at which hydrogel could not be observed any more in the PBS solution.

4.3.5. Immobilization of glucose oxidase

Glucose oxidase was immobilized by dissolving an excess amount (4000 U/L) of glucose oxidase into a 10 w/w% solution of HB PEGDA-co-GMA. The solution was placed in a shaker for 96 hours in 4°C. Afterwards, the solution was placed in a centrifuge vial and centrifuged at 11,000 RPM for separating the unimmobilized enzyme. Separation was possible as the polymer had a higher density than water and two phases were observed after centrifugation; a yellowish polymer at the bottom and a clear liquid on top. The supernatant was removed and H₂O was added for further centrifugation. The final product (a water soluble, GO enzyme-conjugated HB PEGDA-co-GMA copolymer) was dissolved in chloroform-D (CDCl₃) and ¹H NMR analysis was carried out on a 400 MHz Varian NMR spectroscopy system. Data were analyzed using MesReNova 6.1 processing software. The results were compared with the spectrum of the control HB PEGDA-co-GMA polymer.

4.3.6. ROS production in HB PEGA-co-GMA/HA-SH

Following the procedure of making ROS-producing hydrogels in Chapter 3, Section 3.3.2, 250 U/L and 500 U/L GO- /2.5 w/w% glucose-loaded hydrogels were prepared. These two enzyme concentrations and one glucose concentration were selected from the range of previously used concentrations based on the most favorable results from the HB PEGDA/HA-SH experiments.

When preparing the HB PcG with GO enzyme solution, the pre-hydrogel solution was left to react for 96 hours at 4°C with the enzyme to allow immobilization to occur before being crosslinked with the glucose-loaded HA-SH solution.

ROS pertitanic acid assay sampling and protocol were similar to those described in Chapter 3, Section 3.3.3.

4.3.7. Alamar Blue cytocompatibility test

Alamar Blue cytocompatibility test sample preparation, protocol, and data analysis were similar to those performed in Chapter 3, Section 3.3.4.

4.4. Results and Discussion

4.4.1. Chemical characterization of HB PEGDA-co-GMA

GPC analysis showed that after 8 hours reaction polymer weight-average molecular weight (M_w) was 10,126 Da, number-average molecular weight (M_n) was 4,616 Da, polydispersity index was 2.2, and molar conversion from monomer to polymer

was 73.15%. These properties were obtained from the Agilent GPC software by integrating the GPC curve measured on samples polymerized at the corresponding time (Figure 4.7).

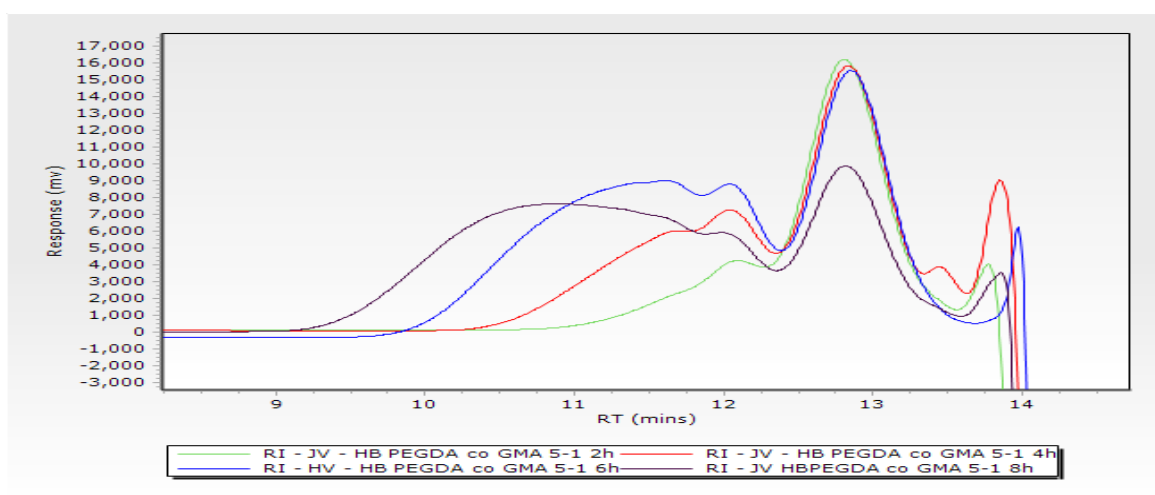


Figure 4.7: GPC profile of HB PEGDA-co-GMA (5:1 PEGDA to GMA molar ratio) synthesized via DE-ATRP reaction.

Comparing with the RAFT-synthesized HB PEGDA, the yield for this DE-ATRP reaction was approximately twice. However the homogeneity of the HB PcG polymer was lower given the high polydispersity index of 2.2 compared to HB PEGDA (1.5). This was likely due to the copolymer nature and the distribution of the GMA in the polymer chains causing irregularity.

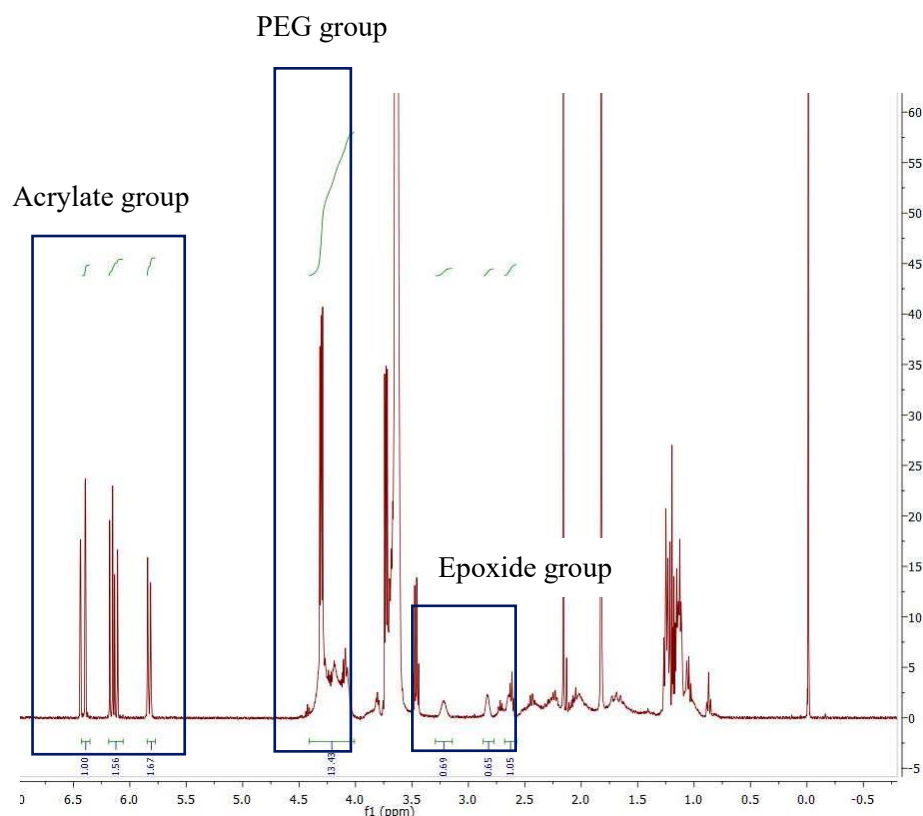


Figure 4.8: ^1H NMR spectrum of HB PEGDA-co-GMA (5:1).

^1H NMR spectra (Figure 4.8) allowed the analysis of the branched structure and amount of pendant acrylate groups. The pendant acrylate groups were identified as three characteristic chemical shifts at 6.4-5.8 ppm. The oxirane/epoxide group was identified as three shifts found at 2.6-3.3 ppm. The PEG groups were identified as the chemical shift at 4.34-3.95 ppm. Degree of hyperbranching was 29.8 mol% for vinyl group content and 19.4 mol% for epoxide group content. As the average degree of hyperbranching is between 40-60%, this material can be considered a low hyperbranched polymer based on vinyl content only. However, if degree of hyperbranching is based on its total functional groups (epoxide and vinyl), the degree of hyperbranching was 49.2 mol% which is an average degree of hyperbranching compared to the high degree of hyperbranching of HB PEGDA (57 mol%)¹³.

4.4.2. Gelation time

Gelation time results are shown in Figure 4.9. In comparing the gelation times of hydrogels based on HB PcG with those based on HB PEGDA at the same composition, HB PcG based hydrogels consistently required a higher time for crosslinking. This can be attributed to the lower vinyl content in HB PcG than in HB PEGDA. Like HB PEGDA/HA-SH hydrogels discussed in Chapter 2, Section 2.4.2.1, HB PcG/HA-SH demonstrated a similar trend with decreasing gelation times with an increase of polymeric material concentration.

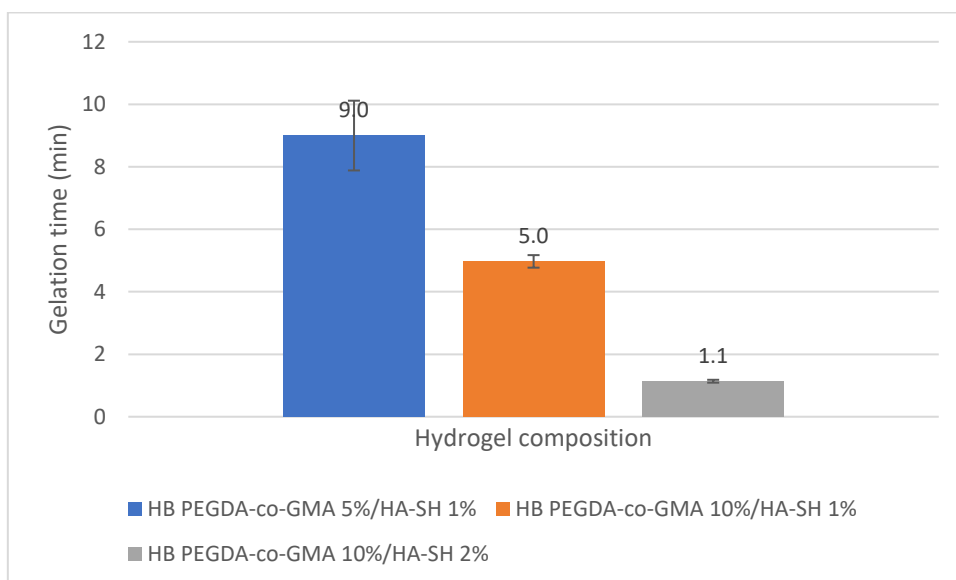


Figure 4.9: Gelation time of HB PEGDA-co-GMA/HA-SH hydrogels of varying compositions.

By increasing the HB PcG content from 5 w/w% to 10 w/w% in constant 1 w/w% HA-SH, the gelation time reduced from 9 minutes to 5 minutes, being 1.8 times faster. This change was less drastic than that observed for HB PEGDA/HA-SH 5.0-1.0 to 10-1.0 where the gelation time became 9.3 times faster. A possible reason is that the presence of epoxide groups in the hyperbranched copolymer interact as well with the thiol groups or inhibit the acrylate groups from reacting with the thiol

groups (it was observed that this polymer is less prone to self-crosslinking than DE-ATRP synthesized HB PEGDA). Another cause is due to the hyperbranched copolymer having a lower amount of vinyl groups per gram than the original material.

By increasing the HA-SH content from 1 w/w% to 2 w/w% in constant 10 w/w% HB PcG, the gelation time, the gelation time was 4.5 times faster. This can be attributed to the increased availability of HA-SH thiol groups coming into contact with the vinyl groups in HB PcG.

4.4.3. Rheological characterization of hydrogel

4.4.3.1. Frequency sweep

Recalling from Chapter 2, the frequency sweep profiles of the HB PcG/HA-SH hydrogels 10-1.0 and 5.0-1.0 at 10% oscillation strain are depicted in Figure 4.10. For a perfect solid, these storage and loss values are $G''=0$ and $G'=a \text{ finite value}$ ¹⁴. For a perfect liquid, $G''=a \text{ finite value}$ and $G'=0$ ¹⁴. As hydrogels are neither perfect solids or perfect liquids, their G' and G'' values are higher than zero. When $G''>G'$, the sample is considered more viscous than elastic (solution), when in $G''<G'$, the sample is more elastic than viscous (hydrogel). From Figure 4.10, in both 5.0-1.0 and 10-1.0 compositions, the storage modulus was higher than the loss moduli at each frequency, hence the material was in hydrogel form.

Storage modulus is also connected to how well-crosslinked a material is. A hydrogel that has more crosslinked junctions is able to store more deformation energy in an elastic manner. When comparing the G' values at the same frequency (e.g. 100 Hz), HB PEGDA/HA-SH 10-1.0 G' was 1.29 MPa and HB PcG/HA-SH

10-1.0 G' was 1.26 MPa. This result was found in each frequency measurement conducted for both hydrogels. This means both hydrogels showed approximately the same rheological properties.

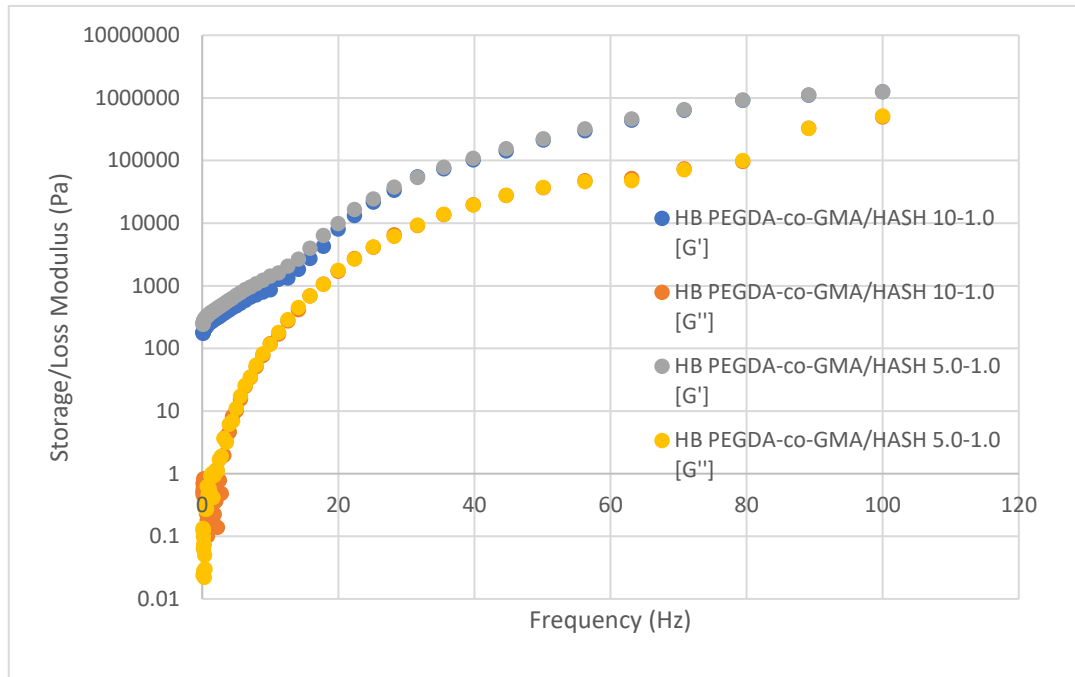


Figure 4.10: Frequency sweep of HB PEGDA-co-GMA/HA-SH 10-1.0 and 5.0-1.0 hydrogels at 10% strain.

4.4.3.2. Strain sweep

In Figure 4.11, the strain sweep profile of the HB PEGDA-co-GM/HA-SH 10-1.0 hydrogel is reported, at a constant frequency of 10 Hz. As in Figure 4.10, the storage modulus G' was higher than the loss modulus G'' at each strain which is characteristic of a hydrogel that behaves more like a solid than a liquid. However, with increasing the strain, G'' initially decreased, reaching a minimum, then increasing. The behavior of G' was similar, although the decrease was less pronounced and the minimum was reached at higher strain than for G'' . This is

from the material “relaxing” after the initial strain exerted on it¹⁵. Relating this to biomedical applications, the hydrogel showed the potential to undergo stresses during its use.

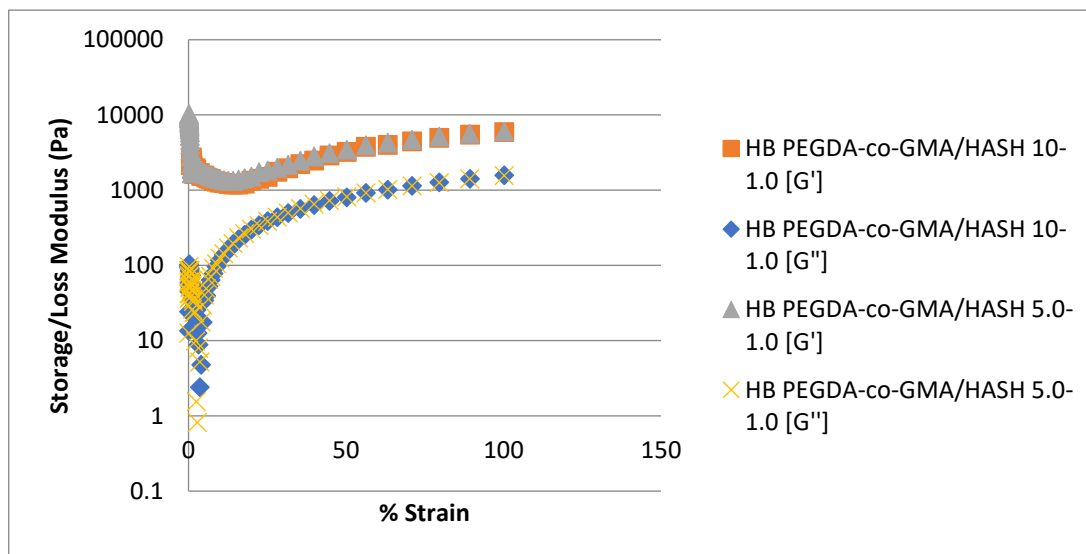


Figure 4.11: Strain sweep of HB PEGDA-co-GMA/HA-SH 10-1.0 and 5.0-1.0 hydrogels at 10 Hz oscillation frequency.

4.4.4. Physical characterization of hydrogel

4.4.4.1. Water adsorption profile

In Figure 4.12, HB PcG/HA-SH 10-1.0 showed a faster water uptake in the beginning than HB PEGDA/HA-SH 10-1.0. By day 20, the HB PcG hydrogel had already absorbed 139% of its weight in water while HB PEGDA showed only 13%. This rapid swelling however caused a faster degradation as the H₂O adsorbed by the hydrophilic parts of the hyperbranched polymer might have uncoiled the

polymer network and hydrolyzed some parts. After the measurement at day 22, the calculated water uptake was found to have dropped to 73% before complete degradation in PBS by day 26.

On the other hand, the water adsorption of HB PEGDA/HA-SH 10-1.0 hydrogel gradually increased with time and the hydrogel was still present after 43days.

HB PEGDA/HA-SH 10-1.0 as a hydrogel has a lower rate of degradation and lower initial water uptake than HB PEGDA-co-GMA/HA-SH 10-1.0 as the former has a higher vinyl content per gram polymer. This means that the HB PEGDA hydrogel is more crosslinked than HB PcG at the same weight concentration and its polymer chains uncoil and expand much slower as water permeates the interstices of the hydrogel matrix.

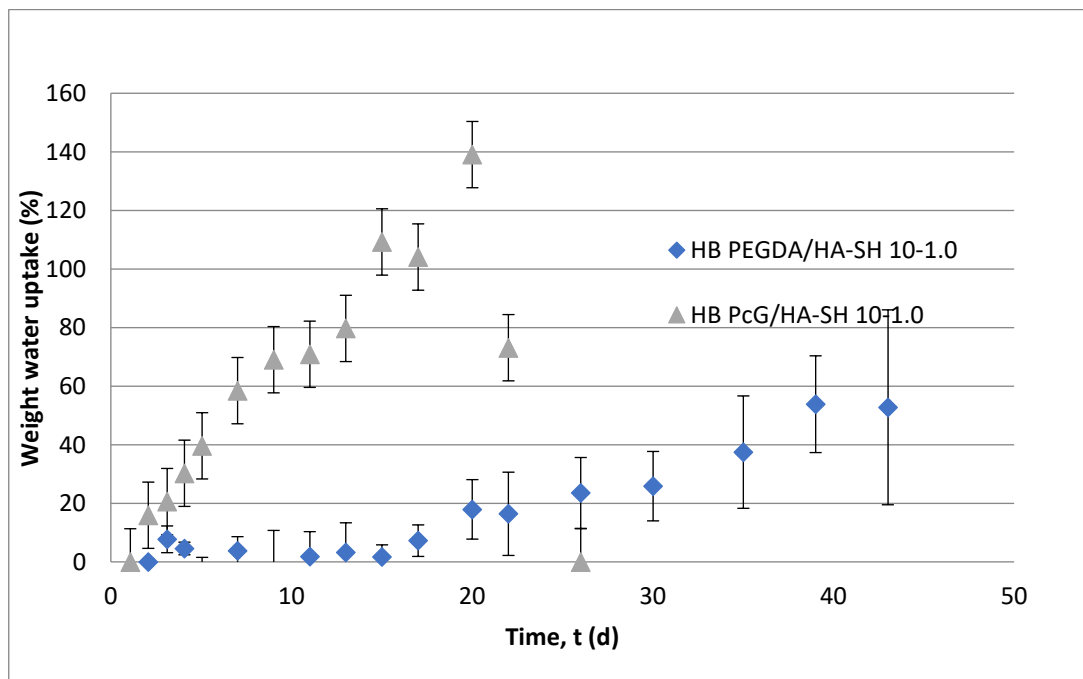


Figure 4.12: Swelling profile of HB PEGDA-co-GMA/HA-SH 10-1.0 and HB PEGDA/HA-SH 10-1.0.

4.4.5. Immobilization of glucose oxidase

The epoxide group can be confirmed by the presence of two peaks at 3.2 and 2.8 ppm in the ^1H NMR spectra. Enzyme was immobilized into the polymer by reacting the enzyme amine groups with the epoxide groups in glycidyl methacrylate for 96 hours. The polymer/enzyme mix was then centrifuged at 11,000 rpm and 37°C to remove the unimmobilized enzyme before analyzing the conjugated polymer by ^1H NMR. Figure 4.13 showed new shift from 2.0 to 2.2 ppm which was attributed to the presence of the enzyme covalently bound to the polymer and a decrease in the original shift at 3.5 ppm as the epoxide group concentration is reduced (but not fully removed, meaning some epoxy groups still remain) as it reacts and conjugates with amine, amide, and thiol functional groups in the GO enzyme.

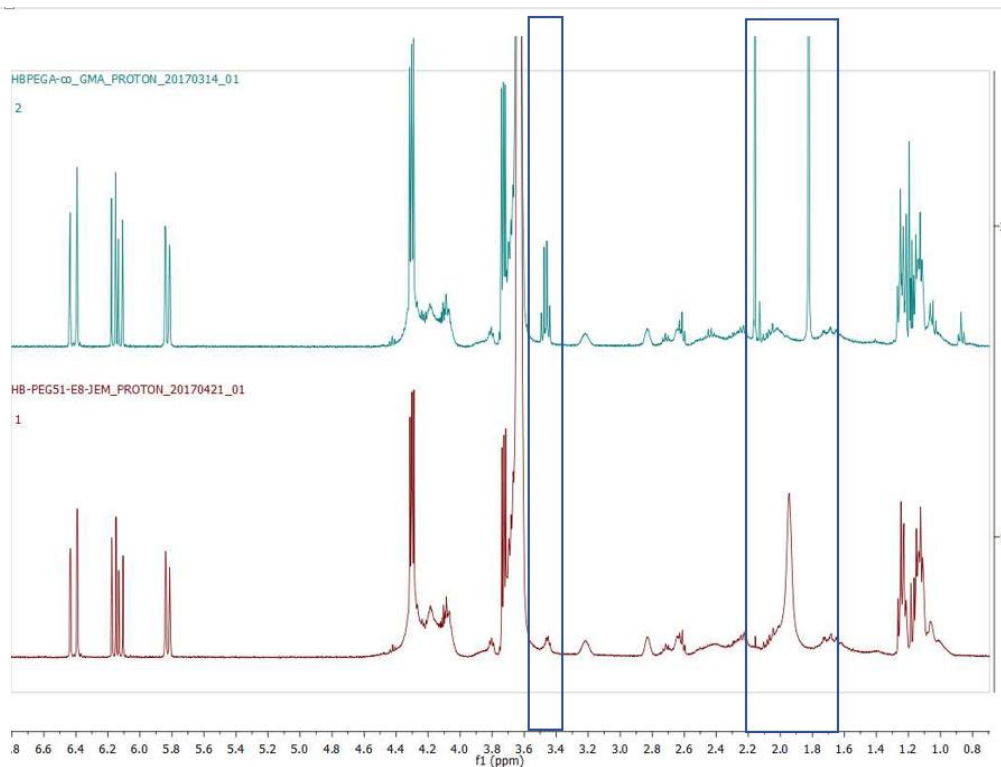


Figure 4.13: ^1H NMR spectra of [1] HB PEGDA-co-GMA with Glucose Oxidase Enzymes (in red), [2] HB PEGDA-co-GMA (in teal)

To confirm the presence of active immobilized GO enzymes, centrifuged HB PEGDA-co-GMA polymer (to remove any unimmobilized enzymes in the polymer solution) was crosslinked with 2.5 w/w% glucose-loaded HA-SH to form an HB PcG/HA-SH 10-1.0 hydrogel. The amount of H₂O₂ formed by this hydrogel was quantified after 24 hours. Pertitanic assay results show that 2.17±0.82 mM H₂O₂ was produced from the immobilized enzymes in the HB PEGDA-co-GMA/HA-SH 10-1.0 hydrogel. This concentration is much lower than the targeted 10-20 mM H₂O₂ a day production, but this nonetheless shows that partial immobilization of biologically active / functional glucose oxidase in the hydrogel can occur.

4.4.6. ROS production in HB PEGDA-co-GMA/HA-SH 10-1.0

Figure 4.14 shows the ROS production results of HB PEGDA-co-GMA/HA-SH 10-1.0 at varying enzyme concentrations for both 24 h and 48 h with the glucose concentration held constant at 2.5 w/w%. When comparing the effect of 250 U/L and 500 U/L GO concentrations, there was no significant difference during the first 24 hours (8.29±0.89 and 8.77±1.11 mM H₂O₂ respectively). However, for t = 48 h the difference between the two concentrations (11.21±1.58 and 13.37±1.62 mM H₂O₂ respectively) was more statistically significant.

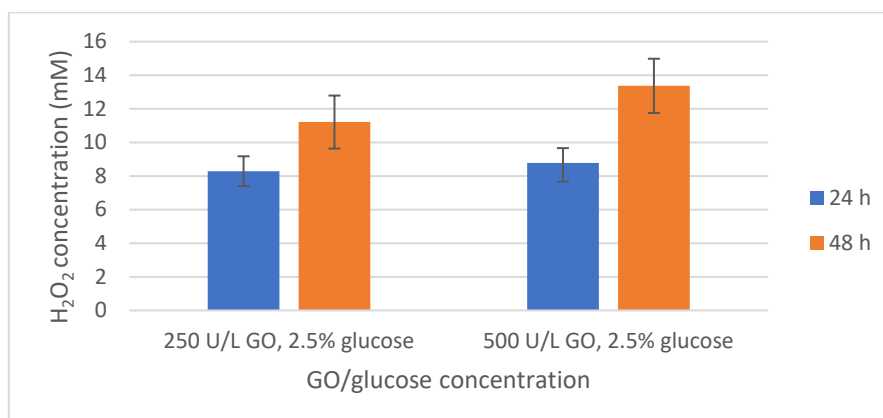


Figure 4.14: H_2O_2 production in HB PEGDA-co-GMA/HA-SH 10-1.0 at varying concentrations of GO enzyme (glucose concentration 2.5 w/w%) after 24 and 48 hours.

A comparison between HB PcG/HA-SH and HB PEGDA/HA-SH hydrogels (at the same time measurement, GO concentration, and glucose concentration) showed that HB PcG/HA-SH produced significantly lower H_2O_2 . The reduced H_2O_2 production could be attributed to GO being immobilized and unable to diffuse and react with glucose. Another reason could be a partial denaturation of the immobilized GO. In future in-depth studies, the active enzyme to denatured enzyme can be quantified through measuring the total protein content in the material.

However, when considering the influence of incubation time on H_2O_2 production, for HB PcG/HA-SH, H_2O_2 increased from 24 h to 48 h at both GO concentrations of 250 U/L and 500 U/L. This was not found for HB PEGDA/HA-SH hydrogel with the difference in concentrations being statistically insignificant. This means that the HB PcG/HA-SH hydrogel was more active in producing consistently more H_2O_2 beyond 24 hours, allowing reaction with diffusing glucose. On the contrary, for HB PEGDA/HA-SH hydrogel, GO enzyme may diffuse out of the hydrogel as a function of time.

4.4.7. Alamar Blue cytocompatibility test

Figure 4.15 shows the results for the indirect cytocompatibility testing of HB PcG/HA-SH hydrogels that were loaded with GO enzyme and glucose using NIH/3T3 mouse fibroblast cells after 24 hours. Positive control represents the cell viability on tissue culture plates.

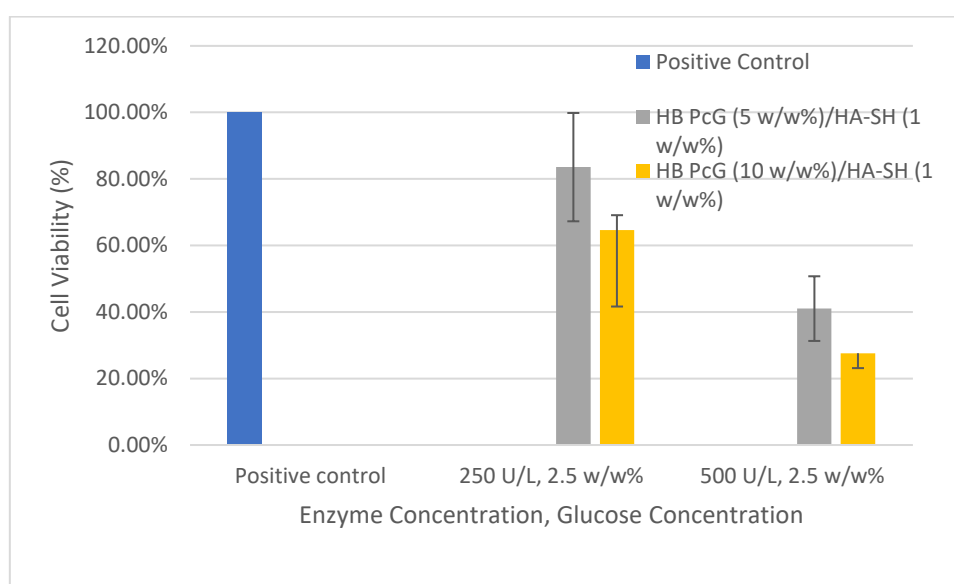


Figure 4.15: Cell viability of NIH/3T3 cells with HB PcG/HA-SH 10-1.0 and 5.0-1.0 hydrogels loaded with two different enzyme concentrations (250 U/L and 500 U/L) at a constant glucose concentration (2.5 w/w%) after 24 hours.

As H_2O_2 concentration produced in HB PcG/HA-SH 10-1.0 was lower than the corresponding H_2O_2 concentration produced in HB PEGDA/HA-SH, the lower cytocompatibility was not caused by the H_2O_2 produced.

HB PcG/HA-SH 5.0-1.0 was then tested to determine the effect of the amount of the enzyme-immobilized HB PcG polymer on the cytocompatibility of the hydrogel. There was a higher cell viability for HB PcG/HA-SH 5.0-1.0 with respect to HB PcG/HA-SH 10-1.0 which can be probably attributed to the lower amount of

glycidyl methacrylate groups as a concentration of GMA monomers at around 5 mM has been observed to cause a decrease in viability for human lymphocytes¹⁶. It is probable that some exposed epoxide functional groups (which did not react or conjugated with an enzyme) in the hydrogel could have caused the cytotoxic effect.

Finally, cytotoxicity increased with increasing enzyme amount from 250 to 500 U/L due to increased H₂O₂ production similar to what has been observed in Chapter 3 regarding HB PEGDA/HA-SH hydrogels loaded with similar GO concentrations.

4.5. Conclusions

HB PEGDA-co-GMA was successfully synthesized via DE-ATRP method as a liquid polymer enzyme-immobilizing substrate (as most substrates in enzyme immobilization tend to be solid) capable of immobilizing GO enzyme and to crosslink into a hydrogel in the presence of HA-SH. This material had a vinyl content of 29.8 mol% and epoxide content of 19.4 mol%. When compared to the original HB PEGDA polymer, HB PcG's degree of functionalization is lower but still considered to be a normal hyperbranched polymer.

The gelation time that ranged from 1.1 to 9 minutes depending on the amount of polymer in the hydrogel; the higher the HB PcG and HA-SH concentration, the lower the required gelation time will be. HB PcG/HA-SH 10-1.0 hydrogel was capable of considerable swelling up to 139% of its weight after 20 days and then fully degrading after 26 days.

HB PcG immobilized glucose oxidase enzymes which actively produced H₂O₂ in the presence of glucose. After 24 hours, at 250 U/L GO and 2.5 w/w% glucose, HB PcG/HA-SH 10-1.0 produced 8.29±0.89 mM H₂O₂. This still falls close to the

desired concentration target of 10-20 mM H₂O₂ after 24 hours even if HB PEGDA/HA-SH 10-1 at similar GO and glucose concentrations produced higher yields (it is likely some enzymes were hydrolyzed or deactivated during the immobilization process). Despite its potential for enzyme immobilization applications, for this specific research on wound healing, the HB PcG/HA-SH 10-1.0 hydrogel (with 250 U/L GO enzyme and 2.5 w/w% glucose) yielded low cytocompatibility using NIH/3T3 cells and did not appear suitable for use as an *in situ* wound healing device.

In the future HB PEGDA-co-GMA could be explored for immobilizing other enzymes than GO for alternative applications. However, cytocompatibility issues can be resolved by decreasing the GMA used (possibly at a 10:1 HB PEGDA to GMA molar ratio) or by improving the immobilization process to cap all of the epoxide groups. Other monomers that have the potential to immobilize enzymes such as vinyl acetate may also be investigated in future studies to explore the synthesis of other hyperbranched functionalized copolymers.

4.6. References

- (1) Datta, S.; Christena, L. R.; Rajaram, Y. R. S. Enzyme Immobilization: An Overview on Techniques and Support Materials. *3 Biotech* **2013**, 3 (1), 1–9. <https://doi.org/10.1007/s13205-012-0071-7>.
- (2) Bianco, P.; Haladjian, J.; Bourdillon, C. Immobilization of Glucose Oxidase on Carbon Electrodes. *J. Electroanal. Chem.* **1990**, 293 (1–2), 151–163. [https://doi.org/10.1016/0022-0728\(90\)80059-F](https://doi.org/10.1016/0022-0728(90)80059-F).
- (3) Li, Z. F.; Kang, E. T.; Neoh, K. G.; Tan, K. L. Covalent Immobilization of Glucose Oxidase on the Surface of Polyaniline Films Graft Copolymerized

with Acrylic Acid. *Biomaterials* **1998**, *19* (1–3), 45–53.

[https://doi.org/10.1016/S0142-9612\(97\)00154-3](https://doi.org/10.1016/S0142-9612(97)00154-3).

- (4) Ekinci, O.; Boyukbayram, A. E.; Kiralp, S.; Toppare, L.; Yagci, Y. Characterization and Potential Applications of Immobilized Glucose Oxidase and Polyphenol Oxidase. *J. Macromol. Sci. Part A Pure Appl. Chem.* **2007**, *44* (8), 801–808.
<https://doi.org/10.1080/10601320701407300>.
- (5) Valentova, O.; Marek, M.; Svec, F.; Stamberg, J. Comparison of Different Methods of Glucose Oxidase Immobilization. *Biotechnol. Bioeng.* **1981**, *XXIII* (1981), 2093–2104.
- (6) Zhang, D. H.; Yuwen, L. X.; Li, C.; Li, Y. Q. Effect of Poly(Vinyl Acetate-Acrylamide) Microspheres Properties and Steric Hindrance on the Immobilization of *Candida Rugosa* Lipase. *Bioresour. Technol.* **2012**, *124*, 233–236. <https://doi.org/10.1016/j.biortech.2012.08.083>.
- (7) KIM, K.-O.; KIM, B.-S. Immobilization of Glucose Oxidase on a PVA/PAA Nanofiber Matrix Reduces the Effect of the Hematocrit Levels on a Glucose Biosensor. *J. Fiber Sci. Technol.* **2017**, *73* (1), 27–33.
<https://doi.org/10.2115/fiberst.fiberst.2017-0004>.
- (8) Zhou, L.; Jiang, Y.; Ma, L.; He, Y.; Gao, J. Immobilization of Glucose Oxidase on Polydopamine-Functionalized. **2015**, 1007–1017.
<https://doi.org/10.1007/s12010-014-1324-1>.
- (9) Wang, W.; Zheng, Y.; Roberts, E.; Duxbury, C. J.; Ding, L.; Irvine, D. J.; Howdle, S. M. Controlling Chain Growth: A New Strategy to Hyperbranched Materials. *Macromolecules* **2007**, *40* (20), 7184–7194.
<https://doi.org/10.1021/ma0707133>.
- (10) A, S.; Xu, Q.; Zhou, D.; Gao, Y.; Vasquez, J. M.; Greiser, U.; Wang, W.; Liu, W.; Wang, W. Hyperbranched PEG-Based Multi-NHS Polymer and

- Bioconjugation with BSA. *Polym. Chem.* **2017**, *8*, 1283–1287.
<https://doi.org/10.1039/C6PY01719C>.
- (11) Zheng, Y.; Li, S.; Weng, Z.; Gao, C. Hyperbranched Polymers: Advances from Synthesis to Applications. *Chem. Soc. Rev.* **2015**, *44* (12), 4091–4130.
<https://doi.org/10.1039/C4CS00528G>.
- (12) Deshmukh, M.; Singh, Y.; Gunaseelan, S.; Gao, D.; Stein, S.; Sinko, P. J. Biodegradable Poly(Ethylen Glycol) Hydrogels Based on a Self-Elimination Degradation Mechanism. *Biomaterials* **2011**, *31* (26), 6675–6684. <https://doi.org/10.1016/j.biomaterials.2010.05.021.Biodegradable>.
- (13) Wang, D.; Zhao, T.; Zhu, X.; Yan, D.; Wang, W. Bioapplications of Hyperbranched Polymers. *Chem. Soc. Rev.* **2015**, *44* (12), 4023–4071.
<https://doi.org/10.1039/C4CS00229F>.
- (14) Moura, M. J.; Figueiredo, M. M.; Gil, M. H. Rheological Study of Genipin Cross-Linked Chitosan Hydrogels. *Biomacromolecules* **2007**, *8*, 3823–3829.
- (15) Zuidema, J. M.; Rivet, C. J.; Gilbert, R. J.; Morrison, F. A. A Protocol for Rheological Characterization of Hydrogels for Tissue Engineering Strategies. *J. Biomed. Mater. Res. Part B Appl. Biomater.* **2014**, *102* (5), 1063–1073. <https://doi.org/10.1002/jbm.b.33088>.
- (16) Poplawski, T.; Pawlowska, E.; Wisniewska-Jarosinska, M.; Ksiazek, D.; Wozniak, K.; Szczepanska, J.; Blasiak, J. Cytotoxicity and Genotoxicity of Glycidyl Methacrylate. *Chem. Biol. Interact.* **2009**, *180* (1), 69–78.
<https://doi.org/10.1016/J.CBI.2009.02.001>.

Part II

Chapter 5 Preparation and Characterization of Wound Healing Thermoplastic Polyurethane Patches

<

5.1. Abstract

In this chapter, the physicochemical and mechanical properties of a set of four commercially available thermoplastic polyurethanes (TPUs) are discussed. TPUs were characterized in order to determine their suitability to be used as wound patches, which will be further discussed in this and later chapters. Polyurethanes have been used in many wound healing applications, mainly for their versatility. A polyurethane is made of monomer units joined by carbamate (urethane) linkages, which are formed from the reaction of isocyanates and alcohols. A thermoplastic polyurethane or TPU is a type of polymer that becomes pliable or mouldable above its melting temperature and solidifies upon cooling.

Suitable TPUs for electrospinning wound healing scaffolds were selected among the four available ones. The selected material should be biocompatible in order to

be used for wound healing applications, for this reason medical grade TPUs were considered. Other requirements include hydrophilicity, water adsorption ability and mechanical properties similar to currently available wound patches. TPUs were processed into films by solvent-casting method for the characterization of their properties. The physicochemical properties of TPUs were thus characterized. Hydrophilicity of the films was measured through static contact angle tests and water adsorption measurements as a function of time. Degradation rate was also characterized. Finally, the tensile mechanical properties of the films were evaluated (elastic modulus, tensile strength, and ultimate elongation percentage).

Two TPUs satisfied the requirements: Lubrizol SP60D60 (TPU A) and Lubrizol SP93A100 (TPU C). Their ability to be electrospun into fibrous patches was evaluated. Through a trial and error procedure, the parameters for electrospinning the polymers were optimized. Different combinations of settings of polymer solution concentration and solvent type, voltage, solution flowrate for electrospinning the samples were tried and then fibre morphology was analyzed by SEM. The desired morphology was to have thin, consistent fibres with no defects at a range of 10-1000 nm.

As SP93A100 gave more bead-like defects during electrospinning, instead of consistently fibrous texture as in the case of SP60DO, SP60D60 (simply coded as TPU A) was selected to be optimal for further studies on wound healing fibrous patches. This material is an aliphatic polyether TPU with the following properties: static contact angle of $72.0 \pm 2.9^\circ$; water absorbance percentage of $44.7 \pm 4.9\%$ after 24 hours and $60.6 \pm 3.0\%$ after 4 weeks; Young's modulus of 25.1 ± 1.5 MPa, ultimate tensile strength of 10.4 ± 0.7 MPa, and ultimate elongation percentage of $386 \pm 63\%$. Optimal electrospinning parameters for this polymer were: 15 w/v% solution concentration in 90 v/v% CHCl_3 , 10 v/v% formic acid, 20 kV voltage; 20 cm distance between the spinneret and the metal collector, and solution feed rate of

1.5 mL/h. Such electrospinning parameters yielded elastic, fibrous patches with an average fibre diameter of $1.12 \pm 30 \mu\text{m}$.

The obtained fibrous patches were surface grafted with GO enzyme using a facile and versatile mussel inspired surface functionalization approach as discussed in the next Chapter.

This part of the Ph.D activity was performed at Politecnico di Torino.

5.2. Introduction

Electrospinning is a process which enables nanofibres to be formed by an electrostatically driven jet of polymer solution¹. These fibres are collected as membranes with diameters ranging from 2 nm to $10 \mu\text{m}$ ^{1,2}. Figure 5.1 depicts the general layout of an electrospinning set-up: a polymer solution is loaded into a syringe and extruded out through the syringe nozzle at a constant rate using a syringe pump. A positive electrode is attached to the syringe needle and a negative electrode is attached to a flat metal collector where the fibres will deposit. Once a potential difference is applied, generally 10-40 kV through the system, the polymer shoots out as a fibrous thread, moving from the positive charge (syringe needle) to the negative charge (collector²⁻⁴).

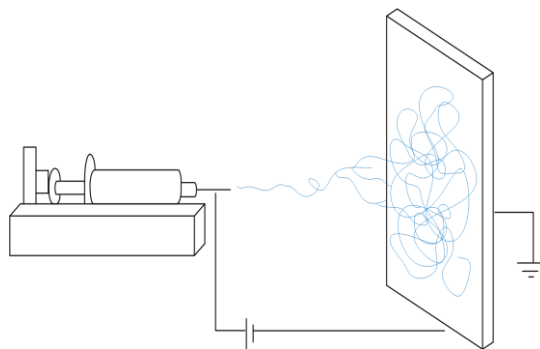


Figure 5.1: Schematic of formation of electrospun fibres.

As this polymer solution is propelled outwards the needle with the application of sufficient voltage, its shape transforms from a spherical tip into a cone shaped figure when the repulsive electrostatic force is less than the surface tension in the polymer solution, as shown in Figure 5.2⁵. This phenomenon is called the Taylor cone. When this repulsive electrostatic force is greater than the surface tension, a charged jet occurs, and the polymer is ejected out in varying directions results in the fibres having a broad diameter divergence.

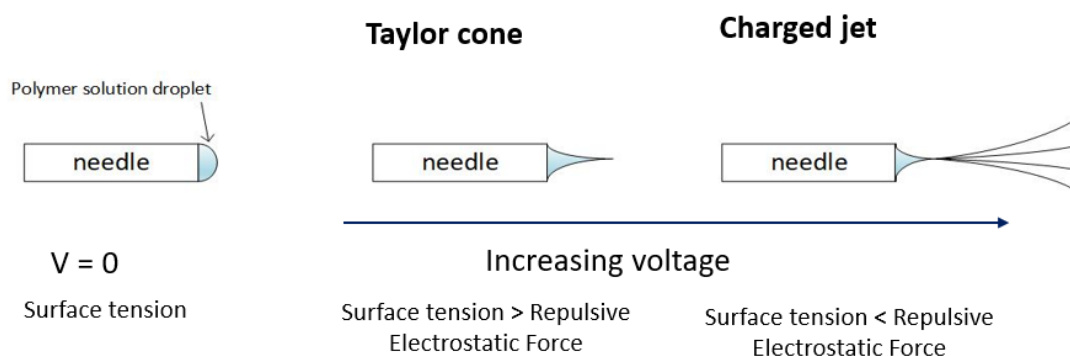


Figure 5.2: Effect of applied voltage on electrospinning fibres.

Thus, one of the most important parameters to optimize is the potential difference applied. If it is too low, the polymer solution cannot be electrospun as it is incapable of forming a Taylor cone. This property differs for each type of polymer solution, as it depends on surface tension and conductivity. Alternatively, by adding an organic acid such as formic acid into the polymer solution, the solution conductivity can be increased leading to thin consistent fibres respect to the original solution when the same voltage is applied⁶.

Electrospun fibres present several properties that can be advantageous in the biomedical field. First of all they can mimic the fibrous structure of the extracellular matrix (ECM) and provide a scaffold for cells to grow out on biodegradable and bioresorbable materials⁷. Fibre diameters can be in the nanometer scale and provide

a large surface area for cells to adhere and grow⁷. While cells attached on a microfibre structure tend to assume a flat morphology, cells adherent on a nanofibrous matrix grow three-dimensionally assuming an *in vivo*-like morphology⁸.

Electrospun fibres can also be surface modified in order to immobilize bioactive molecules, including enzymes. Such substrates are advantageous for surface modification thanks to their high surface area leading to high density of functionalising molecules. One of the possible techniques used to surface modify electrospun fibres is via "mussel-inspired" coatings, which will be treated in the next Chapter⁹.

Electrospun polymer fibres are suitable for wound healing applications due to having characteristics such as: oxygen permeability, biomimetic structure, and depending on the type of polymer used they can possess an adequate hydrophilicity to support cell adhesion¹⁰. Fibrous membranes can also be modified or functionalized to have antibacterial properties that prevent infections as the wound is healing. These characteristics are also similar to those of hydrogels described in previous Chapters. Other desired characteristics are adequate elasticity and tensile strength to withstand wear and stresses as the patient moves about during the wound healing process.

Several electrospun fibres have already been put to use in the commercial biomedical applications such as artificial heart valves that were developed by Xeltis, which they advertised to serve as a scaffold for new cardiac tissue to grow in and eventually replace the scaffold as the material degrades¹¹. They have also been used as a synthetic bone regeneration scaffold such as Rebossis by Ortho ReBirth¹².

For wound healing applications, antibacterial nanofibre mats have been fabricated to reduce chronic wound biofilms. One of the methods was to incorporate silver into the fibre matrix of the mat^{13,14}. In other works, plant-based antimicrobials such as shikonin, alkannin, or murivenna oil have been loaded into electrospun fibres and displayed antibacterial activity against *S. aureus* and *E. coli*¹⁵⁻¹⁷.

Suitable polymers for electrospinning wound healing patches should meet several properties: mainly biocompatibility, hydrophilicity, elasticity, and tensile strength similar to currently available wound patches. Tensile strength and percent elongation at break for a gelatin-based bioadhesive wound dressing material was reported to be 12.7 MPa and 40.4% respectively¹⁸. PCL electrospun nanofibres had a tensile strength of 12 MPa and elongation at break of 98%¹⁹. A comparative study on commercial wound dressing mechanical properties (including Medifoam N, a commercial TPU foam; Allevyn; Biatain; Askina; Lyofoam Extra; Cellosorb Adhesive, etc.) have been reported to have the following a tensile strength range of 0.108-2.43 MPa and percent elongation at break of 180%-1101%²⁰. Hence, tensile strength and elongation at break should be ideally in this range.

5.2.1. Thermoplastic Polyurethanes

Polyurethanes have been used in many wound healing applications, mainly for their versatility. A polyurethane is made of monomer units joined together by carbamate (urethane) linkages, which are formed from the reaction of isocyanates and alcohols²¹. A thermoplastic polyurethane or TPU is a type of polymer that becomes pliable or mouldable at a certain elevated temperature and solidifies upon cooling.

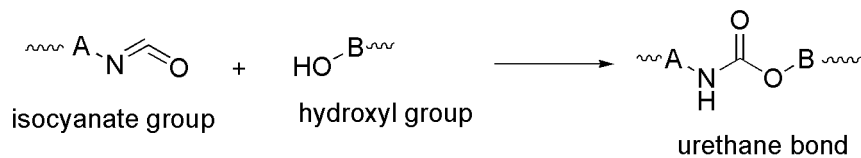


Figure 5.3: Chemical structure of urethane bond by reaction of an isocyanate group and a hydroxyl group. When difunctional monomers react, a linear polyurethane forms.

As many medical grade TPUs are commercially available, in this work one of these TPUs was selected and processed into an electrospun fibrous patch for wound healing applications. Specifically, the focus of Part II in this research (conducted in Politecnico di Torino) was based on the application of a commercially available TPU for fabricating a wound healing device. The steps of the work were: i) electrospinning TPU into a fibrous patch, ii) surface modification of the patch to make its surface reactive, iii) grafting of glucose oxidase enzyme on the modified patch surface, iv) production of H_2O_2 by this functionalized fibrous patch exploiting a glucose source, iv) testing patch biological properties, such as cytocompatibility.

Tecophilic brand polyurethanes produced by Lubrizol have been used in biomedical electrospinning research, with additional substances such as murivenna oil to improve hemocompatibility in wound healing and in the fabrication of ventricles for an artificial heart^{17,21,22}. In this work, commercially available polyurethanes from Lubrizol were selected based on their hydrophilicity and water absorption properties. The work was then addressed to obtain reproducible fibrous membranes with regular morphology for subsequent modification with GO enzyme. This allowed to finally select on TPU material allowing fibre production with no defects. The use of a biocompatible material is expected to speed up the preclinical and clinical tests needed for the future approval and application of the functionalized membrane.

5.3. Materials and methods

Chloroform (CHCl₃), formic acid (FA), phosphate buffer solution (PBS) - pH 7.4 tablets were purchased from Sigma Aldrich, Italy.

5.3.1. Thermoplastic Polyurethanes for electrospinning

Thermoplastic aliphatic polyurethanes: Lubrizol Tecophilic SP-93A-100, SP-60D-60, SP-80A-150, Lubrizol Tecoflex SP-80A-150 were provided by Velox GmbH, Germany.

As a shorthand, the TPUs were given the codes:

- A = Tecophilic SP-60D-60
- B = Tecophilic SP-80A-150
- C = Tecophilic SP-93A-100
- D = Tecoflex SP-80A-150

A summary of TPU properties as reported in their specification sheets and provided in Table 5.1^{23,24}:

Table 5.1. Summary of reported physical and mechanical properties of Lubrizol TPUs.

	SP-80A-150	SP-93A-100	SP-60D-60	SG-80A-150
Shore Hardness	70A	83A	41D	72A
Specific Gravity	1.10	1.13	1.15	1.04
Ultimate Tensile (MPa)				
Dry	13.79	15.17	57.23	39.99
Wet	4.83	9.65	21.37	-
Ultimate Elongation (%)				
Dry	1000%	1040%	500%	600%
Wet	600%	620%	300%	-
Water Absorption	150%	100%	60%	-

To test their properties, TPU films were prepared via the solvent casting method. This consisted of dissolving 1 g of TPU in 10 mL chloroform and pouring the polymer solutions into 10 cm diameter glass dishes, taking care that no bubbles were formed. These were left overnight under vented hood to evaporate chloroform. The films were then peeled out and cut into the appropriate sample shapes needed for the characterizations.

5.3.2. Physical and mechanical properties of TPU cast films

Tests were performed on TPU films to determine their physical mechanical properties to select suitable TPUs for wound healing patches. Primarily, one important factor in TPU selection was surface hydrophilicity as it would improve surface functionalization via mussel inspired coating. Additionally, hydrophilic materials are also useful to absorb wound exudates. It is also ideal that the mechanical properties of the TPUs are in the range of the values listed for several commercial wound dressings mentioned in Section 5.2.

5.3.2.1. Static Contact Angle

Static contact angles were measured at room temperature using a CAM 200 Instrument (KSV NIMA, Biolin Scientific, Finland) equipped with an Attention Theta software (Biolin Scientific, Finland) for data acquisition. Three Milli-Q water droplets (volume 5 μ L) were deposited on each 1 cm x 5 cm TPU film sample and data were collected thereafter for 10 s with a time frame of 10 ms. The data were expressed as mean value \pm SD from 6 measurements.

5.3.2.2. Water Absorption and dry weight loss measurements

TPU film samples were cut to obtain squared samples of 1 cm per 1 cm area. Each dry sample was weighed (W_0) and placed in a bijoux vial. Next 5 mL of 7.4 pH PBS was pipetted into the vial and samples were incubated at 37°C for specific time points, including short term analysis (2, 4, 6, 8, 24 hours) and long term measurements (1, 2, 3, 4 weeks). At each time point, the samples were withdrawn from vials and placed in a paper towel until they were free of water droplets and weighed to measure the wet weight of the sample at time t (W_{Wt}). The samples were then dried in the incubator overnight to remove the absorbed moisture. The samples were weighed to measure their dry weight at time t (W_{Dt}). W_{Dt} lower than W_0 this was an indication of degradation or dissolution. Measurements for each TPU type were carried out in quadruplicates. <

The equation for water absorption used is:

$$\%adsorption_t = \frac{W_{Wt} - W_0}{W_0} * 100\%$$

The equation for dry weight loss is:

$$\%degradation_t = \frac{W_0 - W_{Dt}}{W_0} * 100\%$$

5.3.2.3. Tensile mechanical Testing

The mechanical properties such as tensile strength, Young's modulus, and elongation at break are important factors in characterizing TPUs for wound dressing applications. These factors indicate the ability of the material to maintain integrity during the processing, surface modification, and application on wounds (especially when the patient is moving). Films were cut into dog bone shapes with the test area having dimensions: 5 mm x 15 mm. Thickness was measured by a digital caliper.

The cross sectional area was calculated as the thickness multiplied by 5 mm. Stress was calculated as the measured force over this cross sectional area. Samples were measured in triplicates per TPU type.

Mechanical properties of the films were measured using a Universal Testing Machine MT[®]S QTest[™]/10. The traction force was applied along the length of the samples at a displacement rate of 10 mm/min with a 50 N load cell. A readout of the maximum length (L_{max}) was also given by the testing machine which can be used for calculating the ultimate elongation percentage with the original length (L_0) of the sample. The equation used is:

$$\text{Ultimate Elongation \%} = \frac{L_{max} - L_0}{L_0} * 100\%$$

↳

5.3.3. Electrospinning of TPU patches, imaging of electrospun fibres, and optimization of process parameters

An electrospinning apparatus (Linari Engineering SRL, Italy) was used to obtain the electrospun TPU fibrous membranes. This includes the syringe pump and voltage supply. In finding the optimum parameters, the following range of values were used:

- Voltage: 20-25 kV
- Syringe pump feed rate: 1.0-1.5 mL/h
- Polymer concentration in solvent: 10-15 w/v%
- Solvent type: chloroform (pure); chloroform (90 v/v%) + formic acid (10 v/v%)

The distance between the spinneret and the metal collector was set at 20 cm and the polymer solution was extruded out of a 21 G metal needle. After the optimal settings using chloroform were obtained, with respect to the voltage, feed rate, and polymer

concentration, the set-up was further optimized by observing if an improvement in fibre consistency would be obtained in modifying the organic solution from pure chloroform to an organic solution consisting of 10 v/v% formic acid (FA) and 90 v/v% CHCl₃. The addition of FA was considered to increase conductivity in the polymer solution through an increased level of free ions (CHOO⁻ and H⁺)²⁵.

After electrospun fibres were formed and collected, they were analysed under a scanning electron microscope (SEM) with regards to their morphological properties. Scanning Electron Microscopy was performed using a LEO 1420 microscope (Zeiss, Germany) at 20 kV and a working distance of 15 mm. The diameters of the fibres in electrospun membranes were measured on SEM images using ImageJ software. Measurements in the diameter were taken from thirty random locations and one-way ANOVA was used to determine if there is a significant difference in the fibre diameters from the electrospinning set-ups that were used.

5.4. Results and discussion

5.4.1. Static contact angle of TPU cast films

Figure 5.4 shows the static contact angle measurements of the different solvent-cast TPU films. In contact angle measurements, a material which gives a value less than 90° is considered to be hydrophilic²⁶. The hydrophilic TPUs were: A (72±2.9°) and C (78.6±0.4°). ANOVA test showed that at a significance level of 0.05 the contact angles between all the materials were significantly different from each other (p-value <0.00001). It is worth noting that while the differences between TPU A and TPU C were statistically significant, the averages of the two materials were close in value that they could be similar enough in terms of hydrophilic property. This

property of hydrophilicity is important to allow the material to be functionalised by mussel-inspired strategy.

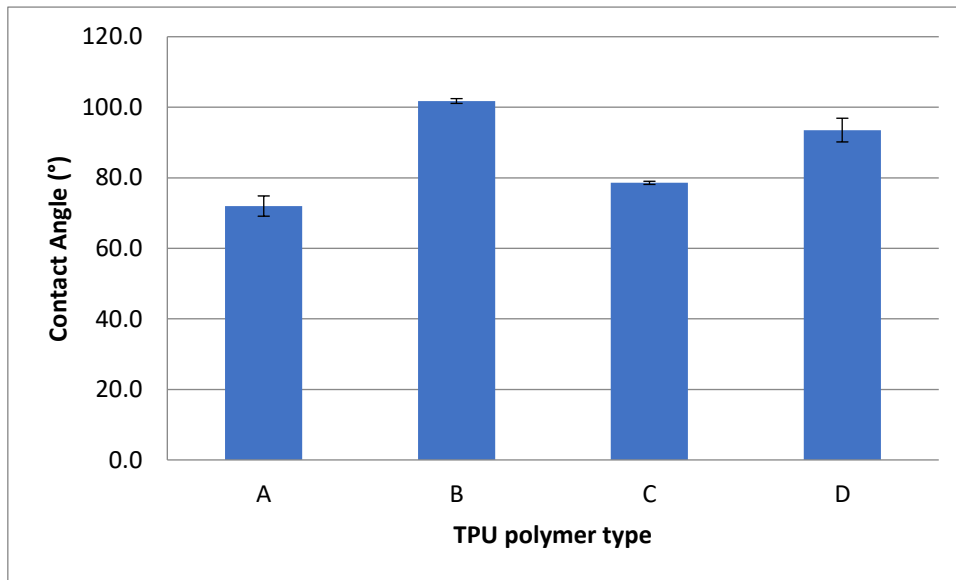


Figure 5.4: Static Contact Angle Measurements of TPUs. Columns are the average values and bars are the standard deviation.

5.4.2. Swelling and degradation results of TPUs

Figure 5.5 shows the short term swelling (2-24 hours) of the TPUs while Figure 5.6 shows the long term swelling of the TPUs (1-4 weeks). In the long-term study, samples were also monitored to detect signs of significant degradation or dissolution.

In Figure 5.5, A, B, and C TPUs displayed the ability to swell and take in water despite B had a low surface hydrophilicity in the contact angle test. When the TPUs were ranked based on highest to lowest percent water absorption from all the time points, B was found to have the highest, then followed by C, A, and finally D. As D was not part of the Tecophilic polymer series (which are water adsorbing TPUs),

it was not unexpected that it did not swell or adsorb water given that its material product sheet did not mention any water retention values as it did for A, B, and C.

The water adsorption of TPU A and TPU C slightly decreased after the first 8 hours before increasing to the starting value after 24 hours. There was a slight decrease in the measurement of water adsorption for B from 1 hours ($96.9 \pm 7.0\%$) to 3 hours ($73.8 \pm 6.5\%$) but it eventually returned to $97.2 \pm 4.3\%$ after 24 hours. The reason for the decreased water adsorption is not clearly known but it is probable that the polymer interstices in the film were expanding (more water could be absorbed) and contracting (less water could be absorbed) before approaching equilibrium swelling value.

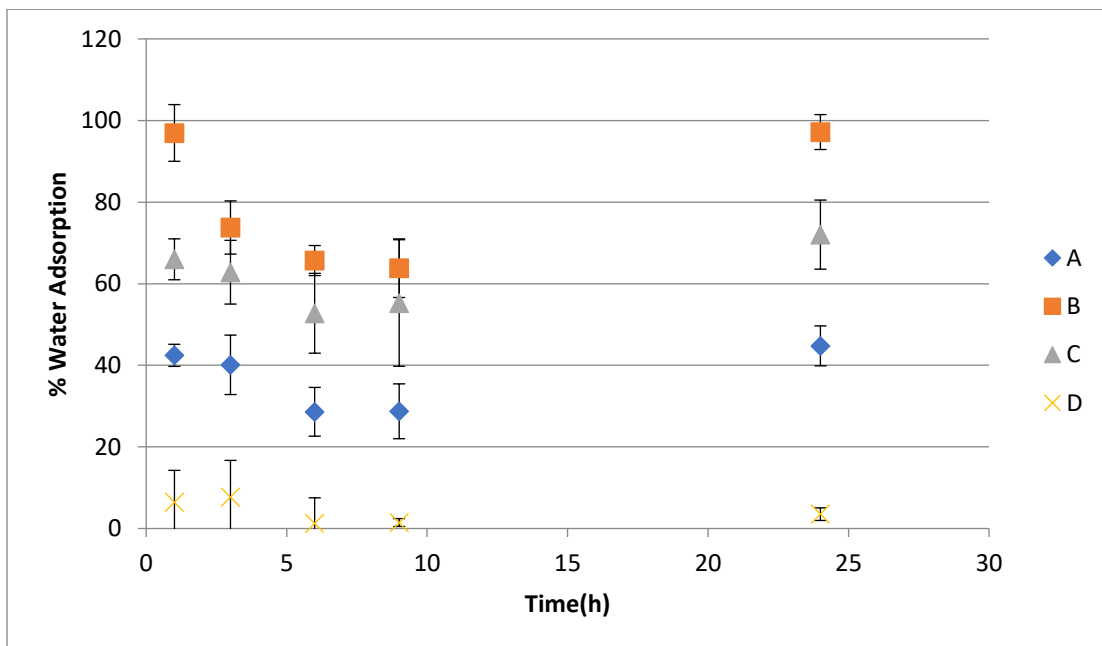


Figure 5.5: Short-term water adsorption results for TPUs.

As shown in Figure 5.6, for TPU B water adsorption percentage increased to around 120 % from 1 to 2 weeks; for TPU C it was around 100% from 1 to 3 weeks and then slightly decreased to $92.3 \pm 2.1\%$, after 4 weeks; in the case of TPU A water

adsorption was around 40% from 1 to 3 weeks and increased to $60.6 \pm 3.0\%$, after 4 weeks. In the case of TPU D, water adsorption was close to 0% at each time-point. In summary, after 4 weeks, TPUs B, C, and A had the water adsorbing values of $122.3 \pm 5.5\%$, $92.3 \pm 2.1\%$, and $60.6 \pm 3.0\%$, respectively. These values are similar to the reported water adsorption data in the Lubrizol material data sheet with TPU B, C, A having 150%, 100% and 60% water adsorption percentage, respectively.

Looking at the water absorption values from the short-term and long-term data, it was observed that despite some fluctuations, TPUs A, B, and C retained a certain minimum water content throughout the experiment. This can be attributed to the water retained through hydrophilic interactions with the polymer.

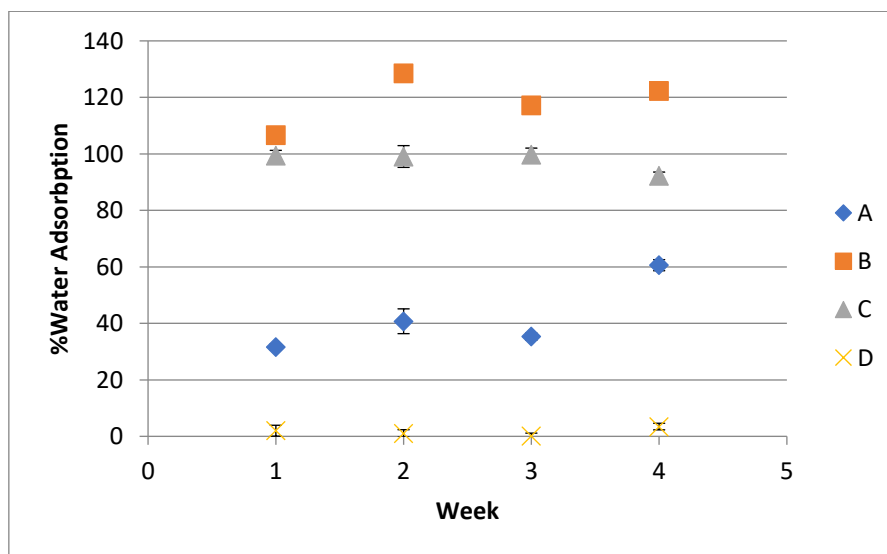


Figure 5.6: Long-term water adsorption results for TPUs.

Regarding material degradation, no significant change in the dry mass (less than 1% its original weight) was observed after 4 weeks (data not reported). It can be concluded that TPU A and B showed slight variations in water adsorption within 20%, while TPU C showed wider variations in water adsorption within 40%. TPU

D did not adsorb water. No signs of degradation could be detected for each TPU up to 4 weeks.

5.4.3. Mechanical test results

Figure 5.7 shows the stress strain curves of the four TPU films (obtained from a Trial 1 out of the 4 sets performed) to show their general trend. In each trial, the ultimate tensile strength and Young's modulus was calculated before being reported in Figure 5.8 as the average of these values. In comparing the values with commercial wound dressings, a material is considered suitable for electrospinning if it has the following mechanical properties: 0.108-2.43 MPa for ultimate tensile strength and percentage of elongation at break of 180%-1101%²⁰.

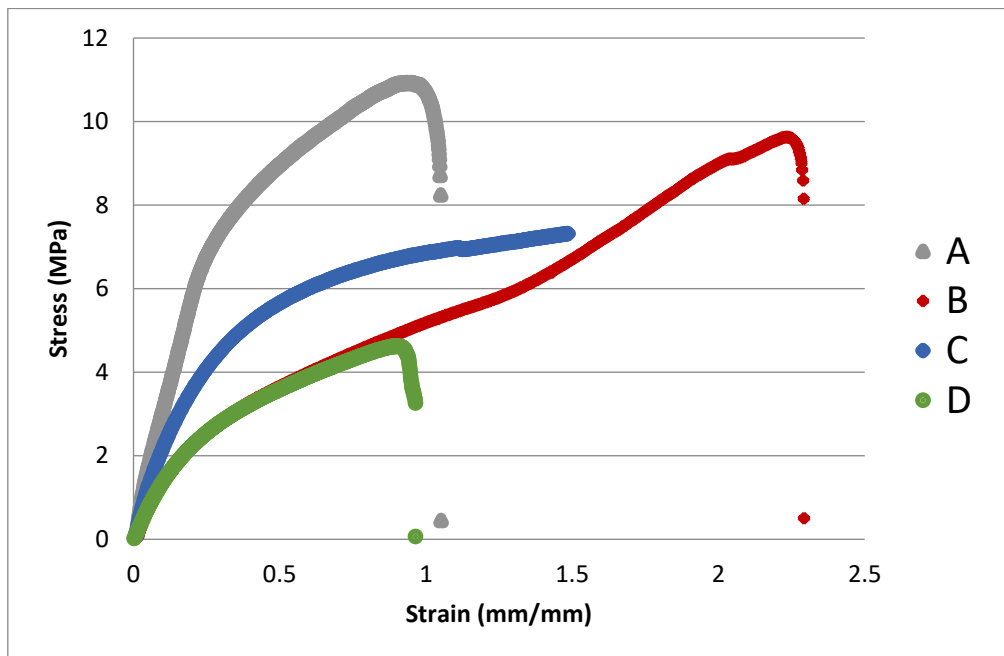


Figure 5.7: Stress-strain curves of the four TPUs (Trial 1 measurements).

Figure 5.8 shows the dry ultimate tensile strength (UTS) and Young's modulus of the TPU samples. TPU B (27.8 ± 3.5 MPa) had the highest ultimate tensile strength, followed by TPU D (13.1 ± 0.9 MPa), TPU A (10.4 ± 0.7 MPa), and finally TPU C (7.6 ± 0.5 MPa). All of the TPUs had UTS values higher than the upper limit of 2.43 MPa, which means that they have better tensile properties than the current wound dressings and can withstand the wear and stresses that wound dressings undergo.

A high Young's modulus means that the material is relatively stiff and it will only change its shape slightly when a load is applied. For most polymers, they are ranged from <10 to 10^4 MPa with foams being the lowest in value and an elastomer such as rubber having approximately 0.3 MPa^{27,28}. TPU A (25.2 ± 1.5 MPa) had the highest Young's modulus, followed by TPU C (14.0 ± 0.3 MPa), TPU B (10.4 ± 2.0 MPa), and finally TPU D (5.9 ± 2.4 MPa). As expected, TPU D which is from a flexible series (Tecoflex) instead of the hydrophilic series (Tecophilic) had the most elastic property among the TPU.

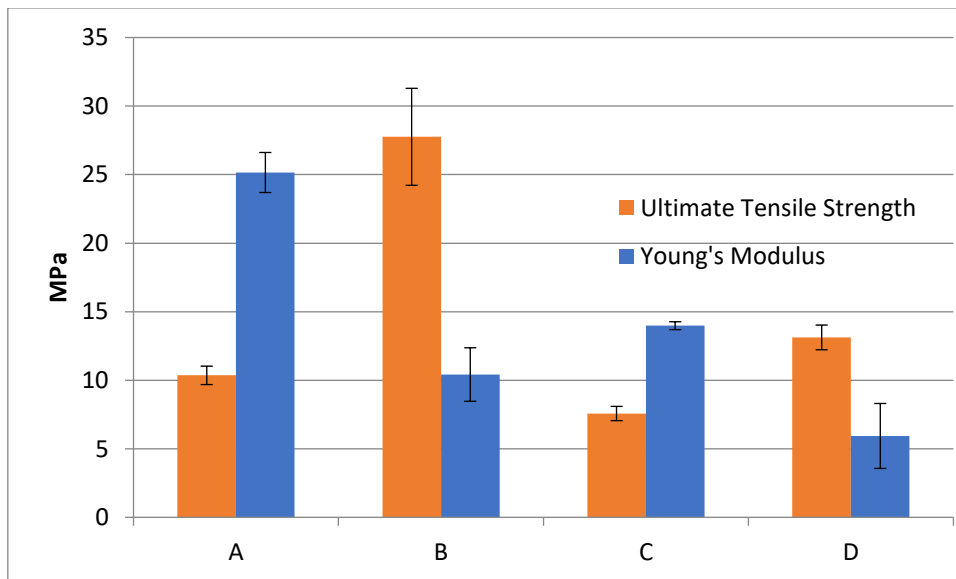


Figure 5.8: Ultimate tensile strength properties of TPUs.

Figure 5.9 shows the stress vs elongation profile of the TPUs obtained from Trial 1. The ultimate elongation percentage was taken as the average maximum length, L_{max} , from the four measurements for each TPU performed.

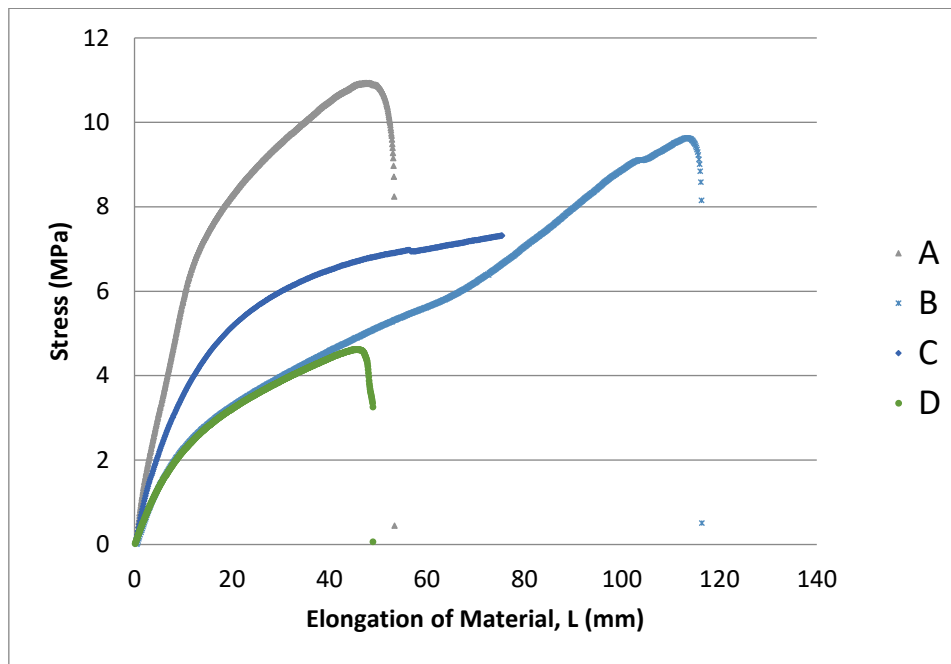


Figure 5.9: Stress-elongation curves of the four TPUs (Trial 1 measurements).

Figure 5.10 shows the ultimate elongation percentage of the TPUs: they were stretched to lengths several times their original length before breaking in two pieces. All TPUs could undergo wide deformation without rupture, which is desirable in wound dressing that undergo physical and mechanical stresses when applied to patients. TPU B had the highest percentage of elongation of $833 \pm 115\%$, followed by TPU D ($742 \pm 116\%$), TPU C ($397 \pm 26\%$), and TPU A ($386 \pm 63\%$). The percent elongation between TPU B and TPU D had no statistical difference found between them. Also the percentage elongation between TPU A and C appeared similar enough and upon further t-test analysis it was found that there was no statistical difference to be found between them ($p = 0.79$). All of these values, even the lowest

which is TPU A fall in the range of acceptable ultimate percent elongation for wound dressing materials.

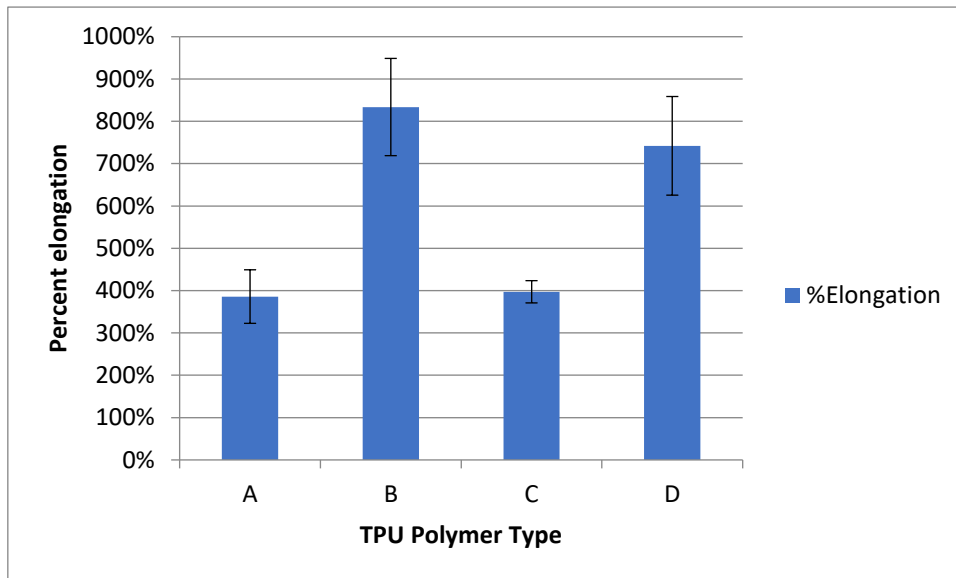


Figure 5.10: Ultimate Elongation Percentage of TPUs.

All of the polymers had mechanical properties that fall in the range commercial wound dressings, making them acceptable to be processed into wound healing materials.

5.4.4. Electrospinning of whitelisted TPUs and morphological characterization

5.4.4.1. Morphological characterization of electrospun TPU patches

Among the TPUs, TPU A (SP-60D-60) and C (SP-93A-100) were selected to be used for electrospinning as they had the lowest static contact angle values, : $72 \pm 2.9^\circ$ for TPU A and $78.6 \pm 0.4^\circ$ for TPU C (suggesting hydrophilicity) and

they were able to retain water at least 40% of their weight ($44.7\pm 2.7\%$ for A and $72.0\pm 5.0\%$ for C). Hydrophilic behaviour is required for further functionalization by mussel-inspired approach (Chapters 6-7). Water retention ability is an important property for wound healing as for example it allows exudate adsorption. Finally, mechanical properties as reported in Section 5.4.3 were within the range of values for the ultimate tensile strength and ultimate percent elongation for commercial wound dressings.

Selected polymers were electrospun at varying flowrates and voltages while the distance of needle to collector (20 cm) and polymer in chloroform concentration (15 w/v%) were kept constant. Morphology of electrospun membranes is shown in Figure 5.11 and 5.12.

Figure 5.11 shows electrospun TPU A membranes prepared using different flowrates and voltages: it was observed from comparing Fig 5.11a with Fig. 5.11c (flowrate held constant at 1.0 mL/h) and Fig. 5.11b with Fig. 5.11d (flowrate held constant at 1.5 mL/h) that more defects and more irregular fibre diameters were obtained at a voltage of 25 kV respect to 20 kV, thus the voltage of 20 kV is the more favourable parameter. Furthermore, the fibres were more uniform in Fig. 5.11b (flowrate 1.5 mL/h) than in Fig. 5.11a (flowrate 1.0 mL/h). Best morphology for TPU A fibrous patches was the one fabricated using 1.5 mL/h and 20 kV as presented in Figure 5.11b.

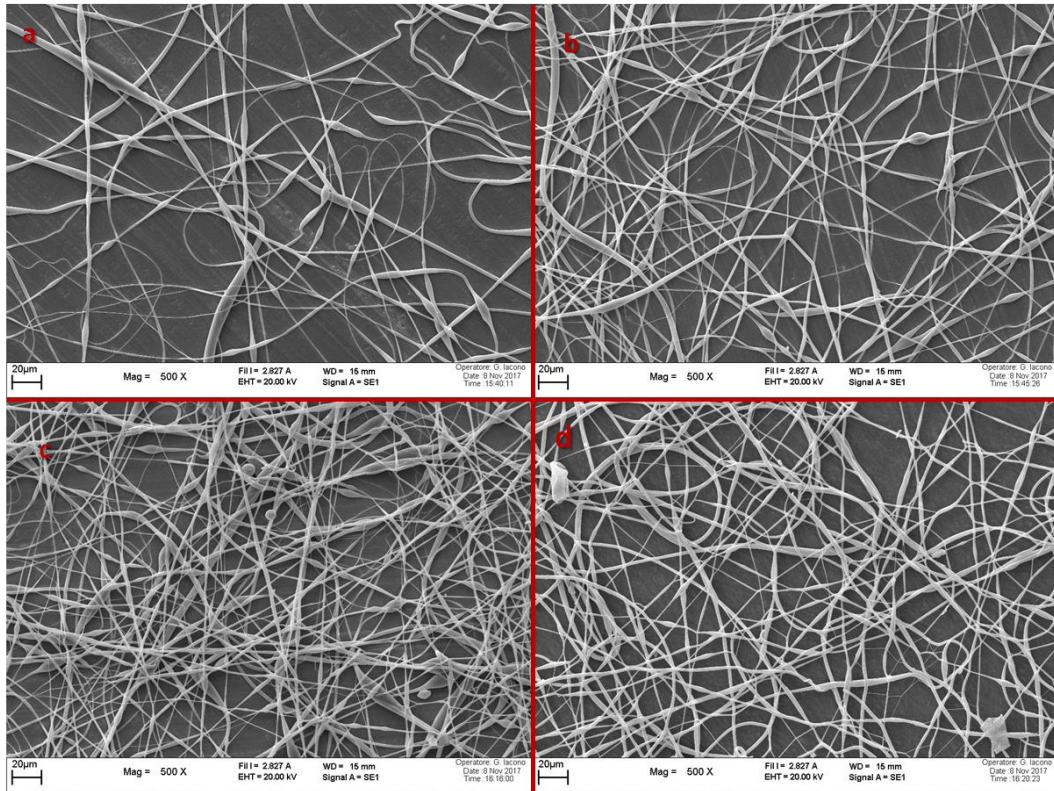


Figure 5.11: TPU A (SP-60D-60) electrospun fibres: a) 20 kV + 1.0 mL/h, b) 20 kV + 1.5 mL/h, c) 25 kV + 1.0 mL/h, d) 25 kV + 1.5 mL/h

Figure 5.12 shows electrospun TPU C membranes prepared using different flowrates and voltages: it was observed that comparing Fig. 5.12a with Fig. 5.12c (flowrate held constant at 1.0 mL/h) and Fig. 5.12b with Fig. 5.12d (flowrate held constant at 1.5 mL/h) that more defects and more irregular fibre diameters were obtained at a voltage of 25 kV than 20 kV, thus the voltage of 20 kV is the more favourable parameter. Furthermore, the fibres were more uniform in Fig. 5.12a (flowrate 1.0 mL/h) than in Fig. 5.12b (flowrate 1.5 mL/h). Best morphology of TPU C patches was the one fabricated with 1.0 mL/h and 20 kV as presented in Fig. 5.12a.

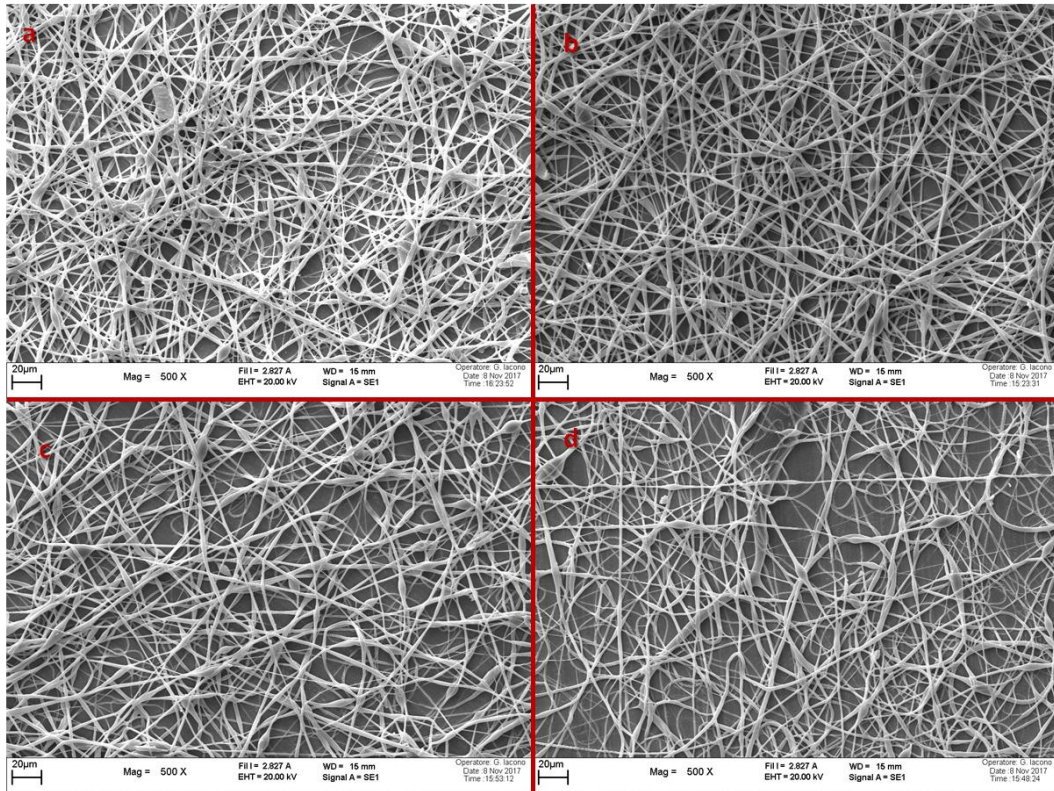


Figure 5.12: Type C (SP-93A-100) TPU electrospun fibres: a) 20 kV + 1.0 mL/h, b) 20 kV + 1.5 mL/h, c) 25 kV + 1.5 mL/h, d) 25 kV + 1.0 mL/h

Figure 5.13 shows the effect of 10 w/v% polymer solution concentration on fibre morphology. Parameters kept constant in this setup were: 25 kV applied voltage, 1.5 mL/h flowrate, 20 cm distance between collector and needle. TPU A samples were beads sprayed onto the collector while TPU C appeared to have some small fibres connecting one bead to another.

Surface tension decreased with concentration, leading to spraying in the case of TPU A. In the case of TPU C, beaded defect were present due to incomplete solvent evaporation. Hence, 10% was not a correct solution concentration to be used for electrospinning.

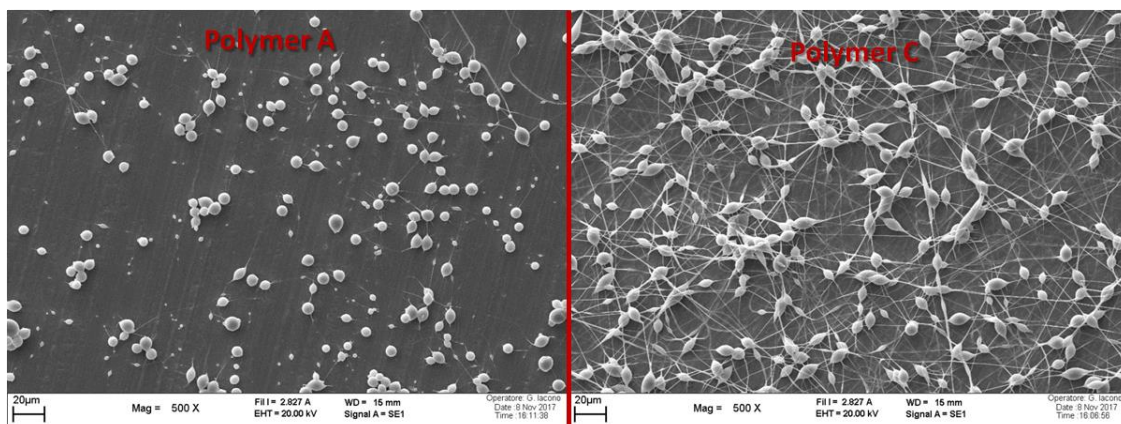


Figure 5.13: TPU A (left) and C (right) electrospun in 10 w/v% chloroform.

The next step in the electrospinning optimization was to find a co-solvent that would improve the conductivity of the solution in order to create thinner fibres. This was done by dissolving the polymers in a blend of 90 v/v% chloroform and 10 v/v% formic acid to provide ionic charges of HCOO^- and H^+ in the solution. Polymer concentration was still maintained at 15 w/v% in this solvent mixture. The best electrospinning parameters for TPUs A and C selected using chloroform solutions were then applied to polymer solutions in solvent mixture. These parameters are summarized in Table 5.2.

Table 5. 2. Shorthand for electrospinning parameter set-ups

	I	II	III	IV
Polymer (TPUs)	C	C	A	A
Concentration (w/v%)	15	15	15	15
Voltage (kV)	20	20	25	20
Flowrate (mL/h)	1	1.5	1.5	1.5
Nozzle-collector distance (cm)	20	20	20	20

Figures 5.14 to 5.17 show the comparison of SEM morphology of membranes electrospun using parameters in Table 5.2 with and without the addition of formic acid to the polymer solution. Generally, while some defects can still be observed, upon SEM observation the fibres in the chloroform/formic acid (CHCl₃/FA) solution had better consistency and appeared thinner than their counterparts. Thus, the addition of formic acid, increasing the conductivity of TPU polymer solution, was an effective approach for improving electrospinning.

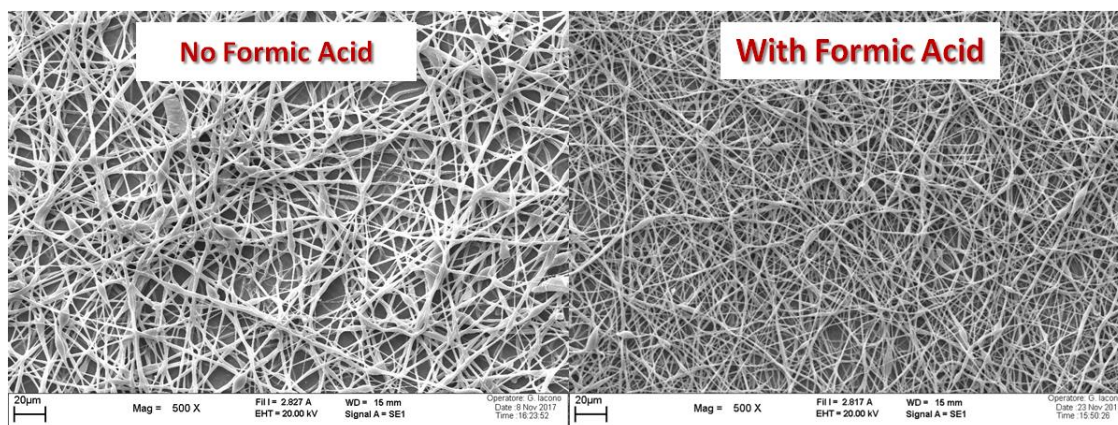


Figure 5.14: Electrospinning Setup I

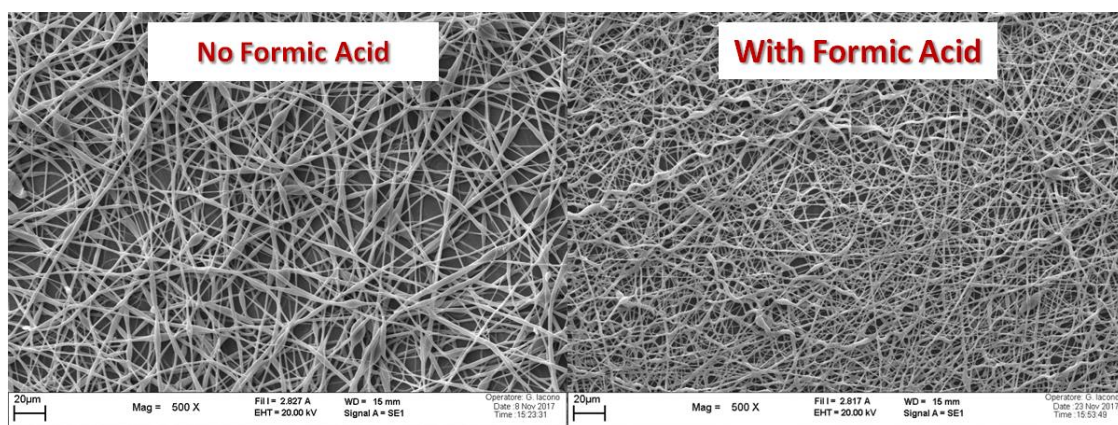


Figure 5.15: Electrospinning Setup II

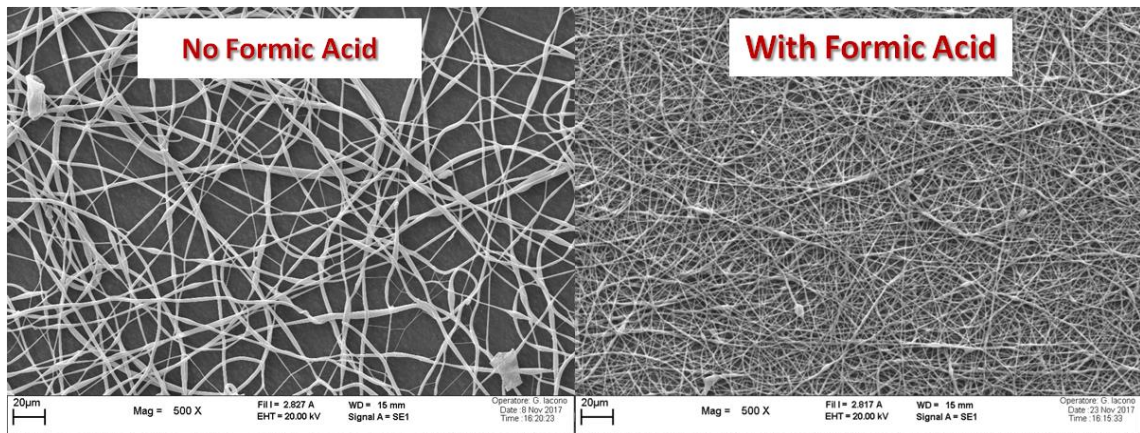


Figure 5.16: Electrospinning Setup III

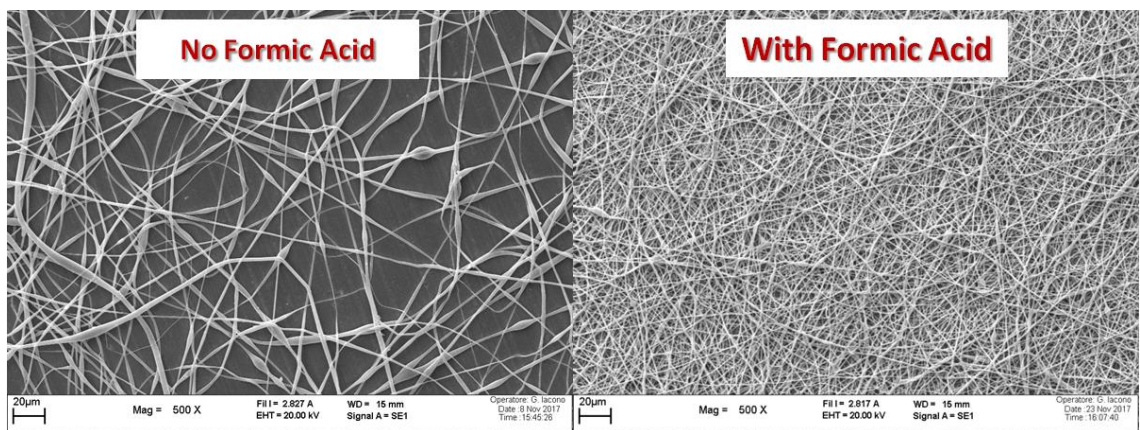


Figure 5.17: Electrospinning Setup IV

Using ImageJ software, the diameters of the fibres were measured by taking 30 random measurements in the SEM images. Values are plotted in Figure 5.18 and tabulated for further clarification in Table 5.3. By adding formic acid into the solvent, in a setup with the same operating parameters, the fibres became much thinner and more uniform based on their decreased standard deviation. Additionally they could densely deposit on the collector (Fig. 5.14-5.17).

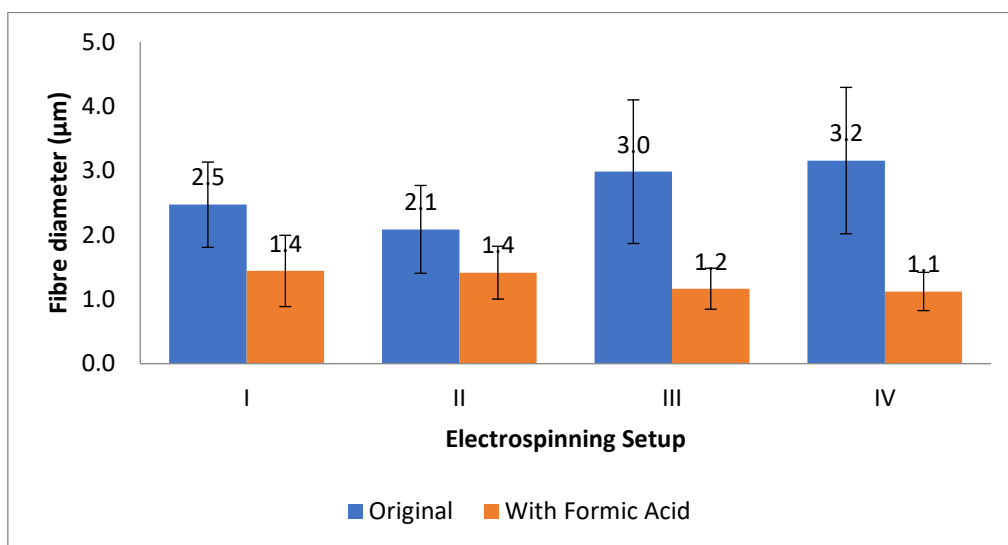


Figure 5.18: Measurement of average fibre diameters.

<

Table 5.3. Tabulation of fibre diameters of electrospun TPUs

	Chloroform only				Chloroform + Formic Acid			
	I	II	III	IV	I	II	III	IV
Average (µm)	2.5	2.1	3.0	3.2	1.4	1.4	1.2	1.1
SD (µm)	0.7	0.7	1.1	1.1	0.6	0.4	0.3	0.3
Min (µm)	1.4	1.0	0.8	1.4	0.7	0.7	0.7	0.7
Max(µm)	3.7	3.6	5.6	6.4	3.1	2.2	1.8	1.7
% SD	26.8	32.7	37.4	36.1	38.4	29.0	27.3	26.5

TPU A or Lubrizol Tecophilic SP60D60 was finally selected based on its hydrophilic properties, good mechanical performance, and when electrospun in different parameters it gave the thinnest and most consistent fibres. The polymer solution was also much more convenient than TPU C to handle as it was not too viscous nor too runny and did not clog the electrospinning needle as often as TPU C did when being electrospun.

The optimal electrospinning parameters were: 15 w/v% TPU A solution concentration in an organic solvent that consists of 90 v/v% chloroform and 10 v/v% formic acid; flowrate of 1.5 mL/h through a 21 G needle placed at a distance of 20 cm from the collector with an applied voltage of 20 kV. The final electrospun product appeared as a thin elastic sheet. Upon SEM analysis of this material, a network of thin fibres randomly arranged to form a mesh-like structure of randomly arranged fibres was observed.

5.5. Conclusions

In this work, four types of commercially available TPUs were characterized: Lubrizol Tecophilic SP60D60 (TPU A), Lubrizol Tecophilic SP80A150 (TPU B), Lubrizol Tecophilic SP93A100 (TPU C), Lubrizol Tecoflex SP80A150 (TPU D). Considering tensile mechanical properties, these materials showed ultimate tensile strength and elongation percentage at break values which were within the reported ranges for commercially available polymer wound dressings. Hence, the selection was mainly based on hydrophilicity (static contact angle and percentage of water absorption). Based on that, TPU A and TPU C were electrospun at different parameters and their morphology was assessed based on reduced number of defects, fibre thickness, and fibre consistency.

Finally, TPU A/Lubrizol Tecophilic SP60D60 (an aliphatic polyether as described in the material data sheet) yielded the most optimal results for electrospinning as it produced the thinnest fibre diameters with the lowest standard deviation, suggesting uniform structure. Optimal electrospinning parameters were: 15 w/v% polymer in organic solution (90 v/v% CHCl₃, 10 v/v% formic acid), 20 kV voltage, 20 cm distance between the spinneret and the metal collector, 1.5 mL/h feed rate through

a 21 G needle. Such random fibrous patches showed an average fibre diameter of $1.1 \pm 0.3 \mu\text{m}$.

In terms of physical and mechanical properties, films of the selected TPU had a static contact angle of $72.0 \pm 2.9^\circ$, water absorbance of $44.7 \pm 4.9\%$ after 24 hours and $60.6 \pm 3.0\%$ after 4 weeks, ultimate tensile strength of $10.4 \pm 0.7 \text{ MPa}$, and Young's modulus of $25.1 \pm 1.5 \text{ MPa}$, elongation percentage of $386 \pm 63\%$. The final electrospun product appeared as a thin, elastic sheet. Upon SEM imaging of this material, a network of thin fibres randomly arranged to form a mesh-like structure was revealed. This would be useful for applications where the loading of drugs or antibacterial agents should be performed. It also has the potential to act as a scaffold for cells to grow into and to be utilized for wound healing purposes. In later chapters, its application as a honey-mimetic wound healing device via polyDOPA surface modification to graft glucose oxidase enzymes will be explored and discussed.

5.6. References

- (1) Khil, M.-S.; Cha, D.-I.; Kim, H.-Y.; Kim, I.-S.; Bhattarai, N. Electrospun Nanofibrous Polyurethane Membrane as Wound Dressing. *J. Biomed. Mater. Res. Part B* **2003**, *67*, 675–679. <https://doi.org/10.1002/jbm.b.10058>.
- (2) Wang, N.; Burugapalli, K.; Song, W.; Halls, J.; Moussy, F.; Zheng, Y.; Yanxuan, M.; Wu, Z.; Li, K. Tailored Fibro-Porous Structure of Electrospun Polyurethane Membranes, Their Size-Dependent Properties and Trans- Membrane Glucose Diffusion. *J Memb Sci.* **2015**, *25* (8), 713–724. <https://doi.org/10.1097/MCA.000000000000178>. Endothelial.
- (3) Liu, Y.; Zhou, G.; Liu, Z.; Guo, M.; Jiang, X.; Taskin, M. B.; Zhang, Z.; Liu, J.; Tang, J.; Bai, R.; et al. Mussel Inspired Polynorepinephrine Functionalized Electrospun Polycaprolactone Microfibers for Muscle Regeneration. *Sci. Rep.* **2017**, *7* (1), 1–10. <https://doi.org/10.1038/s41598-017-08572-z>.

- (4) Xie, M.; Wang, J.; Wang, X.; Yin, M.; Wang, C.; Chao, D.; Liu, X. The High Performance of Polydopamine-Coated Electrospun Poly(Ether Sulfone) Nanofibrous Separator for Lithium-Ion Batteries. *Macromol. Res.* **2016**, *24* (11), 965–972. <https://doi.org/10.1007/s13233-016-4140-3>.
- (5) Kim, M.-R.; Park, S.-H.; Kim, J.-U.; Lee, J.-K. Dye-Sensitized Solar Cells Based on Polymer Electrolytes. *Sol. Cells - Dye. Devices* **2012**, No. November. <https://doi.org/10.5772/22237>.
- (6) Agrahari, V.; Agrahari, V.; Meng, J.; Mitra, A. K. *Electrospun Nanofibers in Drug Delivery*; Elsevier, 2017. <https://doi.org/10.1016/b978-0-323-42978-8.00009-7>.
- (7) Agarwal, S.; Wendorff, J. H.; Greiner, A. Use of Electrospinning Technique for Biomedical Applications. *Polymer (Guildf)*. **2008**, *49* (26), 5603–5621. <https://doi.org/10.1016/j.polymer.2008.09.014>.
- (8) Duque Sánchez, L.; Brack, N.; Postma, A.; Pigram, P. J.; Meagher, L. Surface Modification of Electrospun Fibres for Biomedical Applications: A Focus on Radical Polymerization Methods. *Biomaterials* **2016**, *106*, 24–45. <https://doi.org/10.1016/j.biomaterials.2016.08.011>.
- (9) Xie, J.; Michael, P. L.; Zhong, S.; Ma, B.; MacEwan, M. R.; Lim, C. T. Mussel Inspired Protein-Mediated Surface Modification to Electrospun Fibers and Their Potential Biomedical Applications. *J. Biomed. Mater. Res. - Part A* **2012**, *100 A* (4), 929–938. <https://doi.org/10.1002/jbm.a.34030>.
- (10) Liu, M.; Duan, X. P.; Li, Y. M.; Yang, D. P.; Long, Y. Z. Electrospun Nanofibers for Wound Healing. *Mater. Sci. Eng. C* **2017**, *76*, 1413–1423. <https://doi.org/10.1016/j.msec.2017.03.034>.
- (11) Xeltis. The world's first polymer-based technology platform enabling ETR : Xeltis <http://xeltis.com/technology/> (accessed Apr 6, 2019).
- (12) Ortho reverse | The world's first! Cotton-shaped artificial bone filler material Rebossis birth -ORTHOREBIRTH- <http://orthorebirth.com/?lang=ja> (accessed Apr 6, 2019).
- (13) Heo, D. N.; Yang, D. H.; Lee, J. B.; Bae, M. S.; Kim, J. H.; Moon, S. H.; Chun, H. J.; Kim, C. H.; Lim, H. N.; Kwon, I. K. Burn-Wound Healing Effect of Gelatin/Polyurethane Nanofiber Scaffold Containing Silver-Sulfadiazine. *J. Biomed. Nanotechnol.* **2013**, *9* (3), 511–515. <https://doi.org/10.1166/jbn.2013.1509>.
- (14) Wang, Y. .; Li, P. .; Xiang, P. .; Lu, J. .; Yuan, J. .; Shen, J. . Electrospun Polyurethane/Keratin/AgNP Biocomposite Mats for Biocompatible and Antibacterial Wound Dressings. *J. Mater. Chem. B* **2016**, *4* (4), 635–648. <https://doi.org/10.1039/c5tb02358k>.

- (15) Han, J.; Chen, T. X.; Branford-White, C. J.; Zhu, L. M. Electrospun Shikonin-Loaded PCL/PTMC Composite Fiber Mats with Potential Biomedical Applications. *Int. J. Pharm.* **2009**, *382* (1–2), 215–221. <https://doi.org/10.1016/j.ijpharm.2009.07.027>.
- (16) Kontogiannopoulos, K. N.; Assimopoulou, A. N.; Tsivintzelis, I.; Panayiotou, C.; Papageorgiou, V. P. Electrospun Fiber Mats Containing Shikonin and Derivatives with Potential Biomedical Applications. *Int. J. Pharm.* **2011**, *409* (1–2), 216–228. <https://doi.org/10.1016/j.ijpharm.2011.02.004>.
- (17) Manikandan, A.; Prasath, M.; Kumar, S. Formation of Functional Nanofibers Electrospun Polyurethane and Murivenna Oil with Improved Haemocompatibility for Wound Healing. **2017**, *61*, 106–113.
- (18) Zaman, H. U.; Islam, J. M. M.; Khan, M. A.; Khan, R. A. Physico-Mechanical Properties of Wound Dressing Material and Its Biomedical Application. *J. Mech. Behav. Biomed. Mater.* **2011**, *4* (7), 1369–1375. <https://doi.org/10.1016/j.jmbbm.2011.05.007>.
- (19) Baker, S. R.; Banerjee, S.; Bonin, K.; Guthold, M. Determining the Mechanical Properties of Electrospun Poly-ε-Caprolactone (PCL) Nanofibers Using AFM and a Novel Fiber Anchoring Technique. *Mater. Sci. Eng. C* **2016**, *59*, 203–212. <https://doi.org/10.1016/j.msec.2015.09.102>.
- (20) Lee, S. M.; Park, I. K.; Kim, Y. S.; Kim, H. J.; Moon, H.; Mueller, S.; Jeong, Y. I. L. Physical, Morphological, and Wound Healing Properties of a Polyurethane Foam-Film Dressing. *Biomater. Res.* **2016**, *20* (1), 1–11. <https://doi.org/10.1186/s40824-016-0063-5>.
- (21) Burke, A.; Hasirci, N. Polyurethanes in Biomedical Applications. *Biomater. From Mol. to Eng. Tissues* **2004**, 83–105. https://doi.org/10.1007/978-0-306-48584-8_7.
- (22) Józwiak, A. B.; Kielty, C. M.; Black, R. a. Surface Functionalization of Polyurethane for the Immobilization of Bioactive Moieties on Tissue Scaffolds. *J. Mater. Chem.* **2008**, *18* (19), 2240. <https://doi.org/10.1039/b719025e>.
- (23) Tecoflex™ TPU - Lubrizol <https://www.lubrizol.com/Life-Sciences/Products/Tecoflex-TPU> (accessed Mar 11, 2019).
- (24) Tecophilic™ TPU - Lubrizol <https://www.lubrizol.com/Life-Sciences/Products/Tecophilic-TPU> (accessed Mar 11, 2019).
- (25) Navamathavan, R.; Panth, H. R.; Park, S.-J.; Nirmala, R.; Kim, H. Y.; Nam, K. T.; Yi, C. Effect of Solvents on High Aspect Ratio Polyamide-6 Nanofibers via Electrospinning. *Macromol. Res.* **2010**, *18* (8), 759–765.

<https://doi.org/10.1007/s13233-010-0808-2>.

- (26) Commentary, G. De Finitions for Hydrophilicity, Hydrophobicity, and Superhydrophobicity: Getting the Basics Right. *J. Phys. Chem. Lett.* **2014**, *5*, 686–688. <https://doi.org/10.1021/jz402762h>.
- (27) Cambridge University. Young's Modulus and Specific Stiffness <http://www-materials.eng.cam.ac.uk/mpsite/properties/non-IE/stiffness.html> (accessed Apr 21, 2019).
- (28) Kishore, K.; Gayathri, V. Estimation of Young's Modulus of Elastomers Using Thermomechanical Analyzer. *J. Polym. Sci. Part C Polym. Lett.* **1981**, *19* (1), 475–478.

↳

Chapter 6 Preparation and Characterization of "Bio-artificial" Electrospun TPU Wound Healing Patch

6.1. Abstract

This chapter describes GO enzyme surface functionalization mediated by 3,4-dihydroxyphenylalanine (DOPA)-based coating - polyDOPA (PDA) - with the aim to prepare ROS-producing electrospun wound patches, made of a medical grade commercially available thermoplastic polyurethane (TPU). One commercially available TPU was selected for its hydrophilic properties, tensile strength, elongation properties, and was processed by electrospinning to form membranes which pores may allow glucose and H₂O₂ diffusion (Chapter 5), facilitating both the formation and the release into the wound of antibacterial H₂O₂. Electrospun TPU fibrous patches discussed in Chapter 5 were proposed as the protective covering of the wound dressing hydrogels discussed in Chapters 2-3, while providing an additional source of antibacterial ROS.

The current chapter clarifies the design of the GO-functionalized TPU wound patches. The theoretical background behind the DOPA-mediated method of functionalization and surface modification of the wound patch with GO is here discussed while the subsequent chapters deal with the experimental preparation of the functionalized TPU patches. TPU patches could also be used alone (without the underlying hydrogel) and ROS could also be produced by periodically adding a glucose-releasing hydrogel on the top of the TPU covering (Chapter 8).

This “bio-artificial” wound healing patch, based on a synthetic polymer (TPU) and a natural component (GO) was developed at Politecnico di Torino.

6.2. Introduction

6.2.1. Improved design for wound healing and protection

Taking the concept of enzyme immobilization from Chapter 4, this is here applied to the development of a dual-purpose wound patch that can both protect the antibacterial hydrogel (e.g. HB PEGDA/HA-SH loaded with glucose oxidase and glucose) from outside contamination and provide an additional method of ROS production through its surface-immobilized GO enzyme. Additionally, this system differs from the immobilized-GO system in Chapter 4 in that the immobilized enzymes are confined on the substrate surface instead of being immobilized throughout the hydrogel.

This wound patch should let H_2O_2 be formed from glucose embedded in the bottom HB PEGDA/HA-SH hydrogel or added on its top through an additional top hydrogel and allow H_2O_2 diffuse into the bottom hydrogel layer.

6.2.2. Requirements of wound healing patches

In designing wound healing devices, the material should meet the following general requirements: cover the wound to prevent infection, provide a moist and warm environment, and be physically and chemically compatible to the nature of the wound¹. Additional specific requirements of wound patch here designed are hydrophilicity and porous structure. The desired wound healing properties have been discussed more in depth in Chapter 1 and 5.

6.2.3. State of the art of polymers for wound healing patches

Apart from wound healing hydrogels which were previously discussed from Chapters 1 to 4, other polymeric wound patches also exist with different wound healing functionalities such as foams, fibres, and films.

Porous polymer foams have been applied in wound healing and are commercially available such as Simpurity, a polymer pad which was reported to have an absorption capacity of more than 10 times its weight among its listed properties². Wound dressings made of polyurethane flat foams have been produced by Finesse Medical, Ltd³.

Among a list of polymer processing technologies, electrospinning polymers into non-woven fibres provide particular interest in wound healing applications as they are capable of exhibiting a texture similar to textiles while having a porous structure that would allow the drainage of wound exudates and the permeation of oxygen into the wound for healing⁴.

Other properties that make electrospun fibres relevant to wound healing are: i) their ability for long term delivery of bioactive compounds to tissues at the wound site, ii) ability for physical protection of the wound, iii) loading of up to 40% of drugs, with the release controlled by manipulating the type and composition of the fibres^{4,5}.

Electrospun fibres can also be surface modified in order to immobilize enzymes. Enzyme grafting was mediated by “mussel-inspired” pre-coating⁶⁻⁸. For this research, thermoplastic polyurethanes (TPUs) were selected as the polymer substrate for electrospinning, surface functionalization, and immobilization given their established versatility in wound healing applications⁹⁻¹¹. The substrate used in this chapter was Lubrizol SP60D60 TPU fibre patch fabricated in Chapter 5, which was coded here simply as TPU since only one type of polyurethane was used.

6.2.4. Coating techniques for wound healing patches

To give the TPU adhesive properties for the purposes of adhering to the hydrogel tissue and immobilizing GO, the concept of mussel-inspired coatings was exploited. This mussel-inspired coating is based on the substance secreted by mussels which is a type of liquid protein that hardens rapidly into a solid, water-resistant adhesive material¹². This liquid protein was found to contain 3,4-dihydroxyphenylalanine (DOPA), a catechol containing amino acid¹². When L-DOPA is in a basic solution such as pH 8.5 and has access to oxygen (i.e. the solution is aerated by stirring or shaking), it oxidizes to form polyDOPA. The chemical structure of L-DOPA is shown in Figure 6.1. Upon oxidation, it may deposit onto almost any type of substrate (metals, glass, polymers, etc.), coating the material in the form of a crosslinked and branched polymer, polyDOPA⁸.

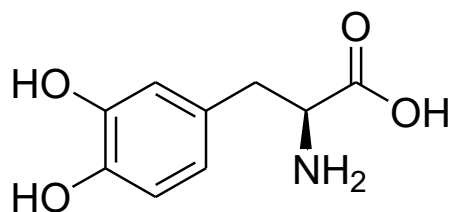


Figure 6.1: Chemical structure of L-DOPA

6.2.4.1. Applications of polyDOPA coatings

Figure 6.2 shows the oxidation of L-DOPA into polyDOPA¹³. Upon L-DOPA oxidation, polyDOPA (PDA) deposits itself into the substrate: this coating contains a type of functional group, called quinone, to which various molecules can be grafted, such as bioactive molecules, growth factors, and enzymes¹⁴ (see Figure 6.4 for these types of reactions).

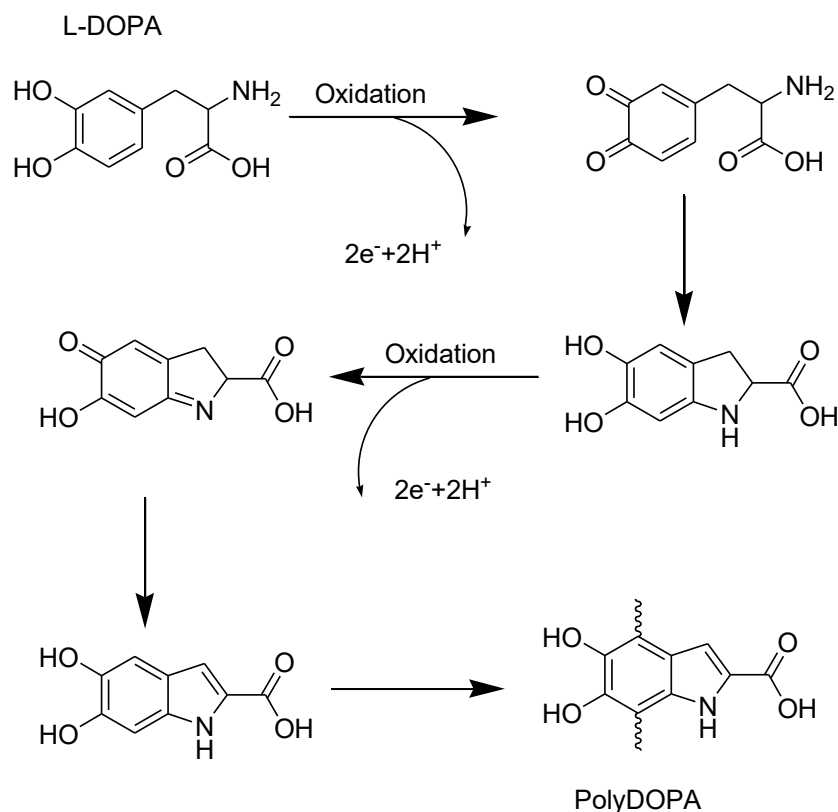


Figure 6.2: Oxidation process of L-DOPA into polyDOPA

Polydopamine was used for coating materials in some studies (derived from dopamine) while other studies utilized polyDOPA (produced from DOPA) and authors generally assigned the acronym PDA to the coatings. For this study, PDA will refer only to polyDOPA. Such coating is used in a wide variety of biomedical applications, having adhesive properties for surface functionalization in binding bioactive molecules, growth factors, enzymes, and biomimetic molecules (e.g. gelatin and chitosan)¹⁵⁻¹⁷. Figure 6.3 shows polyDOPA and polydopamine formation from their monomer units and their polymer structure.

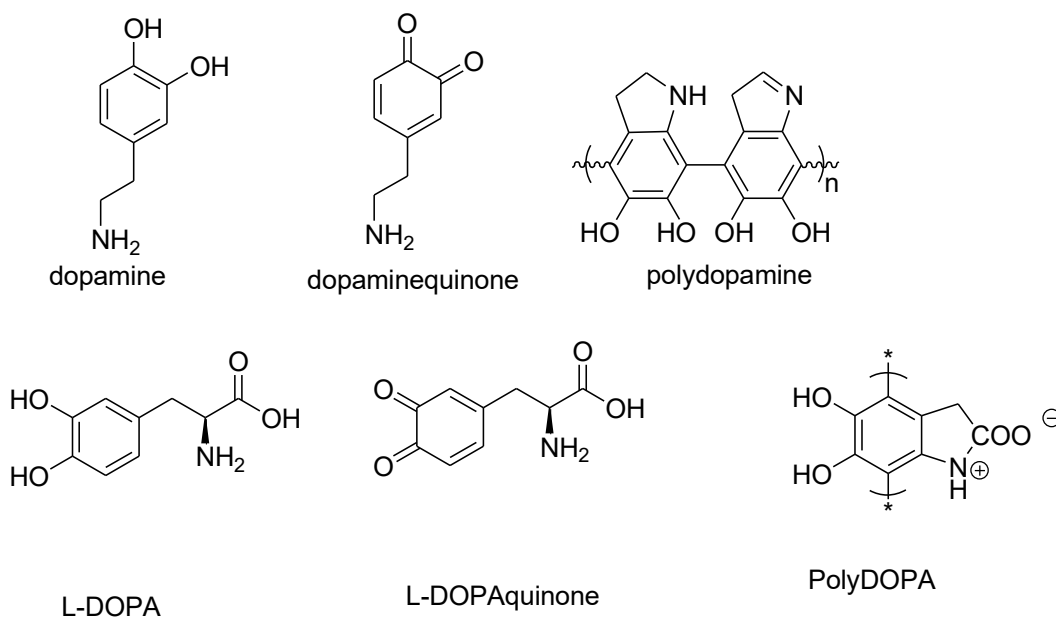


Figure 6.3: Structure of L-DOPA, dopamine, and their polymer derivatives

The coating process by self-oxidation requires immersing the material in a dopamine or in a DOPA solution (e.g. 2 mg/ml dopamine in, pH 8.5 in TRIS buffer 10 mM) for 8-24 hours¹⁷⁻²². By using a catalyst (organic or inorganic) this reaction has the potential to be made much quicker, reducing the required time for surface modification and potentially resulting in a thicker PDA coating in the substrate.

What makes PDA versatile for binding an array of organic molecules is its ability to covalently react with functional groups such as imidazole, amine, or thiols as reported in Figure 6.4²³. In immobilizing enzymes, the main mode for conjugating them to the PDA-coated substrate is to take advantage of Michael type addition which can occur in mild aqueous conditions.

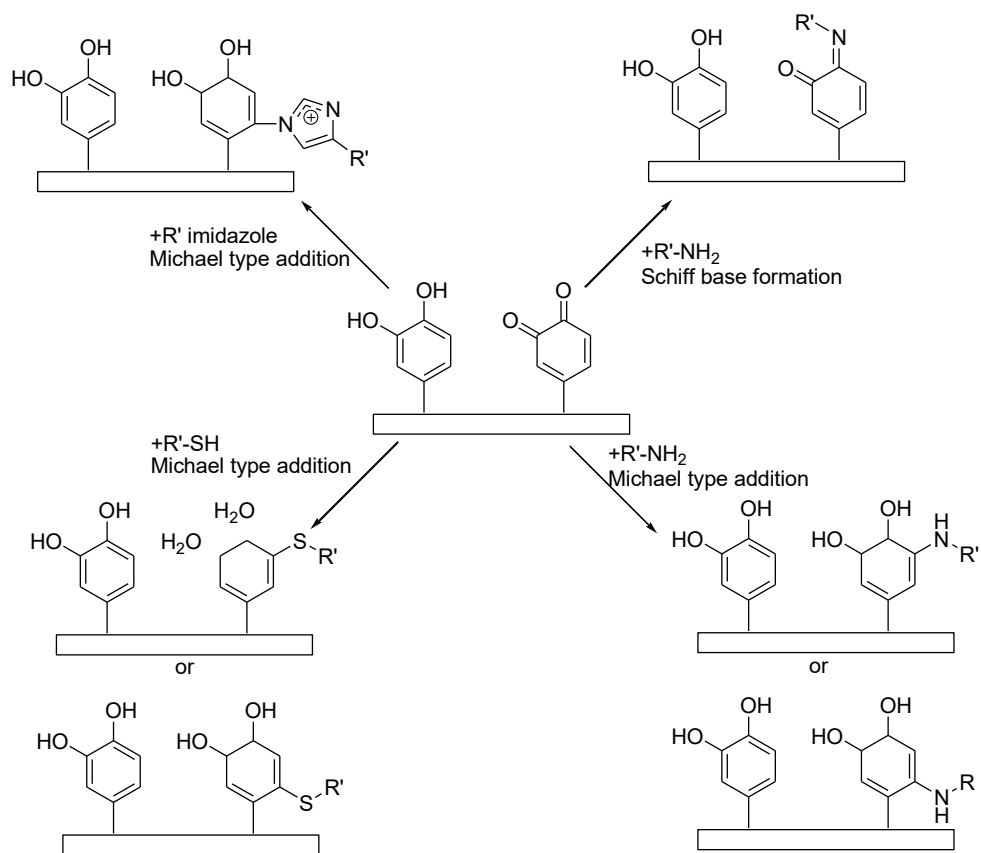


Figure 6.4: Possible reaction pathways in a PDA-coated surface (R' = polymeric backbone). Image drawn by the author, modified from Bazaka, K., et al. (2015)²⁴.

6.2.4.2. Immobilization of enzymes on PDA-coated surfaces

In a study carried out by Zhou L., et al (2014), graphene oxide was coated with polydopamine and the model enzyme was glucose oxidase²⁵. Results showed that the following properties were improved after immobilization: thermal and pH stability, storage stability, and resistance towards GO-denaturing agents, with the immobilized enzyme activity almost identical to the free enzyme activity²⁵. Thus, an electrospun TPU can be fabricated and coated with PDA, as shown in Figure 6.5, creating an intermediate material, TPU-PDA. When coated, the material exhibits a light brown to black colour due to the PDA deposition on the substrate.

Using an oxidizing catalyst, the rate of deposition can be manipulated and increased.

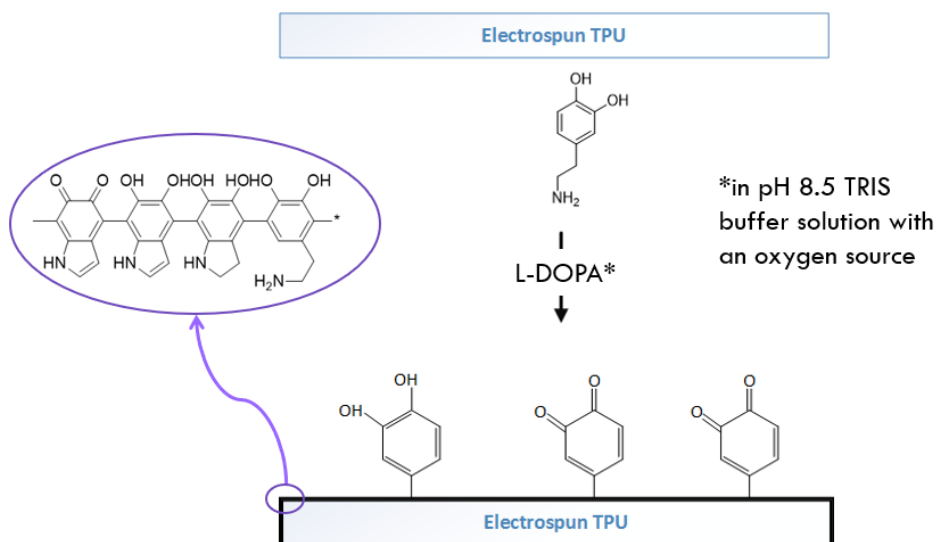


Figure 6.5: PDA-coating of electrospun thermoplastic polyurethane fibre patch (end-product named as TPU-PDA).

After the fibre patch was coated with PDA, glucose oxidase was immobilized onto the TPU-PDA material by immersing the substrate into a GO solution. Through primarily Michael type addition of R'-NH₂ functional groups, the enzyme binds itself to the PDA substrate, where the quinone groups form from catechols, as shown in Figure 6.6. The lateral amine groups of the enzyme (such as those found in arginine, lysine, and glutamine) reacts with the quinone groups in the PDA coating and the enzyme is grafted into the TPU fibre substrate.

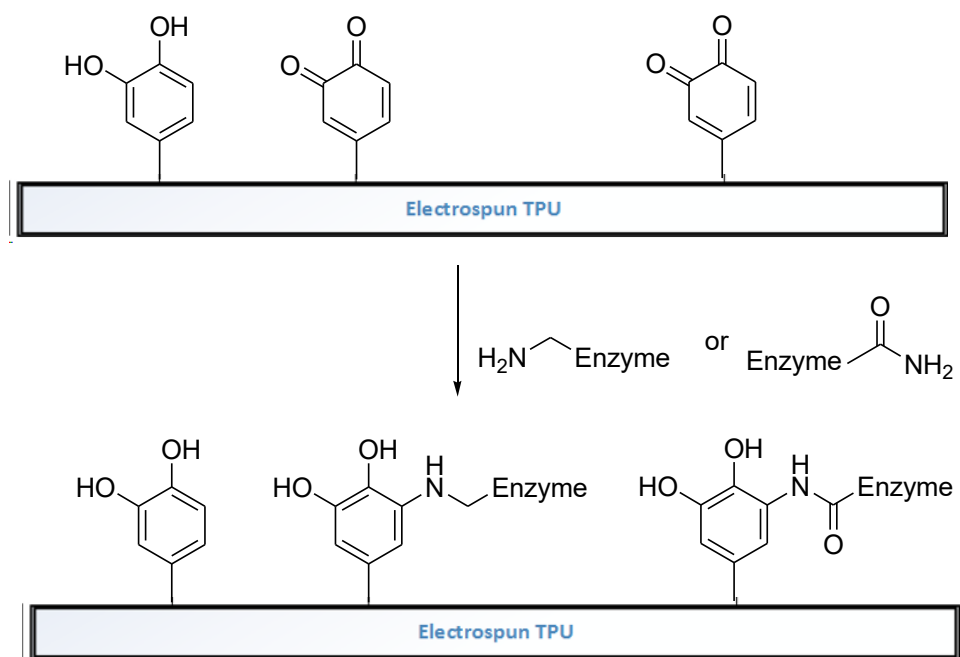


Figure 6.6: Enzyme immobilization on TPU-PDA (end-product named as TPU-PDA-GO).

Figure 6.7 shows a few of the possible reaction pathways of three amino acids that can be found in enzymes with the quinone groups in a PDA-coated material. They show the amino acids grafted at one site in the phenol ring however, they can also graft itself in other locations as depicted in Figure 6.4.

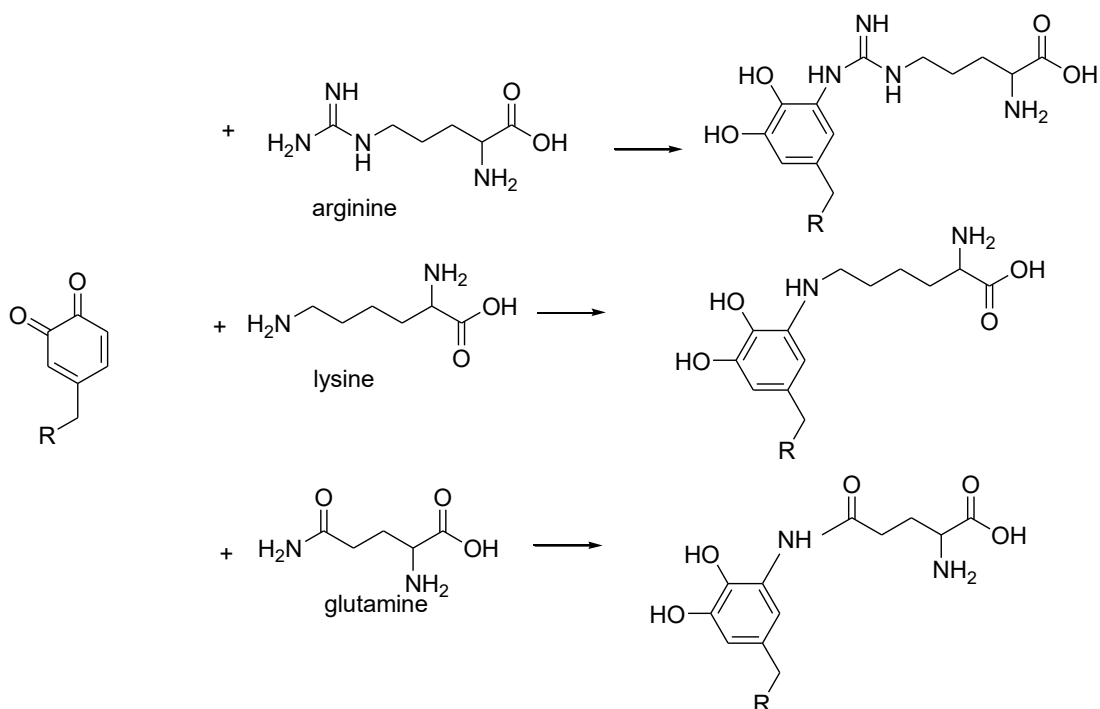


Figure 6.7: Reaction of several amino acids with a quinone group found in a PDA-coated substrate.

6.3. Theoretical design of multilayer wound healing patch

In the next chapters 7 to 8, the development of a glucose oxidase-immobilized, PDA-coated, electrospun TPU (TPU-PDA-GO) fibre patch will be described. The electrospun fibre patch (with its fabrication and characterization process described in chapter 5) can be used as a protective covering for the HB PEGDA/HA-SH hydrogel containing GO enzyme and glucose, as depicted in Figure 6.8 which schematically shows the multilayer wound patch. This protective fibre patch can also serve as an additional ROS source, exploiting both glucose contained in the bottom hydrogel and released from an additional top hydrogel. Particularly, the top glucose-loaded hydrogel can be removed and replaced to replenish the glucose

source, during the wound healing process without the need to peel off the HB PEGDA/HA-SH hydrogel and the TPU-PDA-GO wound patch.

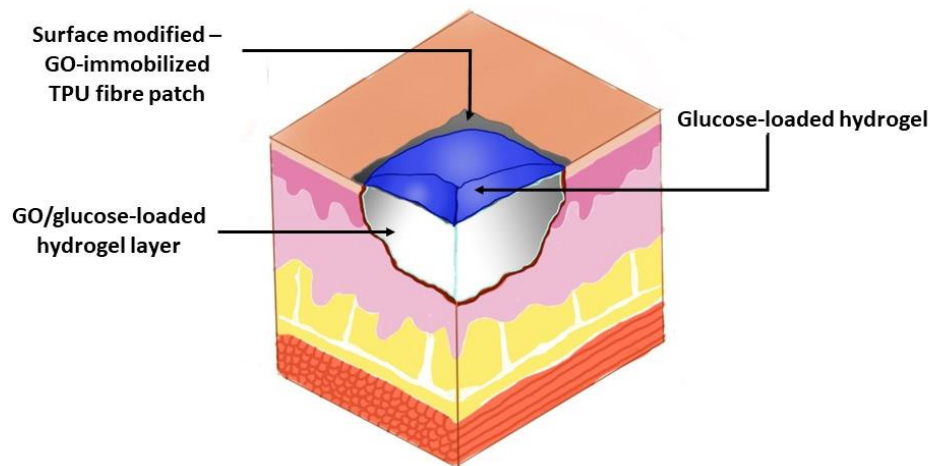


Figure 6.8: Overall multilayer antibacterial ROS-producing wound healing device

An alternative use for the fibre mat is to directly place it on the wound surface without the GO/glucose loaded bottom hydrogel and to deliver a replenishable glucose source on top of the TPU-PDA-GO fibre mat.

This represents an innovative application. In the previous literature, Lin CC., et al. (2016) showed that PDA-coated electrospun fibre mats cultured with adipose-derived stem cells were capable of osteogenesis¹⁵. A PDA-coated electrospun fibre mat has also been used as a wound healing scaffold when grafted with basic fibroblast growth factor in the study carried out by Sun, X., et al. (2014)²⁶.

In this work, TPU-PDA-GO will potentially function as an antibacterial wound healing patch to be used alone or in combination with HB PEGDA/HA-SH hydrogel and will help tissue regeneration acting as a tissue scaffold.

The next chapters will deal with the development of the TPU-PDA-GO electrospun fibre patch and finally the glucose-loaded top hydrogel as well as their relevant physicochemical properties.

6.4. References

- (1) Mir, M.; Murtaza, .; Ali, N.; Barakullah, A.; Gulzar, A.; Arshad, . Munam; Fatima, S.; Asad, M. Synthetic Polymeric Biomaterials for Wound Healing: A Review. **2018**, *7*, 1–21. <https://doi.org/10.1007/s40204-018-0083-4>.
- (2) Simpurity™ Polymer Pad Wound Dressing | WoundSource
<https://www.woundsource.com/product/simpurity-polymer-pad-wound-dressing> (accessed Mar 4, 2019).
- (3) Polyurethane Flat Foam Dressings - Finesse Medical
https://www.finessemedical.com/go/products/wound_management/polyurethane_foam/flat-foam-dressings (accessed Mar 4, 2019).
- (4) Faglie, A.; Neuenschwander, P.; Thompson, J.; Lee, S.-Y.; Gizaw, M.; Chou, S.-F. Electrospun Fibers as a Dressing Material for Drug and Biological Agent Delivery in Wound Healing Applications. *Bioengineering* **2018**, *5* (1), 9. <https://doi.org/10.3390/bioengineering5010009>.
- (5) Liu, M.; Duan, X.-P.; Li, Y.-M.; Yang, D.-P.; Long, Y.-Z. Electrospun Nanofibers for Wound Healing. *Mater. Sci. Eng. C* **2017**, *76*, 1413–1423. <https://doi.org/10.1016/j.msec.2017.03.034>.
- (6) Liu, Y.; Zhou, G.; Liu, Z.; Guo, M.; Jiang, X.; Taskin, M. B.; Zhang, Z.; Liu, J.; Tang, J.; Bai, R.; et al. Mussel Inspired Polynorepinephrine Functionalized Electrospun Polycaprolactone Microfibers for Muscle Regeneration. *Sci. Rep.* **2017**, *7* (1), 1–10. <https://doi.org/10.1038/s41598-017-08572-z>.
- (7) Zhang, H.; Bré, L. P.; Zhao, T.; Zheng, Y.; Newland, B.; Wang, W. Mussel-Inspired Hyperbranched Poly(Amino Ester) Polymer as Strong Wet Tissue Adhesive. *Biomaterials* **2014**, *35* (2), 711–719. <https://doi.org/10.1016/j.biomaterials.2013.10.017>.

- (8) Xie, J.; Michael, P. L.; Zhong, S.; Ma, B.; MacEwan, M. R.; Lim, C. T. Mussel Inspired Protein-Mediated Surface Modification to Electrospun Fibers and Their Potential Biomedical Applications. *J. Biomed. Mater. Res. - Part A* **2012**, *100 A* (4), 929–938. <https://doi.org/10.1002/jbm.a.34030>.
- (9) Kim, S. E.; Heo, D. N.; Lee, J. B.; Kim, J. R.; Park, S. H.; Jeon, S. H.; Kwon, I. K. Electrospun Gelatin/Polyurethane Blended Nanofibers for Wound Healing. *Biomed. Mater.* **2009**, *4* (4), 044106. <https://doi.org/10.1088/1748-6041/4/4/044106>.
- (10) Heo, D. N.; Yang, D. H.; Lee, J. B.; Bae, M. S.; Kim, J. H.; Moon, S. H.; Chun, H. J.; Kim, C. H.; Lim, H. N.; Kwon, I. K. Burn-Wound Healing Effect of Gelatin/Polyurethane Nanofiber Scaffold Containing Silver-Sulfadiazine. *J. Biomed. Nanotechnol.* **2013**, *9* (3), 511–515. <https://doi.org/10.1166/jbn.2013.1509>.
- (11) Józwiak, A. B.; Kielty, C. M.; Black, R. a. Surface Functionalization of Polyurethane for the Immobilization of Bioactive Moieties on Tissue Scaffolds. *J. Mater. Chem.* **2008**, *18* (19), 2240. <https://doi.org/10.1039/b719025e>.
- (12) Kaushik, N. K.; Kaushik, N.; Pardeshi, S.; Sharma, J. G.; Lee, S. H.; Choi, E. H. Biomedical and Clinical Importance of Mussel-Inspired Polymers and Materials. *Mar. Drugs* **2015**, *13* (11), 6792–6817. <https://doi.org/10.3390/md13116792>.
- (13) Sajitha, M.; Vindhyasarumi, A.; Gopi, A.; Yoosaf, K. Shape Controlled Synthesis of Multi-Branched Gold Nanocrystals through a Facile One-Pot Bifunctional Biomolecular Approach. *RSC Adv.* **2015**, *5* (119), 98318–98324. <https://doi.org/10.1039/C5RA19098C>.
- (14) Ding, Y. H.; Floren, M.; Tan, W. Mussel-Inspired Polydopamine for Bio-Surface Functionalization. *Biosurface and Biotribology* **2016**, *2* (4), 121–

136. <https://doi.org/10.1016/j.bsbt.2016.11.001>.
- (15) Lin, C. C.; Fu, S. J. Osteogenesis of Human Adipose-Derived Stem Cells on Poly(Dopamine)-Coated Electrospun Poly(Lactic Acid) Fiber Mats. *Mater. Sci. Eng. C* **2016**, *58*, 254–263. <https://doi.org/10.1016/j.msec.2015.08.009>.
- (16) Cho, H. J.; Madhurakkat Perikamana, S. K.; Lee, J. H.; Lee, J.; Lee, K. M.; Shin, C. S.; Shin, H. Effective Immobilization of BMP-2 Mediated by Polydopamine Coating on Biodegradable Nanofibers for Enhanced in Vivo Bone Formation. *ACS Appl. Mater. Interfaces* **2014**, *6* (14), 11225–11235. <https://doi.org/10.1021/am501391z>.
- (17) Kao, C. T.; Lin, C. C.; Chen, Y. W.; Yeh, C. H.; Fang, H. Y.; Shie, M. Y. Poly(Dopamine) Coating of 3D Printed Poly(Lactic Acid) Scaffolds for Bone Tissue Engineering. *Mater. Sci. Eng. C* **2015**, *56*, 165–173. <https://doi.org/10.1016/j.msec.2015.06.028>.
- (18) Xu, J.; Xu, N.; Zhou, T.; Xiao, X.; Gao, B.; Fu, J.; Zhang, T. Polydopamine Coatings Embedded with Silver Nanoparticles on Nanostructured Titania for Long-Lasting Antibacterial Effect. *Surf. Coatings Technol.* **2017**, *320*, 608–613. <https://doi.org/10.1016/j.surfcoat.2016.10.065>.
- (19) Su, L.; Yu, Y.; Zhao, Y.; Liang, F.; Zhang, X. Strong Antibacterial Polydopamine Coatings Prepared by a Shaking-Assisted Method. *Sci. Rep.* **2016**, *6* (1), 24420. <https://doi.org/10.1038/srep24420>.
- (20) Liu, Y.; Zhang, Z.; Lv, H.; Qin, Y.; Deng, L. Surface Modification of Chitosan Film via Polydopamine Coating to Promote Biomineralization in Bone Tissue Engineering. *J. Bioact. Compat. Polym.* **2017**, 088391151771322. <https://doi.org/10.1177/0883911517713228>.
- (21) Xie, M.; Wang, J.; Wang, X.; Yin, M.; Wang, C.; Chao, D.; Liu, X. The High Performance of Polydopamine-Coated Electrospun Poly(Ether

- Sulfone) Nanofibrous Separator for Lithium-Ion Batteries. *Macromol. Res.* **2016**, *24* (11), 965–972. <https://doi.org/10.1007/s13233-016-4140-3>.
- (22) Ponzio, F.; Barthès, J.; Bour, J.; Michel, M.; Bertani, P.; Hemmerlé, J.; D’Ischia, M.; Ball, V. Oxidant Control of Polydopamine Surface Chemistry in Acids: A Mechanism-Based Entry to Superhydrophilic-Superoleophobic Coatings. *Chem. Mater.* **2016**, *28* (13), 4697–4705. <https://doi.org/10.1021/acs.chemmater.6b01587>.
- (23) Lynge, M.; Schattling, P.; Stadler, B. Recent Developments in Poly (Dopamine) - Based Coatings for Biomedical Applications. *Nanomedicine* **2015**, *10*, 2725–2742. <https://doi.org/10.2217/nnm.15.89>.
- (24) Bazaka, K.; Jacob, M. V; Chrzanowski, W.; Ostrikov, K. Anti-Bacterial Surfaces: Natural Agents, Mechanisms of Action, and Plasma Surface Modification. **2015**. <https://doi.org/10.1039/c4ra17244b>.
- (25) Zhou, L.; Jiang, Y.; Ma, L.; He, Y.; Gao, J. Immobilization of Glucose Oxidase on Polydopamine-Functionalized. **2015**, 1007–1017. <https://doi.org/10.1007/s12010-014-1324-1>.
- (26) Sun, X.; Cheng, L.; Zhao, J.; Jin, R.; Sun, B.; Shi, Y.; Zhang, L.; Zhang, Y.; Cui, W. BFGF-Grafted Electrospun Fibrous Scaffolds via Poly(Dopamine) for Skin Wound Healing. *J. Mater. Chem. B* **2014**, *2* (23), 3636–3645. <https://doi.org/10.1039/c3tb21814g>.

Chapter 7 PolyDOPA Surface Coatings of Selected Wound Healing Thermoplastic Polyurethane Patch

7.1. Abstract

In this work, polyDOPA (PDA) coating was deposited on electrospun TPU fibre patches to produce TPU-PDA surface functionalized patches. PDA functionalization was performed as an intermediate coating for further surface grafting with GO enzyme. As a novelty, this chapter focuses on the use of an oxidizing enzyme, lactoperoxidase (LPO) to reduce the time required for PDA surface functionalization.

TPU fibre patches were immersed in a solution of DOPA at alkaline pH in aerated conditions: DOPA underwent oxidation into polymerizing DOPAquinone, gradually forming polyDOPA. The rates of DOPA oxidation changed based on the addition of different quantities of LPO. Based on absorbance measurements of polyDOPA solutions at 450 nm, it was found that the addition of 1.4 U/mL LPO to DOPA solution (2 mg/mL in 10 mM TRIS buffer at pH 8.5) reduced the coating

time from 7 hours to 2.5 hours respect to enzyme-free conditions. PDA-coating procedures using LPO were set at 3 hours to assure adequate coating.

Thus, the introduction of LPO in a DOPA (or even dopamine) solution may be used to reduce the time needed for PDA formation by dip-coating, to make this type of surface functionalization more efficient. This part of the activity was carried by the Ph.D student at Politecnico di Torino.

7.2. Introduction

7.2.1. Oxidation mechanism of mussel inspired L-3,4-dihydroxyphenylalanine (DOPA)

Mussels have been observed in marine environment to adhere to all types of surfaces, sustaining their bonds through mussel adhesive proteins or MAPs¹. There are 7-8 different proteins found in the mussel byssal threads, and six of these contain high concentrations of L-3,4-dihydroxyphenylalanine (L-DOPA)². A synthesized adhesive version of this when applied to surface-functionalized materials is polyDOPA (PDA) which is formed from the oxidation of L-DOPA (other studies utilize the conversion of dopamine into polydopamine). Figure 6.3 below shows for both L-DOPA and dopamine the structure of the original compounds, the quinone derivatives, and their forms as a polymer.

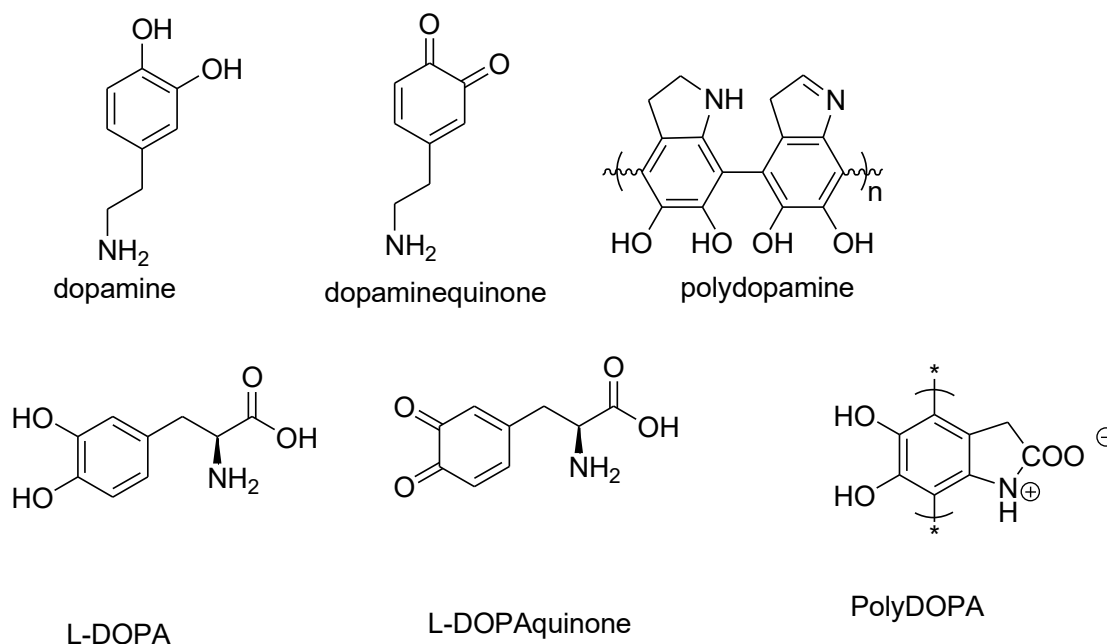


Figure 6.3: Structure of L-DOPA, dopamine, and their polymer derivatives.

The auto-oxidation of DOPA and dopamine have been treated in various studies. In the presence of oxygen, dopamine is found to oxidize into dopaminequinone which may polymerise forming polydopamine³. By altering the pH of a DOPA or dopamine solution, its oxidation can be manipulated; for example, the addition of small amounts of acid can inhibit the oxidation process⁴. The step by step oxidation reaction from L-DOPA to polyDOPA was presented in Figure 6.2 in Chapter 6⁵. Through its mussel adhesive-like properties, this material deposits itself into various types of substrates, including electrospun TPU fibres.

In material science applications aimed at mimicking mussel adhesive property, polyDOPA or polydopamine films may be formed on the surface of substrates incubated in a dopamine or DOPA solution at basic pH (typically at pH 8.5)⁶. This is due to the spontaneous oxidation of dopamine or DOPA followed by its polymerization and deposition onto the substrate surface.

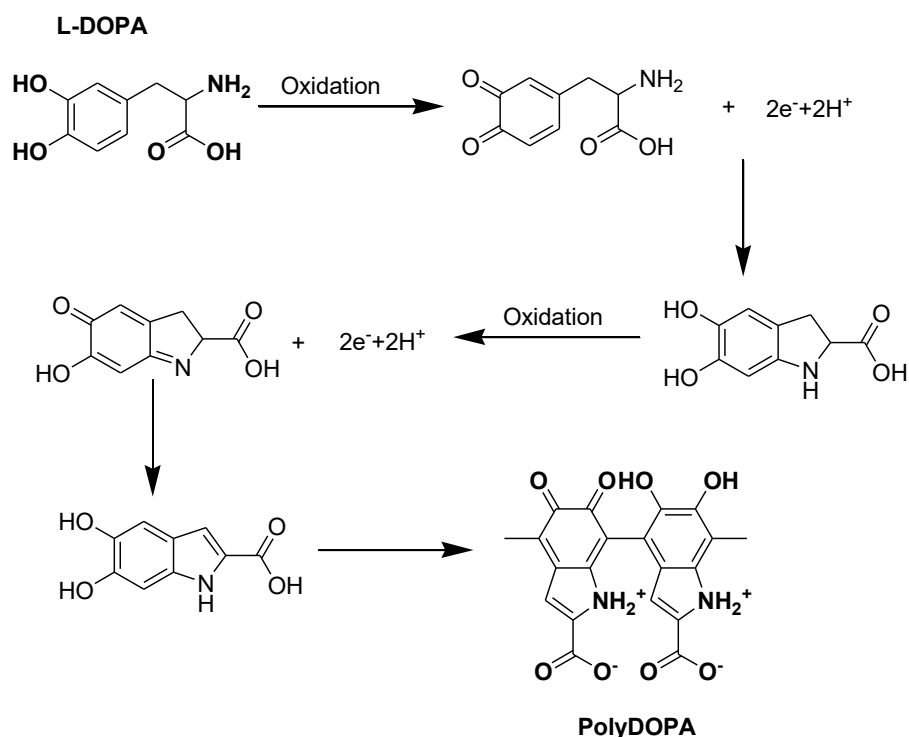


Figure 6.2: Oxidation process of L-DOPA into polyDOPA

A surface-coated polyDOPA or polydopamine material can be grafted with compounds or large molecules that contain imidazole, amine, and thiol groups which react with the o-quinone group formed in the oxidation of DOPA or dopamine (see Figure 6.4). This allows it to immobilize enzymes, growth factors, natural polymers (eg. gelatin), etc. onto its surface. It was observed that the o-quinone group was particularly reactive to compounds with amine and thiol groups of the functional groups named⁷.

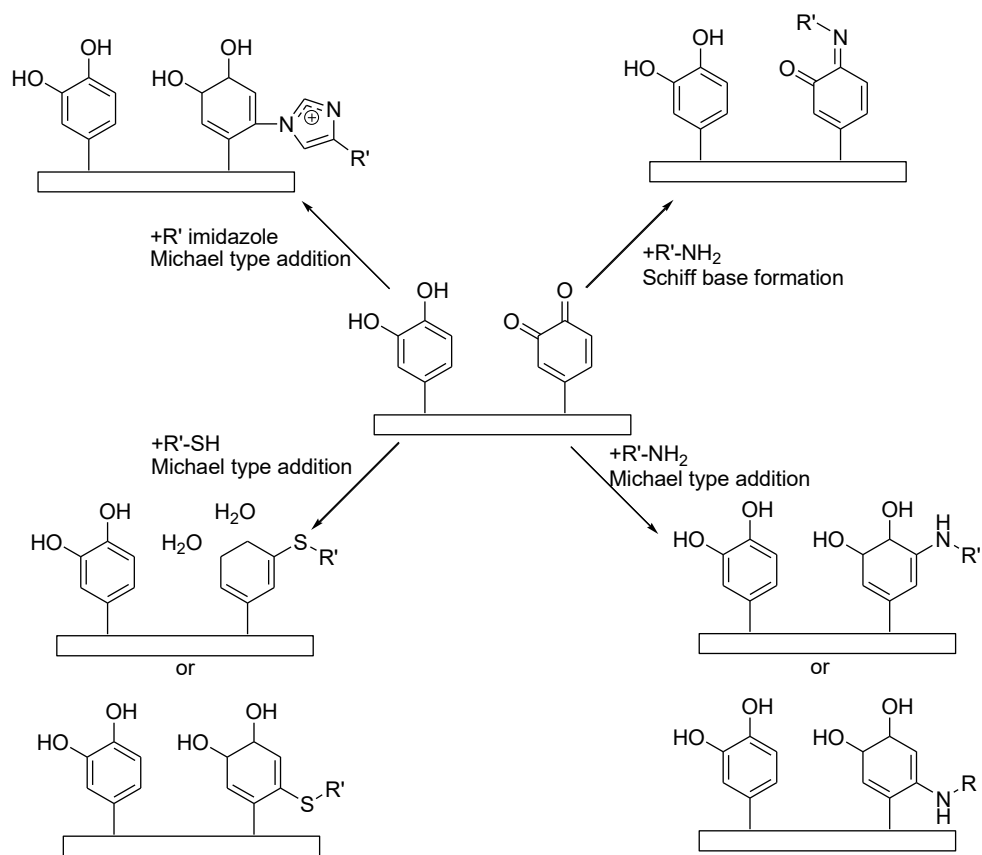


Figure 6.4: Possible reaction pathways in a PDA-coated surface (R' = polymeric backbone). Image drawn by author, modified from Bazaka, K., et al. (2015)⁸.

7.2.2. Enhancing rate of oxidation of DOPA

One possible coating process requires immersing the material in a dopamine solution (e.g. 2 mg/ml dopamine in pH 8.5 in TRIS buffer (10 mM)) for 8-24 hours⁹⁻¹⁴). While being immersed, the material – depending on its chemical nature- might undergo changes in its physicochemical and mechanical properties as a result of material hydrolytic degradation in the basic environment. Reduction in coating time could be useful in preserving the material physicochemical characteristics.

Several studies investigated various agents for increasing the rate of oxidation of DOPA into PDA. Self-polymerisation of DOPA or dopamine can be improved by increasing the aeration of the solution (e.g. by increasing the rate of agitation or

shaking) or temperature, as reported by Zhou, P., et al (2014)¹⁵. Another study by Ruch, D., et al (2011) increased the rate of oxidation by adding metal ions such as copper (Cu^{2+}) or iron (Fe^{3+}), as the metal ions are reduced and gains electrons, the DOPA becomes oxidized and loses electrons as shown in Figure 6.2¹⁶.

Different oxidizing agents may be used, including hydrogen peroxide, potassium permanganate, benzoyl peroxide, acetone, etc¹⁷. Even oxygen itself serves as an oxidizing agent to DOPA (in turn, DOPA acts as a reducing agent to oxygen with trace amounts of hydrogen peroxide produced as a result⁴). As oxidation proceeds, these reagents are consumed and eventually depleted. However, for enzymes they act merely as catalysts to enhance the oxidation rate and are not consumed in the oxidation process. In this research, enzymes were used as they do not actively take part to the reaction.

7.2.3. Oxidizing enzymes

Dopamine was found to be oxidized by several enzymes including lactoperoxidase (LPO), prostaglandin H synthase, xanthine oxidase, etc³. Among these enzymes LPO is the cheapest, it is commercially available, and easily obtained from bovine milk¹⁸. LPO is stable over a broad pH range of 4-11, which includes the typical pH for PDA-coating preparation by self-polymerisation¹⁹. Literature on the oxidizing effect of enzymes on dopamine did not describe their use for polydopamine coating applications, they mainly investigated the mechanism of dopamine oxidation in relation to Parkinson's disease and other neurodegenerative diseases in the presence of lactoperoxidase and other previously mentioned enzymes³. Thus, the approach in using LPO enzyme for surface coating materials with polyDOPA or polydopamine (starting from L-DOPA and dopamine, respectively) is a completely novel approach.

The main objective of this chapter was to develop a novel, easy and fast process for the preparation of PDA-coated electrospun TPU membranes (previously fabricated in Chapter 6) using LPO oxydising enzyme, optimizing the process conditions.

7.3. Materials and methods

Lubrizol Tecophilic SP-60D-60 was purchased from Velox GmbH, Germany and processed into electrospun fibres as described in Chapter 6. 3-(3,4-Dihydroxyphenyl-2,5,6-d3)-D,L-alanine (D,L-DOPA), TRIS buffer, Lactoperoxidase enzyme (LPO, EC number 1.11.1.7, 200 U/mg activity) were purchased from Sigma Aldrich, Italy.

7.3.1. Preparation of LPO enzyme solutions

A stock solution of 200 U/mL LPO was prepared by dissolving 10 mg of LPO in 8.5 pH TRIS Buffer. From this solution, different LPO solutions were derived, as listed in Table 7.1, left column. These LPO solutions were mixed with an equal volume of DOPA solution (4 mg/L) in TRIS buffer solution. The final L-DOPA concentration in these solutions was 2 mg/mL, which is the concentration used in most of the PDA-coating studies^{14,20-22}. On the other hand, LPO concentration in these solutions is reported in the middle column of Table 7.1

Table 7.1. LPO enzyme concentrations used and their respective set-up codes.

LPO solution concentration (U/mL)	LPO concentration in the coating solution (U/mL)	Set-up Code
0	0	LPO 0 or Control
0.35	0.175	LPO 0.18
0.70	0.35	LPO 0.35
2.10	1.05	LPO 1.1
2.80	1.40	LPO 1.4

7.3.2. Study of DOPA oxidation rate with lactoperoxidase

In these experiments, the control solution was DOPA (2 mg/mL) without any enzyme added (LPO 0). In scintillation glass vials with a magnetic stirrer inside, 5 mL of 4 mg/mL DOPA solution was pipetted. Afterwards, 5 mL of the various LPO enzyme concentrations were added as well (see Table 7.1). Each vial was stirred at 300 rpm, with the vial uncovered in order for sufficient oxygenation to take place.

At different time points, 100 μ L samples of each set-up was taken out and put into a well of a 96-well plate. Measurements were done in six replicates. The absorbance of the solution was measured at 450 nm using a Perkin Elmer Victor X3 multi-mode plate reader. In a previous study on the optical properties of eumelanin (dopamine is one of its major components) the researchers found that the optical density measured at given wavelengths, including 450 nm, could be considered an indication of extent of oxidation²³. The same concept was here used to measure the amount of DOPA oxidized into PDA from the solution absorbance intensity at 450 nm wavelength. The absorbance intensity of the TRIS buffer solution at 450 nm was also measured to establish a baseline. Time points for measurements were fixed every 30 minutes for 7 hours. "Full oxidation" absorbance was assumed as the reading of the control PDA solution after 7 hours incubation without the enzyme. This was based on previous studies by Irene Carmagnola et al. (in course of

publication), which showed efficient PDA coating of polymer substrate after 7 hours incubation in a DOPA solution (2 mg/mL).

7.3.3. Surface coating of electrospun TPU with polyDOPA (PDA) with/without LPO enhancement (Part I)

Scintillation vials containing the LPO + DOPA solutions were prepared similarly to the procedure previously mentioned in Table 7.1. A piece of electrospun TPU (1 cm x 1 cm) was immersed in each of these solutions. Absorbance readings of the solutions were performed every 30 minutes for 7 hours as described in the previous Section 7.3.2. This part of the study was carried out to study whether the deposition of PDA on the substrate could yield a reduction in the solution absorbance measurements, as compared to measurements at Section 7.3.2. After the immersion, the film samples were washed in TRIS buffer thrice and dried before they were used for analysis.

7.3.4. Surface coating of electrospun TPU with polyDOPA (PDA) with/without LPO enhancement (Part II) – Scaled-up Surface Modification

Based on results from Section 7.3.2 and 7.3.3, two enzyme concentrations were selected for PDA coating of a larger quantity of TPU fibres to be used for further characterization and application studies.

Figure 7.1 illustrates the set-up used for coating trials. In 250 mL beakers, 250 mL of DOPA only, LPO 1.4 + DOPA, or LPO 1.1 + DOPA solutions were prepared (close to the brim but not spilling). In each beaker, 4 strips (1 cm x 6 cm) of electrospun TPU were immersed with one end clipped to a rod. Beakers were stirred at 300 rpm with no covering to allow oxygenation of the solution. After 3 hours, 2 strips from each setup were taken out and washed with TRIS buffer pH 8.5 several

times. After 7 hours, the final 2 strips from each setup were taken out and washed several times with deionized water. A small portion of the films were cut and were used for SEM imaging and FTIR analysis, which are described later.



Figure 7.1: PDA-coating set-up for electrospun TPU fibres; the scheme of the set-up is shown on the left and the actual final product (TPU-PDA-LPO-1.4-7) is shown on the right.

7.3.5. SEM analysis of PDA-coated TPU

Scanning Electron Microscopy was performed using a LEO 1420 microscope (Zeiss, Germany) at 20 kV and a working distance of 15 mm. The diameters of the fibres in electrospun membranes were measured on SEM images using ImageJ software. Any difference in the morphology of the coated fibrous patches compared to the uncoated fibrous patches was analyzed.

Coated and uncoated samples were analyzed by SEM. To prepare the samples for SEM analysis, samples of the modified fibre patch were cut into 2 mm x 2 mm squares and mounted onto SEM sample holder using conductive tape. The samples were coated with a thin layer of gold using a sputter-coating machine (30 mA, 50 seconds) to improve its conductivity for imaging.

7.3.6. FTIR-ATR analysis of PDA-coated TPU

Attenuated Total Reflectance Fourier Transform InfraRed Spectra (ATR-FTIR) of PDA-coated TPU was obtained at room temperature in the spectral range from 4000 to 400 cm^{-1} using a Perkin–Elmer Spectrum 100 equipped with an ATR accessory (UATR KRS5) with diamond crystal. The spectra, obtained as a result of 16 scans with a resolution of 4 cm^{-1} , were analyzed using the Perkin–Elmer Spectrum Software. Spectra were recorded on the uncoated TPU fibrous patch, the enzyme-free PDA-coated TPU fibrous patch (TPU-PDA), enzyme-PDA coated fibrous patch (TPU-PDA-LPO) to compare coating efficiency in each case.

7.4. Results and discussion

7.4.1. PDA deposition as a function of LPO concentration

Figure 7.2 reports images of a 24-multiwell plate containing the DOPA solution and different enzyme concentrations (0-1.4 U/L LPO) after 30 min, 3 hours, and 5 hours incubation. All the DOPA-LPO starting solutions were transparent and indicate no oxidation has taken place yet. After 30 minutes, solutions displayed a progressively darker colour as the LPO concentration increased. Images also show that each type of solution became darker with increasing time. By hour five, the solution colours were nearly indistinguishable in terms of shade and could be differentiated precisely by measuring solution absorbance at 450 nm.

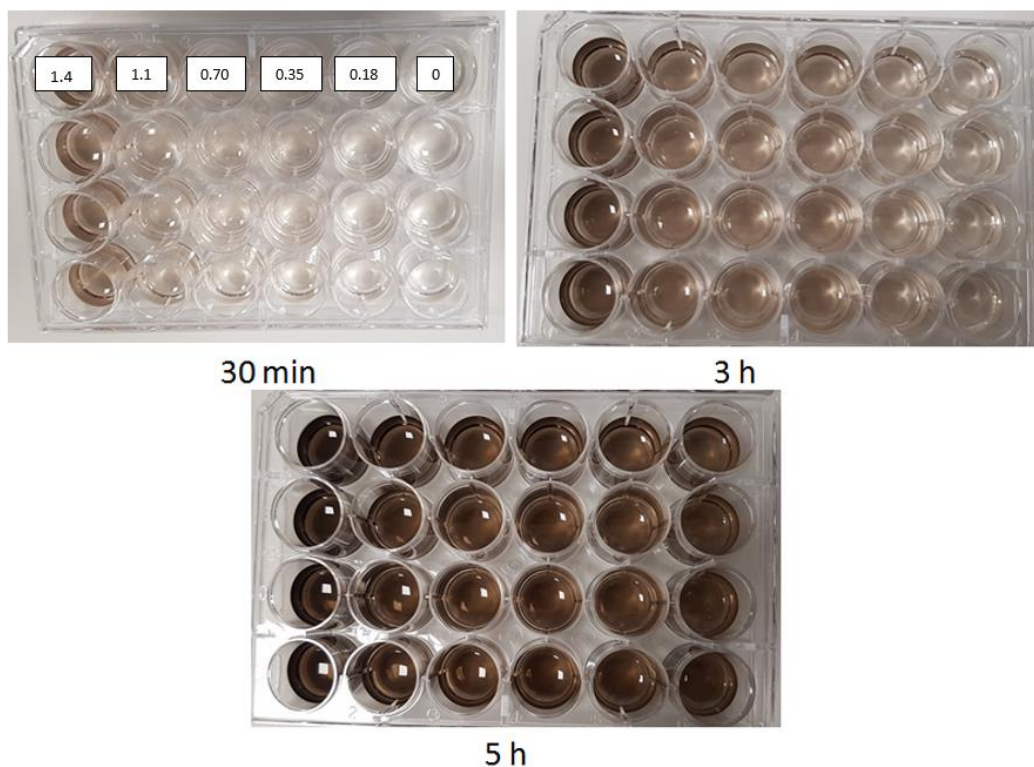


Figure 7.2: Images of L-DOPA solutions (2 mg/mL) oxidizing into PDA with 0-1.4 U/mL LPO concentrations (1 column = 4 wells = 1 LPO concentration set-up) at different times (30 min, 3h and 5h)

Figure 7.3 presents the measured absorbance of the solutions at a wavelength of 450 nm as a function of time. The absorbance intensity value of control/LPO 0 solution after 7 hours (0.764) was considered a reference of significant DOPA oxidation to PDA, based on previous investigation at Politecnico di Torino (data under publication). Hence, this value was used as a reference when comparing the oxidation extent of LPO-containing DOPA solutions relative to the enzyme-free DOPA solution.

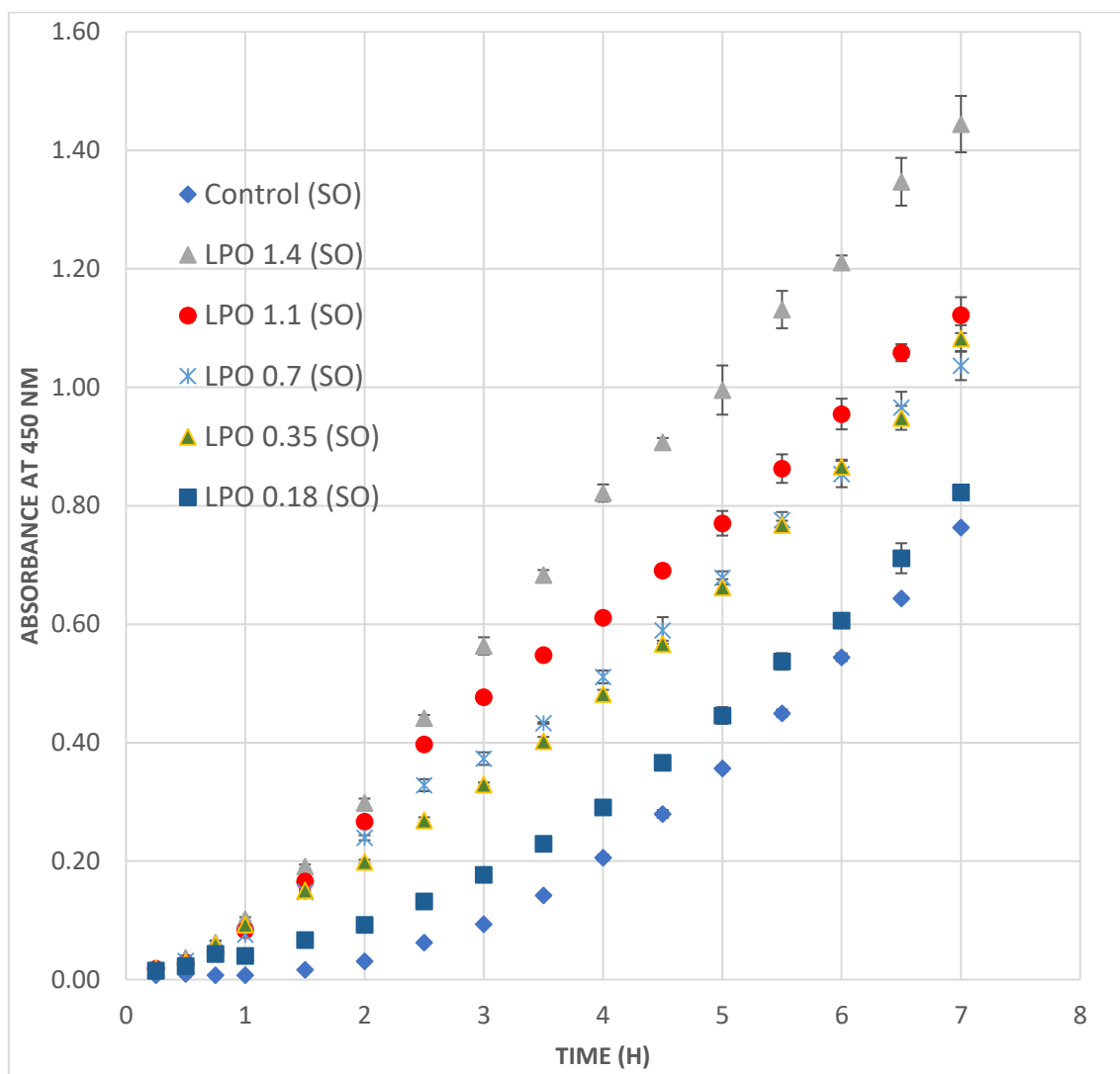


Figure 7.3: Absorbance intensity at 450 nm of DOPA solutions containing different enzyme amounts as a function of time, as indicative of PDA formation (SO = Solution only).

Figure 7.4 reports the measured absorbance intensity of solutions at 450 nm when TPU patch was incubated in the solution at different times. By adding TPU membrane to the PDA-forming solutions, their absorbance intensity decreased respect to that of the corresponding solutions shown in Figure 7.3. This was attributed to PDA partially depositing on TPU film instead of remaining dispersed in the solution.

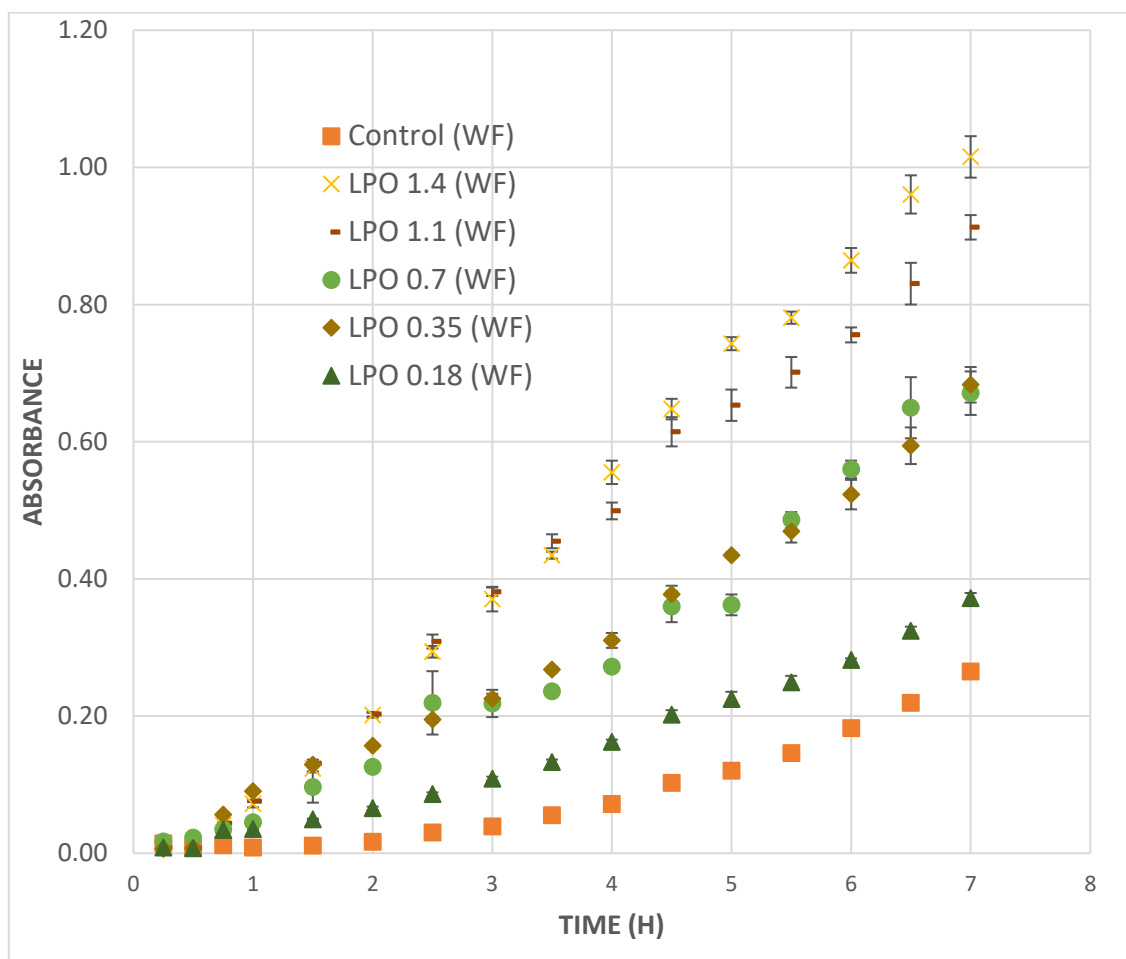


Figure 7.4: Absorbance intensity at 450 nm as a function of time for DOPA solutions containing different enzyme amounts, during the incubation of a TPU patch. Absorbance values were indicative of PDA deposition on the film, when compared to results in Figure 7.3 (SO = Solution only).

Figure 7.5 compares the behaviour of absorbance intensity for the DOPA solution without (SO) and with (WF) TPU film incubation, in the absence of LPO enzyme, as a function of time. The absorbance intensity of the solution after TPU membrane incubation for 7 h was 0.265 while it was 0.764 in the absence of TPU film. Assuming concentration of PDA in the system is proportional to absorbance, this means that approximately 65% of the formed PDA (at that time) deposited on the film, and that about 35% of the formed PDA remained dispersed in the solution.

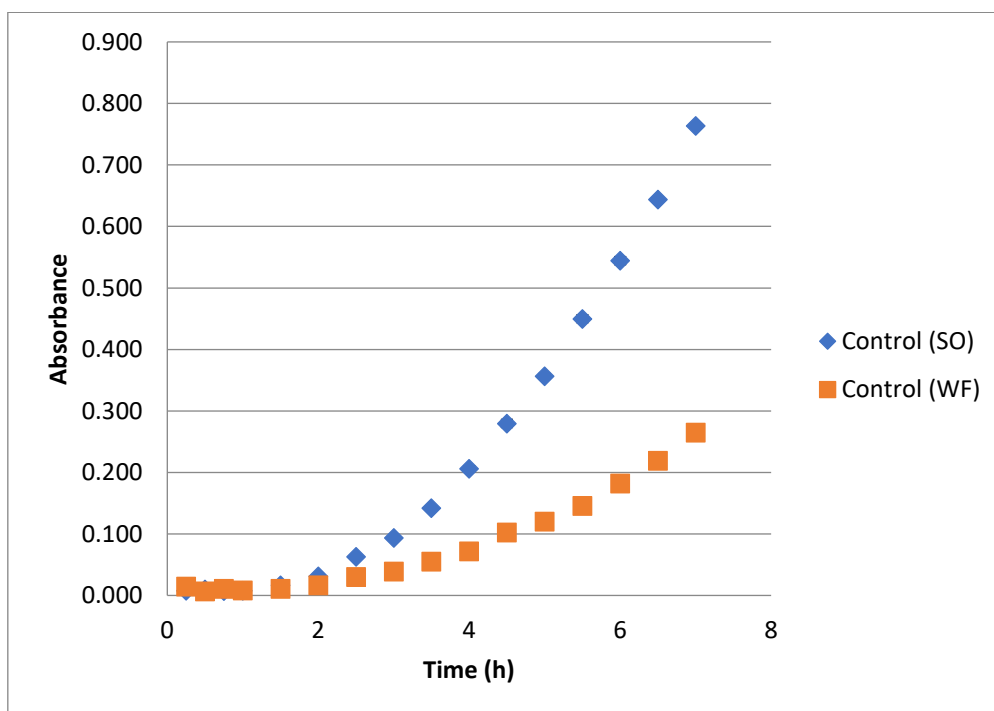


Figure 7.5: Comparison of absorbance values of DOPA solutions with the same concentration (LPO 0) with and without TPU film, as a function of time.

When the rate of PDA oxidation increased in the presence of the enzyme, the difference in the WF versus SO set-ups decreased as the amount of PDA that deposited in the film in faster-oxidizing solutions was only a smaller fraction compared to the overall oxidized PDA present in the solution. Figure 7.6 shows the behavior of absorbance values for LPO 1.4 with and without TPU film incubation. After 7 hours, the absorbance intensity of LPO 1.4 solution at WF condition was lower than in the absence of TPU film (SO condition). However, this difference was reduced compared to the measured difference between SO and WF solutions not contacting the enzyme (Figure 7.5). In the case reported in Figure 7.6, around 30% of formed PDA was deposited while 70% remained in the solution. This means that at a high LPO concentration (1.4 U/mL), the presence of a substrate incubated in the DOPA-LPO solution caused a reduced decrease in the overall amount of polyDOPA in solution. Adding LPO enzyme increased the rate of oxidation and more PDA was formed which only partially could deposit on the substrate. Hence,

in the presence of LPO enzyme, the same solution volume could be used to coat more samples at the same time. For the procedure of coating, four TPU films were incubated in the same DOPA solution volume as described in Section 7.3.4, using conditions: LPO 0 and LPO 1.4 (referred to as oxidizing parameters) used with two coating times, the original 7 hour coating time and a reduced coating time that will be determined in the next section.

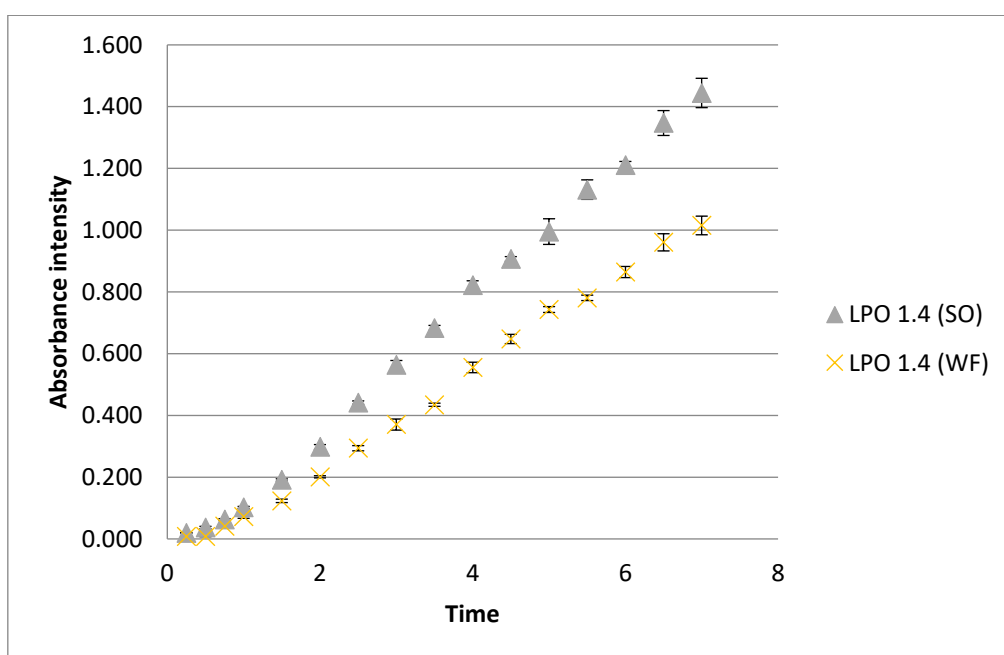


Figure 7.6: Comparison of absorbance times DOPA solutions of the same concentration (LPO 1.4) with and without TPU film.

7.4.2. Determining time for “reference” oxidation level

The absorbance values reported in Figure 7.3 were used to calculate the oxidation percentage of DOPA at time t in the presence of LPO, respect to the reference oxidation level of DOPA without enzyme after 7 h, following the equation below:

$$\begin{aligned}
 \text{Percent oxidation } (O\%_{LPO\ xx,t\ h}) &= \frac{Abs_{LPO\ xx,t\ h}}{Abs_{LPO\ 0,7\ h}} * 100\% \\
 &= \frac{Abs_{LPO\ xx,t\ h}}{0.764} * 100\% \quad (\text{eq. 7.1})
 \end{aligned}$$

Where:

$Abs_{LPO\ xx, t\ h}$ = Absorbance of sample with LPO concentration xx at time t . (for example: the absorbance of sample with 1.1 U/mL LPO at 4.5 hours is written as $Abs_{LPO\ 1.1, 4.5h}$.)

$Abs_{LPO\ 0, 7h}$ = Absorbance of sample with LPO concentration 0 U/mL at time 7 h

Using equation 7.1, the absorbance intensity values could be used to calculate an oxidation percentage respect to the control set-up (Figure 7.7). At LPO concentration higher than 0.35 U/mL, the reference oxidation absorbance value (100%) could be reached at earlier times than 7 hours, which suggested that surface functionalization of substrates incubated in these solutions could occur faster than without enzyme.

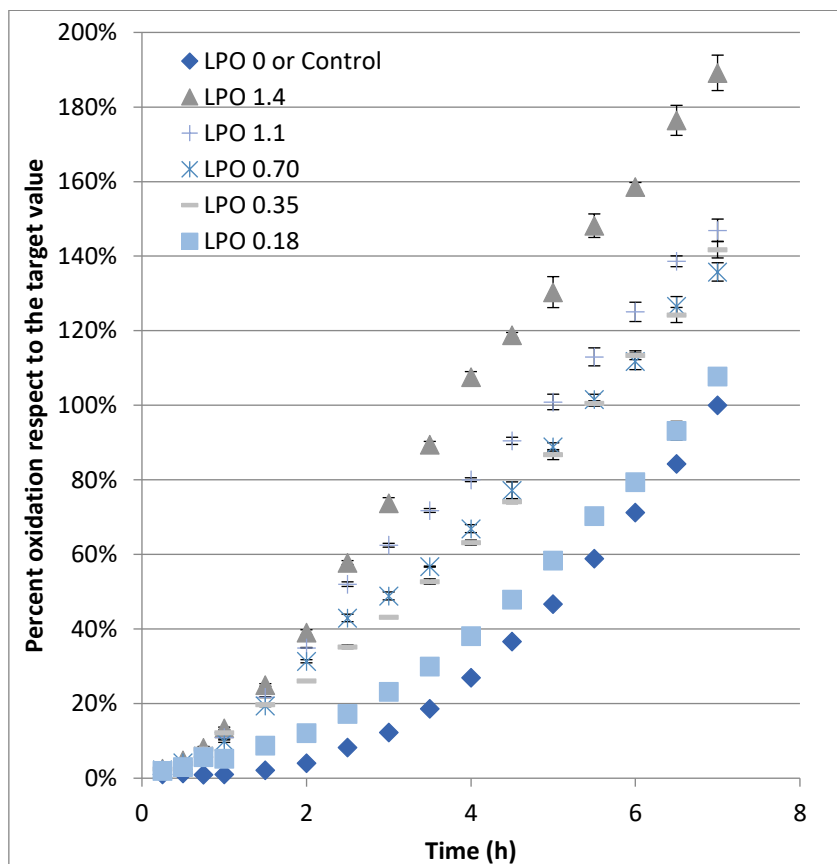


Figure 7.7: Percentage oxidation of DOPA solutions in different conditions respect to the control set-up (SO)

This data analysis was also applied to the absorbance values of the DOPA-LPO solutions that contained film samples (Figure 7.8). Particularly, for LPO 1.4 after 2.5 hours, the percentage of oxidation was 110% relative to the reference value: absorbance intensity was 383% higher than the control after 2.5h. By adding an extra 30 minutes into this coating time, it can be assumed that sufficient coating is achieved by hour 3 for LPO 1.4.

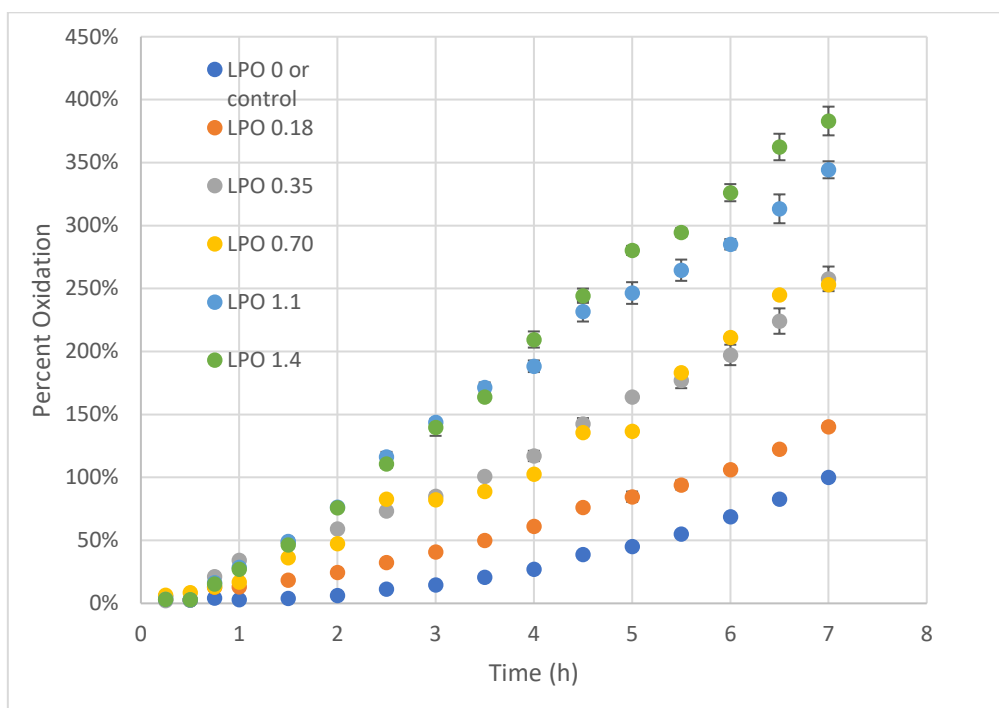


Figure 7.8: Percentage oxidation of DOPA solutions in different conditions respect to the control set-up (WF)

Looking at Figures 7.7 and 7.8, 100% oxidation rate increased in solutions that contained LPO. The oxidation time to achieve a certain oxidation level was found to decrease (meaning the reaction was much faster) by increasing the amount of LPO in the solution. The 100% reference oxidation time for each set-up was calculated by interpolating between two data time points with one having an absorbance intensity higher than 0.764 (100% or reference value) and the second having an absorbance intensity lower than 0.764. The basic interpolation (with Ox % for absorbance and t for the corresponding time point) is:

$$\frac{Ox \%_1 - Ox \%_2}{t_1 - t_2} = \frac{Ox \%_1 - Ox \%_3}{t_1 - t_3}$$

where $Ox \%_1 > 100\%$ and $Ox \%_3 < 100\%$ which are known values and t_2 is the unknown "complete" oxidation time. A sample calculation for the complete oxidation time of LPO 1.4 is as follows:

Given data for LPO 1.4: at $t = 3.5\text{ h}$, $Ox \%_{LPO\ 1.4,\ 3.5\text{ h}} = 89.5\%$; at $t = 4$, $Ox \%_{LPO\ 1.4,\ 4\text{ h}} = 107.6\%$

Calculation:

$$\frac{107.6\% - 100\%}{4 - t_{100\%}} = \frac{107.6\% - 89.5\%}{4 - 3.5}$$

$$t_{100\%} = \mathbf{3.8\text{ h}}$$

The same calculation was done for the solutions, which contained TPU film: oxidation (absorbance value) after 7 hours for the control/LPO 0 set-up (WF) was used as a reference value to calculate the approximate time needed for reference oxidation. The calculated values are summarized and illustrated in Figure 7.9 below.

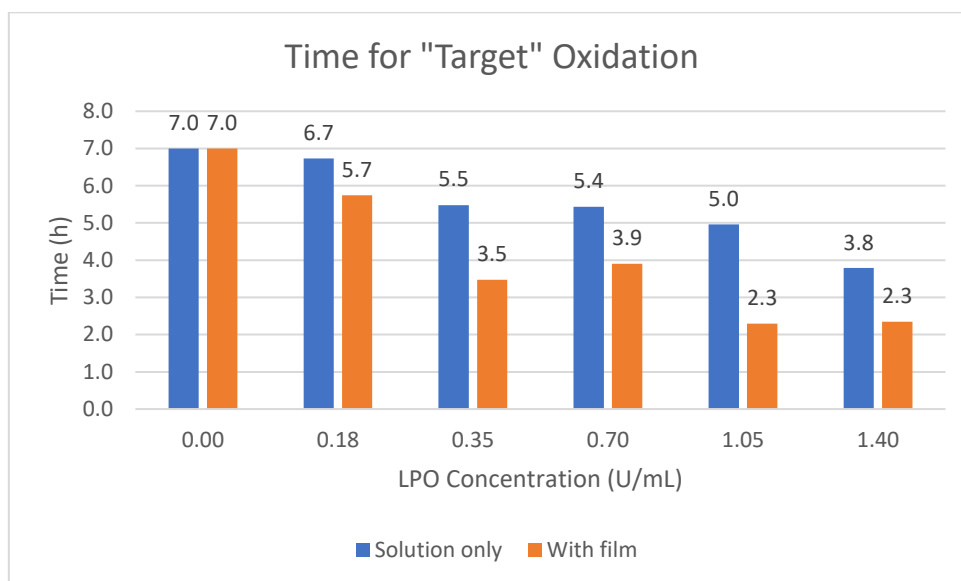


Figure 7.9: Estimated time for reference oxidation in PDA-forming set-ups with LPO concentrations from 0 to 1.4 U/mL

7.4.3. SEM analysis of PDA coated TPU

Concerning the procedure of coating larger surfaces described in Section 7.3.4, three LPO set-ups were used for SEM imaging, LPO 1.1 and LPO 1.4, along with LPO 0 as the control. The TPUs of these LPO-based set-ups were coated with PDA at two different settings: 3 hours and 7 hours.

Results from SEM analysis are shown in Figure 7.10 at a magnification of 5000x. The fibre diameter for the unmodified TPU was reported in Chapter 5 ($1.12 \pm 0.30 \mu\text{m}$).

PDA deposited on the TPU membranes (Figure 7.10 b-d) altered the fibre morphology with the appearance of larger areas (of a few microns) connecting close fibres as emphasized in the green and purple squares in the reported images. This feature was more evident with increase of the amount of LPO used.

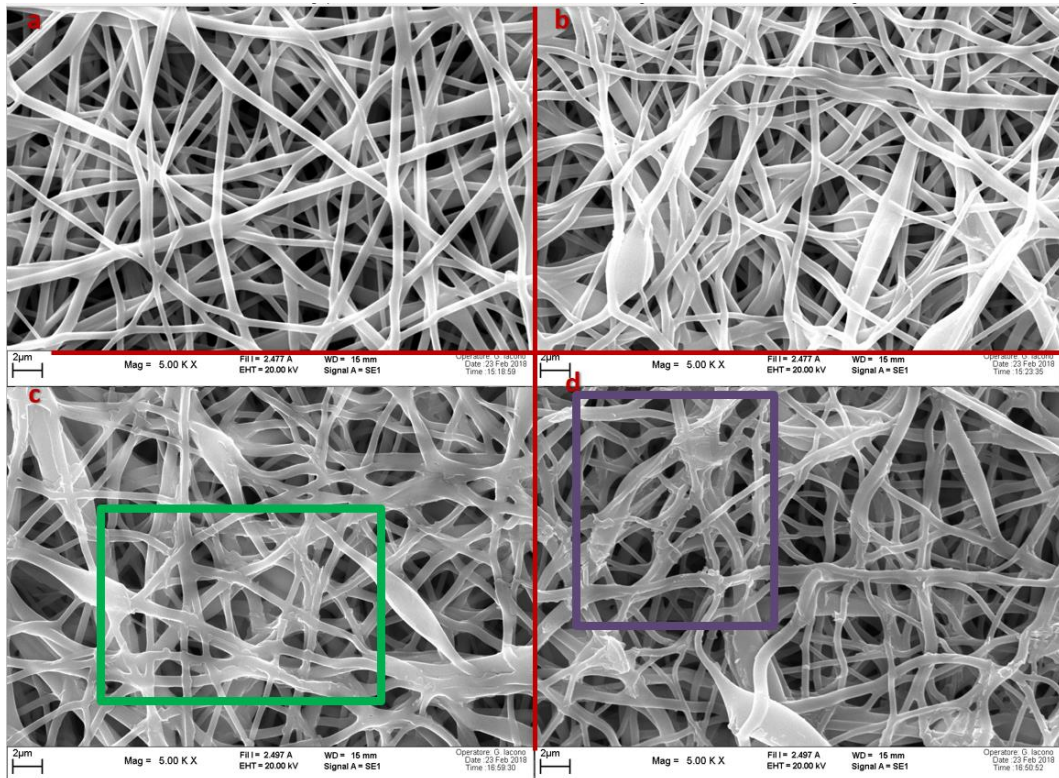


Figure 7.10: SEM images (5000x magnification) of electrospun TPU fibrous membranes: a) uncoated, b) PDA-coated (7h), no LPO, c) PDA coated (7 h), 1.1 U/mL LPO, d) PDA coated (7h), 1.4 U/mL LPO.

Figure 7.11 presents the percentage difference of average fibre diameters for the coated respect to uncoated TPU membranes. Higher standard deviations were observed in the more LPO-concentrated set-ups. This could be attributed to the PDA depositing more preferentially in some areas.

Statistical analysis was used to compare the data and showed that there was a significant difference in fibre diameter change for the all PDA-coated materials (including LPO 0) when compared to the unmodified/uncoated fibre diameter. Starting with the lowest concentration, LPO: there was a very significant difference in the measured fibre diameters for the unmodified TPU with the LPO 0 coated TPU ($p = 0.01$).

However when comparing the fibre diameter change of LPO 0 with other LPO concentrations, there was no significant difference between them. For example, in comparing the fibre diameters of LPO 0 with LPO 1.4, there was no significant difference found between them ($p = 1.00$). This was the case as well for the other LPO concentrations used when compared with LPO 0, that the difference in fibre diameters was not significant.

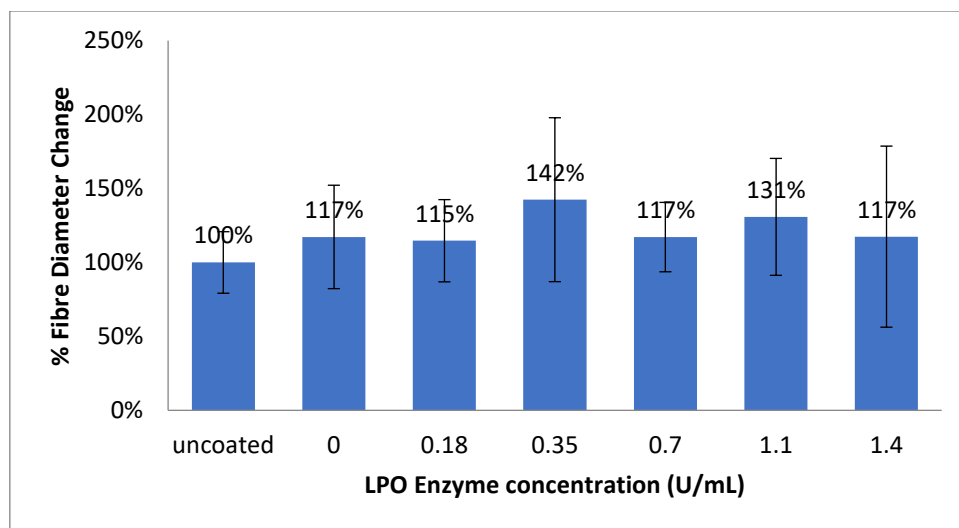


Figure 7.11. Percentage of fibre size difference when coating electrospun TPU fibres with PDA in the presence of difference LPO concentrations. Data were derived from an average of 40 measurements per each SEM image by ImageJ software.

Overall, relative to the original fibre diameter, the PDA-coated samples were thicker by as much as 15-42% as PDA deposited on the fibre mats as evidenced by the darkened colour of the samples.

7.4.4. FTIR analysis of PDA coated TPU

Figure 7.12 shows the FTIR spectra of three samples: uncoated TPU in purple; PDA-coated (without using LPO) in red, and PDA-coated (using LPO 1.4) TPU

membrane in green. To maximize the amount deposited on the TPU, samples prepared with a PDA coating time of 7 h were used in the analysis.

From the information that can be gathered in the material specification sheet, Lubrizol SP-60D-60 (the TPU used in this experiment) was classified as an aliphatic polyether thermoplastic polyurethane. The strong absorbance band at 1098 cm^{-1} was assigned to the C-O stretching and confirms the presence of ether bonds in the polymer backbone. Other characteristic absorption bands of polyurethanes were observed. These included C=O stretching of urethane bonds (1691 cm^{-1}) and N-H bending of urethane bonds (1524 cm^{-1}). The low absorption at around 2900 cm^{-1} was assigned to the C-H stretching of aliphatic backbone.

I

FTIR analysis of the PDA-coated TPUs suggested the presence of polyDOPA. In detail the absorption band at 3322 cm^{-1} was attributed to the O-H stretching of the catechol groups, the peak close to 3000 cm^{-1} was assigned to the stretching of C-H and the absorption at 1524 cm^{-1} and 1490 cm^{-1} was due to the C=C stretching of aromatic ring. Furthermore, a strong increase of the absorption due to the C=O stretching was also observable, attributed to quinone functionalities.

On the other hand, there was no significant difference in FTIR spectra between the PDA-coated with or without the LPO enzyme. It is possible that a part of the LPO enzyme remained grafted to the PDA coating, however used LPO catalyst amount was low and hence difficult to be detected by FTIR-ATR analysis. Additionally, main FTIR-ATR adsorption bands of proteins (e.g. Amide I and Amide II) partially or totally overlap with bands in TPU-PDA spectra.

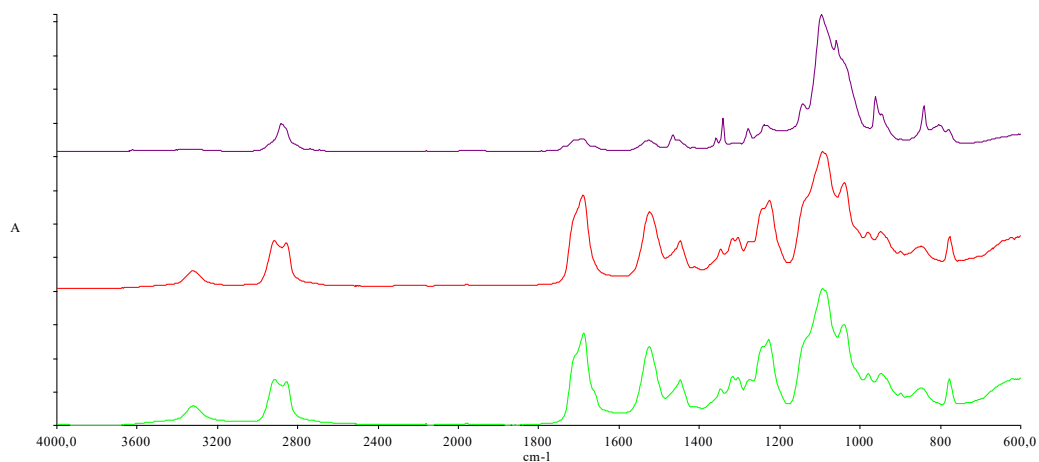


Figure 7.12: FTIR spectra of TPU membranes: purple = TPU; red = TPU-PDA (LPO 0); green = TPU-PDA (LPO 1.4). Coating time for reported spectra was 7 hours.

7.5. Conclusions

Electrospun TPU fibres previously fabricated in Chapter 6 were successfully coated with PDA: the white fibre mats gradually turned into varying degrees of brown to black depending on the coating parameters (use of an oxidizing enzyme catalyst and time used for coating). PDA coating by self-polymerization in oxidizing conditions took approximately 7 hours based on previous studies performed at Politecnico di Torino.

LPO is an oxidizing enzyme that enhances the rate of oxidation of DOPA and PDA formation without taking part to the reaction. Based on absorbance measurements at 450 nm, it was found that the addition of 1.4 U/mL LPO to a DOPA solution (2 mg/mL in 10 mM TRIS buffer at pH 8.5) can reduce the coating time from 7 hours to 2.5 hours. In the next PDA-coating procedures, the reduced coating time was set at 3 hours. Measured fibre diameters of the PDA coated samples were observed to be 15-42% thicker than the uncoated fibres.

Thus, introducing LPO in a DOPA (or even dopamine) solution could reduce time needed for PDA dip-coating applications, making this type of surface functionalization more efficient. In the next chapter, the ability of PDA-coatings to covalently graft proteins will be investigated and characterized.

7.6. References

- (1) Kaushik, N. K.; Kaushik, N.; Pardeshi, S.; Sharma, J. G.; Lee, S. H.; Choi, E. H. Biomedical and Clinical Importance of Mussel-Inspired Polymers and Materials. *Mar. Drugs* **2015**, *13* (11), 6792–6817. <https://doi.org/10.3390/md13116792>.
- (2) Qin, Z.; Buehler, M. J. Molecular Mechanics of Mussel Adhesion Proteins. *J. Mech. Phys. Solids* **2014**, *62* (1), 19–30. <https://doi.org/10.1016/j.jmps.2013.08.015>.
- (3) Muñoz, P.; Huenchuguala, S.; Paris, I.; Segura-Aguilar, J. Dopamine Oxidation and Autophagy. *Parkinsons. Dis.* **2012**, *2012*. <https://doi.org/10.1155/2012/920953>.
- (4) Herlinger, E.; Jameson, R. F.; Linert, W. Spontaneous Autoxidation of Dopamine. *J. Chem. Soc. Perkin Trans. 2* **1995**, No. 2, 259. <https://doi.org/10.1039/p29950000259>.
- (5) Sajitha, M.; Vindhyasarumi, A.; Gopi, A.; Yoosaf, K. Shape Controlled Synthesis of Multi-Branched Gold Nanocrystals through a Facile One-Pot Bifunctional Biomolecular Approach. *RSC Adv.* **2015**, *5* (119), 98318–98324. <https://doi.org/10.1039/C5RA19098C>.
- (6) Ding, Y. H.; Floren, M.; Tan, W. Mussel-Inspired Polydopamine for Bio-Surface Functionalization. *Biosurface and Biotribology* **2016**, *2* (4), 121–136. <https://doi.org/10.1016/j.bsbt.2016.11.001>.
- (7) Lynge, M.; Schattling, P.; Stadler, B. Recent Developments in Poly (Dopamine) - Based Coatings for Biomedical Applications. *Nanomedicine* **2015**, *10*, 2725–2742. <https://doi.org/10.2217/nnm.15.89>.
- (8) Bazaka, K.; Jacob, M. V; Chrzanowski, W.; Ostrikov, K. Anti-Bacterial Surfaces: Natural Agents, Mechanisms of Action, and Plasma Surface Modification. **2015**. <https://doi.org/10.1039/c4ra17244b>.
- (9) Xu, J.; Xu, N.; Zhou, T.; Xiao, X.; Gao, B.; Fu, J.; Zhang, T. Polydopamine Coatings Embedded with Silver Nanoparticles on Nanostructured Titania

- for Long-Lasting Antibacterial Effect. *Surf. Coatings Technol.* **2017**, *320*, 608–613. <https://doi.org/10.1016/j.surfcoat.2016.10.065>.
- (10) Su, L.; Yu, Y.; Zhao, Y.; Liang, F.; Zhang, X. Strong Antibacterial Polydopamine Coatings Prepared by a Shaking-Assisted Method. *Sci. Rep.* **2016**, *6* (1), 24420. <https://doi.org/10.1038/srep24420>.
- (11) Liu, Y.; Zhang, Z.; Lv, H.; Qin, Y.; Deng, L. Surface Modification of Chitosan Film via Polydopamine Coating to Promote Biomineralization in Bone Tissue Engineering. *J. Bioact. Compat. Polym.* **2017**, 088391151771322. <https://doi.org/10.1177/0883911517713228>.
- (12) Xie, M.; Wang, J.; Wang, X.; Yin, M.; Wang, C.; Chao, D.; Liu, X. The High Performance of Polydopamine-Coated Electrospun Poly(Ether Sulfone) Nanofibrous Separator for Lithium-Ion Batteries. *Macromol. Res.* **2016**, *24* (11), 965–972. <https://doi.org/10.1007/s13233-016-4140-3>.
- (13) Kao, C. T.; Lin, C. C.; Chen, Y. W.; Yeh, C. H.; Fang, H. Y.; Shie, M. Y. Poly(Dopamine) Coating of 3D Printed Poly(Lactic Acid) Scaffolds for Bone Tissue Engineering. *Mater. Sci. Eng. C* **2015**, *56*, 165–173. <https://doi.org/10.1016/j.msec.2015.06.028>.
- (14) Ponzio, F.; Barthès, J.; Bour, J.; Michel, M.; Bertani, P.; Hemmerlé, J.; D’Ischia, M.; Ball, V. Oxidant Control of Polydopamine Surface Chemistry in Acids: A Mechanism-Based Entry to Superhydrophilic-Superoleophobic Coatings. *Chem. Mater.* **2016**, *28* (13), 4697–4705. <https://doi.org/10.1021/acs.chemmater.6b01587>.
- (15) Zhou, P.; Deng, Y.; Lyu, B.; Zhang, R.; Zhang, H.; Ma, H.; Lyu, Y.; Wei, S. Rapidly-Deposited Polydopamine Coating via High Temperature and Vigorous Stirring: Formation, Characterization and Biofunctional Evaluation. *PLoS One* **2014**, *9* (11), 0–9. <https://doi.org/10.1371/journal.pone.0113087>.
- (16) Ruch, D.; Ponche, A.; Gracio, J. J. de A.; Addiego, F.; Bernsmann, F.; Ball, V.; Michel, M.; Toniazzi, V. Dopamine–Melanin Film Deposition Depends on the Used Oxidant and Buffer Solution. *Langmuir* **2011**, *27* (6), 2819–2825. <https://doi.org/10.1021/la104981s>.
- (17) Brown, T.; LeMay, H. E. J.; Bursten, B. E.; Murphy, C. J.; Woodward, P. *Chemistry: The Central Science*, 12th Editi.; Prentice hall, 2012.
- (18) Bafort, F.; Parisi, O.; Perraudin, J. P.; Jijakli, M. H. Mode of Action of Lactoperoxidase as Related to Its Antimicrobial Activity: A Review. *Enzyme Res.* **2014**, *2014*. <https://doi.org/10.1155/2014/517164>.
- (19) Boscolo, B.; Leal, S. S.; Salgueiro, C. A.; Ghibaudi, E. M.; Gomes, C. M. The Prominent Conformational Plasticity of Lactoperoxidase: A Chemical

- and PH Stability Analysis. *Biochim. Biophys. Acta - Proteins Proteomics* **2009**, *1794* (7), 1041–1048. <https://doi.org/10.1016/j.bbapap.2009.03.003>.
- (20) Zhang, H.; Bré, L. P.; Zhao, T.; Zheng, Y.; Newland, B.; Wang, W. Mussel-Inspired Hyperbranched Poly(Amino Ester) Polymer as Strong Wet Tissue Adhesive. *Biomaterials* **2014**, *35* (2), 711–719. <https://doi.org/10.1016/j.biomaterials.2013.10.017>.
- (21) Sun, X.; Cheng, L.; Zhao, J.; Jin, R.; Sun, B.; Shi, Y.; Zhang, L.; Zhang, Y.; Cui, W. BFGF-Grafted Electrospun Fibrous Scaffolds via Poly(Dopamine) for Skin Wound Healing. *J. Mater. Chem. B* **2014**, *2* (23), 3636–3645. <https://doi.org/10.1039/c3tb21814g>.
- (22) Xie, J.; Michael, P. L.; Zhong, S.; Ma, B.; MacEwan, M. R.; Lim, C. T. Mussel Inspired Protein-Mediated Surface Modification to Electrospun Fibers and Their Potential Biomedical Applications. *J. Biomed. Mater. Res. - Part A* **2012**, *100 A* (4), 929–938. <https://doi.org/10.1002/jbm.a.34030>.
- (23) Liu, Y.; Ai, K.; Lu, L. Polydopamine and Its Derivative Materials: Synthesis and Promising Applications in Energy, Environmental, and Biochemical Fields. *Chem. Rev.* **2014**, *114*, 5057–5115.
- (24) Boroujeni, M. B.; Nayeri, H. Stabilization of Bovine Lactoperoxidase in the Presence of Ectoine. *Food Chem.* **2018**, *265* (May), 208–215. <https://doi.org/10.1016/j.foodchem.2018.05.067>.
- (25) Luo, H.; Gu, C.; Zheng, W.; Dai, F.; Wang, X.; Zheng, Z. Facile Synthesis of Novel Size-Controlled Antibacterial Hybrid Spheres Using Silver Nanoparticles Loaded with Poly-Dopamine Spheres. *RSC Adv.* **2015**, *5* (18), 13470–13477. <https://doi.org/10.1039/C4RA16469E>.

Chapter 8 Surface modification of TPU-PDA patches with glucose oxidase

8.1. Abstract

This chapter first discusses the immobilization of glucose oxidase into a PDA-coated electrospun TPU fibre patches (TPU-PDA). Two types of TPU-PDA fibre patches were prepared: without LPO and with 1.4 U/mL LPO with the materials coated either for 3 hours or 7 hours. These four prepared TPU-PDA samples were immersed 10,000 U/L glucose oxidase enzyme for 24 hours to allow the enzyme to bind to the PDA layer. TPU-PDA-0-7-GO (TPU-PDA with no LPO and 7 hours coating grafted with glucose oxidase) showed an enzymatic activity of 12.6 ± 2.0 U GO/g while TPU-PDA-1.4-7 (TPU-PDA with 1.4 U/mL LPO and 7 hours coating grafted with glucose oxidase) showed 16.4 ± 3.8 U GO/g activity. The samples were then characterized in terms of morphological structure by SEM and FTIR-ATR analyses before and after surface functionalization, and their ability to produce H_2O_2 in the presence of a glucose source was tested using a colorimetric pertitanic acid assay which was also used to determine enzyme activity.

The second part of the chapter is dedicated to the preparation of a gelatin methacrylate hydrogel for glucose loading to be used in combination with TPU-PDA-GO electrospun membranes. Gelatin methacrylate was synthesized by functionalizing gelatin with methacrylic anhydride, characterized by FTIR-ATR analysis, and crosslinked by UV irradiation with an intensity of 4 mW/cm² at a wavelength of 365 nm. Finally 10 w/v% glucose loaded hydrogel with a 15 w/v% GelMA composition was prepared. A 100 μL volume of this hydrogel in combination with a 1 cm by 1 cm TPU-PDA-GO membrane (prepared using 1.4 U/mL lactoperoxidase enzyme as a catalyst) could produce 3.69±0.50 mM H₂O₂ per day when coated by immersing the patch in a DOPA-oxidizing solution for 7 hours, as assessed by colorimetric pertitanic acid assay. While this combination did not produce as much H₂O₂ as that formed by GO/glucose-laden HB PEGDA/HA-SH hydrogels (using the same hydrogel volume in the same PBS volume, i.e. 100 μL hydrogel in 5 mL PBS), the TPU-PDA membrane demonstrated to be capable of efficient GO immobilization on its surface.

8.2. Introduction

The immobilization of glucose oxidase on the PDA coated TPU fibre surface was done by a Michael type addition of the enzyme, involving the amine groups of the enzyme and the quinone groups of the PDA. This reaction was discussed in more detail in Chapter 6, with Figure 6.6 depicting grafting of GO enzyme on the PDA-coated thermoplastic polyurethane (TPU) polymer.

In Chapter 7, PDA was coated on an electrospun TPU fibre patch with and without the aid of an oxidizing agent, lactoperoxidase (LPO). This was done in order to reduce the time required for coating. This study compared the effect of coating time

on the amount of active glucose oxidase that was immobilized per gram of modified TPU fibre. The materials coated in a DOPA-oxidizing solution containing LPO (with PDA formed and deposited onto its surface) for 3 hours performed as well as the materials coated for 7 hours with no LPO enzyme: this confirmed that the addition of LPO was a viable solution for reducing the time required to coat substrates with polyDOPA or polydopamine.

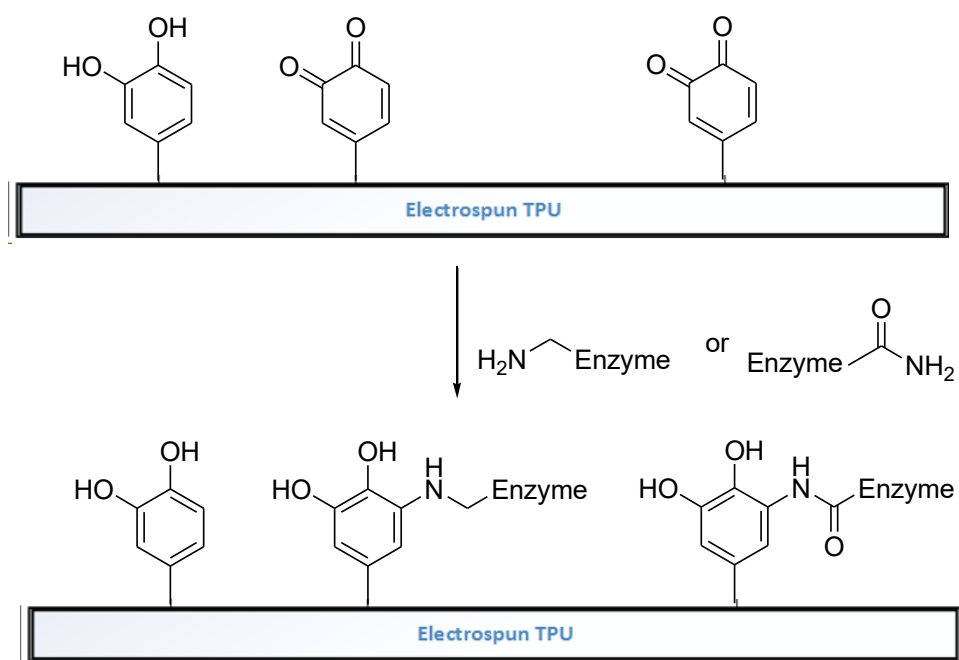


Figure 6.6: Enzyme immobilization on TPU-PDA (end product named as TPU-PDA-GO).

The main purpose of this enzyme-grafting process was to obtain TPU fibre patches with immobilized glucose oxidase on their surface. When this patch is applied together with a glucose source for wound dressing applications, this material would catalyze glucose in the presence of oxygen and produce hydrogen peroxide as shown in Figure 1.4. With H₂O₂ being produced from this material, this would supplement the H₂O₂ produced from the HB PEGDA/HA-SH 10-1.0 hydrogel from

Chapter 3 and aid the wound healing process as it covers the hydrogel from exposure.

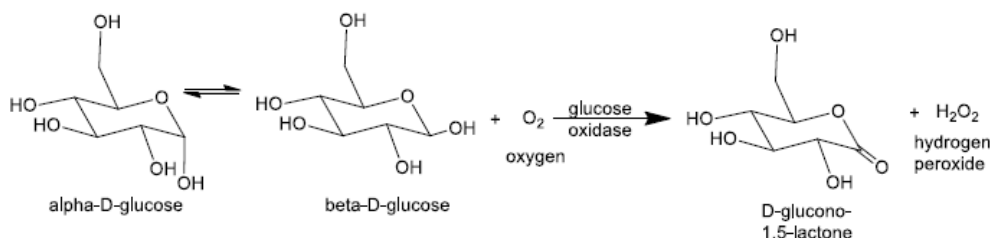


Figure 1.4: ROS formation of H₂O₂ from glucose catalyzed by glucose oxidase (GO).

8.3. Materials and methods

Glucose oxidase, Phosphate Buffer Solution pH 7.4 tablets, sulfuric acid, porcine skin gelatin, methacrylic anhydride, titanium oxysulfate, glucose, Irgacure 2959 were purchased from Sigma Aldrich, Italy.

PDA-coated electrospun TPU fibres (TPU-PDA) were prepared as described in Chapters 5 (preparation of TPU fibres) and 7 (coating of PDA under different oxidation conditions and coating times). The samples are coded as listed in Table 8.1 based on the addition of LPO enzyme catalyst and the coating time the samples underwent.

In Table 8.1, the “Sample Code (before GO grafting)” describe the parameters used for coating the samples as performed in Chapter 7. For example, TPU-PDA-0-3 refers to the sample with no LPO added with the samples immersed in the oxidizing DOPA solution for 3 hours. TPU-PDA-1.4-3 refers to the sample with 1.4 U/mL LPO added to increase the oxidation rate and immersed in the DOPA solution for 3 hours as well. Once these samples were grafted with glucose oxidase enzyme, the

“-GO” was added in to their material name as listen in “Sample Code (after GO grafting)”. Additionally, when a sample is mentioned such as TPU-PDA-0, this refers to the collective set of TPUs coated without LPO both at 3 hours and 7 hours.

Table 8.1. The glucose oxidase grafted sample codes

Sample Code (before GO grafting)	LPO added (U/mL)	Coating time (h)	Sample Code (after GO grafting)
TPU-PDA-0-3	0	3	TPU-PDA-GO-0-3
TPU-PDA-0-7	0	7	TPU-PDA-GO-0-7
TPU-PDA-1.4-3	1.4	3	TPU-PDA-GO-1.4-3
TPU-PDA-1.4-7	1.4	7	TPU-PDA-GO-1.4-7

8.3.1. Gelatin methacrylate

Gelatin methacrylate (GelMA) was synthesized to serve as the glucose loaded hydrogel as it requires non-expensive reagents and an easy synthesis protocol as established by Nichol, JW, et al., 2010¹. Briefly, 3 g of porcine skin gelatin was dissolved in 30 mL phosphate buffer solution (PBS) pH 7.4 at 60°C. Once gelatin was completely dissolved, the temperature was lowered to 50°C and 6 mL of methacrylic anhydride was added dropwise and the solution was reacted for 1 hour. After the acrylation step, 120 mL PBS 7.4 was added to the solution to dilute it. The solution was placed in a dialysis tube with a molecular weight cut-off of 3500 Da and it was dialyzed in deionized water for 5 days to remove any unreacted methacrylic anhydride. The solution was then freeze-dried and the recovered samples were stored in a waterproof container in a refrigerator with a temperature of 4°C.

Figure 8.1 shows the functionalization of gelatin with methacrylic anhydride to form gelatin methacrylate. The presence of the vinyl groups in GelMA allow it to be crosslinked with the addition of a photoinitiator and irradiated under UV light or to react with a thiol group like HA-SH, as was performed with other acrylate functionalized polymers such as HB PEGDA and HB PEGDA-co-GMA (see Chapter 2 and 4)

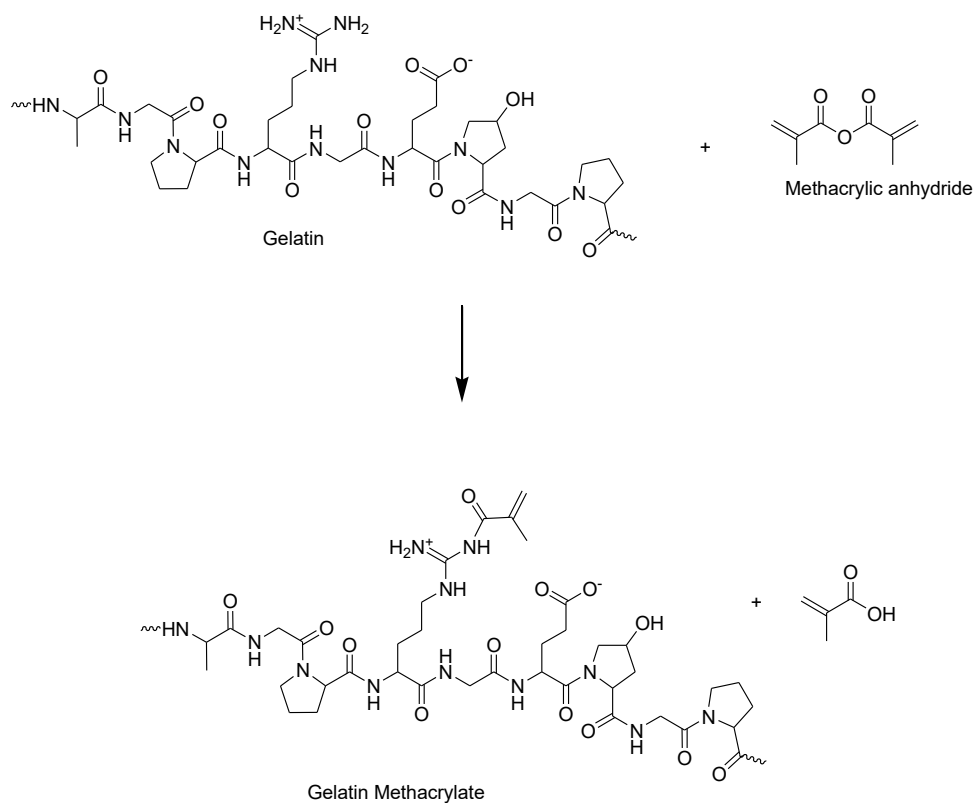


Figure 8.1: Chemical structure of gelatin functionalized to gelatin methacrylate (GelMA) with methacrylic anhydride.

8.3.1.1. Preparation of glucose-loaded GelMA hydrogel

GelMA was selected as the glucose-loaded hydrogel for several reasons: 1) the synthesis process and purification were relatively simple (especially compared to the preparation of HB PEGDA and HA-SH), 2) the material is stable in oxygen and does not self-crosslink (HA-SH requires to be prepared and stored with Argon), 3) only two reagents were required (gelatin and methacrylic anhydride), 4) it was able to crosslink under UV light with the addition of a photoinitiator, 5) it has been used in biomedical engineering applications and has been tested to be cytocompatible¹⁻³.

To prepare the glucose-loaded hydrogel samples, 300 mg of GelMA was dissolved in 2 mL of modified PBS pH 7.4 solution (containing 0.5 w/v% Irgacure and 10 w/v% glucose) at 50°C. After the samples were dissolved, 100 µL of the prepared solutions were pipetted into the hydrogel moulds previously used in Chapter 2 and 3 for preparation of HB PEGDA/HA-SH samples. Hydrogels within moulds were placed under a UV LED lamp and crosslinked for 10 minutes with an intensity of 4 mW/cm² at a wavelength of 365 nm with a LED lamp to surface distance of 10 cm. Figure 8.2 shows the different steps done in the preparation of the hydrogel samples.

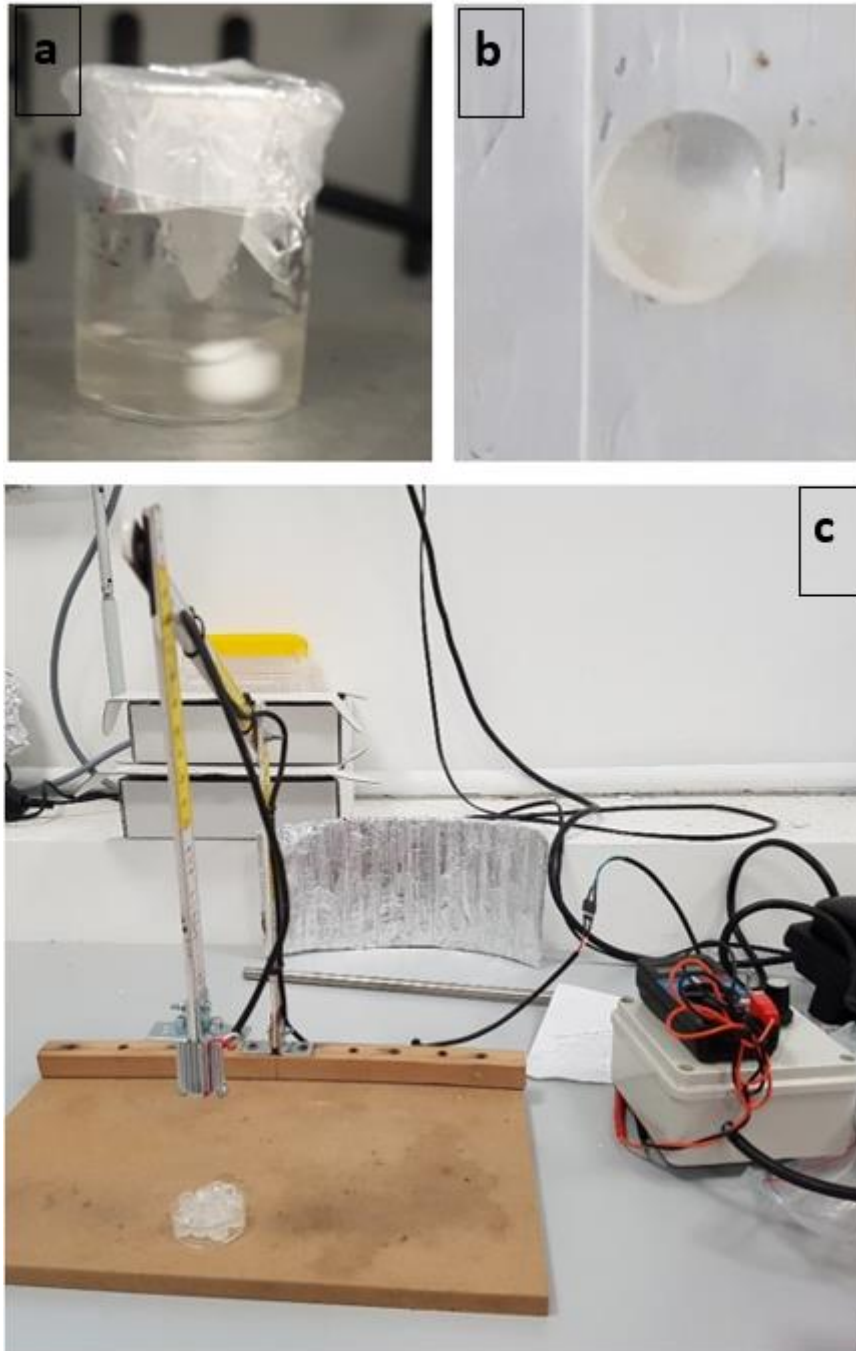


Figure 8.2: a) 15 w/v% GelMA solution in “modified” PBS (with 10 w/v% glucose and 0.5 w/v% Irgacure 2959 in PBS pH 7.4). b) UV-crosslinked 100 μ L glucose-loaded GelMA hydrogel (diameter 7.5 mm). c) UV-crosslinking set-up of the GelMA hydrogels with intensity of 4 mW/cm² at 365 nm wavelength.

8.3.2. Surface grafting of glucose oxidase on PDA-TPU patch

A 10,000 U/L solution of glucose oxidase in PBS pH 7.4 was prepared in a 250 mL beaker. While grafting of compounds in polyDOPA is usually done in TRIS buffer solution pH 8.5 (this solution was also used for PDA-coating of the fibre samples) PBS pH 7.4 was used to avoid denaturation or inactivation of the GO enzyme in a basic solution. Strips of TPU-PDA fibres (of different oxidizing and coating parameters, see Table 8.1) were immersed in the solution for 24 hours with constant stirring at 300 rpm. Afterwards, the strips were removed and washed twice in PBS to remove any traces of unattached GO enzymes.

8.3.3. Tests for analyzing the presence of immobilized glucose oxidase

8.3.3.1. SEM analysis

Scanning Electron Microscopy was performed using a LEO 1420 microscope (Zeiss, Germany) at 20 kV and a working distance of 15 mm. The diameters of the fibres in electrospun membranes were measured on SEM images using ImageJ software. Any difference in the morphology of the coated fibrous patches compared to the uncoated fibrous patches was analyzed. The maximum magnification that can be obtained from this instrument was 5000x.

Coated and uncoated samples were analyzed by SEM. To prepare the samples for SEM analysis, samples of the modified fibre patch were cut into 2 mm x 2 mm squares and mounted onto SEM sample holder using conductive tape. The samples were coated with a thin layer of gold using a sputter-coating machine (30 mA, 50 seconds) to improve conductivity for imaging.

8.3.3.2. FTIR-ATR analysis

Attenuated Total Reflectance Fourier Transform InfraRed Spectra (ATR-FTIR) of PDA-coated TPU was obtained at room temperature in the spectral range from 4000 to 400 cm^{-1} using a Perkin–Elmer Spectrum 100 equipped with an ATR accessory (UATR KRS5) with diamond crystal. The spectra, obtained as a result of 16 scans with a resolution of 4 cm^{-1} , were analyzed using the Perkin–Elmer Spectrum Software. Spectra were recorded on the PDA-coated TPUs (TPU-PDA samples), GO-grafted TPU-PDA-samples (TPU-PDA-GO), gelatin powder, and dried gelatin methacrylate (GelMA).

8.3.3.3. ROS production of GO-immobilized TPU patch

8.3.3.3.1. Enzyme activity in the material

In this experiment, the activity of the active glucose oxidase was measured by measuring the H_2O_2 produced after 5 hours using a pertitanic acid assay⁴. 1 cm by 1 cm strips of TPU-PDA-GO samples were cut, weighed, and placed in bijoux vials and 5 mL glucose solution (10 w/v% glucose in PBS pH 7.4) was added. The samples were incubated at 37°C for 5 hours and then their H_2O_2 concentrations were measured using the pertitanic assay discussed in Section 3.3.3. The equation used for calculating their enzyme activity in terms of U/g material (with 1 U = μmol H_2O_2 converted/minute) was:

$$\text{Activity of material} = \frac{[\text{Volume of solution (L)}] \left[\text{Concentration} \left(\frac{\mu\text{mol}}{\text{L}} \right) \right]}{[\text{time (min)}][\text{mass sample (g)}]}$$

8.3.3.3.2. ROS production with a glucose-loaded hydrogel source

This part of the study examines the ability of a glucose-loaded hydrogel to diffuse into the GO-grafted TPU and produce hydrogen peroxide. 1 cm by 1 cm strips of TPU-PDA-GO samples were cut and placed in bijoux vials along with 100 μ L glucose-loaded GelMA hydrogels prepared from Section 8.3.1.1. Figure 8.3 shows the two materials as arranged within the vial. Afterwards, 5 mL of PBS pH 7.4 was added into the vials and the samples were incubated at 37°C for 24 hours. The hydrogen peroxide concentration of the samples were then measured using the pertitanic acid assay. The difference between this procedure and that of Section 8.3.3.3.1 is that glucose in the hydrogel has to be released and diffuse outwards to the surrounding media before coming into contact with the TPU-PDA-GO material.



Figure 8.3: TPU-PDA-GO-1.4-7 (1 cm x 1 cm) with 100 μ L glucose-loaded GelMA hydrogel.

8.4. Results and discussion

8.4.1. Morphological analysis for GO-immobilized TPU patch

Figures 8.4 and 8.5 depict the SEM images of electrospun TPU fibre patch samples which were coated with PDA in varying conditions (see Table 8.1) before and after GO was grafted into their matrix. In both images, spherical particles (indicated by red arrows in the figures), previously not observed in TPU and TPU-PDA SEM images from Chapter 7, were detected on certain areas of the fibres, forming a rougher look than the uncoated fibres. These particles could be aggregations of GO enzyme grafted on TPU-PDA surface that is abundant in quinone groups. Figure 8.4 shows the TPU-PDA material with no GO enzyme and the corresponding samples grafted with GO enzyme. PDA was found to deposit itself preferably in areas of fibre intersection based on results from Chapter 7. For the TPU material immersed in GO solution, particles were also found on other parts of the fibre matrix, and not just at the junctions. Fibre porous structure was kept after GO functionalization.

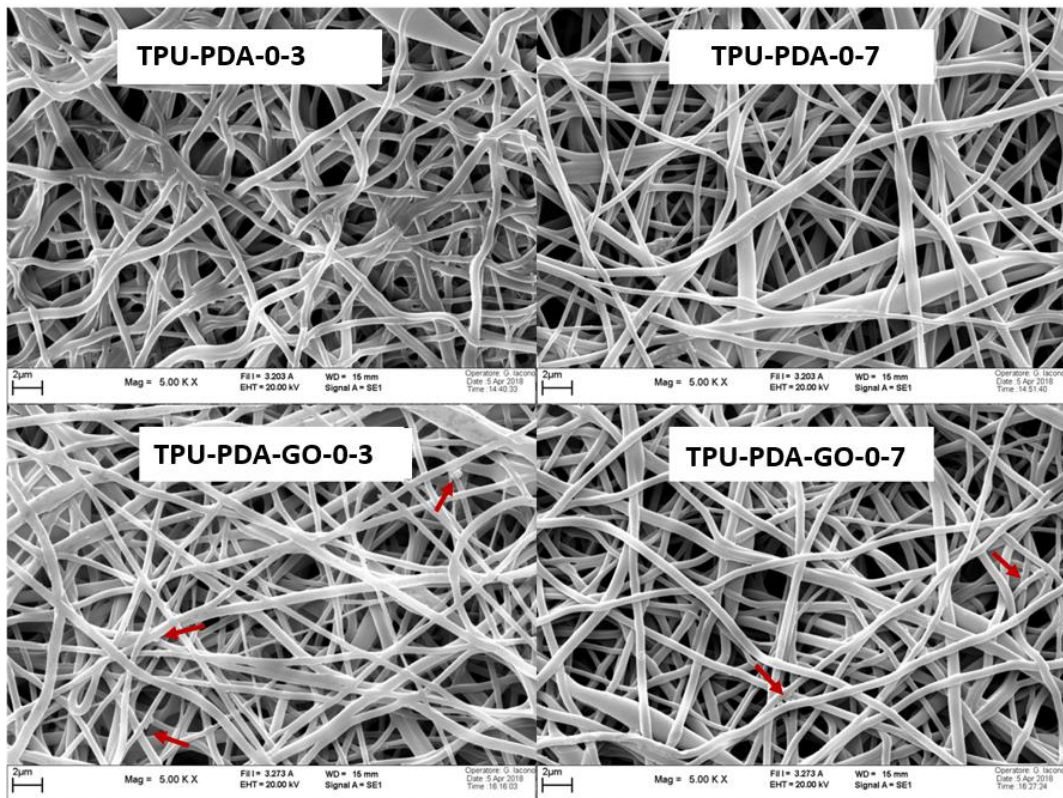


Figure 8.4: SEM images of TPU-PDA-LPO-0 coated for 3h and 7h (see the code), then immersed in GO enzyme solution for 24 hours.

Figure 8.4 shows the TPU-PDA material coated with PDA in the presence of 1.4 U/mL LPO for 3 hours and 7 hours compared to the same samples with grafted GO. In analogy to Figure 8.3, small spherical particles could be observed on the GO-grafted fibres, which could indicate the presence of glucose oxidase enzyme that was immobilized on the PDA-coated fibres. Fibre porous structure was kept after GO functionalization.

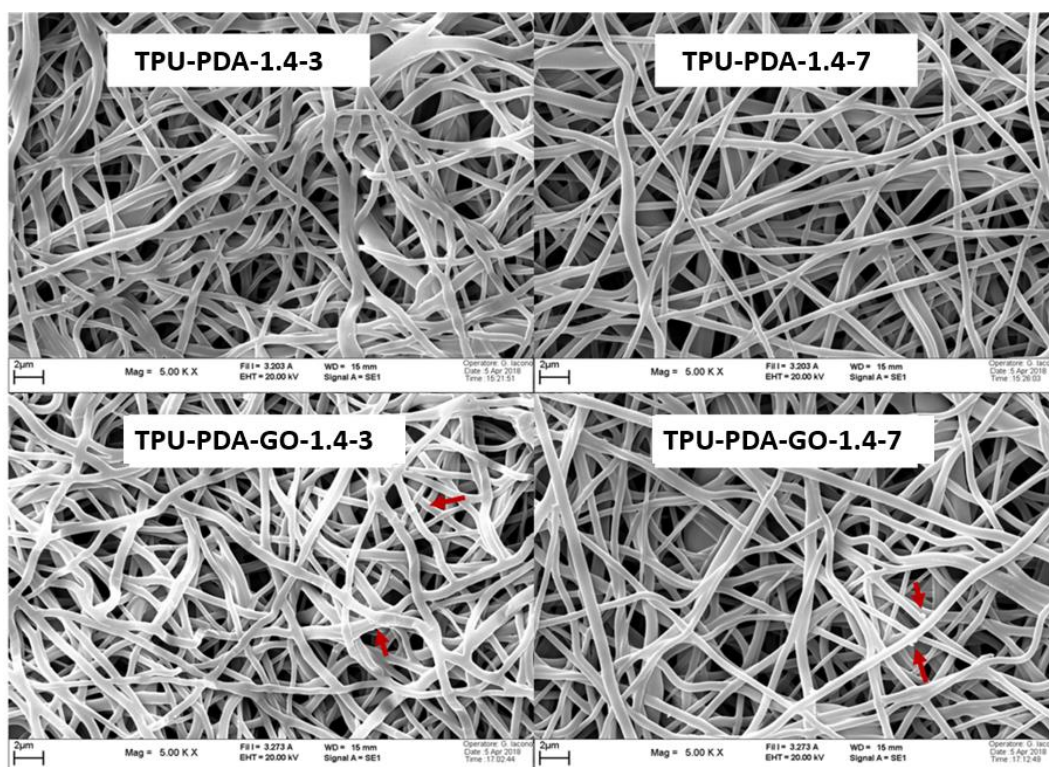


Figure 8.5: SEM images of TPU-PDA-GO-1.4 coated at 3h or 7h (see code), then immersed in GO enzyme solution for 24 hours.

8.4.2. FTIR-ATR analysis

TPU (Lubrizol Tecophilic SP60D60) was purchased as a biomedical grade thermoplastic polyurethane. The chemical structure of the material is unknown: the only available information is that TPU is an aliphatic polyether.

Figure 7.12 in Chapter 7 showed the FTIR-ATR spectra of the original TPU and TPU coated with PDA without the use of lactoperoxidase, and with the use of 1.4 U/mL LPO during a 7 hour coating period. On the other hand, Figures 8.6 to 8.10 show the FTIR spectra of the GO-immobilized PDA-coated TPU fibre samples.

There was no discernible difference in the spectra of GO-immobilized materials respect to spectra reported in Chapter 7 for TPU-PDA-0-7 and TPU-PDA-1.4-7 (Figure 7.12). It is possible that the absorption bands of used enzymes (both GO and LPO), being present at low quantities, are masked by the absorption bands of TPU-PDA spectrum

In more details, spectra in Figure 8.6 to Figure 8.10 showed:

- (i) The characteristic bands of the aliphatic polyether TPU, such as the strong absorbance band at 1098 cm^{-1} assigned to the C-O stretching and confirming the presence of ether bonds in the polymer backbone, C=O stretching of urethane bonds (1691 cm^{-1}) and N-H bending of urethane bonds (1524 cm^{-1}). The low absorption band at around 2900 cm^{-1} was assigned to the C-H stretching.

- (ii) The characteristic bands of PDA coating, such as the absorption at 3322 cm^{-1} attributed to the O-H stretching of the catechol groups, the band at 3000 cm^{-1} assigned to the stretching of C-H, the absorption band at 1524 cm^{-1} and 1490 cm^{-1} due to the C=C stretching of aromatic rings, an increased intensity of the C=O stretching band at 1110 cm^{-1} associated with quinone groups.

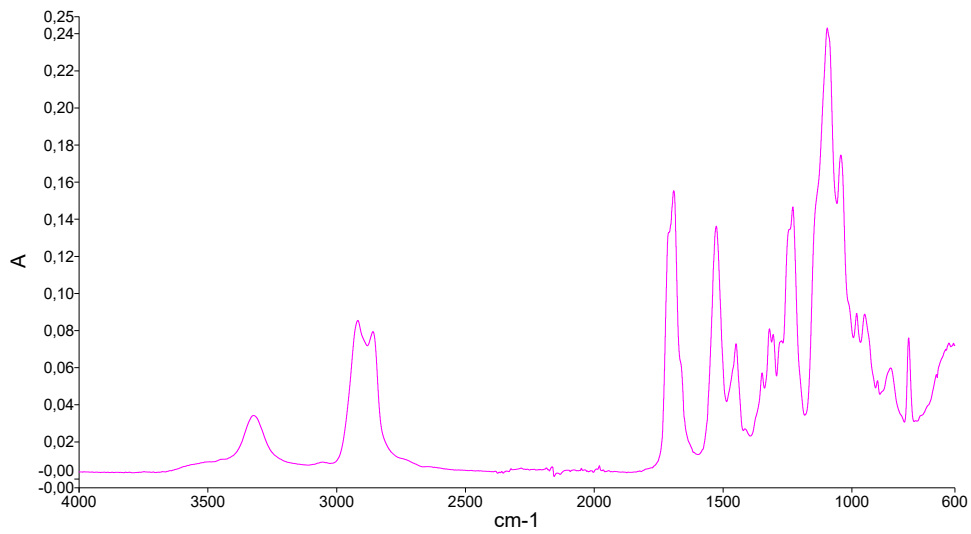


Figure 8.6: FTIR spectra of TPU-PDA-GO-0-3

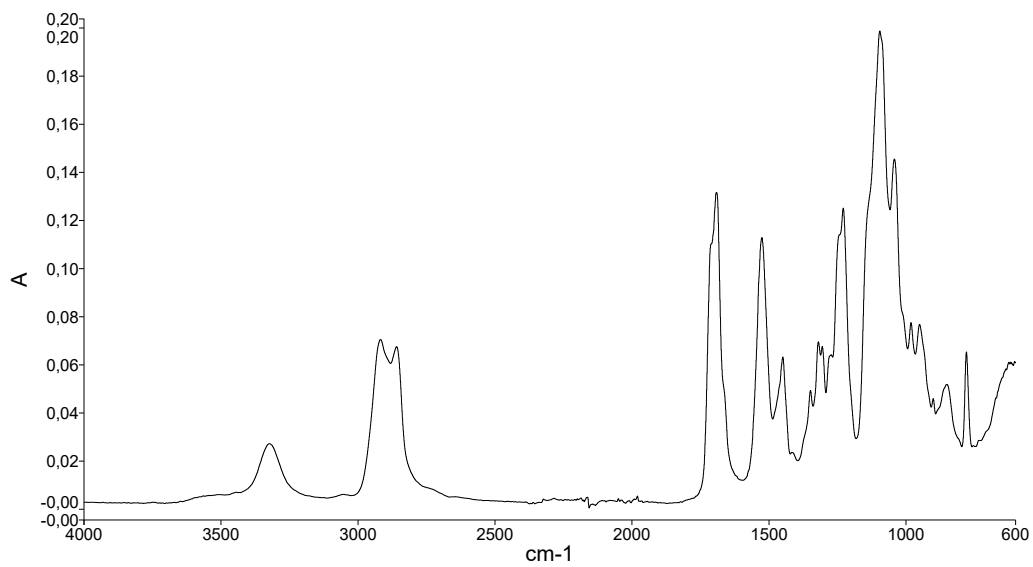


Figure 8.7: FTIR spectra of TPU-PDA-GO-0-7

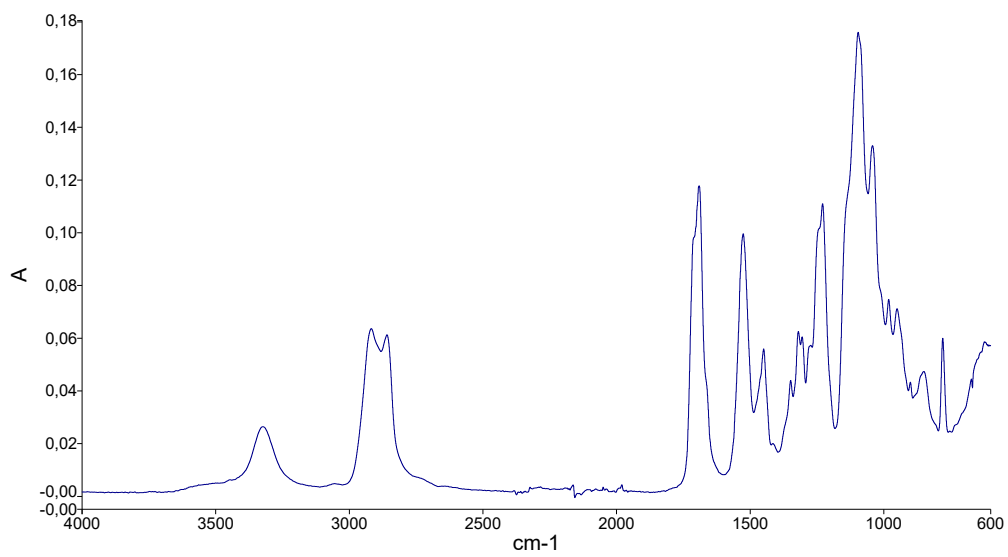


Figure 8.8: FTIR spectra of TPU-PDA-GO-1.4-3

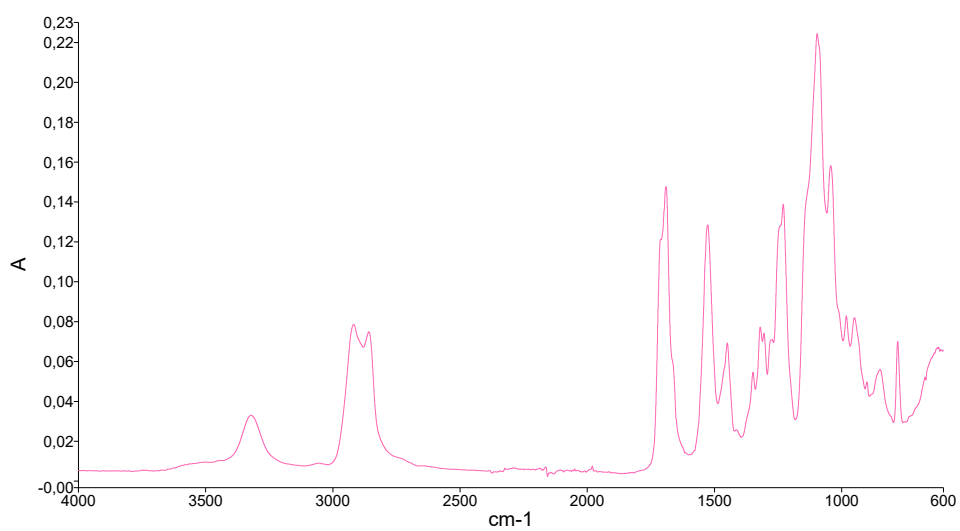


Figure 8.9: FTIR spectra of TPU-PDA-GO-1.4-7

In a previous study that characterized the FTIR spectrum of glucose oxidase, the following bands of note were reported: 1650 cm^{-1} (amide I band); 1540 cm^{-1} (amide II band); 1400 cm^{-1} (carboxylate groups)⁵. In the FTIR-ATR spectra of the TPU-PDA-GO fibre patches, main absorbance bands were in a close wavelength range respect to GO FTIR spectrum. Hence FTIR-ATR analysis could not detect GO grafting. The presence of GO in the TPU-PDA-GO fibre patches could be confirmed based on the ability of the functionalised material to produce hydrogen peroxide (enzyme activity) which will be discussed later.

Figure 8.10 and 8.11 show the FTIR spectra for gelatin methacrylate. Figure 8.10 is the FTIR spectrum obtained by the Ph.D student (presented as % transmission to be more easily compared with Figure 8.11) and Figure 8.11 is the FTIR spectrum of gelatin and GelMA from a study done by Zhou, X., et al. (2016) that also utilized the same protocol used by Nichol, et al. (2010)^{2,6}. Figure 8.11 was reprinted with permission.

The spectrum of GelMA (Figure 8.10) was similar to that of gelatin (Fig. 8.11). A strong peak was present at 1650 cm^{-1} related to amide I (C=O stretching). The band at $1500\text{--}1570\text{ cm}^{-1}$ was due to amide N-H bending while the band at $3200\text{--}3400\text{ cm}^{-1}$ was attributed to N-H and O-H stretching. The peak at 3062 cm^{-1} was due to C-H stretching. The peak due to carbon double bond in GelMA should be detected at 1640 cm^{-1} indicating the grafting of methacrylate anhydride, however it overlapped with the amide I peak. Hence FTIR-ATR analysis could not evidence the presence of MA functionalities which should be analyzed with different techniques (e.g. NMR analysis).

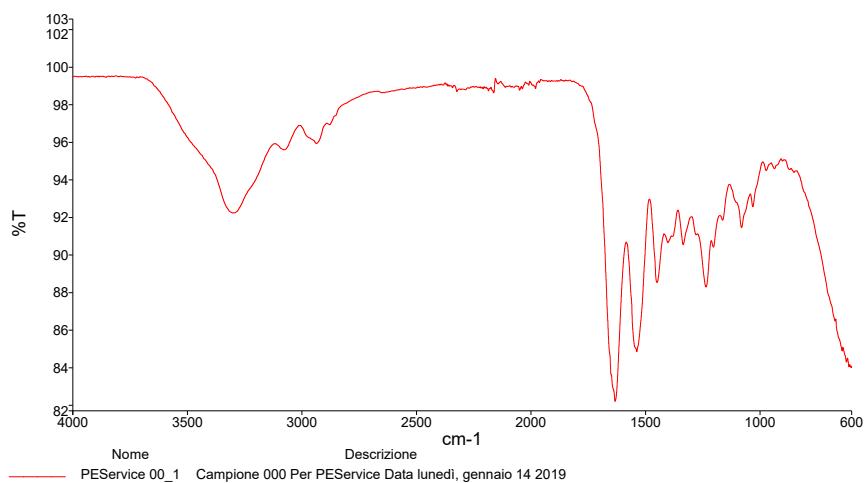


Figure 8.10: FTIR spectra of gelatin methacrylate reported as a function of percent transmittance.

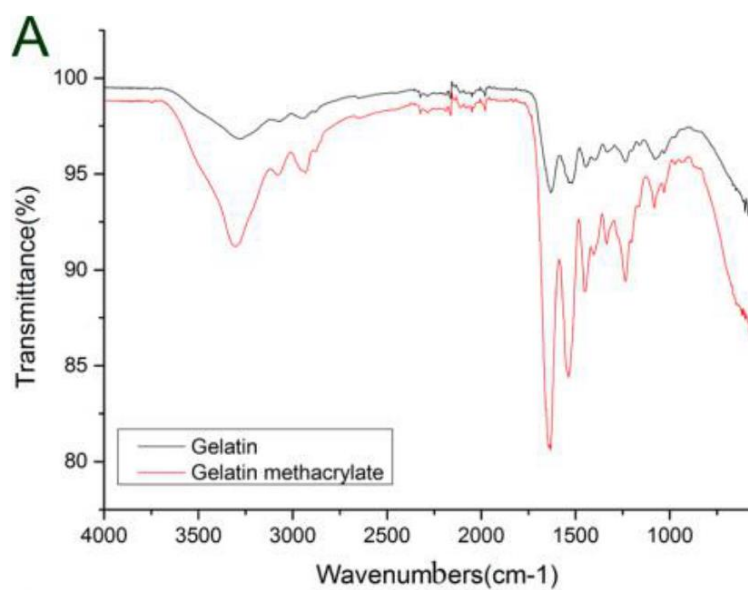


Figure 8.11. FTIR spectra of gelatin and GelMA from a study by Zhou, X., et al (2016)⁶. Reprinted Figure 3.A, reproduced with permission: Copyright (2019) American Chemical Society.

8.4.3. ROS production of GO-immobilized TPU patch

8.4.3.1. GO enzyme in TPU-PDA-GO materials

In order to confirm the presence of GO in the TPU, the materials were tested for their ability to produce H₂O₂ by reacting the material with glucose and then quantifying the H₂O₂ formed. The GO enzyme activity is quantified as the μmol H₂O₂ produced per minute by a gram of TPU-PDA-GO fibre patch. The simplified equation used to obtain this was:

$$\text{Activity of material} = \frac{[0.005 L] \left[\text{Concentration} \left(\frac{\mu\text{mol}}{L} \right) \right]}{[300 \text{ min}][\text{mass sample (g)}]}$$

Since the experiment measured the H₂O₂ concentration produced over a span on 300 minutes (5 hours) by the TPU-PDA-GO sample of a certain mass immersed in a 5 mL PBS pH 7.4 solution containing 10 w/v% glucose, the remaining data to obtain was the H₂O₂ concentration and mass. Figure 8.12 present the processed data from this enzyme activity analysis based on the ability of GO grafted into TPU-PDA to produce hydrogen peroxide in the presence of glucose.

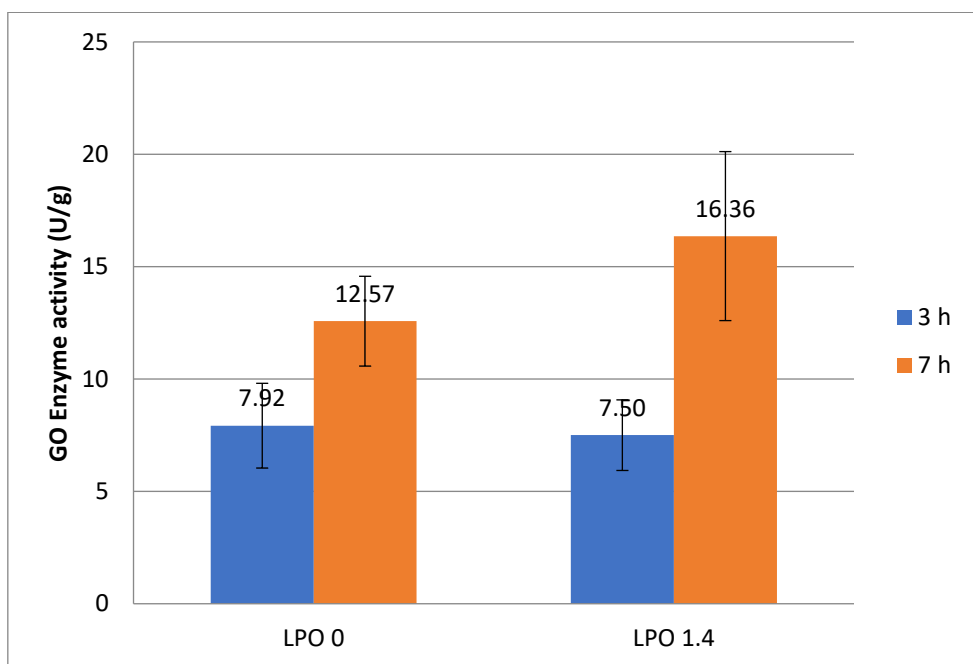


Figure 8.12: GO enzyme activity in TPU-PDA-GO fibre patches.

In comparing the effect of coating time (3 hours versus 7 hours) on GO enzyme activity for TPU-PDA-GO-0 samples, it was found that differences in enzyme activity of the materials were statistically significant ($t(4) = 2.9342$, $p = 0.0426$) from each other. For TPU-PDA-GO-1.4, the role of coating times was also considered to be a significant factor ($t(4) = 3.7662$, $p = 0.0197$) on GO enzymatic activity of the material. This means that PDA coating time plays a key role on the amount of immobilized active glucose oxidase enzyme.

Statistical analysis showed that the difference of GO enzyme activity between TPU-PDA-GO-0-3 and TPU-PDA-GO-1.4-3 was not statistically significant ($p = 0.78$). This means that even with greater oxidation in TPU-PDA-GO-1.4-3, the amount of GO deposited into the fibre patch for materials with a PDA coating time of 3 hours were approximately identical. The difference between TPU-PDA-GO-0-7 and TPU-PDA-GO-1.4-7 was also not statistically significant ($p = 0.20$). It is also a possibility that the amount of quinone groups where enzymes could be immobilized

in TPU-PDA-GO-1.4 was greater than the control setting, but had been partially grafted with lactoperoxidase enzyme reducing the possibility to graft more glucose oxidase.

Since it was found that coating time plays a more significant role on GO enzyme activity immobilized into the fibre patch, future studies ought to try the addition of a concentration lower than 1.4 U/mL LPO (such as 0.7 U/mL LPO) with a coating time of 5 hours as a compromise between the two parameters (while still reducing the time required for target oxidation).

8.4.3.2. ROS production of TPU-PDA-GO with a glucose-loaded hydrogel

Figure 8.13 shows the H₂O₂ concentration of the TPU-PDA-GO materials when used with a glucose-loaded GelMA hydrogel after 24 hours. From previous studies, 10-20 mM H₂O₂ has been selected as the set production target per day that was reported to stimulate angiogenesis in wounds⁷. TPU-PDA-GO plus GelMA hydrogel has been developed to be used in conjunction with HB PEGDA/HA-SH 10-1.0 hydrogel selected to attain this target concentration. However, if TPU-PDA-GO plus GelMA hydrogel two-layer system might produce alone the target ROS concentration, it could be used as an alternative device for wound healing. On the other hand, the three-layer system should be carefully evaluated for its cytotoxicity effects if producing much more hydrogen peroxide than the target concentration.

In comparing the effect of coating time (3 hours versus 7 hours) on H₂O₂ produced for TPU-PDA-GO-0 + glucose-loaded GelMA hydrogel samples, differences were not statistically significant ($p = 0.60$). On the contrary, for TPU-PDA-GO-1.4, differences in the results obtained at different coating times were statistically

significant ($p = 0.02$). This means that the role of PDA coating time is probably more significant for samples that have an added amount of lactoperoxidase to enhance the rate of DOPA oxidation.

Statistical analysis showed that the difference of H_2O_2 produced between TPU-PDA-GO-0-3 and TPU-PDA-GO-1.4-3 was not statistically significant ($p = 0.17$). The difference between TPU-PDA-GO-0-7 and TPU-PDA-GO-1.4-7 was also not statistically significant ($p = 0.10$). As with the statistical analysis from Section 8.4.3.1, the effect of added lactoperoxidase did not improve the activity of GO enzyme within the material.

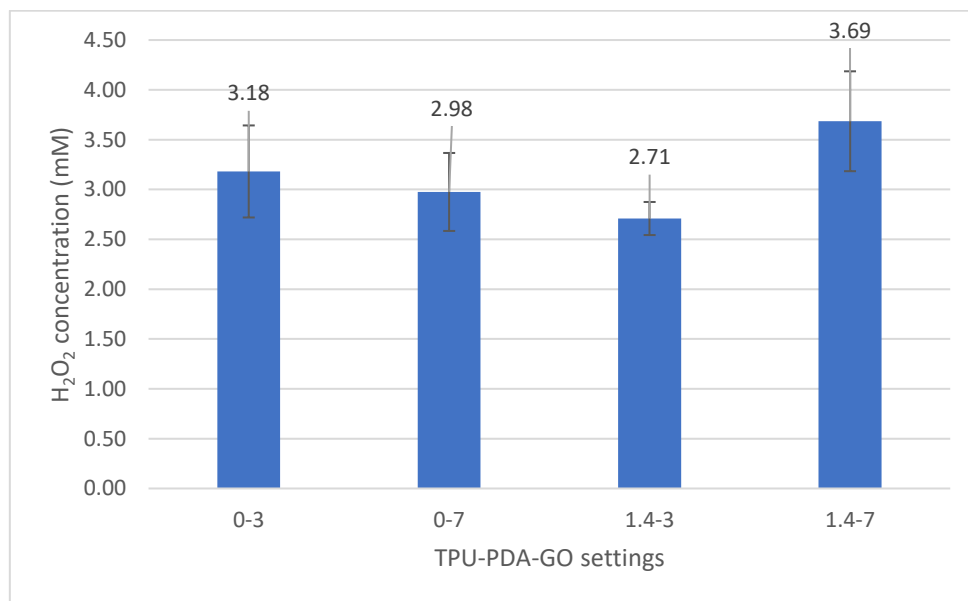


Figure 8.13: ROS production (after 24 hours) of TPU-PDA-GO patches with glucose-loaded GelMA hydrogel.

This experiment has proven that TPU-PDA-GOs can produce hydrogen peroxide when provided with a glucose source that can diffuse into the electrospun fibre and react with the immobilized glucose oxidase. This means that the GO-grafted PDA-coated TPU device can provide more ROS to the wound site if necessary, such as

for vulnerable patients that require an extra concentration of ROS and the protection from exposure provided by the TPU material. However, this also means that the LPO enhancement performed in Chapter 7 did not provide an added amount of grafted GO enzyme that could be immobilized, even if the measured degrees of oxidation in the DOPA solution and TPU material were significantly higher.

8.5. Conclusions

Glucose oxidase was successfully grafted into a PDA-coated electrospun TPU fibre patch. The material that produced the highest activity was TPU-PDA-GO-1.4-7 with an activity of 16.36 ± 3.76 U/g glucose oxidase. When used with a 100 μ L glucose-loaded GelMA hydrogel, 3.69 ± 0.50 mM H_2O_2 was produced after 24 hours. PDA coating time played a more significant role on the amount of grafted GO respect to the use of LPO enzyme catalyst. For this application, the use of LPO did not bring any improvements to this specific application of GO-grafting despite the observed enhanced oxidation as reported in Chapter 7. It is recommended for further studies to explore lower concentrations of LPO with coating times of around 5 hours (still lower than 7 hours required for coating with no enzyme) since there is a chance that the presence of LPO causes an interference with the grafting of glucose oxidase into the PDA-coated TPU fibre patches. However, TPU-PDA-GO-1.4-3 and TPU-PDA-GO 1.4-7 were used for cytocompatibility assays in Chapter 9 as single substrates, bilayer wound healing devices with glucose-loaded GelMA, and trilayer wound healing devices with honey-mimetic HB PEGDA/HA-SH and glucose-loaded GelMA hydrogels.

In this chapter, gelatin methacrylate was synthesized and crosslinked into a hydrogel under UV radiation with the addition of a photoinitiator. This material served to be a viable option for being loaded with glucose. More data and the

characterizations performed on this polymer can be found in the appendices, including its use in other applications.

It is also recommended that images of the fibre patches can be obtained at magnifications of 20,000x and higher before and after GO enzyme grafting by using more advanced SEM instruments that can accomplish this. This would give a more comprehensive view of confirming whether or not there are smaller enzyme particles that can be found grafted into the fibres other than the clusters found in the SEM images.

8.6. References

- (1) Nichol, J. W.; Koshy, S. T.; Bae, H.; Hwang, C. M.; Yamanlar, S.; Khademhosseini, A. Cell-Laden Microengineered Gelatin Methacrylate Hydrogels. *Biomaterials* **2010**, *31* (21), 5536–5544. <https://doi.org/10.1016/j.biomaterials.2010.03.064>.
- (2) Hutson, C. B.; Nichol, J. W.; Aubin, H.; Bae, H.; Yamanlar, S.; Al-Haque, S.; Koshy, S. T.; Khademhosseini, A. Synthesis and Characterization of Tunable Poly(Ethylene Glycol): Gelatin Methacrylate Composite Hydrogels. *Tissue Eng. Part A* **2011**, *17* (13–14), 1713–1723. <https://doi.org/10.1089/ten.tea.2010.0666>.
- (3) Wang, Z.; Abdulla, R.; Parker, B.; Samanipour, R.; Ghosh, S.; Kim, K. A Simple and High-Resolution Stereolithography-Based 3D Bioprinting System Using Visible Light Crosslinkable Bioinks. *Biofabrication* **2015**, *7* (4), 45009. <https://doi.org/10.1088/1758-5090/7/4/045009>.
- (4) Eisenberg, G. Colorimetric Determination of Hydrogen Peroxide. *Ind. Eng. Chem. Anal. Ed.* **1943**, *15* (5), 327–328.

<https://doi.org/10.1021/i560117a011>.

- (5) Chey, C. O.; Ibupoto, Z. H.; Khun, K.; Nur, O.; Willander, M. Indirect Determination of Mercury Ion by Inhibition of a Glucose Biosensor Based on ZnO Nanorods. *Sensors (Switzerland)* **2012**, *12* (11), 15063–15077. <https://doi.org/10.3390/s121115063>.
- (6) Zhou, X.; Zhu, W.; Nowicki, M.; Miao, S.; Cui, H.; Holmes, B.; Glazer, R. I.; Zhang, L. G. 3D Bioprinting a Cell-Laden Bone Matrix for Breast Cancer Metastasis Study. *ACS Appl. Mater. Interfaces* **2016**, *8* (44), 30017–30026. <https://doi.org/10.1021/acsami.6b10673>.
- (7) Loo, A. E. K.; Wong, Y. T.; Ho, R.; Wasser, M.; Du, T.; Ng, W. T.; Halliwell, B. Effects of Hydrogen Peroxide on Wound Healing in Mice in Relation to Oxidative Damage. *PLoS One* **2012**, *7* (11). <https://doi.org/10.1371/journal.pone.0049215>.

Part III

Chapter 9 Assembly of Multilayer Wound Healing Patch

9.1. Abstract

In this chapter, the cytocompatibility of four types of TPU-PDA-GO fibre patches and glucose-loaded GelMA hydrogel were evaluated in NIH/3T3 mouse fibroblast cells for 24 hours using an indirect method. These materials were tested first individually and then combined together. After selecting set-ups which kept cell viability, these were assembled together with the honey mimetic HB PEGDA/HA-SH 10-1.0 hydrogel (250 U/L GO and 2.5 w/w% glucose) to form a multilayer wound healing device. The final trilayer set-up which gave the highest cell viability of $58.2 \pm 8.5\%$ was HB PEGDA/HA-SH 10-1.0 hydrogel (250 U/L GO and 2.5 w/w% glucose) + TPU-PDA-GO-0-3 fibre patch + 10 w/v% glucose-loaded GelMA hydrogel. The obtained cytocompatibility for the multilayer was not considerably ideal, hence the GO/glucose concentrations in HB PEGDA/HA-SH 10-1.0 should be tailored when used in combination with TPU-PDA-GO fibre patch and glucose-loaded GelMA. An alternative application would be to apply the TPU-PDA-GO system to protect the *in situ* HB PEGDA/HA-SH 10-1.0 hydrogel dressing from exposure to external environment and, once the glucose from the HB

PEGDA/HA-SH 10.1 hydrogel has almost depleted itself, the glucose-loaded GelMA hydrogel could be applied as an alternative glucose source.

9.2. Introduction

Multilayer wound dressings (sometimes termed as composite wound dressings) are generally organized into three parts: bacterial barrier, absorption layer, and the adhesive¹. The most common types are variations of a pad, cloth, and film with an adhesive applied to the bottom layer for the dressing to adhere to skin.

For hydrogels, a bilayer hydrogel wound dressing under the name Oxyzyme was developed, which has been previously mentioned in Chapter 1^{2,3}. In this material, the bottom hydrogel was loaded with glucose oxidase and the second layer of hydrogel loaded with glucose was applied on top of it. This was one of the honey-based wound healing materials along with Surgihoney⁴.

To combat the rising problem of antibacterial resistance, a multilayer wound healing device was designed utilizing the concept of antibacterial ROS produced by glucose oxidase and glucose within honey. This “honey mimetic” multilayer wound healing device required to fulfill other objectives as well:

- Produce a minimum concentration of 10 mM H₂O₂ per day to stimulate angiogenesis in wound tissue⁵
- Provide sufficient coverage of the wound tissue including irregular surfaces and crevices (obtained with HB PEGDA/HA-SH 10-1.0 hydrogel having *in situ* gelling properties)

- Have extra protection from possible contamination and exposure (this function is intended to be fulfilled by the TPU-PDA-GO fiber patch which has mussel-like adhesive properties that allow adhesion to the hydrogel)
- Additionally, these materials should be in general: hydrophilic, porous, oxygen-permeable to allow the wound to breathe and drain off wound exudates, and biocompatible⁶

Together, these components are combined and shown in Figure 9.1 to show the assembly using the materials produced in previous chapters.

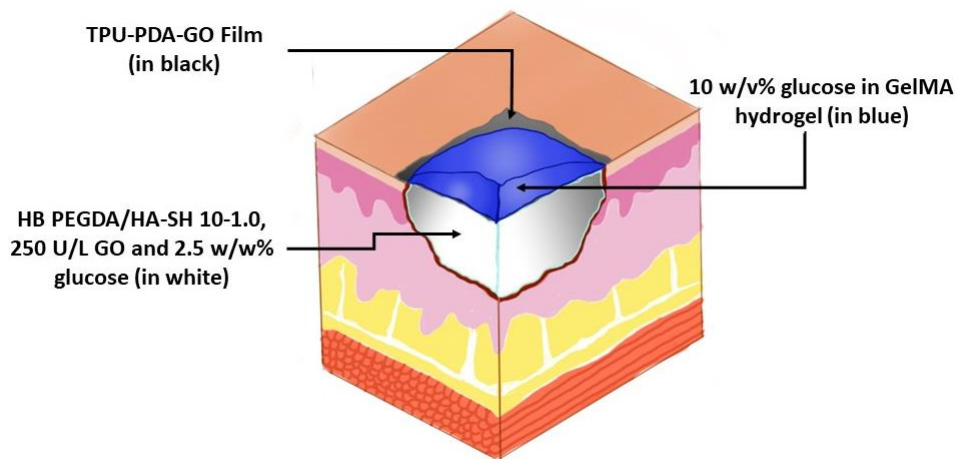


Figure 9.1: Assembly of multilayer wound healing device and their individual components.

In this chapter, the cytocompatibility of TPU-PDA-GO fibres with NIH/3T3 mouse fibroblasts was evaluated before their assembly in the multilayer wound healing device. This analysis was needed to select a biocompatible fibrous layer for the multilayer device in the perspective of further studies. Afterwards, TPU-PDA-GO patch cytocompatibility was evaluated when it was used in combination with a glucose-loaded GelMA hydrogel, similarly to the procedure in Section 3.3.4.

Finally, the components were assembled to form the multilayered wound healing device as shown in Figure 9.1 and evaluated for their cytocompatibility.

9.3. Materials and methods

Phosphate buffer solution tablets (PBS 7.4), High-Glucose Dulbecco's Modified Eagle Medium (DMEM), Fetal Bovine Serum (FBS), Resazurin sodium salt were provided by Sigma Aldrich, Italy. NIH/3T3 mouse fibroblast cells (ATCC® CRL-1658™) were obtained from ATCC, Italy.

9.3.1. HB PEGDA/HA-SH hydrogel

The process for producing this material was described in Chapter 3. The glucose oxidase/glucose concentration used throughout in this study was 250 U/L GO and 2.5 w/w% glucose.

9.3.2. GO-immobilized TPU patch and glucose hydrogel source

The processes for producing these materials were described in Chapter 8. Four types of glucose oxidase enzyme-grafted, polyDOPA-coated electrospun thermoplastic polyurethane fibres (TPU-PDA-GO) were used as previously listed in Table 8.1. UV-crosslinked gelatin methacrylate hydrogel was used as the glucose-laden medium where glucose diffused downwards to the TPU fibers and hydrogen peroxide was produced able to diffuse through the HB PEGDA/HA-SH 10-1.0 hydrogel.

9.3.3. Cytocompatibility of electrospun TPU fibre materials

Cytocompatibility of the materials was evaluated with the assistance of Andrea Gallina, a post-graduate student from Politecnico di Torino.

Pure electrospun TPU fibre mat and TPU-PDA-GO fibre mats were prepared by cutting the fibre patches into 5 mm by 5 mm pieces. They were tested for cytocompatibility using a non-contact method by placing them in a transwell insert in a 24-well plate. Samples were sterilized by UV radiation within a biological hood for 2 hours.

Cytotoxicity of the patches was evaluated using NIH/3T3 mouse fibroblast cells (ATCC® CRL-1658™). Briefly, cell suspension containing 50,000 cells/mL was prepared in full cell medium (High-Glucose Dulbecco's Modified Eagle Mixture, containing 10 v/v% Fetal Bovine Serum) from cells cultured approximately 24 hours previously.

Then, 1 mL of the prepared full cell medium was added to each well in the sterilized plate and incubated at 37°C for 24 hours. After this, the Alamar Blue assay was performed. The transwell inserts were removed and the cells were washed twice with sterile PBS pH 7.4. Then 1 mL of 1X Alamar Blue solution was added to each well, and the plate was returned to incubate for 6 hours at 37°C. Alamar Blue solution was prepared by dissolving 3 mL of resazurin blue in 27 mL PBS pH 7.4 to obtain a 1X or 10 v/v% Alamar Blue solution. Readings were obtained from the Perkin Elmer Victor X3 multimode plate reader. The fluorescence intensity of the

solutions was measured at 595 nm wavelength under excitation at 535 nm wavelength. The percentage of cell viability was calculated as:

$$\begin{aligned} & \text{Cell viability (\%)} \\ &= \frac{\text{Reading of Sample Well} - \text{Reading of Alamar Blue}}{\text{Reading of No treatment Well} - \text{Reading of Alamar Blue}} \\ & * 100\% \quad (\text{eq.6}) \end{aligned}$$

Samples were analysed in quadruplicates. Control samples were also tested consisting of cells cultured in tissue culture polystyrene plates without the presence of electrospun mats.

9.3.4. Assembly of bilayer wound healing patch

The TPU-PDA-GO fibre patch plus glucose-loaded GelMA samples were assembled for cytocompatibility testing as follows: firstly, 5 mm by 5 mm fiber patches of TPU-PDA-GO were prepared as described in Section 9.3.3.

The next step was the preparation of the glucose-loaded GelMA hydrogel beads. To prepare the glucose-loaded hydrogel samples, 300 mg of GelMA was dissolved in 2 mL of PBS solution at pH 7.4 and at 50°C, containing 0.5 w/v% Irgacure and 10 w/v% glucose. After the samples were dissolved, 30 µL of the prepared solutions were pipetted into a flat hydrophobic Teflon-coated surface previously used in Chapter 3 for preparation of HB PEGDA/HA-SH beads. Such beads (still liquid but held in form by surface tension) were placed under an UV LED lamp (at 10 cm distance) and crosslinked for 10 minutes at a power of 4 mW/cm² and a wavelength of 365 nm. These beads are shown in Figure 9.2.

These two components were assembled by spreading out the TPU-PDA-GO fiber patch and gently placing the glucose-loaded GelMA hydrogel bead on top of it. This assembled system is shown in Figure 9.2.

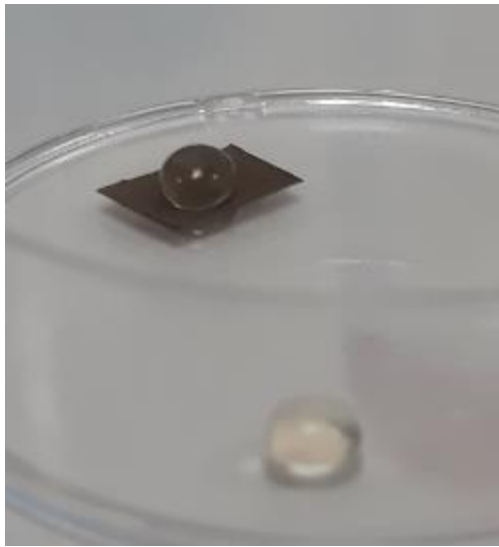


Figure 9.2: Photos of glucose-loaded GelMA hydrogel bead alone, and on the top of a TPU-PDA-GO fibre patch to assemble a bilayer wound healing device.

9.3.5. Cytocompatibility evaluation of bilayer wound healing patch

Cytocompatibility of the materials was evaluated with the assistance of Andrea Gallina, a post-graduate researcher from Politecnico di Torino.

Samples of electrospun TPU and TPU-PDA-GO fibre mats were prepared by cutting the patches into 5 mm by 5 mm pieces. They were tested for cytocompatibility using a non-contact method by placing them on transwell inserts

in a 24-well plate. Samples were sterilized by UV radiation within a biological hood for 2 hours.

Glucose-loaded GelMA hydrogels were prepared as described in Section 9.3.4, separated from the TPU-PDA-GO fibre patches to avoid ROS formation before the evaluation started.

Once both components were sterilized, the GelMA hydrogels were placed within the transwell inserts as shown in Figure 9.3. An extra row of transwell inserts was prepared to test the cytocompatibility of glucose-loaded GelMA hydrogel alone.

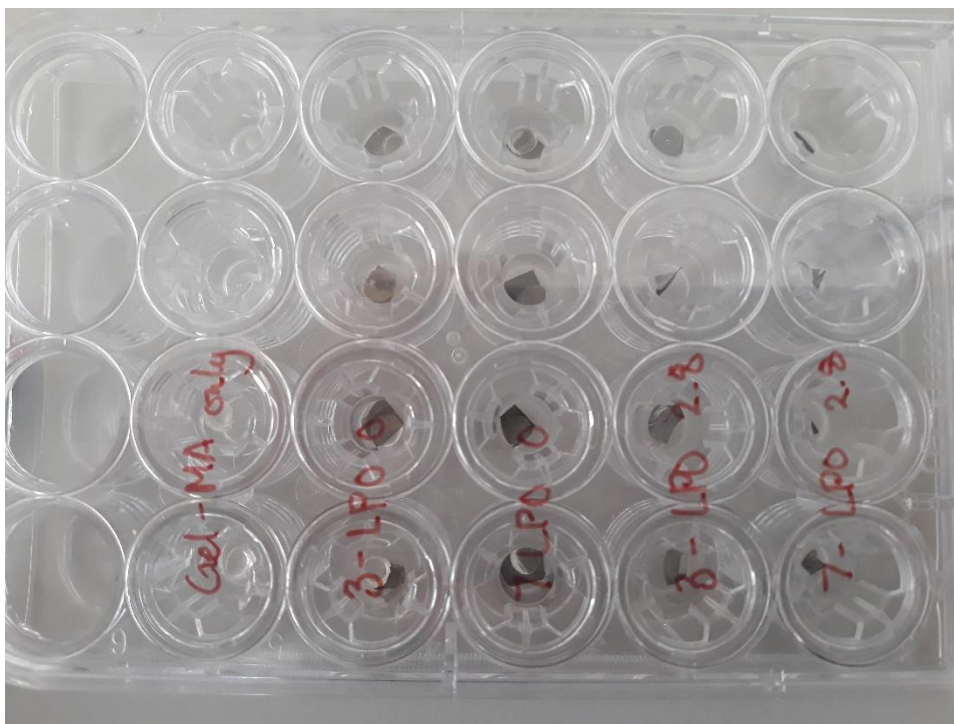


Figure 9.3: Bilayer TPU-PDA-GO + glucose loaded GelMA hydrogel set-ups for cytocompatibility testing.

Cytotoxicity of the patches were evaluated using NIH/3T3 mouse fibroblast cells (ATCC® CRL-1658™). Briefly, cell suspension containing 50,000 cells/mL was

prepared in full cell medium (High-Glucose Dulbecco's Modified Eagle Mixture, containing 10 v/v% Fetal Bovine Serum) from cells cultured approximately 24 hours previously.

Then, 1 mL of the prepared full cell medium was added to each well in the sterilized plate and incubated at 37°C for 24 hours. After this, the Alamar Blue assay was performed. The transwell inserts were removed and the cells were washed twice with sterile PBS at pH 7.4. Then 1 mL of 1X Alamar Blue solution was added to each well, and the plate was returned to incubate for 6 hours at 37°C. Alamar Blue solution was prepared by dissolving 3 mL of resazurin blue in 27 mL PBS pH 7.4 to obtain a 1X or 10 v/v% Alamar Blue solution. Readings were obtained from the Perkin Elmer Victor X3 multimode plate reader. The fluorescence intensity of the wells was measured at 595 nm emission wavelength by excitation at 535 nm wavelength.

In this cytocompatibility assay, the viability of the cells was tested while H₂O₂ was continuously produced by the two components and released into the cell medium. Other experiments included the evaluation of cell viability when the cells were in indirect contact with glucose-loaded GelMA hydrogel and in control conditions (cells cultured in tissue culture polystyrene plates without any sample).

9.3.6. Assembly of trilayer wound healing patch

The final multilayer wound healing device was prepared as follows: Using a 24 well plate as a hydrogel mould, 200 µL HB PEGDA/HA-SH 10-1.0 was poured into each well to form *in situ* and crosslink into a hydrogel. Next, a 1 cm by 1 cm TPU-PDA-GO fibre patch was placed on top of this hydrogel. It was observed that this fibre patch immediately adhered to the hydrogel and was difficult to pull out, which

could be attributed to its mussel-like adhesive property. Finally, 100 μ L cylindrical glucose-loaded GelMA hydrogel pieces (as described in Section 8.3.1.1.) were placed on the top of the TPU-PDA-GO fibre patch. The final assembled device is shown in Figure 9.4

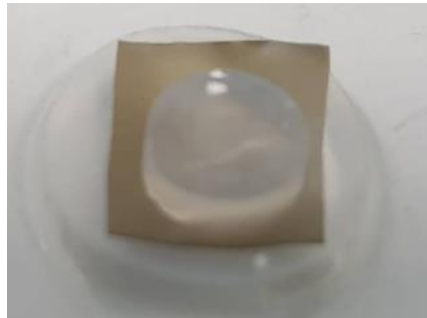


Figure 9.4: Trilayer ROS-producing wound healing device.

9.3.7. Cytocompatibility of trilayer wound healing device

Cytocompatibility of the materials was evaluated with the assistance of Andrea Gallina, a post-graduate researcher from Politecnico di Torino. Since this material was more complex than the previous materials analyzed, the procedure was modified following the ISO 10993 standards for the testing of the biocompatibility of medical devices.

After the multilayer wound dressing was assembled as described in Section 9.3.6, the plate containing the samples was sterilized under UV light for two hours. Then, 1 mL of DMEM was added to each well to collect eluates from the wound healing system after 24 hours. These eluates were filtered through a 0.22 μ m syringe filter for further sterilization.

Separately, another 24 well plate was prepared that had been cultured to contain 50,000 cells per well. The original cell media within these wells were removed and the cell media containing the eluates was introduced into the wells. The plate containing the cells and eluate-extracted cell media was incubated at 37°C for 24 hours.

After this, the Alamar Blue assay was performed. The cell media in each well were pipetted and discarded and the cells were washed in sterile PBS pH 7.4 twice. Then 1 mL of 1X Alamar Blue solution was added to each well, and the plate was returned to incubate for 6 hours at 37°C. Alamar Blue solution was prepared by dissolving 3 mL of resazurin blue in 27 mL PBS pH 7.4 to obtain a 1X or 10 v/v% Alamar Blue solution. Readings were obtained from the Perkin Elmer Victor X3 multimode plate reader. The fluorescence intensity of the wells was measured at 595 nm emission wavelength by excitation at 535 nm wavelength.

In this cytocompatibility assay, the viability of the cells was tested from the eluates in the cell media which contained H₂O₂ produced after 24 hours and possibly some polymer residue from the multilayer components.

9.4. Results and discussion

9.4.1. Cytocompatibility of TPUs

Figure 9.5 presents the non-contact cytocompatibility results of the electrospun TPU fibre patches (modified and unmodified) using NIH/3T3 mouse fibroblast cells after 24 hours.

NT in the figure refers to the set of wells with no treatment introduced as the cells were cultured (positive control). The unmodified TPU fibre patch was also tested

to serve as a control reference to compare its cytocompatibility with the GO-grafted PDA-coated TPU fibres. The TPU fibre gave a positive result in terms of percent cell viability, which was expected as the material used was a commercially available medical grade TPU.

The four GO-grafted TPUs resulted in positive cytocompatibility as they showed percent cell viabilities greater than 80%. This means that the four configurations can be tested for further cytocompatibility testing where it actively produces H₂O₂ with the glucose-loaded GelMA hydrogel.

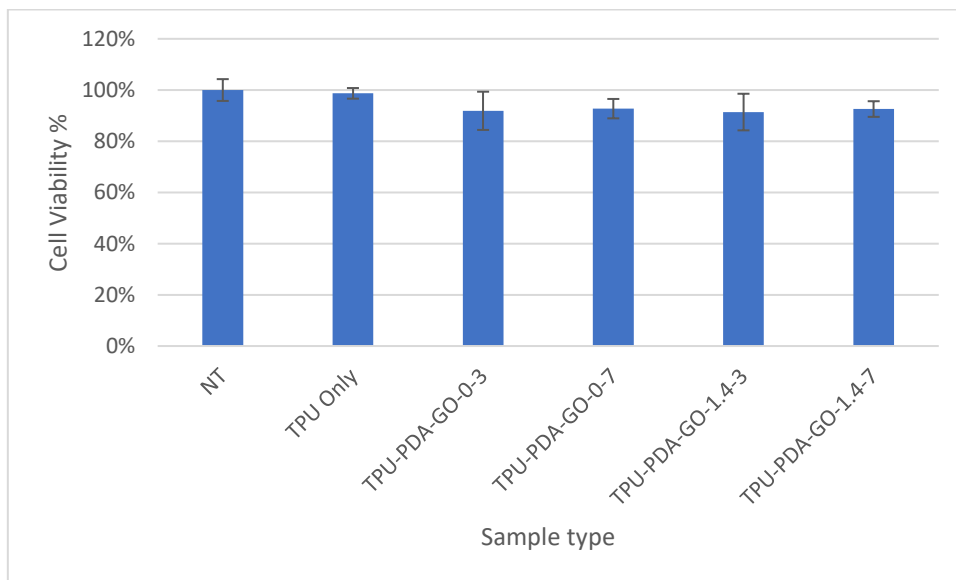


Figure 9.5: Viability of NIH/3T3 cells in indirect contact with electrospun TPU fibre mats (unmodified and GO enzyme grafted) after 24 hours.

9.4.2. Cytocompatibility of bilayer wound healing device

Figure 9.6 presents the non-contact cytocompatibility results of TPU-PDA-GO fiber patches used in conjunction with glucose-loaded GelMA hydrogel, using NIH/3T3 mouse fibroblast cells after 24 hours. NT in the figure refers to the set of

wells with no treatment introduced as the cells were cultured (positive control). The glucose-loaded GelMA was also tested to ascertain whether it was cytocompatible.

Results showed that the glucose-loaded GelMA hydrogel had a cytocompatibility of $86.7 \pm 8.4\%$. A cell viability value above 80% indicates that the material is cytocompatible. However, GelMA hydrogel cytocompatibility was lower than for TPU-PDA-GO fibre patches. The percentage of cell viability of the bilayer samples ranged from 93.8% to 99.0% with not significant differences among tested samples. The slight increase of cell viability percentage in the bilayer device compared to GelMA hydrogel could be attributed to the release of H_2O_2 at low rates, as demonstrated in a previous study which showed H_2O_2 genotoxic and proapoptotic or antiapoptotic effects depending on release kinetics⁷.

As the four sets of materials were cytocompatible when tested in indirect contact with NIH/3T3 fibroblasts after 24 hours, they all could be used for assembly into a trilayer wound healing device for evaluating their cytocompatibility, when used with honey mimetic HB PEGDA/HA-SH hydrogels.

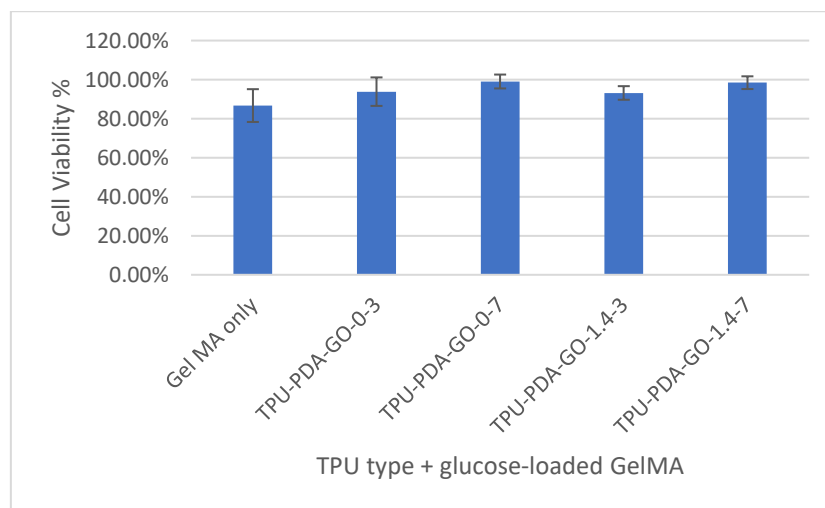


Figure 9.6: Viability of NIH/3T3 cells in indirect contact with electrospun TPU-PDA-GO mats combined with glucose-loaded GelMA hydrogel beads after 24 hours.

9.4.3. Cytocompatibility of trilayer wound healing device

Figure 9.7 presents the cytocompatibility results of NIH/3T3 mouse fibroblast cells after 24 hours using the eluates deriving from the multilayer device (extracted after 24 hours). NT in the figure refers to the set of wells with no treatment introduced as the cells were cultured (positive control). As the composition of HB PEGDA/HA-SH 10-1.0 and GelMA hydrogels were set constant, the materials were differentiated from the TPU-PDA-GO type used. These fibre materials have varying GO enzyme activities (reported as Units GO/gram TPU) thus they produce varying amounts of H₂O₂ depending on their GO activity.

Cytocompatibility values of the trilayer materials were considerably low, with the highest percentage of cell viability when TPU-PDA-GO-0-3, TPU-PDA-GO-0-7 and TPU-PDA-GO-1.4-3 patches were used with a value of $58.2 \pm 8.5\%$, $59.7 \pm 1.0\%$, and $54.2 \pm 6.0\%$, respectively. Samples containing TPU-PDA-GO-1.4-7 patches were not cytocompatible ($17.7 \pm 5.2\%$). GO enzyme assay results showed that TPU-PDA-GO-0-3 patch had the lowest GO amount in terms of U GO/g (7.9 ± 1.9 U GO/g fibre), followed by TPU-PDA-1.4-3 (7.5 ± 1.6 U GO/g fibre), next TPU-PDA-GO-0-7 (12.6 ± 2.0 U GO/g fibre), and TPU-PDA-GO-1.4-7 had the highest GO amount (16.4 ± 3.8 GO U /g fibre), which means that TPU-PDA-GO-1.4-7 patch has approximately twice the activity and the potential to produce twice as much hydrogen peroxide than TPU-PDA-GO-0-3 patch. Hence cytotoxicity in TPU-PDA-GO-1.4-7 containing materials could be due to high production of H₂O₂, deriving from a combined mechanism. As a solution, the GO/glucose concentrations in HB PEGDA/HA-SH hydrogel could be reduced when used in combination with the TPU-PDA-GO fibre patch and glucose-loaded GelMA. An alternative would be to apply the TPU-PDA-GO system to protect the *in situ* HB PEGDA/HA-SH 10-1.0 wound dressing from exposure and once the glucose from

the HB PEGDA/HA-SH 10.1 hydrogel has almost depleted itself, the glucose-loaded GelMA hydrogel could be applied as an alternative glucose source.

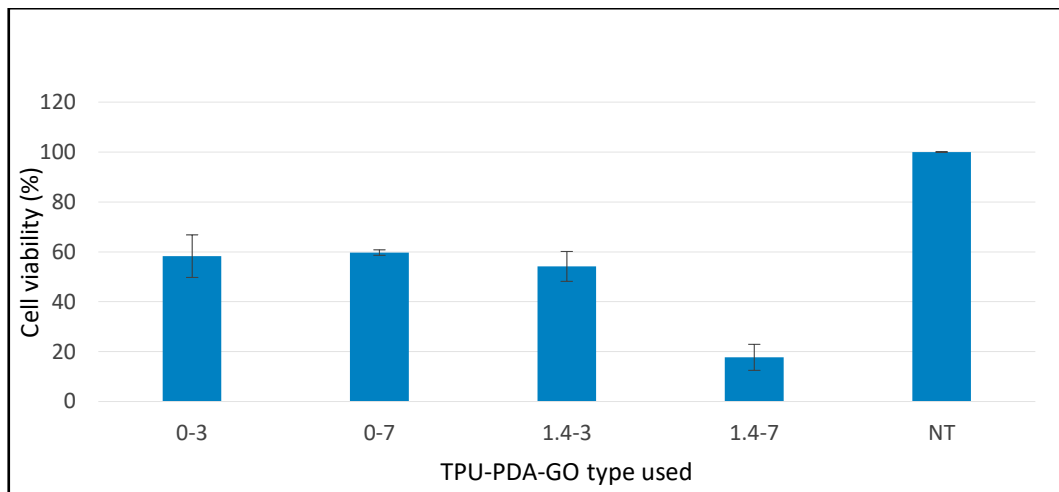


Figure 9.7: Cell viability of NIH/3T3 cells tested with the eluates of the trilayer wound healing device after 24 hours.

Another possible explanation for the low cytocompatibility is possibly due to the amount of H_2O_2 accumulated in 24 hours immediately introduced into the system as opposed to being produced and released throughout the 24 hour time-span. By revising the method to test for the cytocompatibility, a more accurate estimation of the cytocompatibility could be obtained.

9.5. Conclusions

Individually, glucose-loaded GelMA, TPU-PDA-GO-0-3, TPU-PDA-GO-0-7, TPU-PDA-GO-1.4-3, and TPU-PDA-GO-1.4-7 were tested to be cytocompatible in NIH/3T3 mouse fibroblasts after 24 hours culture time, in indirect contact tests. The TPU fibre patches were also cytocompatible when paired together with the

glucose-loaded GelMA, in indirect contact tests. However, when they were used together with HB PEGDA/HA-SH 10-1.0 hydrogels (with 250 U/L glucose oxidase and 2.5 w/w% glucose) cytocompatibility decreased for all sample types. The trilayer set-up which gave the highest cell viability of $58.2 \pm 8.5\%$ was HB PEGDA/HA-SH 10-1.0 hydrogel (250 U/L GO and 2.5 w/w% glucose) + TPU-PDA-GO-0-3 fibre patch + 10 w/v% glucose-loaded GelMA hydrogel. This was closely followed by the trilayer containing TPU-PDA-GO-0-7 ($59.7 \pm 1.0\%$) and TPU PDA-GO-1.4-3 ($54.2 \pm 6.0\%$). For future studies, it is recommended to devise a protocol on simulating the ROS production of the trilayer material for accurate measurement of H_2O_2 concentrations that are released into the media. Additionally optimization studies on the GO concentration of the base HB PEGDA/HA-SH 10-1.0 hydrogel are highly recommended. After these tests have been done, the three trilayer types can then be tested to determine what are their antibacterial properties.

The obtained cytocompatibility for the multilayer was not considerably ideal, thus it is likely that the GO/glucose concentrations in HB PEGDA/HA-SH hydrogel should be reduced when used with the TPU-PDA-GO fibre patch with glucose-loaded GelMA. An alternative would be to apply the TPU-PDA-GO system to protect the *in situ* HB PEGDA/HA-SH 10-1.0 wound dressing from exposure and once the glucose from the HB PEGDA/HA-SH 10.1 hydrogel has almost depleted itself, the glucose-loaded GelMA hydrogel could be applied as an alternative glucose source.

9.6. References

- (1) Composite Wound Dressings | Multi-layered Dressing Products
<https://www.woundsource.com/product-category/dressings/composites>
(accessed Apr 25, 2019).

- (2) Oxyzyme Dressings Datacard
<http://www.dressings.org/Dressings/oxyzyme.html> (accessed May 23, 2018).
- (3) Moffatt, C. J.; Stanton, J.; Murray, S.; Doody, V.; Davis, P. J.; Franks, P. J. A Randomised Trial to Compare the Performance of Oxyzyme® and Iodozyme® with Standard Care in the Treatment of Patients with Venous and Mixed Venous/Arterial Ulceration. *Wound Med.* **2014**, *6*, 1–10.
<https://doi.org/10.1016/j.wndm.2014.08.002>.
- (4) Cooke, J.; Dryden, M.; Patton, T.; Brennan, J.; Barrett, J.; O'Dowd, A.; Godlee, F.; Smith, R.; Coast, J.; Cooke, J.; et al. The Antimicrobial Activity of Prototype Modified Honeys That Generate Reactive Oxygen Species (ROS) Hydrogen Peroxide. *BMC Res. Notes* **2015**, *8* (1), 20.
<https://doi.org/10.1186/s13104-014-0960-4>.
- (5) Loo, A. E. K.; Wong, Y. T.; Ho, R.; Wasser, M.; Du, T.; Ng, W. T.; Halliwell, B. Effects of Hydrogen Peroxide on Wound Healing in Mice in Relation to Oxidative Damage. *PLoS One* **2012**, *7* (11).
<https://doi.org/10.1371/journal.pone.0049215>.
- (6) Faglie, A.; Neuenschwander, P.; Thompson, J.; Lee, S.-Y.; Gizaw, M.; Chou, S.-F. Electrospun Fibers as a Dressing Material for Drug and Biological Agent Delivery in Wound Healing Applications. *Bioengineering* **2018**, *5* (1), 9. <https://doi.org/10.3390/bioengineering5010009>.
- (7) Barbouti, A.; Doulias, P.-T.; Nouis, L.; Tenopoulou, M.; Galaris, D. DNA Damage and Apoptosis in Hydrogen Peroxide-Exposed Jurkat Cells: Bolus Addition versus Continuous Generation of H₂O₂. *Free Radic. Biol. Med.* **2002**, *33* (5), 691–702. [https://doi.org/10.1016/S0891-5849\(02\)00967-X](https://doi.org/10.1016/S0891-5849(02)00967-X).

Chapter 10 General discussion and conclusion

10.1. General discussion

In order to address the problem of the rise of antibacterial resistance to current and future drugs, one solution is to make use of drug free antibacterial methods. In this thesis the proposed method is to exploit one of the antibacterial characteristics of honey, which is the production of antibacterial reactive oxygen species (ROS) such as hydrogen peroxide (H_2O_2) from glucose oxidase enzyme and glucose. Over the course of this research, three types of ROS producing materials have been produced: 1) an *in situ* forming hydrogel that physically encapsulates glucose oxidase and glucose together (HB PEGDA/HA-SH), 2) an *in situ* forming hydrogel that has covalently immobilized glucose oxidase and physically encapsulates glucose (HB PEGDA-co-GMA/HA-SH), 3) a surface modified polyDOPA-coated electrospun thermoplastic polyurethane fibre patch with glucose oxidase immobilized via binding with the poly-DOPA (TPU-PDA-GO) which can convert the glucose (coming from a glucose loaded GelMA hydrogel) it interacts with into H_2O_2 .

Use of GO enzyme/glucose to produce antibacterial ROS (hydrogen peroxide, H₂O₂)

In general, the concept of using glucose oxidase and glucose in order to produce antibacterial H₂O₂ provides many opportunities. This system can be physically encapsulated within a hydrogel or chemically immobilized on a solid substrate (e.g. by binding to a polyDOPA coating) or into a hydrogel (by binding to hydrogel chains containing epoxide groups). The amount of ROS produced by the system and its rate of release can be fine-tuned by manipulating the amounts of glucose oxidase and glucose concentrations. This allows control of the concentrations of the wound healing device to be specific to different kinds of patients. The target range of production was 10-20 mM H₂O₂ per day in order to facilitate angiogenesis as previously reported¹.

HB PEGDA/HA-SH 10-1.0 with 250 U/L glucose oxidase and 2.5 w/w% glucose was able to achieve this range of H₂O₂ production, with 16.0±4.2 mM H₂O₂ after 24 hours. HB PEGDA-co-GMA/HA-SH 10-1.0 with 250 U/L and 2.5 w/w% glucose produced 8.3±0.9 mM H₂O₂ after 24 hours. This reduced production of H₂O₂ in HBPCG/HA-SH is likely to to the reduced movement the enzyme had around the hydrogel system as it was fixed to a certain location whereas in HB PEGDA/HA-SH GO and glucose moved freely within the interstices of the hydrogel matrix, with their interactions resulting in more H₂O₂ produced.

TPU-PDA-GO 1.4-7 fibre patch (i.e. with polyDOPA coating deposited in 7 hours using 1.4 U/mL LPO and grafted with GO to yield 16.4±3.8 U GO/g activity) in combination with 10 w/v% glucose-loaded GelMA hydrogel produced 3.7±0.5 mM H₂O₂ after 24 hours. The average sample weight of the 1 cm by 1 cm TPU patch is 0.0039 grams, which means it has an activity of 0.0063±0.0015 U GO that diffuses the produced H₂O₂ into the 5 mL PBS solution. This means that a maximum of 18.1±4.5 mM H₂O₂ can be produced at the maximum during the 24 hour period.

However, the obtained concentration was only 20% was produced and released into the system as the material was limited by the glucose in GelMA that diffused towards the TPU-PDA-GO layer and reacted with the enzyme. This means that the rate of H₂O₂ production in this bilayer system can be controlled to some degree by manipulating the glucose concentration in GelMA, area of contact between TPU-PDA-GO/GelMA (giving the 100 μL hydrogel a larger diameter), and GelMA hydrogel composition (this study used 15 w/v% but it is possible a higher glucose diffusion can be achieved at lower polymer concentrations).

Information about this ROS-producing system is discussed more in depth in Chapter 3, 4, and 8.

Hyperbranched Polymer Synthesis

For producing novel hydrogels with *in situ* forming characteristics, two types of PEG-based hyperbranched polymers were synthesized: hyperbranched polyethylene glycol diacrylate (HB PEGDA) and hyperbranched polyethylene glycol diacrylate-co-glycidyl methacrylate (HB PEGDA-co-GMA or HB PcG). These polymers contain vinyl groups that can be crosslinked into hydrogels in two ways: by UV-crosslinking when a photoinitiator is added into the system (this was performed on HB PEGDA but not discussed in this research thesis) or by Michael addition thiol-ene crosslinking with a thiolated polymer such as thiolated hyaluronic acid with a defined thiolation degree (HA-SH). The speed at which the hydrogel is formed is proportionally dependent on the amount of hyperbranched polymer and its vinyl group content and can be tailored by changing these two characteristics.

Crosslinking degree affects several hydrogel properties such as gelation time (the more vinyl and thiol groups available for crosslinking, the lesser the gelation time),

water absorption and degradation rate, (a more crosslinked material has a lower water absorption values but also takes longer to degrade).

Their respective chemical data are summarized in the abstracts of Chapter 2 for HB PEGDA and Chapter 4 for HB PEGDA-co-GMA.

Polymer Processing, Surface Modification, and Functionalization

Commercially available biomedical grade thermoplastic polyurethane (TPU) Lubrizol Tecophilic SP-60D-60 was selected to be processed into a fibre mat by electrospinning according to the processing conditions described in Chapter 5. The material was selected due to its established biocompatibility, hydrophilic properties where it has a static contact angle of $72.0 \pm 2.9^\circ$; water absorbance percentage of $44.7 \pm 4.9\%$ after 24 hours and $60.6 \pm 3.0\%$ after 4 weeks (ideal for contact with hydrogels); Young's modulus of 25.1 ± 1.5 MPa, ultimate tensile strength of 10.4 ± 0.7 MPa, and ultimate elongation percentage of $386 \pm 63\%$ (mechanical properties are in the accepted range of commercial wound dressings).

This fibre patch was then coated with PDA, with and without the aid of lactoperoxidase (LPO) enzyme to boost the oxidation process and potentially lower the coating time required (described in depth in Chapter 7). These modified fibre patches (TPU-PDA-LPO) were immersed in a glucose oxidase solution for 24 hours in order to let the enzyme molecules bind and be immobilized into the PDA layer. Various tests in Chapter 8 confirmed the presence of GO and its ability to produce hydrogen peroxide with glucose .

TPU-PDA-0-7-GO (PDA coating for 7 hours without LPO) had an enzymatic activity of 12.6 ± 2.0 U GO/g while TPU-PDA-1.4-7 (PDA coating for 7 hours with 1.4 U/mL LPO) had an enzymatic activity of 16.4 ± 3.8 U GO/g activity.

Synthesis of Glucose Loaded Top Hydrogel

Gelatin methacrylate (GelMA) was synthesized from porcine skin gelatin and functionalized with glycidyl methacrylate following the same procedure proposed by Nichol, JW, et al., 2010². This hydrogel was selected for the following reasons: 1) the synthesis process and purification were relatively simple (especially compared to the preparation of HB PEGDA and HA-SH), 2) the material is stable in oxygen and does not self-crosslink (HA-SH requires to be prepared and stored with Argon), 3) only two reagents were required (gelatin and methacrylic anhydride), 4) it was able to crosslink under UV light with the addition of a photoinitiator, 5) it has been used in biomedical engineering applications and has been tested to be cytocompatible²⁻⁴. This glucose-loaded material was intended to be applied to wounds already crosslinked when placed on top of the TPU-PDA-GO patch similar to the bilayer hydrogel wound dressing system of Oxyzyme⁵⁻⁷.

GelMA hydrogel formed from a 15 w/v% solution with the addition of 0.5 w/v% Irgacure 2959 and exposure to UV radiation for 10 min. Glucose was loaded into the hydrogel at 10 w/v% concentration. Chemical characterization by FTIR-ATR analysis confirmed the functionalization of gelatin with methacrylate functionalities. Characterization of this material can be found in Chapter 8.

ROS Production in Polymer Biomaterials

A colorimetric assay was applied to detect the formation of hydrogen peroxide from the various types of material (thiol-ene hydrogel, TPU patch, or TPU patch with

glucose-laden hydrogel on the top) ⁸. Details of the ROS measurement results can be found in Chapter 3, 4, and 8 with the data summarized below in Table 10.1.

Table 10.1. Summary of materials with their highest H₂O₂-yielding parameters

Material	GO/glucose content	H₂O₂ concentration after 24 hours (mM)
200 μ L HB PEGDA/ HA-SH 10-1.0 in 10 mL PBS pH 7.4	250 U/L GO, 2.5 w/w%	In static conditions: 9.1 \pm 0.9 mM H ₂ O ₂ With shaking: 16.0 \pm 4.2 mM H ₂ O ₂
200 μ L HB PEGDA-co-GMA/ HA-SH 10-1.0 in 10 mL PBS pH 7.4	250 U/L GO, 2.5 w/w%	With shaking: 8.3 \pm 0.9 mM H ₂ O ₂
1 cm x 1 cm (0.0039 g) TPU-PDA-GO-1.4-7 + 100 μ L glucose-loaded GelMA in 5 mL PBS pH 7.4	16.4 \pm 3.8 U GO/g fibre patch, 10 w/v% glucose in GelMA	In static conditions: 3.7 \pm 0.5 mM H ₂ O ₂ Maximum concentration based on activity (static conditions): 18.1 \pm 4.5 mM H ₂ O ₂

Cytocompatibility of ROS-producing Biomaterials

Cytocompatibility of the materials were tested using NIH/3T3 mouse fibroblast cells for 24 hours. The base materials (not producing ROS) such as HB PEGDA/HA-SH 10-1.0, TPU, and TPU-PDA, TPU-PDA-GO, and UV-crosslinked GelMA showed cytocompatibility when analysed individually.

When loaded with GO enzyme and glucose, HB PEGDA/HA-SH 10-1.0 was cytocompatible for GO concentrations between 0 to 250 U/L with 2.5 w/w% glucose. From the material data sheet, glucose oxidase has an activity of 19,290

U/g, thus when converting the enzyme activity concentration to mass concentration for the enzyme solutions used, the prepared solutions were between 0 to 13 mg/L.

5 mm by 5 mm TPU-PDA-GOs used with 30 μ L 10 w/v% glucose-loaded GelMA hydrogel gave cytocompatible results with percentage of cell viability higher than 80%. The cytocompatibility of the bilayer material was designed to keep the testing conditions as similar to the ones used for HB PEGDA/HA-SH 10-1.0 and HB PEGDA-co-GMA/HA-SH 10-1.0 where hydrogels were set to sample sizes of 30 μ L and tested with 30,000 NIH/3T4 cells/mL for 24 hours.

The material HB PEGDA-co-GMA demonstrated low cytocompatibility due to glycidyl methacrylate's unconjugated epoxide bonds that did not graft with an enzyme and was not suitable for wound healing applications however it has the potential to be used in other enzyme immobilization applications, such as immobilizing enzymes for sensor applications and used in enzyme reactor vessels as a catalyst for reactions without requiring separation from the bulk fluid^{9,10}.

Antibacterial Activity of ROS-producing Biomaterials

Antibacterial tests were performed in collaboration with PhD Ayesha Idrees (Politecnico di Torino). HB PEGDA/HA-SH 10-1.0 hydrogels showed zones of inhibition for several bacterial strains at a concentration of 250 U/L GO and 2.5 w/w% glucose: *S. aureus*, *S. epidermidis*, *E. coli*, Methicillin-resistant *S. aureus* (MRSA), Methicillin-resistant *S. epidermidis* (MRSE), *P. aeruginosa*, *A. baumannii*. At an increased concentration of 500 U/L GO and 2.5 w/w% glucose, this hydrogel showed zones of inhibition for all strains mentioned previously and for KPC-2 producing drug resistant *E. coli*.

The antibacterial activity of TPU-PDA-GO material plus glucose loaded GelMA hydrogel was not performed in this thesis but it will be performed in later studies. ROS produced from these materials are additional to those produced by the HB PEGDA/HA-SH hydrogel and aims to prolong the antimicrobial activity of the final device.

Assembly of Multilayer Wound Healing Device

Figure 10.1 shows the assembled multilayer wound healing device with the specific materials used for each layer.

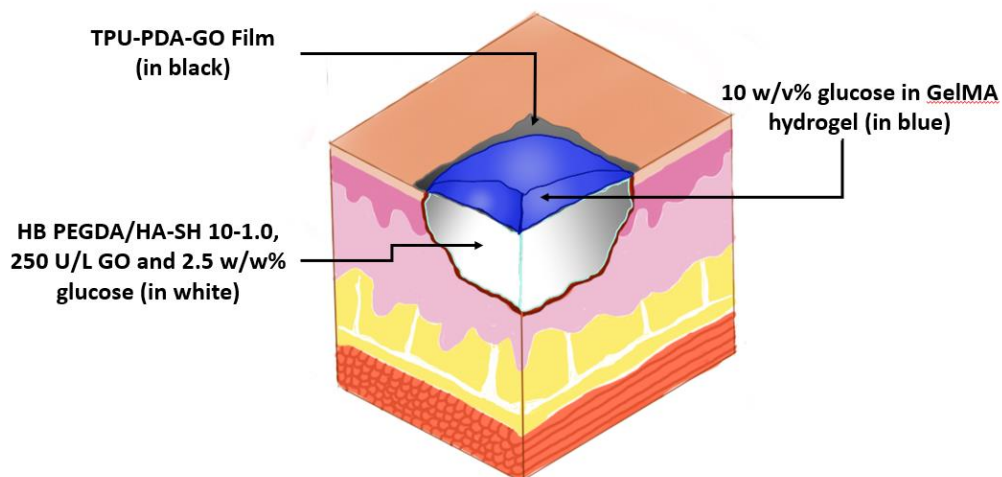


Figure 10.1: Multilayer wound healing device

A multilayer wound material loaded with drug-free ROS producing GO enzyme was developed. The bottom HB PEGDA/HA-SH hydrogel had 250 U/L GO concentration and 2.5 w/w% glucose and this was the base setting of the device, showing cytocompatibility when tested with NIH/3T3 mouse fibroblasts and displaying antibacterial activity.

For the trilayer device, the highest overall cytocompatibility was $58.3\pm 8.5\%$ when using TPU-PDA-GO-0-3 and glucose-loaded (10 w/v%) UV-crosslinked GelMA hydrogel. The other trilayer materials with similar cytocompatibility were the ones that used TPU-PDA-GO-0-7 ($59.7\pm 1.0\%$) and TPU-PDA-GO-1.4-3 ($54.2\pm 6.0\%$). The obtained cytocompatibility for the multilayers were not considerably ideal, thus it is likely that a higher amount of ROS was produced leading to cytotoxicity, with the combined concentration being at least 12.1 ± 1.4 mM H_2O_2 for TPU-PDA-GO-0-3, for example. Due to the lack of HB PEGDA, overall ROS measurements in the trilayer system were not able to be performed but it is possible that the overall concentration is higher with some glucose molecules that have permeated through the TPU-PDA-GO membrane without reacting with the grafted GO to reacting instead with the unimmobilized (thus more mobile) GO in the HB PEGDA/HA-SH 10-1.0 hydrogels.

Hence, GO/glucose concentrations in bottom HB PEGDA/HA-SH 10-1.0 hydrogel should be reduced when used in combination with the TPU-PDA-GO fiber patch with glucose-loaded GelMA top hydrogel. An alternative would be to apply the TPU-PDA-GO system to protect the *in situ* HB PEGDA/HA-SH 10-1.0 wound dressing from exposure and once the glucose from the HB PEGDA/HA-SH 10.1 hydrogel has almost depleted itself, the glucose-loaded GelMA hydrogel could be applied as an alternative glucose source.

The other possible alternative configurations of this wound healing device can be seen in Figure 10.2, using the materials developed in this study. For example, by using Layer 1 and 2, this combination uses the advantage of Layer 1 being a primary antibacterial material-producing wound dressing and Layer 2 as an extra protective film as well as being a secondary source of ROS-producing glucose oxidase enzymes. Layer 2 and Layer 3 used together is another potential combination with in situations where lower ROS concentrations are more desirable.

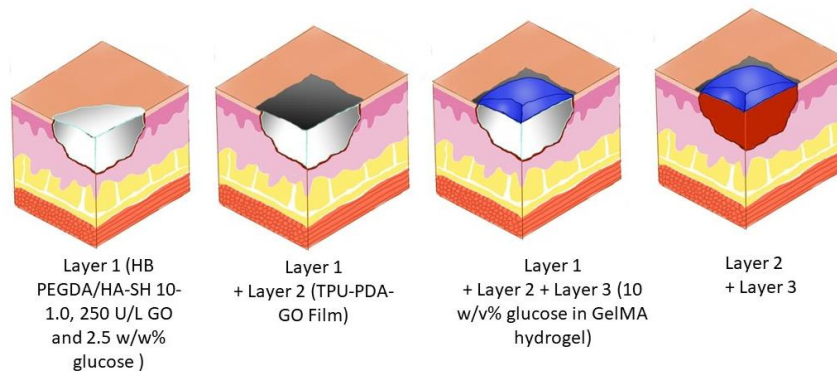


Figure 10.2: Possible configurations for assembling the materials developed in this thesis for an antibacterial wound healing patch using Layers 1 to 3.

10.2. Conclusions and future development

HB PEGDA/HA-SH 10-1.0 hydrogels have proven to be a potentially effective drug-free antibacterial wound healing device that mimic the ROS-producing property of honey. Its quick-forming *in situ* properties allow it to be applied into a wound surface as a liquid, fill irregular crevices in the wound, and rapidly turn into a hydrogel in approximately one minute. The optimal composition of this hydrogel for producing ROS is 250 U/L glucose oxidase and 2.5 w/w% glucose.

Further research should be conducted for the use of a lower GO concentration when the hydrogel is combined with a TPU-PDA-GO fibre patch + glucose-loaded GelMA top hydrogel. Independently, these two sets of medical devices produce good cytocompatibility in NIH/3T3 mouse fibroblasts (after 24 hours) but when used together, ROS concentration reaches a high level causing cytotoxicity.

Another possible explanation for the low cytocompatibility is that in this work the whole amount of H_2O_2 accumulated in 24 hours was tested, rather than the amount

produced throughout the 24 hour time-span. By revising the method to test ROS production, a more accurate estimation of the cytocompatibility could be obtained.

It is also recommended that antibacterial testing can be also performed on the TPU-PDA-GO patches in combination with glucose-loaded GelMA hydrogels to analyse whether they produce antibacterial activity at an equal level respect to HB PEGDA/HA-SH 10-1.0 hydrogels alone.

In imaging studies performed on GO enzyme grafted PDA-TPU-LPO and PDA-TPU systems, higher magnifications than 20,000x should be performed. Due to the limitations of the equipment used, in this study maximum magnification was 5,000x. At a higher magnification, the individual enzyme clusters onto the TPU fibre surface could be easily detected^{11,12}.

For future studies regarding honey-mimetic, drug free antibacterial materials, the system of producing ROS with glucose oxidase and glucose may be tested in other hydrogel matrices, such as thermoresponsive polymers. One of the polymer syntheses performed by the PhD candidate was PLGA(poly(lactic-co-glycolic acid))-PEG (poly(ethylene glycol))-PLGA in supercritical carbon dioxide (see Thesis Appendix A and B). The copolymer was water soluble at room temperature and turned into a gel at around body temperature (35°C) when solution concentration was 20 w/w% PLGA-PEG-PLGA. Data on copolymer synthesis, hydrogel rheological properties, and ROS formation from GO and glucose can be found in the PhD thesis appendices. This preliminary study on thermosensitive hydrogels underlines that the GO/glucose system can be applied over a wide range of hydrogels having different gelation mechanisms.

10.3. References

- (1) Loo, A. E. K.; Wong, Y. T.; Ho, R.; Wasser, M.; Du, T.; Ng, W. T.; Halliwell, B. Effects of Hydrogen Peroxide on Wound Healing in Mice in Relation to Oxidative Damage. *PLoS One* **2012**, *7* (11).
<https://doi.org/10.1371/journal.pone.0049215>.
- (2) Nichol, J. W.; Koshy, S. T.; Bae, H.; Hwang, C. M.; Yamanlar, S.; Khademhosseini, A. Cell-Laden Microengineered Gelatin Methacrylate Hydrogels. *Biomaterials* **2010**, *31* (21), 5536–5544.
<https://doi.org/10.1016/j.biomaterials.2010.03.064>.
- (3) Hutson, C. B.; Nichol, J. W.; Aubin, H.; Bae, H.; Yamanlar, S.; Al-Haque, S.; Koshy, S. T.; Khademhosseini, A. Synthesis and Characterization of Tunable Poly(Ethylene Glycol): Gelatin Methacrylate Composite Hydrogels. *Tissue Eng. Part A* **2011**, *17* (13–14), 1713–1723.
<https://doi.org/10.1089/ten.tea.2010.0666>.
- (4) Wang, Z.; Abdulla, R.; Parker, B.; Samanipour, R.; Ghosh, S.; Kim, K. A Simple and High-Resolution Stereolithography-Based 3D Bioprinting System Using Visible Light Crosslinkable Bioinks. *Biofabrication* **2015**, *7* (4), 45009. <https://doi.org/10.1088/1758-5090/7/4/045009>.
- (5) Oxyzyme Dressings Datacard
<http://www.dressings.org/Dressings/oxyzyme.html> (accessed May 23, 2018).
- (6) Moffatt, C. J.; Stanton, J.; Murray, S.; Doody, V.; Davis, P. J.; Franks, P. J. A Randomised Trial to Compare the Performance of Oxyzyme® and Iodozyme® with Standard Care in the Treatment of Patients with Venous and Mixed Venous/Arterial Ulceration. *Wound Med.* **2014**, *6*, 1–10.
<https://doi.org/10.1016/j.wndm.2014.08.002>.
- (7) Eaton, A. Oxyzyme Application and Removal Video - YouTube
<https://www.youtube.com/watch?v=N5BVAC8oTtU> (accessed May 23,

- 2018).
- (8) Eisenberg, G. Colorimetric Determination of Hydrogen Peroxide. *Ind. Eng. Chem. Anal. Ed.* **1943**, *15* (5), 327–328.
<https://doi.org/10.1021/i560117a011>.
 - (9) Poplawski, T.; Pawlowska, E.; Wisniewska-Jarosinska, M.; Ksiazek, D.; Wozniak, K.; Szczepanska, J.; Blasiak, J. Cytotoxicity and Genotoxicity of Glycidyl Methacrylate. *Chem. Biol. Interact.* **2009**, *180* (1), 69–78.
<https://doi.org/10.1016/J.CBI.2009.02.001>.
 - (10) Gao, X.; Ni, K.; Zhao, C.; Ren, Y.; Wei, D. Enhancement of the Activity of Enzyme Immobilized on Polydopamine-Coated Iron Oxide Nanoparticles by Rational Orientation of Formate Dehydrogenase. *J. Biotechnol.* **2014**, *188*, 36–41. <https://doi.org/10.1016/j.jbiotec.2014.07.443>.
 - (11) Anwar, M. Z.; Kim, D. J.; Kumar, A.; Patel, S. K. S.; Otari, S.; Mardina, P.; Jeong, J.-H.; Sohn, J.-H.; Kim, J. H.; Park, J. T.; et al. SnO₂ Hollow Nanotubes: A Novel and Efficient Support Matrix for Enzyme Immobilization. *Sci. Rep.* **2017**, *7* (1), 15333.
<https://doi.org/10.1038/s41598-017-15550-y>.
 - (12) Leitgeb, M.; Knez, Ž.; Vasić, K. Micro- and Nanocarriers for Immobilization of Enzymes. In *Micro and Nanotechnologies for Biotechnology*; 2016. <https://doi.org/10.5772/63129>.

Appendix A – Synthesis and characterization of thermosensitive PLGA-PEG-PLGA hydrogel

A1. Abstract

A triblock polylactic-co-polyglycolic acid-polyethylene glycol- polylactic-co-polyglycolic acid (PLGA-PEG-PLGA or PPP) polymer was synthesized by the researcher while performing her secondment in the Vornia Ltd., research laboratory utilizing their innovative production technology that allows for production of cleaner biomaterials (medical grade polymers). This material has been commercialized and launched into the market. When dissolved in PBS pH 7.4 or water from 20 w/w% to 30 w/w%, the material behaved as a thermoresponsive hydrogel where the solutions were in liquid state in room temperature but transition into a hydrogel at a temperature of 32°C or higher. When a 20 w/w% PPP polymer solution containing glucose oxidase was mixed with a 20 w/w% PPP polymer solution containing glucose, this hydrogel mixture produced hydrogen peroxide as a result. For PPP hydrogels: 250 U/L GO with 2.5 w/w% glucose produced 6.3 ± 1.6 mM H_2O_2 after 24 hours and 500 U/L GO with 5.0 w/w% glucose produced 10.9 ± 0.5 mM H_2O_2 after 24 hours. The intended application was to use this material as an injectable hydrogel for wound healing purposes where the liquid solution

transforms into a hydrogel upon contact of the solution with human body heat (at a temperature of around 37°C) where this hydrogel behaves as a honey mimetic wound healing device similar to HB PEGDA/HA-SH 10-1.0. What can be gained from this synthesis and hydrogel preparation is that the glucose oxidase/glucose system can be applied to a wide range of hydrogel materials where their behavioural properties (such as gelation time, method of crosslinking, etc.) can be tailored to specific wound healing applications.

A2. Introduction

The researcher aimed to synthesize a triblock poly(lactic-co-glycolic acid)-poly(ethylene glycol)-poly(lactic-co-glycolic acid) (PLGA-PEG-PLGA) polymer making it an environmentally friendly process. The original process was performed by Gao, Y. et al. (2010)¹. Figures A1 to A3 show the polymerization reaction for lactide, glycolide, and poly(ethylene glycol) (PEG) forming a triblock polymer.

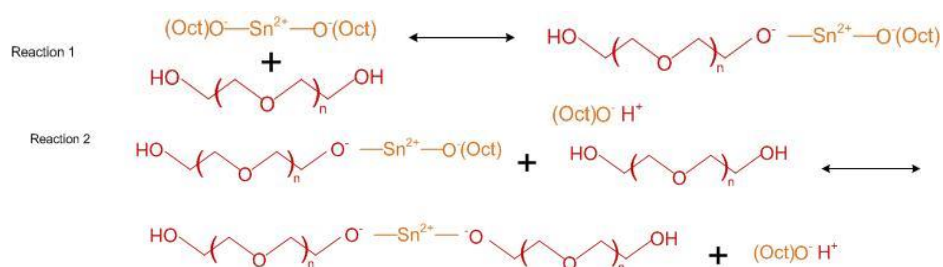


Figure A1: Poly(ethylene glycol) (red) reacting with stannous octanoate (orange)

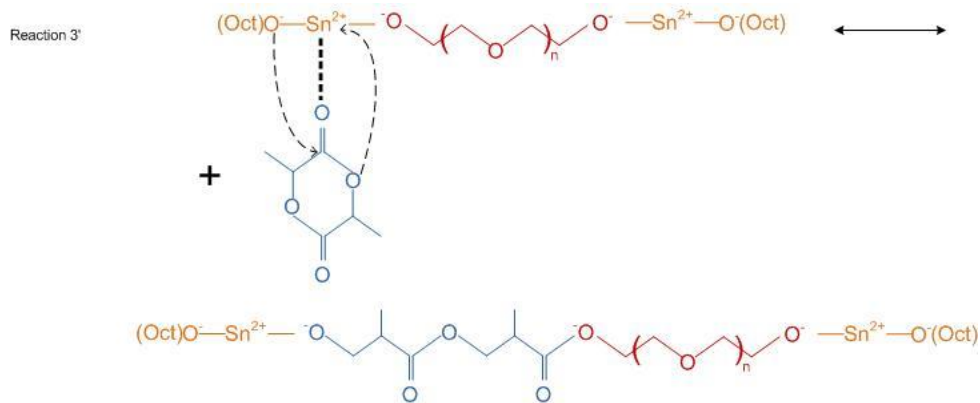


Figure A2.: Ring opening reaction for PLGA-PEG-PLGA

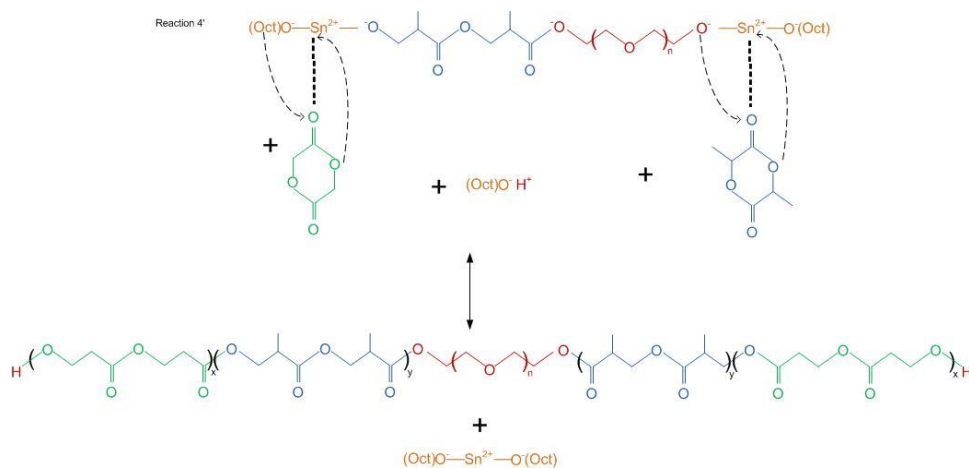


Figure A3. Final PLGA-PEG-PLGA (PPP) product

A3. Materials and methods

Phosphate buffer solution (PBS) pH 7.4 tablets, glucose, glucose oxidase (GO, E.C. 1.1.3.4.), sulfuric acid, titanium oxysulfate were bought from Sigma Aldrich, UK. The reagents for the polymer synthesis were also provided by them.

A3.1. Polymer Synthesis

A copy of the PLGA-PEG-PLGA product brochure, prepared by the PhD candidate during her secondment is shown in Appendix B. Product synthesis is not disclosed for commercial reasons.

A3.2. Chemical characterization by ^1H NMR and Gel Phase Chromatography

See Chapter 2, Section 2.3.4 for the procedure on ^1H NMR and GPC sample preparation and analysis.

A3.3. Determination of gelation temperature

PLGA-PEG-PLGA (PPP) hydrogels were prepared by dissolving PPP at 20, 25, and 30 w/w% in PBS pH 7.4. The temperature where gelation occurs was measured by using a TA Discovery Hybrid Rheometer-2 (DHR-2).

A hydrogel sample was placed in an 8 mm flat disc plate rheometer. The storage modulus profiles were measured from 30°C to 40°C with a step increase of 0.1°C (10% strain, 10 Hz frequency). An increasing storage modulus means that the hydrogel becomes more solid-like.

A3.4. ROS measurement assays

The main purpose of this section is to test the applicability of antibacterial ROS glucose oxidase/glucose hydrogels in non thiol-ene crosslinking polymer system. PLGA-PEG-PLGA was selected to see if the ROS system was applicable to a thermoresponsive hydrogel.

Briefly, two ROS systems were prepared in 20 w/w% PPP: 250 U/L GO and 2.5 w/w% glucose; 500 U/L and 5.0 w/w% glucose. The hydrogels were prepared by mixing 100 μ L Solution A and 100 μ L Solution B. These polymer solutions became hydrogels while incubated at 37°C as shown in Table A.1.

Table A.1. Concentration of GO and glucose used for preparing thermoresponsive PPP hydrogels.

Final hydrogel composition (20 w/w% PLGA-PEG-PLGA)	Solution A (Glucose oxidase containing solution)	Solution B (Glucose containing solution)
250 U/L GO and 2.5 w/w% glucose	PPP composition: 20 w/w% Glucose oxidase concentration: 500 U/L	PPP composition: 20 w/w% Glucose concentration: 5 w/w%
500 U/L and 5.0 w/w% glucose	PPP composition: 20 w/w% Glucose oxidase concentration: 1000 U/L	PPP composition: Glucose concentration: 10 w/w%

Using the procedure described in Chapter 3, Section 3.3.3. the H₂O₂ content of these hydrogels were measured at different time points: 2 hours, 4 hours, 24 hours, and 48 hours.

A4. Results and Discussion

A4.1. Chemical characterization

Figure A.4. outlines the NMR results showing the presence of the polylactide, polyglycolide and PEG groups. Calculations from NMR data gave a lactide:glycolide molar ratio of 7.7:1, a 24.42 wt% PEG, and a molecular weight of 6,143 Da. Meanwhile the GPC results show that Mw was 9,786 Da and Mn was 6,960 Da. The reaction had a molar yield of 98%, which means that 98% of the reagents were reacted in the polymer synthesis.

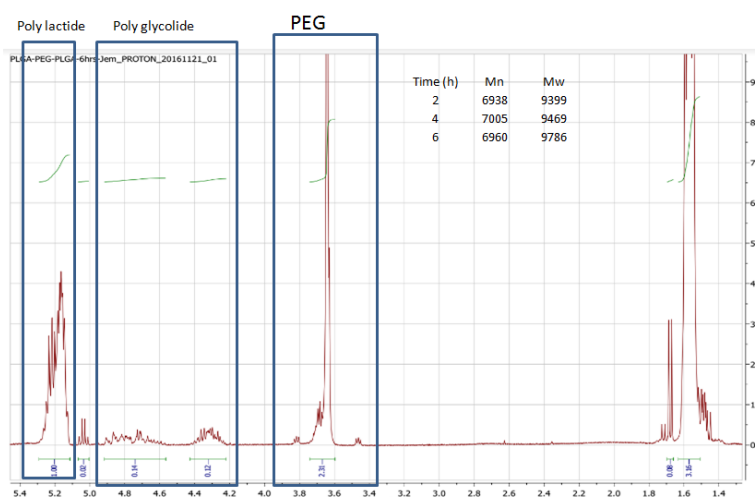


Figure A4: ^1H NMR results of PLGA-PEG-PLGA with the GPC results for the Mn and Mw reported for 2, 4, and 6 hours.

A4.2. Gelation temperature

From Figure A.5, it can be seen that storage modulus increases with respect to temperature up to a certain point before decreasing once again. It was observed that increasing the amount of polymer in the solution decreases the gelation temperature. For concentrations 25 w/w% PPP and 30 w/w% PPP, they became hydrogels at approximately 32°C while 20 w/w% PPP had a gelation temperature of 35°C. This means that for all concentrations, a hydrogel would be formed at body temperature, 37°C. For practical reasons such as ease of dissolving and conserving material, 20 wt% will be used for future studies such as measuring the amount of H₂O₂ produced.

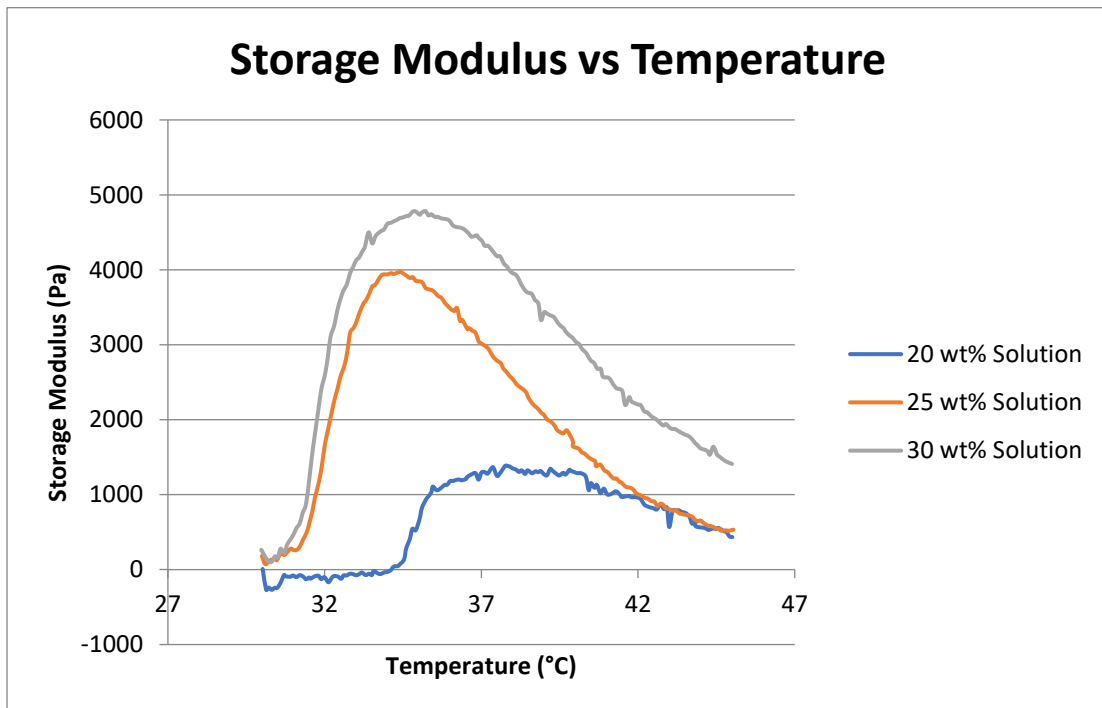


Figure A.5: Storage of 2PLGA-PEG-PLGA hydrogels as a function of temperature.

A4.3. ROS production in thermoresponsive hydrogels

Hydrogen peroxide was successfully produced in the two GO/glucose concentrations used. However, when compared to the HB PEGDA/HA-SH 10-1.0 hydrogels of the same GO/glucose concentrations, the PLGA-PEG-PLGA hydrogels produced H₂O₂ concentrations which were significantly lower than their counterparts. The target H₂O₂ production for ROS-producing hydrogels was 10-20 mM H₂O₂ per day, which was only achieved by the PPP hydrogel with 500 U/L GO and 5.0 w/w% glucose².

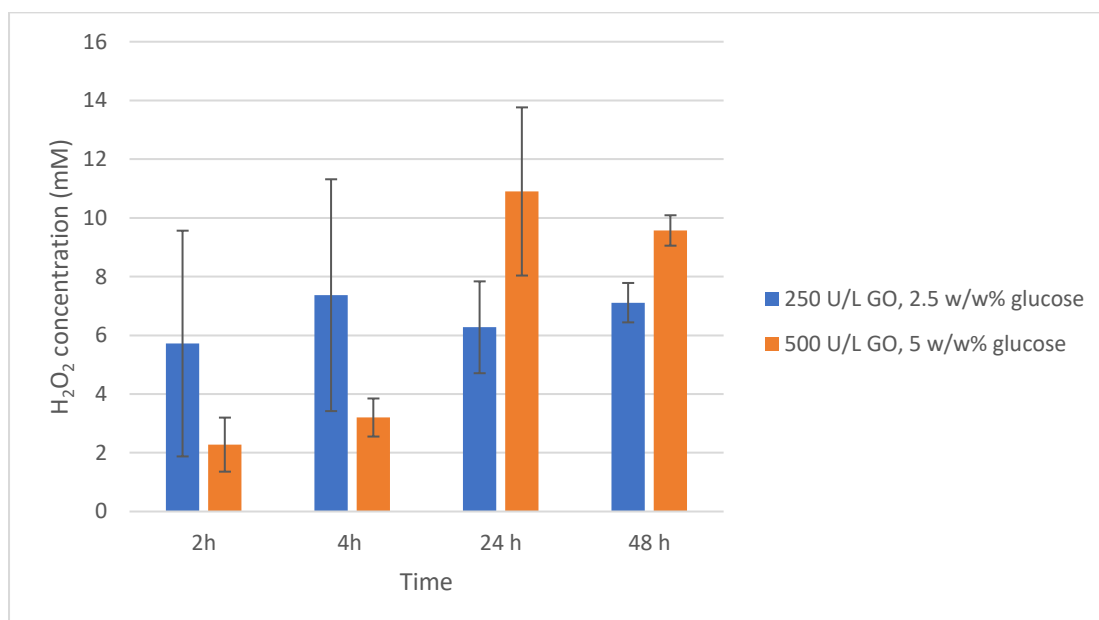


Figure A.6. H₂O₂ production in PLGA-PEG-PLGA at different time points.

The intended application was to use this material as an injectable hydrogel for wound healing purposes where the liquid solution transforms into a hydrogel from the contact of the solution to human body heat (at a temperature of approximately 37°C) where this hydrogel behaves as a honey mimetic wound healing device similar to HB PEGDA/HA-SH 10-1.0.

A.5. Conclusions

The honey-mimetic system (glucose oxidase enzyme/glucose reacting to form hydrogen peroxide) used in the main thesis was also applicable to a thermoresponsive hydrogel of 20 w/w% PLGA-PEG-PLGA with 500 U/L GO and 5.0 w/w% glucose. This material produced 9.6 ± 0.5 mM H_2O_2 in 24 hours. This polymer was developed and synthesized by the PhD candidate during her secondment in Vornia Ltd., Ireland. This material was advertised in the Vornia website briefly before the company was sold to Ashland Specialties Ltd., Ireland.

What can be gained from this synthesis and hydrogel preparation is that the glucose oxidase/glucose system can be applied to a wide range of hydrogel materials where their behavioural properties (such as gelation time, method of crosslinking, etc.) can be tailored to specific wound healing applications.

A.6. References

1. Gao, Y., Sun, Y., Ren, F. & Gao, S. PLGA-PEG-PLGA hydrogel for ocular drug delivery of dexamethasone acetate. *Drug Dev Ind Pharm* **36**, 1131–1138 (2010).
2. Loo, A. E. K. *et al.* Effects of Hydrogen Peroxide on Wound Healing in Mice in Relation to Oxidative Damage. *PLoS One* **7**, (2012).

Appendix B: Brochure copy of Vornia Ltd.s' PLGA-PEG-PLGA

This was written by the PhD candidate and featured in briefly in Vornia website (before the company was purchased by Ashland Specialties, Ltd.)



Vornia Poly D,L-lactide-co-glycolide-co-Polyethylene glycol-co-Poly D,L-lactide-co-glycolide (PLGA-PEG-PLGA)

Poly D,L-lactide-co-glycolide-co-Polyethylene glycol-co-Poly D,L-lactide-co-glycolide (PLGA-PEG-PLGA)

PLGA-PEG-PLGA is a triblock copolymer of Poly D, L-lactide and Glycolide on both ends of Poly Ethylene Glycol. Biocompatible, degradable, thermosensitive, and properties can be easily modified.

It is an amphiphilic triblock copolymer which can self-assemble into micelles in aqueous medium due to the hydrophobic interactions present in the hydrophobic segments. The PEG segment imparts hydrophilicity and improves the biocompatibility of the copolymer. The PLGA segment forms a hydrophobic core and can solubilize hydrophobic drugs. These copolymers are widely used as nanocarriers for the sustained release of drugs.

It is capable of forming a gel at a range of temperatures depending on its composition and concentration in water. It is available in a wide range of both molecular weights and lactide to glycolide ratios. Vornia PLGA is available 10:1 in molar ratio. It is supplied in the form of a bottled polymer solution. Vornia PLGA-PEG-PLGA is produced via a "green" manufacturing process which is completely devoid of solvent residues, resulting in a highly pure resorbable polymer product certified to the ISO 13485 standard for use in medical device and pharmaceutical applications.

Application:

This material has been used in:

- Synthesis of targeted nanoparticles
- Differential drug delivery
- Controlled release of drugs

It is also suitable for:

- Injectable hydrogels
- Wound dressings
- Thermosensitive applications

Standard R&D Grade /Medical Grade

General Specifications:

Molecular Weight:	5 - 10kDa Available to order
Molar Ratio:	10:1 Lactide to Glycolide Available to order
% Purity:	≥98%
Residual Monomer:	≤2%
Heavy Metals (not incl. Sn):	≤ 10ppm
Residual Solvent:	None
Appearance:	Viscous polymer. Typically 1 gram in glass bottle
Storage temperature:	2-8°C
Degradation timeframe:	2-3 weeks

Discounts offered for Bulk orders.

For bulk orders or for customized polymers please contact us directly at info@vornia.com or + 353 (0)1 531 2981

A decorative footer graphic consisting of a grid of light blue lines that form a wavy, undulating pattern across the bottom of the page.

VORNIA BIOMATERIALS